

**Structure-function analysis of the axon
guidance molecules *Sidestep* and *Beaten path
1a* in *Drosophila melanogaster***

Inaugural-Dissertation

zur Erlangung des Doktorgrades
der Mathematisch-Naturwissenschaftlichen Fakultät
der Heinrich-Heine-Universität Düsseldorf

vorgelegt von

Caroline Daniela Stefanie Heymann
aus Dachau

Düsseldorf, Juni 2017

aus dem Institut für Funktionelle Zellmorphologie
der Heinrich-Heine-Universität Düsseldorf

Gedruckt mit der Genehmigung der
Mathematisch-Naturwissenschaftlichen Fakultät der
Heinrich-Heine-Universität Düsseldorf

Referent: Prof. Dr. Hermann Aberle

Korreferent: Prof. Dr. Eckhard Lammert

Tag der mündlichen Prüfung:

Abstract

Precise connectivity between the nervous system and muscles builds the basis for all coordinated movements. During embryogenesis, outgrowing motor axons are guided by diverse attractive and repellent cues from the CNS to the muscles. Various guidance molecules contribute to motor axon pathfinding. In *Drosophila*, two members of the immunoglobulin superfamily, Sidestep (Side) and Beaten path la (Beat), are key molecules regulating this process. Side is expressed in a highly dynamic pattern during embryogenesis and was identified as target-derived attractive guidance molecule marking intermediate and final targets. Beat is expressed in motor axons and is required to detect Side-labeled surfaces.

Previous cell aggregation experiments with transiently transfected S2 cells showed that adhesive aggregates formed only if both Beat and Side were present in these cells. The interaction domains of Beat and Side were now characterized *in vivo*. These studies indicate that the respective first immunoglobulin domains of Beat and Side are sufficient for the interaction of these proteins. Firstly, Beat constructs containing the first immunoglobulin domain are redirected to form clusters with Side constructs containing the first immunoglobulin domain. Secondly, full-length Beat, but not Beat Δ IG1, traps endogenous Side in late stage embryos. Thirdly, deletion of the first immunoglobulin domain of Side and a G187D missense point mutation within this domain in *side*^{l306} abolish the interaction with Beat. As specific Side overexpression leads to an irreversible formation of ectopic neuromuscular junctions, this work also provides evidence that Side does not only guide growth cones, but also induces synaptogenesis.

Former *in vitro* studies indicated that Beat spans the plasma membrane, although it does not contain a classical transmembrane region. This assumption was supported by previous rescue experiments, which were confirmed and expanded in this work. These experiments demonstrate that presynaptic, but not postsynaptic, expression of full-length Beat constructs during embryogenesis rescues the *beat* mutant phenotype, indicating that Beat function is required cell-autonomously. Various GFP-tagged Beat deletion and fusion constructs were further used in live imaging, western blot and surface staining experiments and support the existence of a transmembrane domain located between the two N-terminal immunoglobulin domains and the C-terminal cysteine-rich region, thus characterizing Beat as a type I transmembrane protein. Taken together, these data indicate that Beat and Side interact *in vivo* via their first immunoglobulin domains, thereby building the basis for axon-substrate adhesion during axon guidance.

Zusammenfassung

Die Voraussetzung für die Ausführung koordinierter Bewegungen ist eine korrekte motoneuronale Verschaltung, die während der Embryogenese ausgebildet wird. Anziehende und abstoßende Wegfindungsmoleküle dirigieren die auswachsenden Motoraxone präzise zu ihren Zielen. Verschiedene Moleküle tragen zur axonalen Wegfindung bei. Die zwei Proteine Sidestep (Side) und Beaten path Ia (Beat) aus der Familie der Immunglobuline übernehmen eine wesentliche Funktion in der motoraxonalen Wegfindung. Side ist während der Embryonalentwicklung in einem sehr dynamischen Muster exprimiert und markiert intermediäre und finale Zielzellen. Beat ist in Motoneuronen exprimiert und wird benötigt, um Side-markierte Wege zu detektieren.

Vorangegangene Zell-Aggregationsversuche mit transient transfizierten S2 Zellen zeigten, dass sich adhäsive Aggregate nur ausbilden konnten, wenn sowohl Beat als auch Side in diesen Zellen exprimiert wurden. Die Interaktionsdomänen von Beat und Side wurden im Rahmen dieser Arbeit *in vivo* charakterisiert. Diese Studien deuten darauf hin, dass die jeweiligen ersten Immunglobulin (IG) Domänen von Beat und Side die Interaktion dieser Proteine vermitteln. Bei simultaner Expression von Beat und Side Konstrukten, die ihre jeweilige erste IG Domäne enthalten, überlagern sich die Signale beider Proteine. Vollängen Beat vermag endogenes Side in späten Embryonen in seinem jeweiligen überexprimierten Muster festzuhalten, während Beat Δ IG1 dies nicht bewirkt. Darüber hinaus verhindert eine Deletion der ersten IG Domäne von Side sowie die G187D *missense* Mutation in *side*³⁰⁶ eine Interaktion mit Beat. Da die spezifische Überexpression von Side zur irreversiblen Ausbildung ektopischer neuromuskulärer Endplatten führt, liefert diese Arbeit zudem Hinweise darauf, dass Side auch an der Synaptogenese beteiligt ist.

Frühere *in vitro* Studien deuteten darauf hin, dass Beat die Plasmamembran durchspannt, obwohl es keine klassische Transmembranregion enthält. Diese Annahme wurde durch Rettungsversuche bestätigt, die in dieser Arbeit bestätigt und ausgeweitet wurden, und eine zellautonome Funktion für Beat zeigen: die präsynaptische, jedoch nicht die postsynaptische, Überexpression von Vollängen Beat cDNA rettet den *beat* mutanten Phänotyp. Verschiedene, GFP-markierte Beat Deletions- und Fusionskonstrukte wurden für Aufnahmen im intakten Tier, Western Blot Analysen sowie Oberflächen-Färbungen eingesetzt und stützen das Vorhandensein einer Transmembrandomäne. Zusammenfassend deuten die Daten dieser Arbeit darauf hin, dass Beat und Side *in vivo* über ihre jeweiligen ersten Immunglobulin Domänen interagieren und damit die Basis für die Axon-Substrat Adhäsion bilden.

Table of Contents

ABSTRACT	I
ZUSAMMENFASSUNG	II
TABLE OF CONTENTS	III
1 INTRODUCTION	1
1.1 DROSOPHILA AS MODEL ORGANISM FOR MOTOR AXON GUIDANCE MECHANISMS	1
1.2 EMBRYONIC DEVELOPMENT: NEURONAL DIFFERENTIATION AND MUSCLE DEVELOPMENT ...	2
1.3 THE LARVAL NEUROMUSCULAR SYSTEM	4
1.3.1 <i>Labeling postsynapses with Sh-GFP</i>	6
1.4 MECHANISMS AND GUIDANCE MOLECULES OF AXONAL PATHFINDING	6
1.5 SELECTIVE DEFASCICULATION OF MOTOR AXONS	8
1.5.1 <i>Beaten path Ia</i>	9
1.5.2 <i>Sidestep</i>	10
1.5.3 <i>Side guides motor axons towards their targets in the periphery</i>	11
1.6 THE AXONAL CYTOSKELETON AND THE NAVIGATING GROWTH CONE	13
1.7 TARGET RECOGNITION AND SYNAPTOGENESIS	15
1.8 AIM OF THIS THESIS	17
2 MATERIALS AND METHODS	18
2.1 MATERIAL	18
2.1.1 <i>Equipment, chemicals and reagents</i>	18
2.1.2 <i>Buffers, media and solutions</i>	21
2.1.3 <i>Fly stocks</i>	24
2.1.4 <i>Oligonucleotides</i>	26
2.1.5 <i>Plasmids</i>	32
2.1.6 <i>Antibodies</i>	35
2.1.7 <i>Software</i>	36
2.2 METHODS	37
2.2.1 <i>Fly maintenance</i>	37
2.2.2 <i>Molecular biological methods</i>	40
2.2.3 <i>Microbiological methods</i>	48
2.2.4 <i>Protein biochemical methods</i>	52
2.2.5 <i>Microscopy</i>	57
2.2.6 <i>Contributions</i>	58
3 RESULTS	59
3.1 SIDE AND BEAT MUTANT ALLELES	59
3.1.1 <i>Beat mutant alleles</i>	59
3.1.2 <i>Side mutant alleles</i>	60
3.2 SIDE EXPRESSION DURING EMBRYONIC DEVELOPMENT	63
3.3 SIDE IS CONSTITUTIVELY EXPRESSED IN LARVAE	67
3.4 BEAT EXPRESSION DURING EMBRYOGENESIS.....	69
3.5 SIDE ATTRACTS MOTOR AXONS	72
3.6 OVEREXPRESSION OF SIDE INDUCES SYNAPTOGENESIS.....	74
3.7 SIDE AND BEAT DELETION AND FUSION CONSTRUCTS.....	76
3.8 LARVAL INNERVATION DEFECTS.....	78
3.8.1 <i>Rescue of the beat mutant phenotype</i>	78
3.8.2 <i>Overexpression of Side and Beat induces innervation defects</i>	82
3.9 ANALYSIS OF THE BEAT EXPRESSION PATTERN	89
3.9.1 <i>Presynaptic Beat expression pattern</i>	89
3.9.2 <i>Postsynaptic Beat expression pattern</i>	92
3.10 N- AND C-TERMINAL PART OF BEAT SEGREGATE.....	95
3.11 FULL-LENGTH BEAT IS NOT SECRETED IN VIVO	97

Table of Contents

3.11.1	<i>Surface staining confirms the putative transmembrane domain</i>	98
3.11.2	<i>Degradation of cytosolic GFP verifies the orientation of Beat</i>	101
3.12	INTERACTION OF BEAT AND SIDE IN VIVO	104
3.12.1	<i>Beat and Side interact in simultaneous overexpression</i>	105
3.12.2	<i>BeatnewTM-GFP biochemically interacts with Side-Cherry</i>	109
3.12.3	<i>Overexpression of Beat-GFP traps endogenous Side</i>	110
3.12.4	<i>Interaction of Side and Beat neutralize the attractive effect of Side</i>	114
4	DISCUSSION	119
4.1	MISSENSE MUTATIONS IN SIDE AND BEAT IMPEDE THEIR FUNCTIONALITY	119
4.2	SIDE IS CONSTITUTIVELY EXPRESSED	120
4.3	ENDOGENOUS BEAT EXPRESSION	124
4.4	BEAT IS A TYPE I TRANSMEMBRANE PROTEIN	126
4.4.1	<i>Localization of Beat constructs</i>	126
4.4.2	<i>C- and N-terminus of Beat segregate</i>	128
4.4.3	<i>Orientation of Beat and localization of the transmembrane domain</i>	130
4.5	SIDE ATTRACTS MOTOR AXONS AND INDUCES SYNAPTOGENESIS	131
4.6	BEAT AND SIDE INTERACT VIA THEIR FIRST IG DOMAINS IN VIVO	132
4.6.1	<i>Beat and Side interact in simultaneous overexpression</i>	133
4.6.2	<i>BeatnewTM-GFP biochemically interacts with Side-Cherry</i>	134
4.6.3	<i>Overexpression of Beat-GFP traps endogenous Side</i>	134
4.6.4	<i>Binding of Side to co-overexpressed Beat restores axon guidance</i>	135
4.6.5	<i>Larval innervation defects</i>	136
4.7	CONCLUSION AND OUTLOOK	142
	INDEX OF TABLES	143
	INDEX OF FIGURES	144
	REFERENCES	146
	INDEX OF ABBREVIATIONS	153
	EIDESSTÄTTLICHE ERKLÄRUNG	155
	DANKSAGUNG	156

1 Introduction

The foundation for all later competences like taking up information and reacting by appropriate actions or movements is laid during embryogenesis in all animals. Motor axons need to cover considerable distances in order to connect the brain with their final targets. Analogously, the axons of sensory neurons need to travel long ways from their origin in the periphery to the brain. The navigation of axons occurs in a highly stereotyped manner in both vertebrates and invertebrates and many guidance mechanisms are highly conserved (Araújo and Tear, 2003). The relative simplicity of the segmentally repeated body architecture of embryos and larvae as well as the possibility for precisely targeted genetic manipulations make *Drosophila* one of the favorite model systems to study axon guidance mechanisms (Landgraf and Thor, 2006).

1.1 Drosophila as model organism for motor axon guidance mechanisms

With its bilateral symmetry, *Drosophila* embryos and larvae exhibit a highly stereotypic design of body wall muscles and their innervation pattern. The larval locomotor system is kept together by the translucent, cuticular exoskeleton, which allows for imaging of intact animals. The locomotor system comprises the segmentally repeated set of 30 somatic muscles, which are innervated recurrently by about 35 motoneurons (Landgraf et al., 1997; Van Vactor et al., 1993). These motoneurons project their axons from the cell bodies in the ventral nerve cord to the muscles. In wild-type animals, each muscle is characterized by its shape and position. Analogously, each nerve bundle is defined by its position and synaptic contacts. As every hemisegment is innervated independently, disturbance in axonal guidance can thus be evaluated multiple times in each animal (Hoang and Chiba, 2001).

1.2 Embryonic development: neuronal differentiation and muscle development

The differentiation of neurons begins with the outgrowth of motor axons from the central nervous system (CNS) and the expression of neuron-specific markers at stage 13. The axon of the anterior corner cell (aCC) neuron pioneers the anterior root of the intersegmental nerve (ISN) and is shortly afterwards followed by the axons of the U neurons (Campos-Ortega and Hartenstein, 1997a). After leaving the ventral nerve cord, these pioneer axons probably grow along the segmental transverse branch of the developing trachea and then fasciculate with the first ingrowing sensory axons at stage 14. The posterior root of the ISN is pioneered by the axons of two ventral unpaired median (VUM) neurons and the RP2 neurons, which then fasciculate with the axons of the aCC and U neurons. Later, the axons of the ventral intersegmental neurons (VIN) grow out (Sink and Whittington, 1991) and fasciculate with the aCC and U axons to form the ISN, which innervates the dorsal and dorso-lateral muscles (see Figure 1.1, blue rectangles). The VUM neurons comprise three neurons at the ventral midline, which innervate numerous muscles in the ventral, lateral and dorsal compartment (Campos-Ortega and Hartenstein, 1997a). Their axons bifurcate towards the left and right body half and exit through each of the segmental nerves. Most of the ISN neurons thus project their axons from the anteriorly adjacent hemisegment, except for the RP2 and VUM neurons, which lie within the same neuromere. The axons of the lateral segmental neurons (LSN) together with axons of the VUM neurons form the segmental nerve (SN), which originates from the same hemisegment. The SN is subdivided into the SNa, which innervates the lateral transversal musculature (see Figure 1.1, purple rectangles) and the SNc, which projects to the external ventral muscles (see Figure 1.1, yellow rectangles). The four motoneurons RP1, 3, 4 and 5 were originally identified in the grasshopper embryo (Goodman et al., 1984). Their axons project contralaterally, follow the anterior root of the ISN and then defasciculate at the level of the ventral musculature to pioneer the ISNb and ISNd, which innervate the ventral muscles (see Figure 1.1, dark green and light green rectangles in the background). The two axons of the transverse nerve (TN), which innervate the ventral, transverse muscle (muscle 25, see Figure 1.3) grow out as separate main nerve bundle (Landgraf and Thor, 2006).

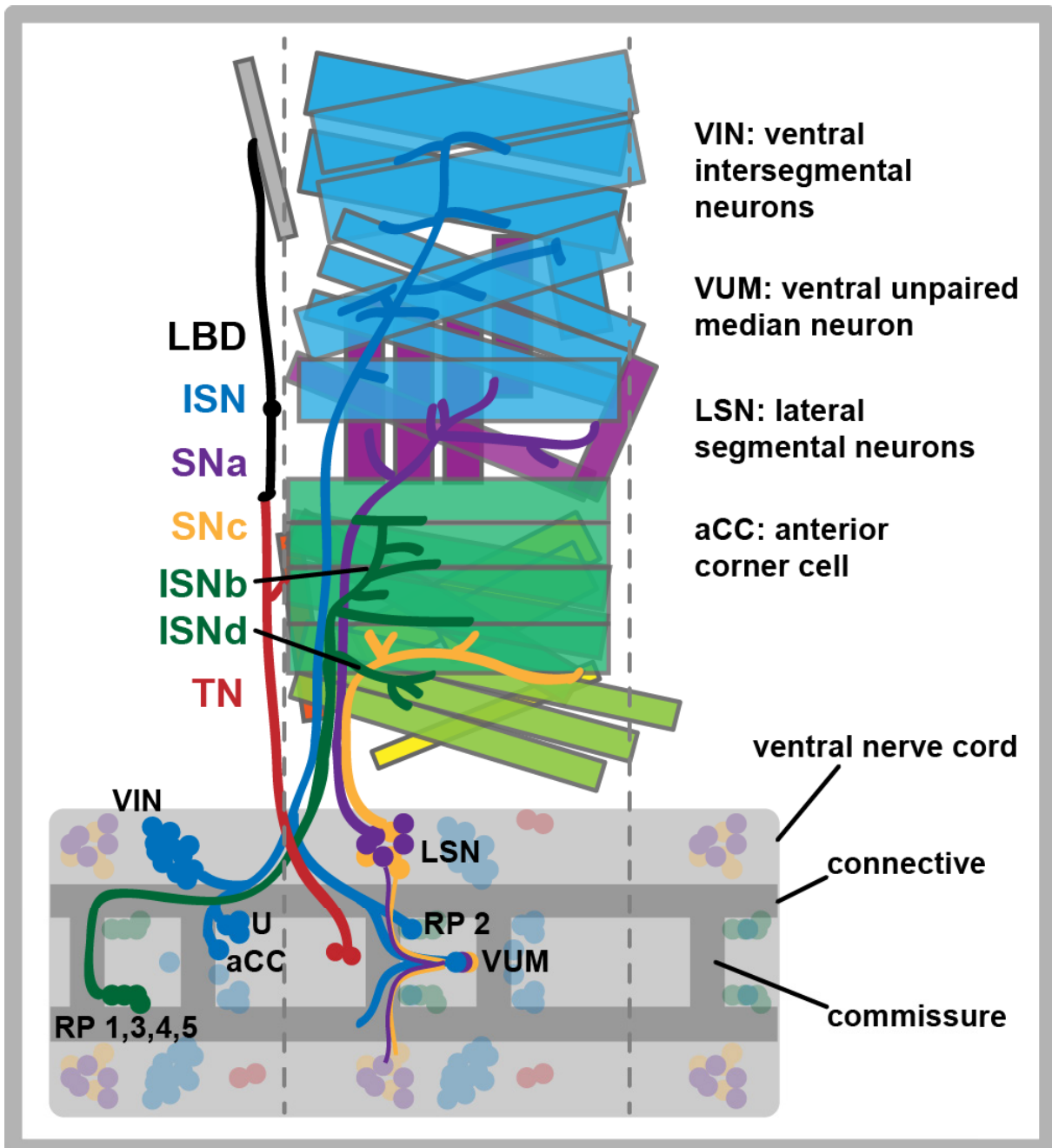


Figure 1.1: Embryonic origin of motor axons.

Schematic diagram of an abdominal hemisegment and the ventral nerve cord of a stage 17 embryo, dorsally viewed from the inside. Motor axons are superimposed on the muscle pattern. The motor neurons originate from the ventral nerve cord (light grey) and grow along the connectives and commissures (dark grey) towards the exit junction of the midline, which is defined as the anastomosis between the intersegmental nerve (ISN) and segmental nerve (SN). Here, the motor axons fasciculate with the pioneer axons and grow into their respective muscle field (muscles = colored rectangles). The RP 1, 3, 4 and 5 neurons are located contralaterally in the anteriorly adjacent neuromere and form the ISNb and ISNd, which innervate the ventral muscle field. The ventral intersegmental neurons (VIN), the U neuron and the anterior corner cell (aCC) neuron also project their axons from the anteriorly adjacent neuromere and form the ISN together with the RP2 and the ventral unpaired median (VUM) neurons. The SNa and the SNc both arise from the lateral segmental neurons (LSN) and from the VUM neurons within the same hemisegment. The transverse nerve (TN) comprises two motor neurons, one innervating muscle 25 and one contacting the lateral bidendritic neuron (LBD), which innervates the alary muscle (grey). Based on models from (Campos-Ortega and Hartenstein, 1997a; Landgraf and Thor, 2006; Landgraf et al., 1997).

Parallel to the outgrowth of motor axons, the formation of the somatic muscles occurs during stages 13 to 15 (Campos-Ortega and Hartenstein, 1997b). Single mesodermal muscle founder cells fuse to naive fusion-competent myoblasts, which then form syncytial cells, the so-called myotubes (Weitkunat and Schnorrer, 2014). These myotubes further grow and are guided towards the tendon attachment sites. After steady attachment in stage 17, the myotubes develop into myofibers and contractile sarcomeres start to form (Weitkunat and Schnorrer, 2014). During this developmental stage, the muscles start to contract. By the end of stage 17, the mature muscular system has developed (see Figure 1.1, colored rectangles). Interestingly, muscle founder cells are important to trigger the defasciculation of outgrowing motor axons into the muscle fields (Landgraf et al., 1999).

1.3 The larval neuromuscular system

The innervation pattern of *Drosophila* larvae is established during embryogenesis. Although the muscle fibers grow enormously from 50 – 500µm from first to third instar larvae, the arrangement and shape of the body wall muscles and motor axons remains constant (de Jossineau et al., 2012; Weitkunat and Schnorrer, 2014). *Drosophila* larvae exhibit bilateral symmetry and comprise three thoracic segments (T1-T3) and eight abdominal segments (A1-A8), as depicted in Figure 1.2.

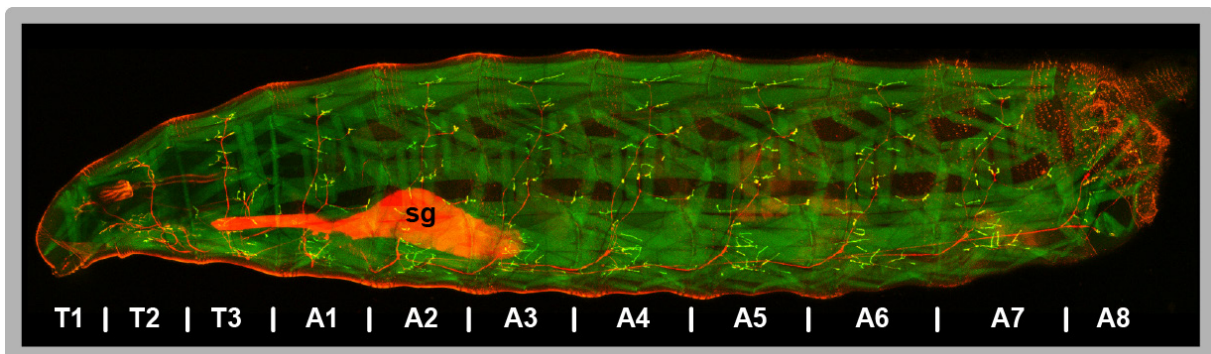


Figure 1.2: Larval neuromuscular system.

Confocal image of a whole-mount third instar larva (OK371 > UAS-DsRed, Sh-GFP). Motoneurons are marked in red and muscles and postsynapses are depicted in green. The larval thoracic segments 1-3 (T1-T3) and abdominal segments 1-8 (A1-A8) are outlined. Salivary glands (sg) also stain in red.

Each hemisegment of A2-A7 exhibits a highly stereotyped pattern of 30 somatic muscles and about 35 innervating motor axons (Bate et al., 1999). The motor axons project from the ventral nerve cord in the larval brain into the periphery in three

principle nerves; the ISN, which innervates the internal muscles, the SN (Bossing et al., 1996; Landgraf et al., 1997; Sink and Whitington, 1991; Van Vactor et al., 1993) and the TN (Landgraf and Thor, 2006).

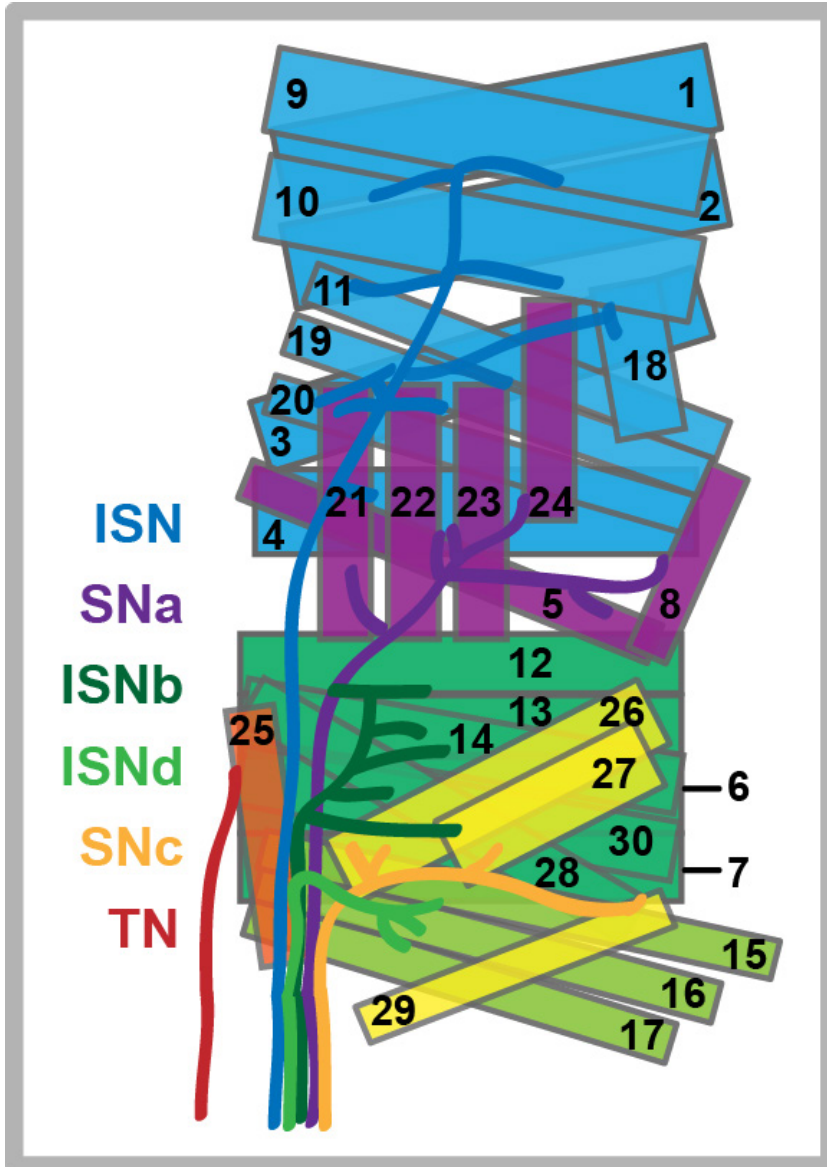


Figure 1.3: Stereotypic innervation pattern of *Drosophila* larval body wall muscles.

Schematic drawing of the repetitive larval pattern of somatic muscles and the approximate branching pattern of the motor axons, viewed from the exterior. Motor axons are superimposed on the muscle pattern. In the abdominal hemisegments A2-A7, the six fascicles ISN, ISNb, ISNd, SNa, SNc and TN innervate the 30 somatic muscles at specific sites in a highly stereotypic manner. Nerve fascicles and the muscles they innervate are depicted in the same color shade. Based on a model from (Beuchle et al., 2007).

The SN and the TN innervate the external body muscles. The intersegmental- and segmental nerves then defasciculate into the five axon bundles ISN, ISNb, ISNd, SNa and SNc (as depicted in Figure 1.3). Each muscle is innervated by one or more motor axons (Bate and Broadie, 1995; Jia et al., 1993). More recent studies showed

that each muscle is innervated only by one motoneuron of a given bouton type, whereas up to four axons of different bouton types can innervate the same muscle (Hoang and Chiba, 2001). A type Ib glutamatergic innervation is present on all muscles. Most muscles receive further innervation from two other motoneurons, which form type Is, type II or type III boutons (Hoang and Chiba, 2001; Landgraf and Thor, 2006).

1.3.1 Labeling postsynapses with Sh-GFP

Zito and colleagues created the useful fusion construct CD8-GFP-Shaker (referred to as Sh-GFP in this work) that enables *in vivo* imaging of the postsynaptic terminals of *Drosophila* neuromuscular junctions (NMJs) (Zito et al., 1999). As muscles only form postsynaptic terminals in the presence of motor axons (Fernandes and Keshishian, 1995), the use of Sh-GFP allows for easy detection of innervation defects in intact larvae. Sh-GFP is under the control of the muscle-specific promoter of *myosin heavy chain* (MHC). The chimeric construct is composed of the extracellular and transmembrane region of the human lymphocyte membrane protein CD8, fused to GFP and coupled with the C-terminal part of the *Drosophila* potassium channel Shaker (Sh). The PDZ-binding domain in the C-terminus of Sh localizes the protein to the postsynapse (Zito et al., 1997). The synaptic localization probably takes place via interaction with Discs large (Dlg), a protein of the Membrane-associated guanylate kinase (MAGUK) family. MAGUK proteins contain multiple PDZ-domains, which enable them to crosslink proteins and link them to the cytoskeleton or to signal-transducing enzymes (Zito et al., 1997). According to the localization of Dlg in type I boutons (Lahey et al., 1994), Sh-GFP labels type Ib and type Is boutons of the NMJ.

1.4 Mechanisms and guidance molecules of axonal pathfinding

During embryonic development of the neuromuscular system, outgrowing motor axons need to navigate over long distances to innervate their final targets. Axons are equipped with a highly perceptible and motile structure at their tip, the growth cone. This sensitive structure is able to percept guidance cues, which can be either repelling or attractive, and transduce them into steering information (Dickson, 2002; Kolodkin and Tessier-Lavigne, 2011). Pioneer axons play an important role as they

locate the correct pathway and make stereotyped contacts with a variety of cell surfaces (Van Vactor et al., 1993). Later outgrowing axons follow and fasciculate with the pioneer axons in a main nerve bundle, as this facilitates the outgrowing. At specific choice points, motor axons defasciculate from the main nerve and grow into the respective muscle fields (Tessier-Lavigne and Goodman, 1996; Van Vactor et al., 1993). If pioneer axons are removed, the guidance of subsequent follower axons is perturbed or delayed. Still, this does not necessarily prevent following axons from locating their appropriate targets (Lin et al., 1995; Raper and Mason, 2010).

Guidance factors can have repellent, attractive or bidirectional functions, depending firstly on the receptor they interact with and secondly on the growth cone they interact with (Colamarino and Tessier-Lavigne, 1995; Raper and Mason, 2010; Raper et al., 1983). The steering information can be mediated over short or long distances, contingent upon the nature of the guidance cue as secreted or membrane-associated molecule (Dickson, 2002). There are four major families of canonical guidance cues, the Netrins, Slits, Semaphorins and Ephrins. Furthermore, certain morphogenes, growth factors and cell adhesion molecules participate in the elaborate process of axonal pathfinding (Kolodkin and Tessier-Lavigne, 2011).

Netrins are bifunctional, secreted molecules (Colamarino and Tessier-Lavigne, 1995), which mediate attraction towards the ventral midline and sometimes also repulsion via receptors of the Deleted in Colorectal Carcinomas (DCC) family (Culotti and Merz, 1998). Netrins send exclusively repulsive signals via members of the Unc5 family of receptors, which sometimes act with DCC as co-receptor (Dickson, 2002; Kolodkin and Tessier-Lavigne, 2011). Slits are large, secreted extracellular matrix molecules, which are expressed by midline glia cells (Rothberg et al., 1988, 1990) and mediate axonal repulsion by interaction with Roundabout (Robo) receptors (Battye et al., 1999; Kidd et al., 1999). Slits thus have an important role in midline guidance and prevent ipsilateral axons from crossing and commissural axons from recrossing the ventral midline (Dickson, 2002). The Semaphorin family comprises secreted and transmembrane molecules, which have repellent and sometimes also attractive function to promote axonal fasciculation and defasciculation (Raper, 2000). They are characterized by a Sema-domain at their N-terminus and act through multimeric receptor complexes including the Plexin family, sometimes with Neuropilins as co-receptor (Dickson, 2002; Kolodkin and Tessier-Lavigne, 2011). Ephrins are bifunctional, cell-surface signaling molecules (Dickson, 2002; Wilkinson

DG, 2001) and probably act exclusively short range. They mediate their regulation on axon guidance and axonal branching via receptor tyrosine kinases of the Eph family (Kolodkin and Tessier-Lavigne, 2011).

The cell adhesion molecules (CAMs) comprise molecules of the immunoglobulin and cadherin superfamily (Kolodkin and Tessier-Lavigne, 2011). Especially Fasciclin II (FasII), a member of the immunoglobulin superfamily and structural homolog of the vertebrate neural cell adhesion molecule NCAM, plays an important role in the selective fasciculation of motor axons (Harrelson and Goodman, 1988; Lin and Goodman, 1994; Lin et al., 1994), as it mediates homophilic binding. In addition to its function during axonal fasciculation, FasII also controls synapse stabilization (Schuster et al., 1996; Zito et al., 1999).

1.5 Selective defasciculation of motor axons

In the periphery, motor axons need to defasciculate from the main nerve bundle in order to immigrate into their target muscle fields and finally establish synaptic connections. Molecules, which control the selective defasciculation of motor axons at specific choice points, comprise the transmembrane protein-tyrosine phosphatase *Drosophila* leukocyte common antigen-related (Dlar), Beaten path Ia (Beat), Sidestep (Side) and the secreted matrix-metalloprotease Tolloid-related (Tlr). Dlar is expressed by a large subset of motoneurons and *dlar* mutant embryos display specific defasciculation defects of the ISNb and ISNd (Desai et al., 1996; Krueger et al., 1996). Outgrowing motoneurons express Beat and *beat* loss of function mutations result in a highly penetrant ISNb defasciculation phenotype (Fambrough and Goodman, 1996; Van Vactor et al., 1993). Side was identified as target-derived transmembrane protein and *side* mutant embryos exhibit severe defasciculation defects, especially of the ISNb, ISNd and SNC, which innervate the ventral muscle field (Sink et al., 2001). Tlr gets secreted from somatic muscles during motor axon pathfinding and mutations in this gene lead to embryonic defasciculation errors, which persist as larval innervation defects (Meyer and Aberle, 2006). Neither the highly related *Drosophila* Tolloid, nor other metalloprotease have so far been associated with similar functions in motor axon defasciculation (Meyer and Aberle, 2006; Nguyen et al., 1994; Serpe et al., 2005).

1.5.1 Beaten path Ia

The function of Beaten path Ia (Beat) in motor axonal pathfinding was discovered in a genetic screen searching for mutations, which perturb neuromuscular connectivity (Van Vactor et al., 1993). *Beat* mutant embryos exhibit highly penetrant ISNb defasciculation defects (Fambrough and Goodman, 1996; Van Vactor et al., 1993). These guidance errors lead to the irreversible formation of NMJs at aberrant positions that persist through all larval stages (Siebert et al., 2009).

Beat is expressed in motor neurons during embryonic development and is enriched in growth cones (Fambrough and Goodman, 1996). The onset of *beat* mRNA expression can be detected at stage 12 in a subset of CNS cells, which are probably early born motoneurons. The number of *beat* expressing cells further increases and the expression level reaches its maximum at stage 13, when motor axons exit the CNS and begin to extend into the periphery. This high expression level persists through stage 14, when the major peripheral motor nerve branches form, and then drops to a lower expression level until stage 17 (Fambrough and Goodman, 1996).

Beat is a small member of the immunoglobulin-superfamily and consists of 427 amino acids. It has two immunoglobulin domains at the N-terminus, an unstructured linker region and a cysteine-rich domain, which contains seven cysteine-residues (Bazan and Goodman, 1997; Pipes et al., 2001).

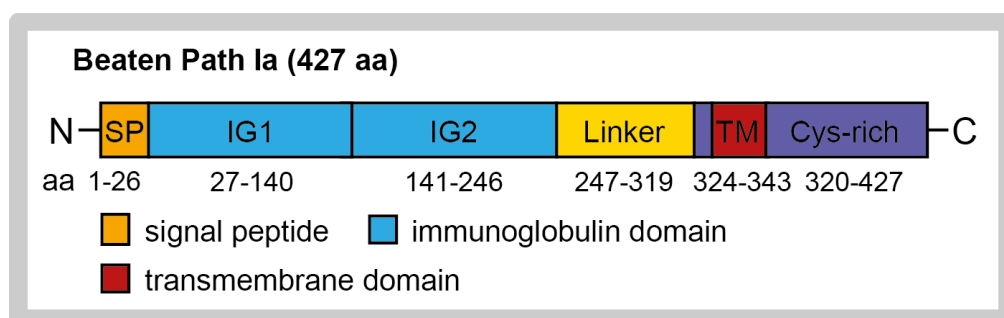


Figure 1.4: Protein structure of Beaten path Ia.

Beat consists of a signal peptide at the N-terminus, which gets cleaved off, followed by two immunoglobulin domains, an unstructured linker region and the cysteine-rich domain, which probably contains a transmembrane domain. N = N-terminus, C = C-terminus.

Based on fuzzy immunohistochemical staining and primary structure predictions, Beat was originally described as secreted anti-adhesive factor, which promotes motor axon defasciculation at choice points (Bazan and Goodman, 1997; Fambrough and Goodman, 1996; Pipes et al., 2001). However, further *in vitro* studies provided biochemical evidence that Beat functions as a membrane-associated receptor or part

of a receptor complex (Siebert et al., 2009). Bioinformatic data of topology prediction algorithms supports the idea of a non-conventional kind of transmembrane region within the cysteine-rich domain at the C-terminal region of Beat (see Figure 1.4).

Pipes and colleagues identified a large protein family of 14 homologous, Beat-like molecules, which all share the presence of two immunoglobulin domains. Eleven of these homologous molecules are located in four different chromosomal clusters, indicating that the expansion of this protein family has been provided in part by gene duplication (Pipes et al., 2001). Full-length cDNAs for *beat Ib*, *beat Ic*, *beat IIa* and *beat VI* have been isolated and the respective protein structures are predicted to be membrane anchored by either a GPI-anchor (in the case of Beat VI) or transmembrane domains. Although many of the *beat*-homologous genes are transcribed in different subsets of CNS neurons, mutations in other *beat* genes lead to much milder guidance phenotypes, indicating redundancy with other genes (Pipes et al., 2001).

1.5.2 Sidestep

The *sidestep* (*side*) gene was identified in two independent genetic screens for axon guidance defects and structural abnormalities of the neuromuscular junction (Aberle et al., 2002; Sink et al., 2001; Van Vactor et al., 1993). *Side* mutant embryos exhibit severe defasciculation defects of the ISNb, ISNd and SNc with motor axons frequently bypassing their ventral target muscle regions (Sink et al., 2001). Further analysis of NMJs in third instar larvae revealed the inability to correct these embryonic guidance defects (Sink et al., 2001). *Side* gain-of-function experiments showed that ectopic expression of *Side* on trachea, hemocytes or muscle precursors causes motor axons to grow abnormally and strongly attracts them to ectopic sites (de Jong et al., 2004; Siebert et al., 2009; Sink et al., 2001). De Jong and colleagues thus postulated an additional role of *Side* in motor axon targeting and synaptogenesis (de Jong et al., 2004).

Side expression follows a highly dynamic spatio-temporal expression pattern during embryogenesis (Kinold, 2016; Siebert et al., 2009; Sink et al., 2001). *Side* can first be detected in stage 10-11 in cells flanking the ventral midline. In early stage 13 embryos, *Side* is expressed in a triangular pattern lateral to the CNS. At stage 14,

ingrowing sensory neurons of the dorsal cluster express Side. From stage 15 to 17, Side expression is detectable on somatic muscles (Sink et al., 2001).

Sidestep belongs to a family of eight closely related proteins, which are all transmembrane proteins of the immunoglobulin superfamily (Aberle, 2009a; Zinn, 2009). Side encodes a protein of 939 amino acids. It contains five immunoglobulin domains, a transmembrane domain and a cytoplasmic tail (see Figure 1.5).

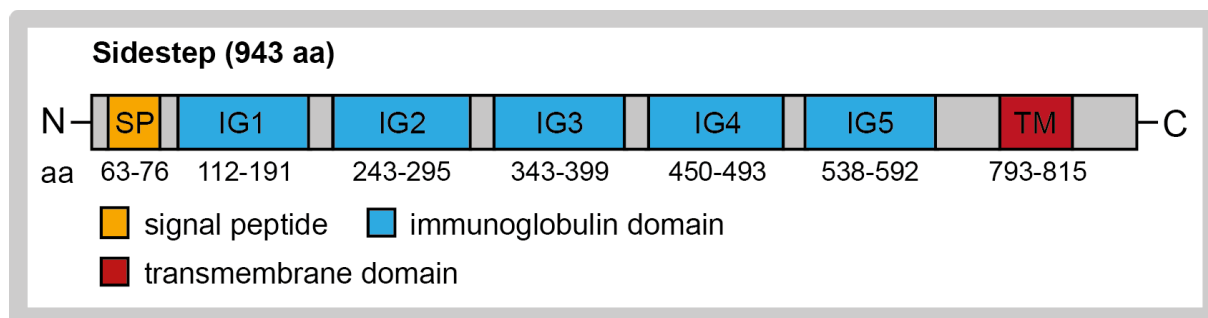


Figure 1.5: Protein structure of Sidestep.

The localization of the Side protein is directed by its N-terminal signal peptide, which gets cleaved off. The Side protein contains five immunoglobulin domains, a transmembrane domain and a short, cytoplasmic tail. N = N-terminus, C = C-terminus.

1.5.3 Side guides motor axons towards their targets in the periphery

The axon guidance phenotypes of *beat* and *side* mutant embryos are highly similar (Fambrough and Goodman, 1996; Sink et al., 2001). These guidance defects persist as innervation defects in *beat* and *side* mutant larvae, which resemble each other strongly. The mentioned similarities and the fact that the defects are not enhanced in *beat* and *side* double mutant larvae (Siebert et al., 2009) indicate a genetic interaction of these molecules. Further experiments showed a consistent association of the motor axon growth cones with Side positive embryonic tissues (Siebert et al., 2009), revealing that outgrowing Beat-expressing motor axons tightly follow a Side-labeled substrate pathway (see Figure 1.6).

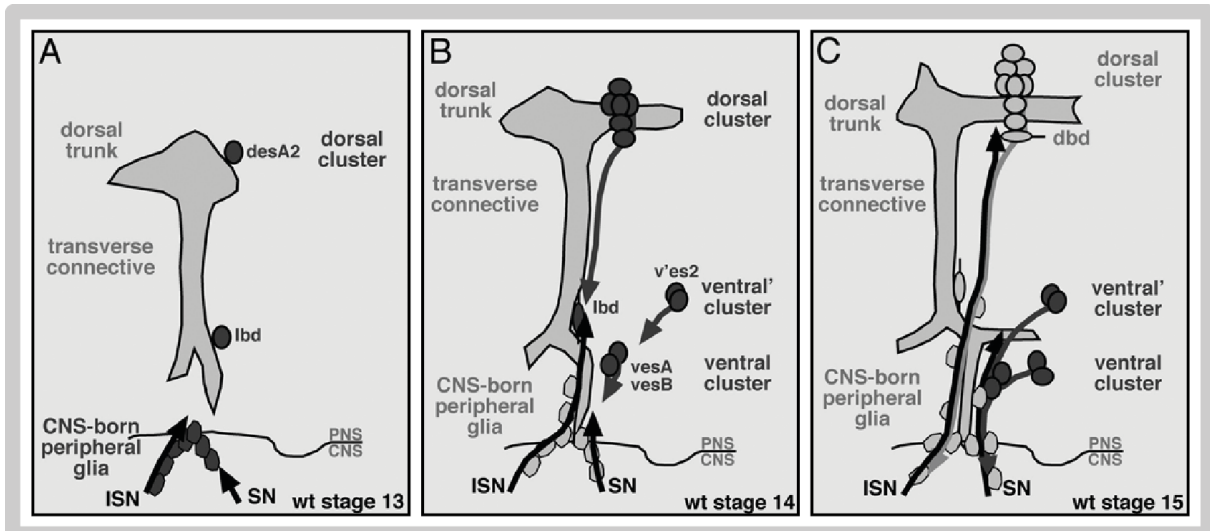


Figure 1.6: Schematic illustration of the dynamic Side expression in spatial relation to the outgrowing motoneurons.

The development of the ISN and SN fascicles is shown. The dorsal trunk and the transverse connective of the trachea are outlined. Motor axons are drawn in black and Side-expressing tissues are depicted in dark grey. A: At stage 13, the pioneer axons of the ISN and SN grow along Side-expressing glia cells towards the exit-junction of the CNS. B: Motor axons of the ISN fasciculate with the ingrowing, Side-expressing sensory axons from the dorsal cluster at the lateral bidendritic neuron (lbd) at developmental stage 14. Around the same time, motor axons of the SN fasciculate with the Side-positive sensory axons of the ventral clusters. C: The motor axons and sensory axons grow oppositely along each other. At the time when the ISN reaches the end of the sensory track, Side is no longer expressed on the dorsal cluster and the motor axons migrate into the muscle fields. Adapted from (Aberle, 2009a).

Biochemical evidence for a direct interaction of Beat and Side was provided by cell aggregation experiments with transiently transfected S2 cells. These studies showed that adhesive aggregates formed only if both Beat-myc and Side-GFP were present in these cells (Siebert et al., 2009).

These data conclude in a model for the navigation of motor axons from the CNS to the final targets by following a Side-labeled pathway (see Figure 1.7), presuming that Beat acts as guidance receptor on the growth cone to percept contact-mediated attraction from intermediate and final targets labeled with Side (Siebert et al., 2009).

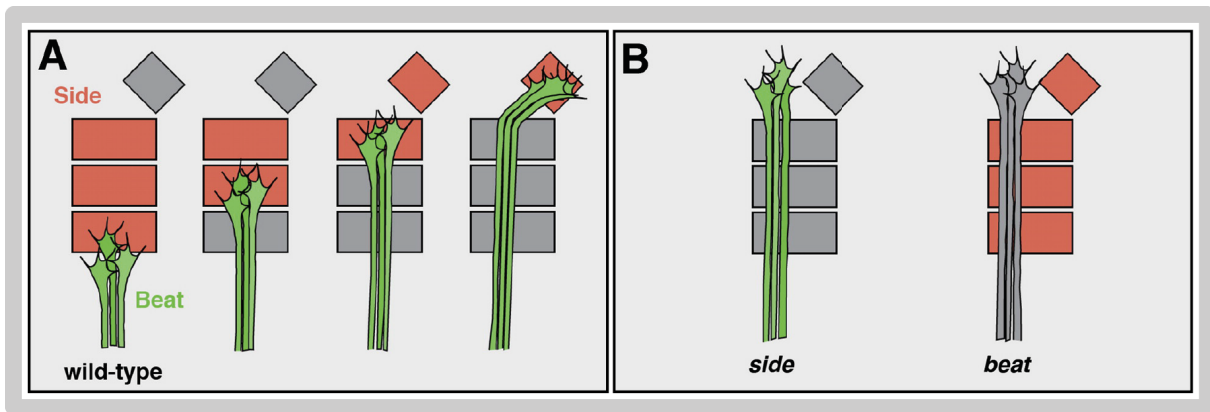


Figure 1.7: Schematic model of Side-expressing tissues guiding Beat-positive motor axons towards their final targets.

Beat-expressing motor axons are labeled in green. Side-expressing tissues are marked in red, Side-negative tissues are grey. A: In wild-type embryos, motor axons recognize and follow the Side-labeled substrate pathway. Contact with the motor axons induces downregulation of Side. B: In *side* mutant embryos, substrates are not labeled and growth cones fail to turn at specific choice points. In *beat* mutant embryos, motor axons do not recognize the Side labeling and thus fail to turn. Side does not get downregulated. Taken from (Siebert et al., 2009).

1.6 The axonal cytoskeleton and the navigating growth cone

The neuronal actin and microtubule cytoskeleton is essential for axon formation, pathfinding and synaptogenesis (Long and Van Vactor, 2013). The bundled microtubules are located in the axon shaft and the center of the growth cone and are required for axon formation and axonal transport (Kevenaar and Hoogenraad, 2015; Kolodkin and Tessier-Lavigne, 2011). Microtubules are polarized polymers, which consist of α - and β -tubulin heterodimers and have a fast-growing plus-end pointing away from the cell body and a minus-end that is more stable (Kevenaar and Hoogenraad, 2015; Long and Van Vactor, 2013). The motility and protrusion of the growth cone is primarily mediated by the actin filaments (Dent et al., 2011; Dickson, 2002). The actin component in the periphery of the growth cone is organized in dense filaments, which radiate into the filopodia, and a loosely interwoven network in between (Lewis and Bridgman, 1992). The so-called F-actin microfilaments are built up by globular actin monomers, which are assembled into long, helical polymers. The fast-growing barbed-end of the F-actin is oriented towards the leading edge at the tip of the filopodia, whereas actin polymers disassemble at the pointed end, providing to the dynamic instability of the actin filaments (Lowery and Van Vactor, 2009). Growth cones constantly protrude and retract their filopodia, scanning the surrounding for positive or negative guidance cues. Attractant and repellent signals are perceived by a multitude of receptors on the surface of the growth cone and transduced in order to

modulate cytoskeletal dynamics and intracellular activity (Long and Van Vactor, 2013). Interestingly, growth cones of individual motor axons can respond differently to the same guidance cues, probably mediated by a unique set of receptors that evaluates the balance between attractive and repellent information. Single microtubules, which extend along the actin filaments into the filopodia, also exhibit high dynamics. Stabilization of a certain filopodial microtubule likely stabilizes directional decisions and thus plays a role in growth cone advance or initiating growth cone turning (Dickson, 2002). Growth cones can also serve as points of attachment to the underlying extracellular matrix (Long and Van Vactor, 2013). This temporary anchorage renders stability for the mechanical forces of axon protrusion and thus promotes axonal elongation into the direction of attachment. The built-up of the axonal cytoskeleton and the different classes of surrounding directional cues are illustrated in Figure 1.8.

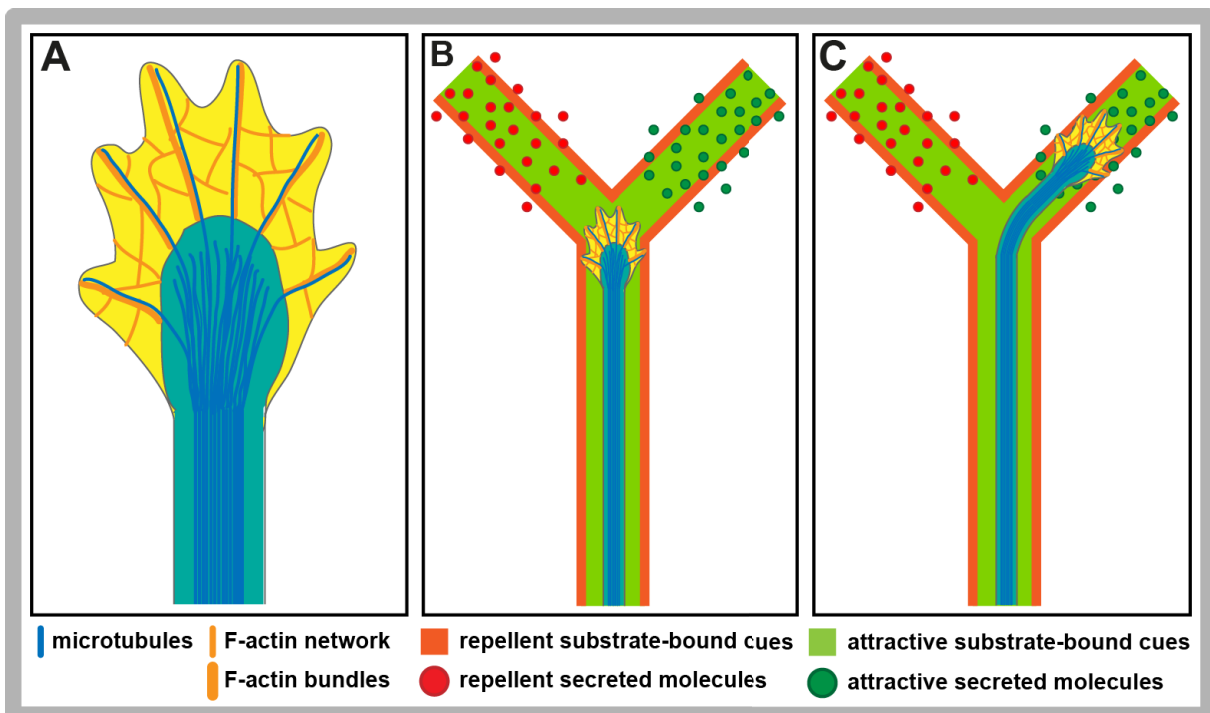


Figure 1.8: Schematic overview of the motor axon cytoskeleton and surrounding guidance cues.

A: Motor axonal microtubule bundles range into the center of the growth cone. In the periphery of the growth cone, F-actin bundles radiate into the filopodia and loose filaments build the intervening F-actin network. Single, highly dynamic microtubules grow along the filopodial actin filaments. The selective stabilization of some of these microtubules induces growth cone advance and turning. B-C: Attractive, adhesive guidance cues build a roadmap for the outgrowing motor axons, whereas repellent, surface-bound molecules prevent the growth cone from migrating off the track. Additionally, secreted positive or negative guidance cues draw growth cones into the correct direction.

1.7 Target recognition and synaptogenesis

Motor axons are precisely guided towards their specific target muscles during embryogenesis. While axon guidance and synaptic target recognition probably share many of the same molecular mechanisms, synaptic targeting must include mechanisms to stop growth cone advance and initiate extensive remodeling of the cytoskeleton (Chiba, 1999; Chiba and Keshishian, 1996; Goodman, 1996). Target recognition involves cellular recognition mechanisms between the growth cone and the muscle fiber, mostly via homophilic cell-adhesion molecules (Chiba et al., 1993; Fernandes and Keshishian, 1995; Jin, 2002). The highly dynamic axonal filopodia as well as muscular motile processes, the so-called myopodia, contribute to the process of pre- and postsynaptic pairing (Featherstone and Broadie, 2000; Goodman, 1996; Ritzenthaler et al., 2000). Several adhesion molecules are expressed by synaptic partners, such as Fasciclin III (Halpern et al., 1991) and Connectin (Nose et al., 1992). The misexpression of synaptogenic molecules in inappropriate partners promotes ectopic formation of synapses (Jin, 2002).

Upon contact of matching partners, synapse formation is initiated during late embryonic development and the motile growth cone is converted into a stable and highly differentiated presynaptic terminal. Both the growth cone and muscle fiber undergo synaptic differentiation (Fernandes and Keshishian, 1995). The axonal growth cone experiences rapid growth and varicosities form in the axonal processes. Directly after the contact between pre- and postsynaptic partners is established, the immature presynaptic terminal releases glutamate and in response, glutamate receptors begin clustering in the postsynaptic area (Featherstone and Broadie, 2000; Marqués, 2005). In contrast to the formation of the muscle fibers, which occurs independently of innervation (Broadie and Bate, 1993a), the molecular and functional specialization of the postsynaptic area is only initiated in the presence of a neuron (Fernandes and Keshishian, 1995). Furthermore, the postsynaptic maturation in *Drosophila* depends upon neuronal excitation (Broadie and Bate, 1993b).

Mature synaptic terminals are classified into different synaptic bouton types (Hoang and Chiba, 2001; Johansen et al., 1989). Firstly, type Ib with relatively large, glutamatergic boutons, which are found on all larval, somatic muscles (Gorczyca et al., 1993). Type Ib boutons cluster in short and minimally branching nerve terminals. Secondly, the medium-sized, glutamatergic type Is boutons, with generally longer and more elaborate terminals bearing them than those in type Ib (Atwood et al.,

1993; Hoang and Chiba, 2001). Thirdly, type II boutons, which have a small diameter and are spread in very long terminals (Johansen et al., 1989). Their neurotransmitters are probably glutamate and octopamine. Fourthly, the medium-sized type III boutons, which contain glutamate and insulin (Gorczyca et al., 1993), a putative neural co-transmitter, and cluster in medium-length terminals. One muscle can be innervated by up to four motor axons, if the synaptic terminals bear boutons of different classes (Hoang and Chiba, 2001).

1.8 Aim of this thesis

Accurate guidance mechanisms build the basis to establish a functional locomotor system. Growth cones steer the outgrowing motor axons along the developing embryonic tissues and precisely encounter and innervate their correct partner muscles. Side was identified as target-derived, attractive guidance molecule in *Drosophila*. It functions in motor axon pathfinding, target recognition and synaptogenesis. Since further studies recognized the genetic connection between Side and Beat within the same pathway and found *in vitro* evidence for the direct interaction of these proteins, this work now aims to elucidate the mechanisms how Beat and Side function and interact in the living animal.

As *side* and *beat* were identified in EMS mutagenesis screens, chances are good to find missense mutations in these alleles, which can give valuable hints about functionally important domains. All available *beat* and *side* mutant alleles shall thus be analyzed by sequencing. *Side* mutant animals will further be tested for immunodetection in histological stainings as well as western blot analysis in order to obtain information about possible truncations of the mutant Side proteins. Since there is currently no specific antibody for the detection of endogenous Beat available, two different anti-Beat antisera are to be generated and shall enable the visualization of Beat expression. Beat was originally characterized as secreted molecule, yet more recent studies provided bioinformatic evidence as well as *in vitro* support that Beat is associated with the plasma membrane and thus may act as receptor on motor axons. This work further aims to confirm the localization of Beat in the plasma membrane by several analyses taking advantage of the different, fluorescently labeled Beat constructs, and the exact location of the predicted transmembrane domain is to be verified. In order to enable structure-function analyses *in vivo*, various Beat and Side deletion and fusion constructs, tagged with GFP and Cherry, respectively, shall be generated and integrated into flies. The interaction domain of Beat and Side shall be characterized in the living animal, using overexpression experiments as well as co-immunoprecipitation with the GFP-tagged Beat constructs and Cherry-tagged Side constructs. These *in vivo* studies aim to help further understanding of the functionally important structures of Beat and Side and the mechanisms of interaction during axon guidance.

2 Materials and Methods

2.1 Material

2.1.1 Equipment, chemicals and reagents

Additionally to the standard lab equipment, the following devices were employed:

Table 2.1: Equipment

Equipment	Manufacturer
Microscopes	
Axio Imager M2	Carl Zeiss MicroImaging GmbH, Jena
Confocal Laser-Scanning-Microscope 710	Carl Zeiss MicroImaging GmbH, Jena
Stereo-microscope Stemi 2000	Carl Zeiss MicroImaging GmbH, Jena
Microinjection	
Glass capillaries with filament (0.69 x 1.2 x 100mm)	Science Products GmbH, Hofheim
Microinjector FemtoJet express	Eppendorf, Hamburg
Micromanipulator PatchMan NP2	Eppendorf, Hamburg
Dissection	
Austerlitz Insect pins Minutiens (x 0.1 mm, stainless steel)	Fine Science Tools GmbH, Heidelberg
Forceps (Dumont, #5)	Fine Science Tools, Heidelberg
Sylgard dissection plates	Roland Vetter Laborbedarf OHG, Ammerbuch
Vannas Spring Scissors straight, 4mm cutting edge	Fine Science Tools, Heidelberg

Table 2.2: Chemicals and solvents

Chemical	Manufacturer
Acetic acid (C ₂ H ₄ O ₂)	Sigma Aldrich Chemicals GmbH, Steinheim
Acrylamide (Rotiphorese Gel 30, 37.5:1)	Carl Roth GmbH & Co. KG, Karlsruhe
Agar	BD (Becton, Dickinson), Sparks, USA
Agarose low EEO	AppliChem GmbH, Darmstadt
6-Aminohexanoic acid (ϵ -Aminocaproic acid)	Carl Roth GmbH & Co. KG, Karlsruhe
Ammonium peroxodisulphate (NH ₄) ₂ S ₂ O ₈ (APS)	Carl Roth GmbH & Co. KG, Karlsruhe

Materials and Methods

Chemical	Manufacturer
Ampicillin	AppliChem GmbH, Darmstadt
Agar	Carl Roth GmbH & Co. KG, Karlsruhe
Bromphenol blue sodium salt	Carl Roth GmbH & Co. KG, Karlsruhe
Chloramphenicol	AppliChem GmbH, Darmstadt
Chlorix (2,8 g/l Sodium hypochloride)	Colgate-Palmolive, Hamburg
Corn grits	Küper, Oberhausen
DAPI	Sigma Aldrich Chemic GmbH, Steinheim
Disodium hydrogen phosphate (Na ₂ HPO ₄)	Grüssig GmbH, Filsum
1,4-Dithiothreit (DTT) (C ₄ H ₁₀ O ₂ S ₂)	Carl Roth GmbH & Co. KG, Karlsruhe
Ethanol absolute	VWR International, Gelenaakbaakn, Belgium
Ethylenediaminetetraacetic acid (EDTA)	Carl Roth GmbH & Co. KG, Karlsruhe
Ficoll 400	Sigma Aldrich Chemic GmbH, Steinheim
Formaldehyde 37%	AppliChem GmbH, Darmstadt
Glycerol	Carl Roth GmbH & Co. KG, Karlsruhe
Glycine	Carl Roth GmbH & Co. KG, Karlsruhe
Heptane	VWR International, Gelenaakbaakn, Belgium
Hydrochloric Acid (HCl) 1N	VWR International, Gelenaakbaakn, Belgium
Injection oil Voltalef 3S	VWR International GmbH, Darmstadt
Injection oil Voltalef 10S	VWR International GmbH, Darmstadt
Kanamycine	AppliChem GmbH, Darmstadt
Malt extract	Aromatic Marketing GmbH, Berlin
Methanol	VWR International BVBA, Gelenaakbaakn, Belgium
Nipagin	Merck, Darmstadt
Normal Donkey Serum (NDS)	Jackson Immunoresearch (USA)
Normal Goat Serum (NGS)	Jackson Immunoresearch (USA)
Nonidet P-40	AppliChem GmbH, Darmstadt
Phenol red	Carl Roth GmbH & Co. KG, Karlsruhe
Potassium Acetate	Carl Roth GmbH & Co. KG, Karlsruhe
Potassium Chloride (KCl)	AppliChem GmbH, Darmstadt
Potassium Dihydrogenphosphate (KH ₂ PO ₄)	AppliChem GmbH, Darmstadt
Powdered milk	Carl Roth GmbH & Co. KG, Karlsruhe

Chemical	Manufacturer
Propionic acid	Sigma Aldrich Chemic GmbH, Steinheim
Sodium Chloride (NaCl)	VWR International BVBA, Gelenaakbaakn, Belgium
Sodium dodecyl sulfate (SDS), ultra pure	Carl Roth GmbH & Co. KG, Karlsruhe
Sodium dihydrogen phosphate (NaH ₂ PO ₄)	Grüssig GmbH, Filsum
di-Sodium hydrogen phosphate (Na ₂ HPO ₄)	Grüssig GmbH, Filsum
Sodium hydroxide - pellets (NaOH)	AppliChem GmbH, Darmstadt
Soy flour	Heirler Cenovis GmbH, Radolfzell
Treacle	Grafschafter Krautfabrik, Meckenheim
TEMED	Carl Roth GmbH & Co. KG, Karlsruhe
Tris- (hydroxymethyl)- aminomethane bufferan	Carl Roth GmbH & Co. KG, Karlsruhe
TRIS blotting-grade	Carl Roth GmbH & Co. KG, Karlsruhe
TRIS-hypochloride	Carl Roth GmbH & Co. KG, Karlsruhe
Tryptone	BD (Becton, Dickinson and Company), Sparks, USA
TritonX-100	Carl Roth GmbH & Co. KG, Karlsruhe
Yeast extract	BD (Becton, Dickinson and Company), Sparks, USA
Yeast powder	Heirler Cenovis GmbH, Radolfzell

Table 2.3: Kits and reagents

Kit or reagent	Manufacturer
BP Clonase Enzyme Mix and Reagents	Invitrogen, Eugene (USA)
Clarity™ Western ECL Substrate Peroxide solution	Bio-Rad Laboratories Inc., Hercules, USA
Clarity™ Western ECL Substrate Luminol/enhancer solution	Bio-Rad Laboratories Inc., Hercules, USA
Complete protease inhibitor cocktail	Roche Diagnostics GmbH, Mannheim
DNeasy Blood & Tissue Kit	QIAGEN, Hilden
dNTPs (dATP, dTTP, dGTP, dCTP)	Fermentas GmbH, St. Leon-Rot
Gene Ruler 1kb DNA-Ladder	Fermentas GmbH, St. Leon-Rot
High Pure Plasmid Isolation Kit	Roche Diagnostics GmbH, Mannheim
Immun-Blot PVDF Membrane, 0.2µm	Bio-Rad Laboratories Inc., Hercules, USA
pENTR/D-TOPO Cloning Kit	Invitrogen, Eugene (USA)
Phenol-Chloroform-Isoamyl alcohol	Carl Roth GmnH & Co. KG, Karlsruhe

PageRuler Prestained Protein Ladder	Thermo Fisher Scientific, Schwerte
Oligo d(T) 18 mRNA Primer	New England BioLabs, Frankfurt am Main
Q5 High-Fidelity DNA Polymerase	New England BioLabs GmbH
QIAquick gel extraction kit	QIAGEN GmbH, Hilden
QIAquick PCR Purification Kit	QIAGEN GmbH, Hilden
RNase Inhibitor, Murine (M0314S)	New England BioLabs, Frankfurt am Main
SYBR Safe DNA Gel Stain	Invitrogen, Darmstadt
ToTALLY RNA Kit	Ambion
SuperScript™ III Reverse Transcriptase	Invitrogen
Whatman™ Chromatography paper 3mm Chr	GE Healthcare GmbH, Solingen

All restriction enzymes were purchased from Fermentas GmbH, St. Leon-Rot. The following enzymes were used in this work with the respective buffers: EcoRI, EcoRV, KpnI, NcoI, NheI, NotI, SacI, Sall, XbaI and XhoI.

2.1.2 Buffers, media and solutions

If not declared else, all buffers, media and solutions are solved in millipore water.

Table 2.4: Buffers

Buffer	Composition
Germline transformation	
10x Injection buffer	1mM Sodium phosphate, pH 6.8 50mM KCl sterile-filter through 0.22µm millipore filter
Phenol red	2% (w/v)
Agarose gel electrophoresis	
50x TAE buffer	2M Tris-base 0.05M EDTA pH 8.2
1% Agarose gel	1% (w/v) Agarose in 1x TAE buffer, boil, cool down to 50°C, add SYBR Safe (3µl per 100ml of gel)
6x DNA loading buffer	0.25% (w/v) Bromophenol blue 15% (w/v) Ficoll in 1x TAE Store at 4°C

Materials and Methods

Buffer	Composition
Plasmid isolation	
Resuspension buffer (buffer 1)	50mM Tris-HCl, pH 8 10mM EDTA 100µg/ml RNase A, store at 4°C
Lysis buffer (buffer 2)	200mM NaOH 1% (w/v) SDS
Neutralization buffer (buffer 3)	3M potassium acetate pH 5.5 with acetic acid
TE Buffer	10mM Tris/HCl, pH 7.6 1mM EDTA, pH 8.0
Immunohistochemistry	
10x PBS	1.37M NaCl 27mM KCl 100mM Na ₂ HPO ₄ 20mM KH ₂ PO ₄ pH 7.4
PTX	0.1% Triton X-100 in 1x PBS
PTX + 5% NGS	5% (v/v) normal goat serum in PTX, store at 4°C
70% Glycerol	70% (v/v) Glycerol in PBS
Co-immunoprecipitation	
Washing buffer	50mM Tris/HCl, pH 7.5 150mM NaCl 1% Nonidet P-40
Lysis buffer	10ml Washing buffer + 1 tablet complete protease inhibitor cocktail (Roche)
Binding buffer	50mM Tris/HCl, pH 7.0
SDS-PAGE	
Running buffer	25mM Tris, pH 8.3 192mM Glycine 0.1% (w/v) SDS
2x Sample buffer	62.5mM Tris/HCl, pH 6.8 10mM DTT 2% (w/v) SDS 10% (v/v) Glycerol 0.02% Bromophenol blue
8% Separating gel (24 ml → 4 gels)	11.1ml millipore H ₂ O 6.4ml 30% Acrylamide 6ml 1.5M Tris, pH 8.8 240µl 10% SDS 240µl 10% APS 24µl TEMED

Materials and Methods

Buffer	Composition
10% Separating gel (24 ml → 4 gels)	9.5ml millipore H ₂ O 8ml 30% Acrylamide 6ml 1.5M Tris, pH 8.8 240µl 10% SDS 240µl 10% APS 24µl TEMED
4% Stacking gel (10 ml → 4 gels)	5.9ml millipore H ₂ O 1.3ml 30% Acrylamide 2.5ml 0.5M Tris pH 6.8 100µl 10% SDS 100µl 10% APS 10µl TEMED
Western blot	
Anode buffer I (ABI)	300mM Tris, pH 9.4
Anode buffer II (ABII)	30mM Tris, pH 9.4
Kathode buffer (KB)	30mM Tris, pH 9.4 40mM ε-Aminocaproic acid 0.1% (w/v) SDS
10x TBS	0.1M Tris-HCl, pH 7.4 1.5M NaCl
10x TBST	0.1M Tris-HCl, pH 7.4 1.5M NaCl 1% (v/v) Tween-20
Blocking solution	5% (w/v) powdered milk in TBST

Table 2.5: Media and solutions

Media and solutions	Composition
Fly breeding	
Standard <i>Drosophila</i> medium	10l Demineralized water 50g Agar 168g Yeast powder 450g Malt extract 95g Soy flour 712g Corn grits 400g Treacle cook 25 min, cool to ~ 65°C, then add 45ml Propionic acid 15g Nipagin
Apple juice agar	3l Demineralized water 1l Apple juice (clear) 100g Sucrose 70g Agar

Media and solutions	Composition
Microbiological media and solutions	
LB medium	10g NaCl 10g Tryptone 5g Yeast extract ad 1l millipore H ₂ O pH 7.0, autoclave, add antibiotics
LB agar	10g NaCl 10g Tryptone 5g Yeast extract 20g Agar ad 1l H ₂ O pH 7.0 autoclave, cool to ~ 50°C, add desired antibiotics, cast petri dishes
Ampicillin stock solution	50mg/ml ampicillin in millipore H ₂ O, store at -20°C
Chloramphenicol stock solution	34mg/ml chloramphenicol in Ethanol, store at -20°C
Kanamycin stock solution	50mg/ml kanamycin in millipore H ₂ O, store at -20°C

2.1.3 Fly stocks

Table 2.6: Fly stocks

Fly stock	Source
General stocks	
w ¹¹¹⁸ (w ⁻)	AG Aberle, stock collection
w ⁻ ; CD8-GFP-Sh, 1A	(Zito et al., 1999)
w ⁻ ; CD8-GFP-Sh, 7A	(Zito et al., 1999)
y ⁻ w ⁻ , M(3xP3-EGFP, vas-Int) ZH2A;; ZH(3xP3-RFP, attP) 51C	(Bischof et al., 2007)
y ⁻ w ⁻ , M(3xP3-EGFP, vas-Int) ZH2A;; ZH(3xP3-RFP, attP) 86Fa	(Bischof et al., 2007)
y ⁻ w ⁻ , M(3xP3-EGFP, vas-Int) ZH2A;; ZH(3xP3-RFP, attP) 86Fb	(Bischof et al., 2007)
w ⁻ ; $\frac{IF}{CyO,act-GFP}$	AG Aberle, stock collection
w ⁻ ; $\frac{Dr}{TM6C,Sb,Tb,e}$	AG Aberle, stock collection
FasII-GFP ^{Mue397}	(Rasse et al., 2005)
y,w; Side ^{MI00149-GFSTF.1} (Side-GFP exon trap)	(Nagarkar-Jaiswal et al., 2015)
Mutant stocks	
w ⁻ ; $\frac{side^{C137}, 7A}{TM3,Sb,Ser,tw-GFP}$	(Aberle et al., 2002)

Fly stock	Source
$W^{-}; \frac{side^{I1563}, 7A}{TM3,Sb,Ser,tw-GFP}$	(Aberle et al., 2002)
$W^{-}; \frac{side^{I306}, 7A}{TM3,Sb,Ser,tw-GFP}$	H. Aberle, unpublished
$W^{-}; \frac{side^{K717}, 7A}{TM3,Sb,Ser,tw-GFP}$	H. Aberle, unpublished
$W^{-}; \frac{side^{D609}}{TM3,Sb,Ser,tw-GFP}$	H. Aberle, unpublished
$W^{-}; \frac{side^{H143}, 7A}{TM3,Sb,Ser,tw-GFP}$	(Sink et al., 2001)
$W^{-}; \frac{beat^{C163}, 1A}{CyO,tw-GFP}$	(Fambrough and Goodman, 1996)
$W^{-}; \frac{beat^2, 1A}{CyO,tw-GFP}$	(Fambrough and Goodman, 1996)
$W^{-}; \frac{beat^3, 1A}{CyO,tw-GFP}$	(Fambrough and Goodman, 1996)
Gal4-driver lines	
$w^{-}, FasII-Gal4^{Mz507}$	gift from B. Altenheim, Mainz
$w^{-}; OK371-Gal4$	(Mahr and Aberle, 2006)
$w^{-}; mef2-Gal4$	gift from C.S. Goodman
$w^{-}; elav-Gal4$	gift from C.S. Goodman
$w^{-}; nSyb-Gal4$	AG Aberle, stock collection
$w^{-}; 5053-Gal4$	(Lopez, 1998)
UAS-effector lines	
$y^{-}w^{-}; UAS-mCD8-GFP$	(Lee and Luo, 1999)
$w^{-}; UAS-NrxIV^{secreted}-GFP$	gift from T. Stork, C. Klämbt, Münster
$w^{-}; UAS-NSlmb-vhhGFP4$	gift from M. Affolter, M. Müller, Basel (Caussinus et al., 2011)
$w^{-}; UAS-Side^{29A}$	(Sink et al., 2001)
$w^{-}; UAS-Side-Cherry (\Phi 51C)$	A. Bauke, master thesis
$w^{-}; UAS-GFP-Side-Cherry (\Phi 86Fb)$	C. Heymann, this work
$w^{-}; UAS-Side\Delta IG1-Cherry (\Phi 51C)$	C. Heymann, this work
$w^{-}; UAS-SideIG1-5-Cherry (\Phi 51C)$	C. Heymann, this work (together with V. del Olmo-Toledo)
$w^{-}; UAS-SideIG1-CD8-Linker-TM-Cherry (\Phi 51C)$	C. Heymann, this work
$w^{-}; UAS-SideIG1-CD8-CD8-Cherry (\Phi 51C)$	C. Heymann, this work (together with V. del Olmo-Toledo)
$w^{-}; UAS-SideIG1-FasII-Cherry (\Phi 51C)$	C. Heymann, this work (together with V. del Olmo-Toledo)
$w^{-}; UAS-Beat^5$	(Fambrough and Goodman, 1996)

Fly stock	Source
w ⁻ ; UAS-Beat-GFP (random)	A. Bauke, master thesis
w ⁻ ; UAS-SP-GFP-Beat-Cherry (Φ 86Fb)	C. Heymann, this work
w ⁻ ; UAS-Beat_1-395-GFP (Φ 86Fb)	C. Heymann, this work (together with V. Kühlmann)
w ⁻ ; UAS-Beat_1-361-GFP (Φ 86Fa)	C. Heymann, this work (together with V. Kühlmann)
w ⁻ ; UAS-Beat_1-345-GFP (Φ 68E)	A. Bauke, master thesis
w ⁻ ; UAS-Beat_1-322-GFP (Φ 68E)	A. Bauke, master thesis
w ⁻ ; UAS-Beat_1-254-GFP (Φ 86Fb)	C. Heymann, this work
w ⁻ ; UAS-BeatΔIG1-GFP (Φ 86Fb)	C. Heymann, this work
w ⁻ ; UAS-Beat-Cys-GFP (Φ 86Fb)	C. Heymann, this work (together with V. del Olmo-Toledo)
w ⁻ ; UAS-BeatnewTM-GFP (Φ 86Fb)	C. Heymann, this work
w ⁻ ; UAS-BeatΔTM-GFP (Φ 86Fb)	C. Heymann, this work
w ⁻ ; UAS-Beat_29-427-GFP (Φ 86Fb)	C. Heymann, this work
w ⁻ ; UAS-Beat_29-322-GFP (Φ 86Fb)	C. Heymann, this work

2.1.4 Oligonucleotides

Table 2.7: Oligonucleotides

Primer designation	Sequence (5' → 3')	Product size
beat sequencing primers (adopted from A. Bauke, Münster)		
BeatEx1F	GGTTGGGTCTTAAGGCGTCAAATG	460 bp
BeatEx1R	CCATCAGGAGAGCATTGTTCTGTG	
BeatEx2F	CGCCTCCGGATGATTTCTATTAG	414 bp
BeatEx2R	GAAGTGCGATTTGCTTATGTTG	
BeatEx3F	CATCTGGCCAACAAGAACGATATG	333 bp
BeatEx3R	CCCCCATCGACAATATAAGCGG	
BeatEx4F	CGATCCGGTTTACCTTTGAACTG	381 bp
BeatEx4R	CCCCTCTCACACCCATTGAAAAG	
BeatEx5F	GAGCCCAGAAACCCAATAAGCC	421 bp
BeatEx5R	GGCACCGTTTCCGTGTTTTGG	
BeatEx6F	GTGGTCACCGATCAACACTTTG	481 bp
BeatEx6R	CCTCCATCTAACTGCAGACGAAC	

Materials and Methods

Primer designation	Sequence (5' → 3')	Product size
BeatEx7F	TGGAGGAAGTTCCAGAATACATCG	559 bp
BeatEx7R	CTGGCGAATGGCACTGGAGTTG	
side sequencing primers (adopted from H. Aberle)		
Side_Ex1F	TTTGCCACATAAATGACGAGAC	411 bp
Side_Ex1R	GCTGTTATTGTTATTGCGAGTA	
Side_Ex3F	TTTCAGGAGTTTCTTCAAGTGC	369 bp
Side_Ex3R	CGTAAGGTGTAGCAAAGGATG	
Side_Ex4,5F	GCCCCCTCACTTACACTTGTAC	506 bp
Side_Ex4,5R	CTAATGAAAAGCTGCCTGACAG	
Side_Ex6,7F	AAGGATACTCCACACAACCTGC	723 bp
Side_Ex6,7R	CCATGCTCCATAAAATAGTCAG	
Side_Ex8F	CAACGTATCCTTTAGCTAATAC	249 bp
Side_Ex8R	GCAGTCTACCAGTTCACCTGTC	
Side_Ex9F	GCCATTGCCGTTTATTATTTTG	303 bp
Side_Ex9R	GAGTGGTAGTGCTGAATGGAGT	
Side_Ex10F	GCAACTTGTTCCTCCCAATAAATG	289 bp
Side_Ex10R	TACCCAGCAACCAACCATATAG	
Side_Ex11F	ATATTTATGAAGCTCCCGATTC	308 bp
Side_Ex11R	GGGGTTAGACAAAACGATAGCT	
Side_Ex12F	TGATTTCAATTCGATTTGGTTC	394 bp
Side_Ex12R	ATGCCGACACCAGTACTGTTTA	
Side_Ex13F	CCCCAGCTTGTCTATGACTATG	418 bp
Side_Ex13R	CCGAACCGTGAGTAAATTTTAA	
Side_Ex14F	TATAAATGCGCCTCTTGTCATG	355 bp
Side_Ex14R	GTGGAAAACAGGACAGAAGAC	
Side_Ex15F	ACGTTTAGTGCCTAACTTTTGG	392 bp
Side_Ex15R	GATGTGGATGTGAATGTGAAGA	
Side_Ex16F	CATGCCATTTATTGTATTTTTC	410 bp
Side_Ex16R	GGGATTGATAAATTGATGACTA	
Side_Ex17F	TATGCCATTGTTGTTGATTTTG	175 bp
Side_Ex17R	GTGTGTGTGTGTGTCTATGTGT	

Table 2.8: Oligonucleotides used for OE-PCR and subsequent Topo-cloning of Beat constructs

Fragment	Template DNA	Primer designation	Sequence (5' → 3')	Product size
SP-GFP-Beat				
Beat SP	pENTR_Beat+Stop	Beatla-712F	CACCATGCGGTTTCCACA GAAT	105 bp
		BeatSP_GFP_R	CTCGCCCTTGCTCACCAT ACCGCTTCCAGCTGCGGT CATCTCTAATG	
GFP	pUASTattB_rfA_eGFP	BeatSP_GFP_F	CATTAGAGATGACCGCAG CTGGAAGCGGTATGGTG AGCAAGGGCGAG	765 bp
		GFP_Beat_R	GAACCCGGACATCCCGTA ACTTGTACAGCTCGTCCA TG	
Beat_1-427	pENTR_Beat+Stop	GFP_Beat_F	CATGGACGAGCTGTACAA GTTACGGGATGTCCGGG TTC	1222 bp
		BeatC_R	TGTTAATTGCCTGATACAT CTGC	
Beat_1-395				
Beat_1-395	pENTR_Beat+Stop	Beatla-712F	CACCATGCGGTTTCCACA GAAT	1189 bp
		Beat1a_1876R	GGAAGTTGCGATGCTCCTG CTG	
Beat_1-361				
Beat_1-361	pENTR_Beat+Stop	Beatla-712F	CACCATGCGGTTTCCACA GAAT	1087 bp
		Beat1a_1774R	GCTCATGTTGCACGTTGC AC	
Beat_IG1-2				
Beat_IG1-2	pENTR_Beat+Stop	Beatla-712F	CACCATGCGGTTTCCACA GAAT	762 bp
		Beatla_IG2	GGCACCGTTTCCGTGTTT TGG	
SP-BeatΔIG1				
SP	pENTR_Beat+Stop	Beatla-712F	CACCATGCGGTTTCCACA GAAT	120 bp
		BeatN_BeatIG2_R	GTTATGAATGGCGCATTG TGAACCCGGACATCCCGT AAAGC	
BeatΔIG1	pENTR_Beat+Stop	BeatN_BeatIG2_F	GCTTTACGGGATGTCCGG GTTCAATGCGCCATTC ATAAC	885 bp
		BeatC_R	TGTTAATTGCCTGATACAT CTGC	

Materials and Methods

Fragment	Template DNA	Primer designation	Sequence (5' → 3')	Product size
SP-BeatCys				
SP	pENTR_Beat+Stop	Beatla-712F	CACCATGCGGTTTCCACA GAAT	103 bp
		BeatSP_Cys_R 2	GACCATCCAACAGGATTG ACTAGCTGCGGTCATCTC TAATG	
BeatCys	pENTR_Beat+Stop	BeatSP_Cys_F 2	CATTAGAGATGACCGCAG CTAGTCAATCCTGTTGGA TGGTC	344 bp
		BeatC_R	TGTTAATTGCCTGATACAT CTGC	
BeatnewTM				
Beat SP, IG1-2 and Linker	pENTR_Beat+Stop	Beatla-712F	CACCATGCGGTTTCCACA GAAT	994 bp
		BeatN_CD8TM_ R	CAAGGGCGCCCAGATGT AGATACAGGATTGACTTG AGCTCG	
newTM from CD8	pCasper_MHC_hCD 8-GFP-Sh	BeatN_CD8TM_ F	CGAGCTCAAGTCAATCCT GTATCTACATCTGGGCGC CCTTG	107 bp
		CD8TM_BeatC_ R	CATCGCCTGCAACGGCG AGTAAAGGGTGATAACCA GTG	
Beat C- terminus	pENTR_Beat+Stop	CD8TM_BeatC_ F	CACTGGTTATCACCTTT ACTCGCCGTTGCAGGCG ATG	272 bp
		BeatC_R	TGTTAATTGCCTGATACAT CTGC	
BeatΔTM				
Beat SP, IG1-2 and Linker	pENTR_Beat+Stop	Beatla-712F	CACCATGCGGTTTCCACA GAAT	991 bp
		BeatN_BeatC_ R	CATCGCCTGCAACGGCG AACAGGATTGACTTGAGC TC	
Beat C- terminus	pENTR_Beat+Stop	BeatN_BeatC_F	GAGCTCAAGTCAATCCTG TTCGCCGTTGCAGGCGAT G	271 bp
		BeatC_R	TGTTAATTGCCTGATACAT CTGC	
SP-Beat_29-427				
SP from human CD8	pCasper_MHC_hCD 8-GFP-Sh	CD8SP_F	CACCATGGCCTTACCAGT GACCGCCTTGCTCCTGCC	85 bp
		CD8SP_Beat_R	GAACTCGAACCCGGACAT CCGGCCTGGCGGCGTGG AG	

Fragment	Template DNA	Primer designation	Sequence (5' → 3')	Product size
Beat_29-427	pENTR_Beat+Stop	CD8SP_Beat_F	CTCCACGCCGCCAGGCC GGATGTCCGGGTTTCGAG TTC	1215 bp
		BeatC_R2	TGTTAATTGCCTGATACAT CTGCTGTTGATCCTGC	
SP-Beat_29-322				
SP from human CD8	pCasper_MHC_hCD8-GFP-Sh	CD8SP_F	CACCATGGCCTTACCACT GACCGCCTTGCTCCTGCC	85 bp
		CD8SP_Beat_R	GAACTCGAACCCGGACAT CCGGCCTGGCGGCGTGG AG	
Beat_29-322	pENTR_Beat+Stop	CD8SP_Beat_F	CTCCACGCCGCCAGGCC GGATGTCCGGGTTTCGAG TTC	900 bp
		Beat322_R	GGATTGACTTGAGCTCGG ACTCAGGCGGGAAGTGG	

Table 2.9: Oligonucleotides used for OE-PCR and subsequent Topo-cloning of Side constructs

Fragment	Template DNA	Primer designation	Sequence (5' → 3')	Product Size
SP-GFP-Side				
SP	pBS-SK-Side	Side-1F	CACCATGCAGCTTTTATT GCCAACA	255 bp
		SideSP_GFP_R	CTCGCCCTTGCTCACCAT ACCGCTTCCCAGGCAAGT CAACAGGAC	
GFP	pUASTattB_rfA_eGFP	SideSP_GFP_F	GTCCTGTTGACTTGCCTG GGAAGCGGTATGGTGAG CAAGGGCGAG	761 bp
		GFP_Side_R	ACCGATTTTCAGTTGCTGC TTGTACAGCTCGTCCATG	
Side	pBS-SK-Side	GFP_Side_F	CATGGACGAGCTGTACAA GCAGCAACTGAAATCGGT	2608 bp
		Side-2817R	CTTCAGCGTTGGATCCAG GGTCGT	
SP-SideΔIG1				
SP	pBS-SK-Side	Side-1F	CACCATGCAGCTTTTATT GCCAACA	275 bp
		SideSP_SideIG2_R	GTGAGTTGAAGAAGTCGA CCGCCGAAACCGATTTCA G	
SideΔIG1	pBS-SK-Side	SideSP_SideIG2_F	CTGAAATCGGTTTCGGCG GTGACTTCTTCAACTCA C	2259 bp
		Side-2817R	CTTCAGCGTTGGATCCAG GGTCGT	

Materials and Methods

Fragment	Template DNA	Primer designation	Sequence (5' → 3')	Product Size
SidelG1-5				
SP+Sidel G1-5	pBS-SK-Side	Side-1F	CACCATGCAGCTTTTATT GCCAACA	2350 bp
		SideLinker_R	GCTGGCGCCGGTGCCCA GG	
SidelG1-CD8-Linker				
SP+Sidel G1	pBS-SK-Side	Side-1F	CACCATGCAGCTTTTATT GCCAACA	748 bp
		SideSP+IG1+ CD8_R	CGACACCCGGAAGTGGC TGCAGAGGAAGAGCTCAT AGC	
CD8-Linker	pCasper_MHC_hCD8-GFP-Sh	SideSP+IG1+ CD8_F	GCTATGAGCTCTTCCTCT GCAGCCAGTTCCGGGTG TCG	521 bp
		CD8_SideTM_R	GGCGGCGAGTATCAGCA GATCACAGGCGAAGTCCA G	
Side C-Terminus	pBS-SK-Side	CD8_SideTM_F	CTGGACTTCGCCTGTGAT CTGCTGATACTCGCCGCC CTTCAGCGTTGGATCCAG GGTCGT	459 bp
		Side-2817R		
SidelG1-CD8-CD8				
SP+Sidel G1	pBS-SK-Side	Side-1F	CACCATGCAGCTTTTATT GCCAACA	748 bp
		SideSP+IG1+ CD8_R	CGACACCCGGAAGTGGC TGCAGAGGAAGAGCTCAT AGC	
CD8-Linker	pCasper_MHC_hCD8-GFP-Sh	SideSP+IG1+ CD8_F	GCTATGAGCTCTTCCTCT GCAGCCAGTTCCGGGTG TCG	521 bp
		CD8_CD8_R	CGACACCCGGAAGTGGC TATCACAGGCGAAGTCCA G	
CD8 incl. TM	pCasper_MHC_hCD8-GFP-Sh	CD8_CD8_F	CTGGACTTCGCCTGTGAT AGCCAGTTCCGGGTGTC G	597 bp
		CD8_R	AACACGTCTTCGGTTCCT GTG	
SidelG1-FasII				
SP+Sidel G1	Side full-length	Side-1F	CACCATGCAGCTTTTATT GCCAACA	751 bp
		SideSP+IG1_ FasII_R	CTGATTCTCAGGGGCATT TGTGCAGAGGAAGAGCT CATAG	

Fragment	Template DNA	Primer designation	Sequence (5' → 3')	Product Size
FasII IG2 to C-terminus	pBS-KS-FasII	SideSP+IG1_FasII_F	CTATGAGCTCTTCCTCTG CACAAATGCCCCTGAGAA TCAG	2218 bp
		FasII_R	CACCGCCGAATTCTTCCC GA	

2.1.5 Plasmids

Table 2.10: General plasmids

Plasmid	Resistance	Source
pBS-KS-FasII	ampicillin	J. Kinold, AG Aberle
pCasper_MHC_hCD8-GFP-Sh	ampicillin	(Zito et al., 1999)
pBS-SK-Side	ampicillin	gift from C. S. Goodman
pENTR_Beat+Stop	kanamycin	A. Bauke, Münster

Table 2.11: Gateway pENTR/D-Topo vectors

Plasmid	Insert	Resistance	Source
pENTR/D-Topo-empty	-	kanamycin	Invitrogen
Beat entry vectors			
pENTR_GFP-Beat	Beat full-length, N-terminally fused to GFP and the endogenous SP	kanamycin	C. Heymann, this work
pENTR_Beat_1-395	Beat aa 1-395	kanamycin	C. Heymann, this work (together with V. Kühlmann)
pENTR_Beat_1-361	Beat aa 1-361	kanamycin	C. Heymann, this work (together with V. Kühlmann)
pENTR_Beat_1-254	Beat aa 1-254	kanamycin	C. Heymann, this work
pENTR_BeatΔIG1	Beat without IG1 (aa 141-427), N-terminally fused to the endogenous SP	kanamycin	C. Heymann, this work
pENTR_BeatCys	Beat Cys-rich domain (aa 320-427), N-terminally fused to the endogenous SP	kanamycin	C. Heymann, this work (together with V. del Olmo-Toledo)

Materials and Methods

pENTR_BeatΔTM	Beat full-length with deleted TM (aa 324-343 missing)	kanamycin	C. Heymann, this work
pENTR_BeatnewTM	Beat full-length, TM replaced by TM of hCD8 (aa 324-343 replaced)	kanamycin	C. Heymann, this work
pENTR_Beat_29-427	SP from hCD8, N-terminally fused to Beat aa 29-427	kanamycin	C. Heymann, this work
pENTR_Beat_29-322	SP from hCD8, N-terminally fused to Beat aa 29-322	kanamycin	C. Heymann, this work
Side entry vectors			
pENTR_GFP-Side	Side full-length, N-terminally fused to GFP and the endogenous SP	kanamycin	C. Heymann, this work
pENTR_SideΔIG1	Side without IG1 (aa 85-192), N-terminally fused to the endogenous SP	kanamycin	C. Heymann, this work
pENTR_SideIG1-5	Side aa 1-782	kanamycin	C. Heymann, this work (together with V. del Olmo-Toledo)
pENTR_SideIG1-CD8-TM	Side IG1 (aa 1-242) fused to hCD8 extracellular part, fused to Side TM and intracellular tail (aa 793-939)	kanamycin	C. Heymann, this work
pENTR_SideIG1-CD8-CD8	Side IG1 (aa 1-242) fused to hCD8 extracellular part, fused to complete CD8 including its TM	kanamycin	C. Heymann, this work (together with V. del Olmo-Toledo)
pENTR_SideIG1-FasII	Side IG1 (aa 1-242) fused to FasII (with deleted IG1)	kanamycin	C. Heymann, this work (together with V. del Olmo-Toledo)

Table 2.12: Gateway destination vectors

Plasmid	Resistance	Source
pUASTattB_rfA_eGFP	chloramphenicol + ampicillin	R. Stephan, Münster
pUASTattB_rfA_mCherry	chloramphenicol + ampicillin	F. Rodrigues, Münster

Plasmid	Resistance	Source
Beat expression vectors		
pUASTattB_GFP-Beat-mCherry	ampicillin	C. Heymann, this work
pUASTattB_Beat_1-395-eGFP	ampicillin	C. Heymann, this work (together with V. Kühlmann)
pUASTattB_Beat_1-361-eGFP	ampicillin	C. Heymann, this work (together with V. Kühlmann)
pUASTattB_Beat_1-254-eGFP	ampicillin	C. Heymann, this work
pUASTattB_BeatΔIG1-eGFP	ampicillin	C. Heymann, this work
pUASTattB_BeatCys-eGFP	ampicillin	C. Heymann, this work (together with V. del Olmo-Toledo)
pUASTattB_BeatΔTM-eGFP	ampicillin	C. Heymann, this work
pUASTattB_BeatnewTM-eGFP	ampicillin	C. Heymann, this work
pUASTattB_Beat_29-427-eGFP	ampicillin	C. Heymann, this work
pUASTattB_Beat_29-322-eGFP	ampicillin	C. Heymann, this work
Side expression vectors		
pUASTattB_GFP-Side-mCherry	ampicillin	C. Heymann, this work
pUASTattB_SideΔIG1-mCherry	ampicillin	C. Heymann, this work
pUASTattB_SideIG1-5-mCherry	ampicillin	C. Heymann, this work (together with V. del Olmo-Toledo)
pUASTattB_SideIG1-CD8-TM-mCherry	ampicillin	C. Heymann, this work
pUASTattB_SideIG1-CD8-CD8-mCherry	ampicillin	C. Heymann, this work (together with V. del Olmo-Toledo)
pUASTattB_SideIG1-FasII-mCherry	ampicillin	C. Heymann, this work (together with V. del Olmo-Toledo)

2.1.6 Antibodies

Table 2.13: Primary antibodies

Antigen	Species	Dilution IHS	Dilution WB	Source
Ankyrin-2XL	rabbit	1:1000	not used	(Koch et al., 2008)
Beat-Cys	rabbit	1:200	1:2000	Custom production at Biogenes
Beat-Cys	guinea pig	1:200	1:1000	
Beat-Linker	rabbit	1:200	1:2000	
Beat-Linker	guinea pig	1:200	1:1000	
Beat-Linker	rabbit	1:200	1:2000	A. Bauke, master thesis
mCherry	mouse	1:100	not used	DSHB (Clone 3A11)
Dlg	mouse	1:400	not used	DSHB
DvGlut	rabbit	1:800	not used	(Mahr and Aberle, 2006)
FasII	mouse	1:50	not used	DSHB (Clone 1D4)
Futsch	mouse	1:100	not used	gift from C. S. Goodman
GFP	rabbit	1:1000	1:5000	Acris Antibodies GmbH (Germany) (clone TP401)
MHC	mouse	1:100	not used	DSHB
Side	mouse	1:20	1:100	DSHB (Clone 9B8)
Tolloid-related	rabbit	not used	1:500	gift from M. O'Connor
α -Tubulin	mouse	not used	1:10000	Sigma Aldrich

Table 2.14: Secondary antibodies

Antigen	Species	Conjugate	Dilution	Source
rabbit	goat	HRP	1:7500	Jackson Immuno-research (USA)
mouse	goat	HRP	1:7500	
guinea pig	goat	HRP	1:7500	
mouse	goat	Cy3	1:500	
rabbit	goat	Cy3	1:500	
mouse	goat	Alexa 488	1:500	
rabbit	goat	Alexa 488	1:500	
mouse	goat	Alexa 647	1:500	

rabbit	goat	Alexa 647	1:500	
guinea pig	donkey	Cy3	1:500	

2.1.7 Software

Table 2.15: Software

Software	Manufacturer
Illustrator	Adobe Systems Incorporated, San José (USA)
Photoshop	Adobe Systems Incorporated, San José (USA)
(Fiji is just) ImageJ	GNU General Public License
Image Lab Software	BioRad Laboratories GmbH, München
MacVector	MacVector Incorporated, Apex (USA)
Excel	Microsoft Corporation, Redmond (USA)
Word	Microsoft Corporation, Redmond (USA)
Zen Blue	Carl Zeiss MicroImaging GmbH, Jena

2.2 Methods

2.2.1 Fly maintenance

Fly stocks were bred on *Drosophila* standard medium in plastic tubes sealed by batting plugs and kept on 18°C, room temperature or 25°C. For crosses, virgin female flies (less than ten hours after hatching at 18°C) and male flies (different ages) of the appropriate genotypes were put together.

2.2.1.1 *Drosophila* embryo collection

Flies of the desired genotypes were mated in small plastic cages on apple juice agar plates and egg-laying was encouraged by adding a dab of fresh baker's yeast. Apple juice agar plates were changed twice a day. Embryos were collected by carefully washing them off the agar using tap water and a soft brush. Embryos were transferred into a sieve, dechorionized with 1.7% hypochlorite for 4 min and rinsed with tap water.

2.2.1.2 Germline transformation

Transgenic fly lines were established by germline transformation using the site-specific Φ C31 integrase method (Bischof et al., 2007). Using this method, purified DNA is injected into early embryos and can be incorporated into the attP target site of the fly genome.

The plasmids used for injection contain a UAS-enhancer and promoter, the coding sequence for the protein of interest, an attB integration site and a mini *white*⁺ marker gene. These expression vectors were generated using the gateway system. The mix for injection is prepared as following:

Table 2.16: Mix for injection

Component	10 μ l mix
10x injection buffer	1 μ l
phenol red	1 μ l
purified plasmid	4 μ g
millipore H ₂ O	ad 10 μ l

The DNA mix for injection was centrifuged at 4°C and maximum speed for 30 min, transferred into a fresh tube and stored at -20°C until use.

About 300 flies containing the desired attP target site (w^- ; $\Phi 51C$ for integration on the 2nd chromosome and w^- ; $\Phi 86Fb$ for integration on the 3rd chromosome) were bred in large fly cages on apple juice agar plates with a dab of fresh baker's yeast. Flies were allowed to lay eggs for about 20 min and the embryos were collected and dechorionized as described above (see 2.2.1.1). The embryos were then aligned on a piece of apple juice agar with their micropile pointing into the same direction. The arranged embryos were glued to a cover slide (22 x 22mm) that was priorly coated with parcel tape heptane glue, dried at room temperature for about 4-7 min and coated with 10S Voltalef oil. 2µl of injection mix were pipetted into a sharpened glass capillary and the capillary was then attached to the FemtoJet microinjector. The DNA was injected into the posterior end of the embryos, where the future germ cells will arise. The slides with the embryos were then transferred into small plastic dishes (x 35mm) and covered with 3S Voltalef oil, which allows oxygen to pass through. These plastic dishes on their part were stored in a large plastic dish (x 145mm) containing a wet filter paper so that the embryos would not dry out. Embryos were kept on 18°C for 2-3 days and hatched first instar larvae were collected and transferred into tubes containing *Drosophila* standard food.

2.2.1.3 Establishment of transgenic fly lines

Hatched flies (F0), which originated from the injected embryos, were crossed to w^- flies in individual crosses. F1 offspring flies emerging from these different crosses were screened by their eye-color, because successful transformation leads to integration of the DNA into the fly genome in F1 progeny and thus to expression of the *white*⁺ marker gene. Positive transformants were crossed to w^- ; IF/CyO (for injection of w^- ; $\Phi 51C$) and w^- ; Dr/TM6C (for injection of w^- ; $\Phi 86Fb$) respectively. The segregation of dominant markers allows for the establishment of the transgenic fly line over a balancer chromosome.

2.2.1.4 Directed gene expression

Gene expression in *Drosophila* can be directed time- and tissue-specifically by using the Gal4/UAS-system (Brand and Perrimon, 1993). The gene for the yeast

transcription factor Gal4 is inserted behind a cell- or tissue-specific enhancer in the *Drosophila* driver-line. The upstream activating sequence (UAS) is cloned in front of the gene of interest and inserted into the genome of the so-called effector line. The gene expression is dependent on activation of the upstream activating sequence. When mating these flies, Gal4 proteins can bind to the UAS-region in the offspring and thus activate gene expression (Figure 2.1).

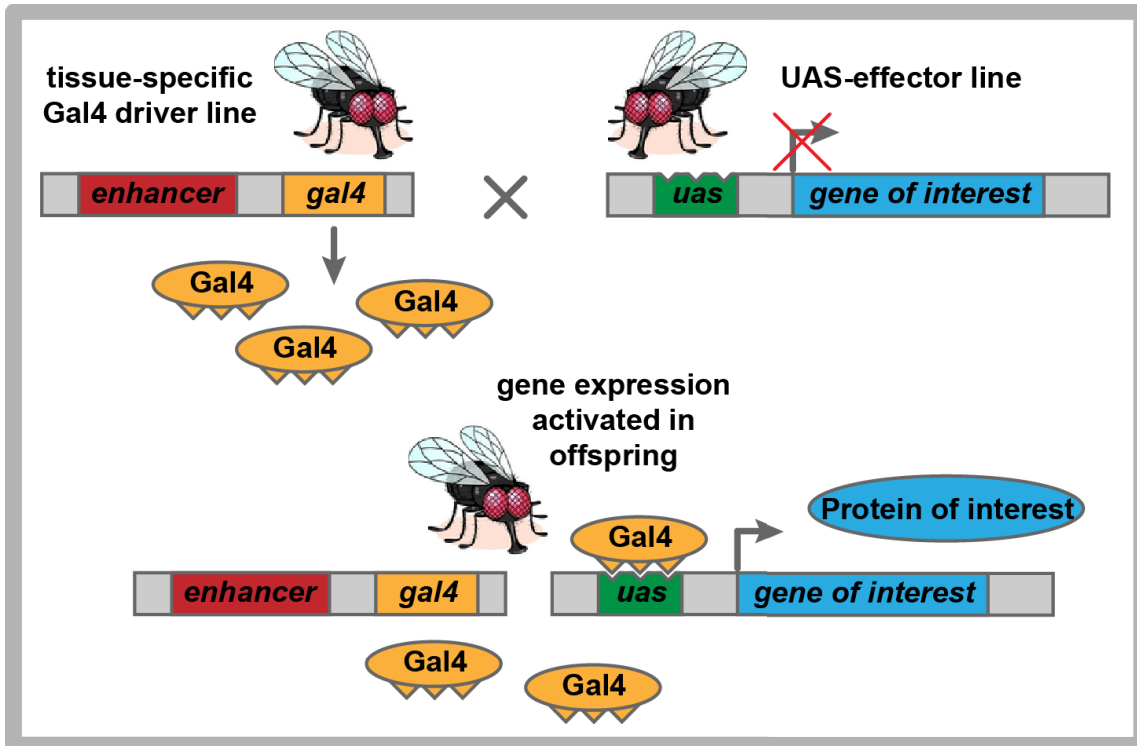


Figure 2.1: Schematic model of directed gene expression via the Gal4/UAS-system.

The transgenic, tissue-specific driver line expresses the yeast transcription factor Gal4. If crossed with flies from a transgenic effector line containing the UAS-region, Gal4 activates the gene transcription in the progeny.

Together with the accessible and versatile method of site-specific integration (Bischof et al., 2007), the directed gene expression opens up many possibilities for analyzing gene functions. This method of the Φ C31 integration allows for the insertion of any desired transgene into specific landing sites in the fly genome and thus greatly facilitates the establishment and reproducibility of Gal4 driver lines and UAS-effector lines.

2.2.2 Molecular biological methods

2.2.2.1 Isolation of genomic DNA from adult *Drosophila* flies

For isolation of total DNA from adult flies, DNeasy Blood & Tissue Kit (QIAGEN) was used. About 100 flies were collected and frozen in 1.5ml reaction tubes at -20°C over night so that subsequent cell disruption would be facilitated. After addition of 180µl PBS, samples were thoroughly pestled with micropestles for 5 min. Then 20µl proteinase K and 200µl buffer AL were added, probes were mixed and incubated at 56°C for 10 min. The addition of 4µl RNase A extinguishes contaminating RNA and samples were incubated 2 min at room temperature. After adding 200µl 100% ethanol, probes were mixed, transferred to the DNeasy columns and centrifuged 1 min at 8000rpm. The filtrate was discarded, 500µl buffer AW1 was added to the column, and centrifuged again for 1 min at 8000rpm. The filtrate was discarded again, 500µl buffer AW2 was added and the column was centrifuged for 3 min at 14000rpm in order to dry the membrane. The column was transferred to a fresh reaction tube and 100µl buffer AE was added, incubated for 1 min and centrifuged for 1 min at 8000rpm. The DNA concentration was estimated photometrically and the DNA was stored at -20°C.

2.2.2.2 RNA isolation

RNA was isolated from dechorionized *Drosophila* embryos or whole larvae using the Totally RNA Kit (Ambion).

Sample disruption and homogenization

Embryos were collected and dechorionized as described above (see 2.2.1.1). About 50mg (ca. 80µl) of embryos were transferred into a 1.5ml reaction tube, pestled in 50-100µl denaturation buffer with a micropestle and the buffer was afterwards filled up to 500µl. For isolation from 3rd instar larvae, about 20 larvae (ca. 30mg) were collected, frozen at -20°C over night and pestled in about 50-100µl of denaturation buffer. All samples were further decomposed by raising the probe up and down through a 23 gauge syringe.

Phenol:chloroform:IAA extraction

1 starting volume of phenol:chloroform:IAA was added to the samples and mixed for 1 min (vortexer). Probes were incubated on ice for 5 min and centrifuged at 4°C and 12000rpm for 5 min. The aqueous (upper) phase was transferred into a fresh reaction tube.

Acid phenol extraction

1/10 volume (v/v) of sodium acetate solution was added and the samples were mixed for 10 sec. 1 starting volume of acid-phenol:chloroform was added to the samples and mixed for 1 min (vortexer). Probes were incubated on ice for 5 min and centrifuged at 4°C and 12000rpm for 5 min. The aqueous (upper) phase was transferred into a fresh reaction tube.

Isopropanol precipitation of the RNA

An equal volume of isopropanol as the aqueous phase from the acid phenol extraction was added and mixed. Samples were precipitated at -20°C for at least 30 min (to over night) and centrifuged at 4°C and 12000rpm for 15 min. The supernatant was discarded and the pellet was washed by adding 300µl 70% ethanol, gentle mixing and centrifugation at 4°C and 7500rpm for 5-10 min. The supernatant was discarded, the pellet was dried and eluted in 50-200µl elution solution. RNA was stored at -80°C.

2.2.2.3 Reverse transcription (cDNA-synthesis)

Reverse transcription is used to generate complementary DNA (cDNA) of an RNA template. This method offers the possibility to amplify transcribed gene sequences by PCR.

7.5µg of RNA in in a total volume of 17.55µl water were incubated at 90°C in a heat block for 2 min and then on ice for another 2-5 min. Then the mastermix (12.45µl) was added and the samples were incubated in a 50°C warm water bath for 1h. The reverse transcriptase was then heat-inactivated at 95°C for 2 min and the probes were then directly transferred on ice. The cDNA was stored at -20°C.

Table 2.17: Reverse transcription

Component	30µl reaction	Final concentration
5x First Strand Buffer	6µl	1x
10mM dNTP Mix (2.5mM each)	1.2µl	400µM
Oligo-dT ₍₁₈₎ Primer	1.2µl	0.5µg/µl
0.1M DTT	1µl	0.1M
murine RNase Inhibitor (40 U/µl)	1µl	1.3 U/µl
SuperScript III Reverse Transkriptase (200 U/µl)	1µl	6.7 U/µl
total volume	12.45µl	

2.2.2.4 Polymerase chain reaction (PCR)

The technique of polymerase chain reaction (PCR) is used to specifically amplify DNA fragments. The reaction requires a template DNA, a pair of primers (ca. 20 bp, synthetically assembled oligonucleotides), the four dNTPs, a heat-stable polymerase and the reaction buffer. A PCR consists of the following steps:

Denaturation: Heating of the double-stranded DNA to 95-98°C leads to melting of the DNA, yielding single-stranded DNA molecules.

Annealing: Lowering the temperature to about 55-65°C allows hybridization of the primers to the single-stranded DNA.

Elongation: Reaction temperature of 72°C (optimum of most polymerases) leads to 5' → 3' assembly of nucleotides, starting from the primers and adding nucleotides to the free 3'-hydroxyl-group of the growing DNA-strand.

Each cycle doubles the number of DNA fragments, leading to exponential DNA-synthesis.

Table 2.18: Standard PCR

Component	50µl reaction	Final concentration
10 mM dNTPs (each 2.5 mM)	1µl	200µM
10 µM forward primer	2.5µl	0.5µM
10µM reverse primer	2.5µl	0.5µM
plasmid template	1µl	0.02-0.2ng/µl
5x Q5 reaction buffer	10µl	1x
Q5 polymerase	0.5µl	0.02U/µl
5x Q5 high CG enhancer (optional for difficult templates)	(10µl)	(1x)
millipore H ₂ O	to 50 µl	

Thermocycling conditions of a standard PCR using Q5 polymerase:

98°C		30 s	
98°C	(denaturation)	10 s	} 30-35 cycles
58-62°C	(annealing)	30 s	
72°C	(elongation)	15-90 s (15-30 s per kb)	
72°C	(final extension)	2 min	

2.2.2.5 Agarose gel electrophoresis

Agarose gel electrophoresis is used for the separation of DNA and RNA fragments. As voltage is applied, the negatively charged nucleic acids migrate towards the anode. Smaller fragments travel quicker than bigger ones and this leads to a separation according to their fragment sizes.

Loading buffer was added to the samples and they were filled into the pockets of the agarose gel. The 1 kb DNA ladder serves as reference for fragment size. Nucleic acid bands were visualized using the ChemiDoc Imager (Biorad).

2.2.2.6 PCR product purification

PCR purification serves to purify the amplified DNA fragments from primers in the PCR reaction mix. For this purpose, the QIAquick PCR purification Kit was used (Qiagen). All centrifugation steps were carried out for 1 min at room temperature and 13000rpm.

5 volumes of buffer PB were added to 1 volume of PCR reaction, mixed and loaded onto the provided column in order to bind the DNA to the membrane. After

centrifugation, the flow-through was discarded and the DNA was washed by adding 750µl of buffer PE. The column was centrifuged, the filtrate discarded and the residual buffer was removed by another centrifugation step. Elution of the DNA from the column was performed by addition of 30µl buffer EB to the column, 5 min incubation at room temperature and subsequent centrifugation. The DNA concentration was determined photometrically and DNA was stored at -20°C.

2.2.2.7 PCR product purification via gel extraction

In order to purify PCR products, which exhibit by-products, DNA bands of the desired fragment size were excised from an agarose gel. Gel extraction was performed using the QIAquick Gel Extraction Kit (Qiagen). All centrifugation steps were carried out for 1 min at room temperature and 13000rpm.

3 gel volumes (w/v) of buffer QG were added to 1 volume of gel and incubated at 50°C for about 10 min until the gel slice was solved completely. 1 gel volume of isopropanol was added, the sample was mixed, applied to the provided column and centrifuged in order to bind the DNA to the column. 500µl buffer QG were added and centrifuged, and then the DNA was washed by applying 750µl buffer PE and following centrifugation. The membrane was dried by another centrifugation step. Elution of the DNA from the column was performed by addition of 30µl buffer EB to the column, 5 min incubation and subsequent centrifugation. The DNA concentration was determined photometrically and the purified DNA was stored at -20°C.

2.2.2.8 Overlap extension PCR (OE-PCR)

With the method of overlap extension PCR, DNA fragments from different sources can be easily assembled *in vitro*. Artificial fusion constructs can thus be created without the need of serial cloning steps and without the requirement of linker parts for restriction enzymes and site-directed mutagenesis can be easily effectuated (Ho et al., 1989).

Primers were designed in a way that the endings of the resulting fragments overlap. The overlapping DNA pieces were then fused together in the so-called overlap PCR.

Table 2.19: Extension PCR

Component	50µl reaction	Final concentration
10mM dNTPs (each 2.5mM)	1µl	200µM
10µM forward primer	2.5µl	0.5µM
10µM reverse primer	2.5µl	0.5µM
plasmid template	1µl	0.02 - 0.2ng/µl
5x Q5 reaction buffer	10µl	1x
Q5 polymerase	0.5µl	0.02U/µl
5x Q5 high CG enhancer (optional for difficult templates)	(10µl)	(1x)
millipore H ₂ O	to 50µl	

Thermocycling conditions of the extension PCR:

98°C		30 s	
98°C	(denaturation)	10 s	} 30 cycles
58-64°C	(annealing)	30 s	
72°C	(elongation)	30-90 s (15-30 s per kb)	
72°C	(final extension)	2 min	

The amplified DNA fragments were visualized by agarose gel electrophoresis and purified either by PCR purification (see 2.2.2.6) or gel extraction (see 2.2.2.7) depending on purity of the DNA-band. The concentration of the purified PCR product was determined.

For subsequent overlap PCR, equimolar amounts of PCR products were applied (e.g. if fragment 1 has twice the size [bp] of fragment 2, only half the amount of DNA [ng] is employed).

Table 2.20: Overlap PCR

Component	50µl reaction	Final concentration
10mM dNTPs (each 2.5mM)	1µl	200µM
fragment 1	required amount	50-800ng
fragment 2	required amount	50-800ng
(fragment 3)	(required amount)	(50-800ng)
5x Q5 reaction buffer	10µl	1x
Q5 polymerase	0.5µl	0.02U/µl

Component	50µl reaction	Final concentration
5x Q5 high CG enhancer (optional)	(10µl)	(1x)
millipore H ₂ O	to 50µl	

Thermocycling conditions of the overlap PCR:

98°C		30 s	
98°C	(denaturation)	10 s	} 15 cycles
60°C	(annealing)	30 s	
72°C	(elongation)	60-90 s (15-30 s per kb)	
72°C	(final extension)	2 min	

In order to amplify explicitly the final, overlapped PCR product, 3µl from the overlap PCR reaction were used as DNA template and amplified with the end primers.

Table 2.21: Purification PCR

Component	50µl reaction	Final concentration
10mM dNTPs (each 2.5mM)	1µl	200µM
10µM forward end primer	2.5µl	0.5µM
10µM reverse end primer	2.5µl	0.5µM
reaction mix from overlap PCR	3µl	
5x Q5 reaction buffer	10µl	1x
Q5 polymerase	0.5µl	0.02U/µl
5x Q5 high CG enhancer (optional)	(10µl)	(1x)
millipore H ₂ O	to 50µl	

Thermocycling conditions of the purification PCR:

98°C		30 s	
98°C	(denaturation)	10 s	} 20 cycles
72°C	(annealing)	30 s	
72°C	(elongation)	60-90 s (15-30 s per kb)	
72°C	(final extension)	10 min	

The amplified DNA fragments were visualized, purified by gel extraction (see 2.2.2.7) and the concentration of the purified PCR product was determined.

2.2.2.9 Topo cloning reaction

Topo cloning is a strategy to directionally clone a blunt-end PCR product into a vector containing a covalently bound topoisomerase and a GTGG overhang. Adding the four bases CACC to the 5'-end of the forward primer enables the directional cloning of the PCR fragment.

For topo cloning, the pENTR/D-TOPO Cloning Kit (Invitrogen) was used. The ratio between the purified PCR product and the pENTR/D-TOPO vector should be 0.5:1 (for smaller PCR fragments) up to 2:1 (for larger PCR fragments).

Table 2.22: Mix for Topo cloning

Component	6µl reaction
Purified PCR product (ca. 5-10ng)	0.5 - 4µl
Salt solution	1µl
TOPO vector (15-20ng/µl, 2580 bp)	1µl
millipore H ₂ O	ad 6µl

The reaction mix was incubated at room temperature for 5-30 min and then used for transformation into One Shot TOP10 *E. coli* (see 2.2.3.1).

Isolated plasmids were checked for potential errors during PCR or cloning by sequencing.

2.2.2.10 Sequencing

The exact nucleotide order of DNA probes was determined by sequencing (performed by MWG Eurofins, Ebersberg). DNA was diluted according to the product size and purity (see Table 2.23). Samples were prepared as following:

Table 2.23: Sample preparation for sequencing

Component	15µl reaction	
DNA	Purified PCR product 150-300 bp	2ng/µl
	Purified PCR product 300-1000 bp	5ng/µl
	Purified plasmid DNA	50-100ng/µl
Primer	15pmol	
millipore H ₂ O	ad 15µl	

Sequences were analyzed using MacVector software. Multiple sequence alignment was performed with MUSCLE (Multiple Sequence Comparison by Log-Expectation).

2.2.3 Microbiological methods

2.2.3.1 Heat shock transformation of chemically competent *E. coli* bacteria

Transformation terms the uptake and incorporation of exogenous DNA, e.g. a plasmid, into bacteria. Bacteria must be in a state of competence to permit transformation. In order to get stably incorporated, the plasmid has to exhibit a so-called origin of replication (ORI), which allows replication independently of the replication of its host's genome. The selection of positive transformants takes place via an antibiotic resistance gene in the plasmid.

Table 2.24: List of employed *E. coli* strains

Bacterial strain (<i>E. coli</i>)	Purpose	Source
XL1 blue	retransformation of general plasmids	Self-made
One Shot TOP10	Gateway cloning	Invitrogen
One Shot ccdB Survival 2T1	retransformation of Gateway destination vectors	Invitrogen

Cells were slowly thawed on ice. About 1µl of the desired plasmid was added to 25-50µl of chemically competent *E. coli* bacteria. The vials were incubated on ice for 30 min, the bacteria were then heat shocked in a 42°C water bath for 30 s and incubated on ice for 2 min. 250µl of pre-warmed SOC medium was added and the bacteria were shaken horizontally at 37°C for 1 h and 300rpm in a thermo shaker. 25-100µl of the transformed cells were spread on selective agar plates and incubated at 37°C over night.

The next day, about 5 clones were picked and used for inoculation of 3ml LB medium containing the respective antibiotic. Cultures were incubated at 37°C on a rotary shaker over night and further used for plasmid isolation (see 2.2.3.2). Glycerol stocks of the respective bacteria were prepared by adding 500µl glycerol to 500µl of bacterial culture and stored at -80°C.

2.2.3.2 Plasmid isolation

Plasmids were isolated from bacteria by minipreparation. Depending on demands of purity, isolation was carried out with- or without the usage of columns.

Quick minipreparation

If plasmids were used for analysis via restriction digest, the following protocol was used.

Overnight cultures were centrifuged for 1 min at 14000rpm at room temperature (RT) and the supernatant was discarded. The pellet was resuspended in 100µl of resuspension buffer and mixed thoroughly. 200µl of lysis buffer were added and samples were carefully mixed by inversion. 150µl of pre-cooled neutralization buffer were added, mixed by inversion and incubated for 5 min on ice. Samples were centrifuged at 4°C for 10 min and 14000rpm. The supernatant was transferred into a fresh tube, the same amount of isopropanol was added, probes were mixed, incubated for 2 min at RT and centrifuged at 4°C for 10 min and 14000rpm. The supernatant was discarded and the pellet was washed by the addition of 750µl of 70% ethanol, mixing and centrifugation at 4°C for 5 min and 14000rpm. The supernatant was discarded and the pellet was dried and eluted in about 50µl TE buffer. Plasmid DNA was stored at -20°C.

Minipreparation using the High Pure Plasmid Isolation Kit (Roche)

If plasmids were subsequently used for LR-reaction or microinjection, the demands on the purity of the DNA were fulfilled by using the following method.

Overnight cultures were centrifuged for 1 min at 14000rpm (RT) and the supernatant was discarded. The pellet was resuspended in 250µl suspension buffer and mixed thoroughly. 250µl of lysis buffer were added, samples were carefully mixed by inversion and incubated at RT for 5 min. 350µl of pre-cooled binding buffer were added, mixed by inversion and incubated on ice for 5 min. Samples were centrifuged at 4°C for 10 min and 13000rpm. The supernatant was transferred onto the provided column, centrifuged at maximum speed for 1 min and the filtrate was discarded. 500µl of wash buffer I were added and centrifuged at maximum speed for 1 min. The filtrate was discarded, 700µl of wash buffer II were added and the column was centrifuged at maximum speed for 1 min. The filtrate was again discarded and the membrane was dried by another centrifugation step at maximum speed for 1 min.

The column was then transferred into a fresh reaction tube, 20-50µl of elution buffer were added, incubated for 1-5 min at RT and the sample was centrifuged for 1 min at maximum speed. In case of further use for Phenol/Chloroform extraction, the elution of the DNA from the membrane was performed with millipore H₂O instead of elution buffer. The concentration was photometrically determined and plasmid DNA was stored at -20°C.

2.2.3.3 Restriction digest of plasmid DNA

Restriction endonucleases cut DNA at specific recognition sequences. Isolated plasmids were digested with restriction enzymes in order to control the size of the vector and the insert as well as the correct orientation of the insert. Typically, the plasmids were examined with enzymes cutting at a unique restriction site (linearization) and with enzymes cutting twice - once within the insert and once within any other region of the plasmid (orientation digest). Enzymes that were used for restriction digest are listed in Chapter 2.1.1.

Table 2.25: Components of a restriction digest

Component	20µl reaction
10x buffer	2µl
Restriction enzyme	0.5µl
Plasmid (ca. 1 µg)	1-5µl
millipore H ₂ O	ad 20µl

Plasmid digests were incubated at 37°C for 2h and visualized by agarose gel electrophoresis.

2.2.3.4 LR recombination reaction

The site-specific recombination properties of bacteriophage lambda provide the foundation for transferring DNA sequences. In this case, DNA sequences from the Gateway entry vector (see Table 2.11) and destination vector (see Table 2.12) are fused to a combination of the cloned DNA sequence and an appropriate tag. This is mediated by the reaction between the attL and attR sites of the Gateway entry- and destination vectors.

Table 2.26: Components of the LR reaction

Component	10µl reaction
Entry vector (50-150ng/reaction)	1-7µl
Destination vector (150ng/reaction)	1µl
LR Clonase II Enzyme Mix	2µl
TE buffer, pH 8	ad 10µl

Samples were incubated for 2h to over night at 25°C and the addition of 1µl Proteinase K and incubation of 10 min at 37°C terminated the reaction. The samples were then used for transformation into One Shot TOP10 *E. coli* (see 2.2.3.1) and for each sample, 50µl and 100µl were plated on LB plates containing ampicillin.

2.2.3.5 Phenol/Chloroform extraction

Phenolic DNA purification serves to eliminate enzymes or other proteins from the original cell extracts. This purification method was used for all plasmids prior to injection into embryos.

About 1-10µg of miniprep plasmid diluted in 250µl of millipore H₂O was mixed with 250µl of phenol/chloroform/isoamyl alcohol and centrifuged for 10 min at maximum speed at RT. The aqueous (upper) phase was transferred to a fresh reaction tube. Yields in final DNA concentration could be elevated by the addition of another 200µl of millipore H₂O to the organic phase, mixing and another centrifugation step at maximum speed. Again, the aqueous (upper) phase was transferred to the fresh tube containing the aqueous phase from the first separation step. 1/20 volume (v/v) of 5 M NaCl and 2 volumes (v/v) of 96% ethanol were added, the mixture was mixed by inversion and incubated for at least 15 min at -80°C (or for a longer time at -20°C). Samples were centrifuged at 4°C and 14000rpm for 10 min, the supernatant was discarded, the pellet was washed with 70% ethanol and centrifuged at 4°C and 14000rpm for another 10 min. The supernatant was discarded again and the pellet was dried at 42°C in the heat block for a maximum of 10 min. The pellet was then eluted in 10-20µl millipore H₂O, the concentration was determined photometrically and the DNA was stored at -20°C. The concentration for subsequent microinjection should be about 300-1000ng/µl.

2.2.4 Protein biochemical methods

2.2.4.1 Antibody generation

Immunohistochemical staining of *Drosophila* embryos offers the possibility to visualize the embryonic expression pattern of a protein of interest. Up to now, there is no antibody commercially available, which is directed against Beaten path Ia. Therefore, two different peptide antibodies directed against a part of the linker-region (aa 286-299: C-LQGEEDDGTEGGLG) and against a part of the Cys-rich domain (aa 376-389: C-VSATKQKQKQRQMQ) respectively (Figure 2.2), were custom-generated at Biogenes. Protein fragments were chosen by high antigenicity properties. Peptides were synthesized with a purity of at least 80% and coupled to hemocyanin as carrier. Polyclonal antisera were generated by immunization of one rabbit and one guinea pig for each peptide.

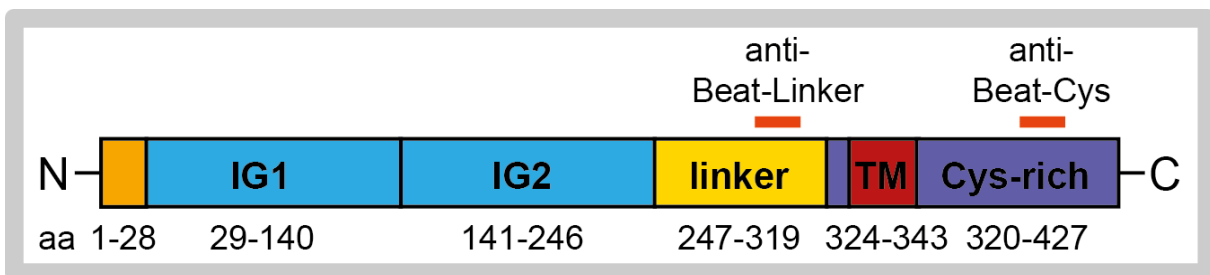


Figure 2.2: Peptide-antibodies generated at Biogenes.

Anti-Beat-Linker: aa 286-299 (LQGEEDDGTEGGLG), anti-Beat-Cys: aa 376-389 (VSATKQKQKQRQMQ).

2.2.4.2 Immunohistochemistry of *Drosophila* embryos

Dechorionized embryos (see 2.2.1.1) were transferred into a reaction tube containing 600µl 3.7% formaldehyde in PBS covered with 600µl heptane and fixed for 20 min on the nutator. The formaldehyde (lower phase) was then removed, 600µl methanol was added and the vitelline membrane was removed by shaking the embryos 1-2 min vigorously. The embryos sink to the bottom whereas the membrane debris goes to the interphase. The upper phase and interphase were then removed and the embryos were washed with 500µl methanol 3 times. At this step, embryos can be stored in methanol at -20°C for a couple of weeks.

Fixed embryos were washed in 750µl PTX 3 times for 10 min on the nutator and unspecific binding sites were blocked by incubation in 400µl PTX + 5% normal goat serum (NGS) for 30 min. Primary antibodies were added and the embryos were

incubated on the nutator at 4°C over night. Embryos were then washed in 750µl PTX 4 times for 10 min, fluorescently labeled secondary antibodies diluted in 400µl PTX + 5% NGS were added and the embryos were incubated on the nutator for 2h at RT in darkness. Embryos were washed 4 times in 750µl PTX for 10 min, rinsed in PBS and covered in 400µl 70% glycerol in PBS. After the embryos have sunken to the bottom of the tube, embryos were mounted for subsequent imaging. Therefore, the tip of a 200µl pipette was cut so that embryos could pass the tip without undergoing too much shearing forces. About 29µl of 70% glycerol containing the stained embryos were added to an object slide, covered by an 18 x 18mm cover slide and sealed with nail polish.

2.2.4.3 Immunohistochemistry of *Drosophila* larval filets

L3 larvae were dissected on sylgard plates using forceps, microscissors and insect pins. Dissection took place in PBS and the resulting larval filets were rinsed twice with PBS, then once with PBS containing 3.7% formaldehyde and then fixed with 1ml PBS containing 3.7% formaldehyde for 15 min and washed with PBS 3 times. Filets were then transferred into a reaction tube containing PTX, washed 3 times for 15 min in 750µl PTX and incubated in 400µl PTX + 5% NGS for one hour in order to block unspecific binding sites. Primary antibodies were added and the filets were incubated on a nutator at 4°C over night. Filets were washed in 750µl PTX 4 times for 15 min and the filets were incubated with fluorescently labeled secondary antibodies diluted in 400µl PTX + 5% NGS for 2 hours at RT in darkness. Filets were washed again 4 times in 750µl PTX for 15 min, rinsed in PBS and covered with 300µl 70% glycerol in PBS. After the filets have sunken to the bottom of the tube, elevated head and tail regions were removed and the preparations were mounted onto object slides in about 25µl 70% glycerol in PBS, covered with 22 x 22mm cover slides and sealed with nail polish.

2.2.4.4 Surface staining of *Drosophila* larval filets

Larvae were dissected in ice-cold PBS and incubated with antibodies in 10 fold higher concentration than used for normal immunohistochemistry for 60 min on ice. Larvae were rinsed twice with ice-cold PBS, then once with ice-cold PBS containing 3.7% formaldehyde and then fixed for 20 min in ice-cold 3.7% formaldehyde in PBS.

Filets were then transferred into a tube containing 750 μ l PTX and washed 3 times for 10 min in PTX. Secondary antibodies were added to 400 μ l PTX + 5% NGS and the probes were incubated on the nutator at RT for 2h, filets were then washed 3 times for 10 min in 750 μ l PTX, rinsed in PBS and then 400 μ l 70% glycerol in PBS was added. Preparations were mounted as described above (see 2.2.4.3).

2.2.4.5 Co-immunoprecipitation

Co-Immunoprecipitation permits the identification of protein-protein interactions. Using this method, an antibody, which is specific for a target protein, is used to indirectly capture proteins that are bound the target protein. Gel electrophoresis and subsequent western blotting enables the visualization of co-precipitated proteins.

Sample preparation

L3 larvae were dissected and the resulting filets were homogenized with a micropestle in lysis buffer (about 15 μ l lysis buffer per larval filet) and incubated on ice for 10 min. Lysates were centrifuged for 15 min at 14000rpm at 4°C and the supernatants were transferred into fresh tubes. 90 μ l of the lysate of each desired genotype (derived from 6 filets) were mixed.

Preclear

80 μ l of soaked protein A-sepharose were added to 180 μ l of the mixed lysates and rotated at 4°C for 1h. This step reduces unspecific interactions between proteins and the protein A-sepharose. Probes were centrifuged for 5 min, 3000g at 4°C and the supernatant was transferred into a fresh reaction tube.

Immunoprecipitation

The precleared lysate was incubated with 5 μ g of anti-GFP antibody over night at 4°C on the test-tube rotator. 80 μ l of protein A-sepharose beads were added and rotated for 3-4h at 4°C. The sample was centrifuged for 5 min at 3000g and 4°C and the supernatant was transferred into a fresh tube for further immunodetection. The sepharose beads were washed 4x with washing buffer at 4°C (addition of 500 μ l washing buffer, 5-10 min incubation on the nutator and centrifugation for 3 min at 3000g and 4°C). 60 μ l of 2x sample buffer were added to the sepharose beads, boiled at 98°C for 5 min and centrifuged for 5 min at 5000rpm and RT. The supernatant was

used for gel electrophoresis (2.2.4.6) and subsequent western blotting (2.2.4.7) with antibodies for the interacting candidate protein.

2.2.4.6 Sodium dodecyl sulfate polyacrylamide gel electrophoresis (SDS-PAGE)

The discontinuous, denaturing and reducing SDS-PAGE allows for the separation of proteins according to their molecular weight. Probes were heat-denatured at 98°C for 5 min (disruption of hydrogen bonds leads to breaking of the secondary and tertiary structures) and reduced (dithiothreitol (DTT) in the sample buffer disrupts covalent disulfide bonds). SDS acts as anionic detergent, which equally anneals to the amino acid chains and overlies the intrinsic charge of a protein. The resulting negative charge is proportional to the molecular weight of the protein. When a voltage is applied, the negatively charged proteins migrate towards the anode. Proteins with a higher molecular weight carry more negative charge than smaller ones and thus migrate slower. The discontinuous PAGE gathers proteins in the stacking gel (which contains less acrylamide than the separating gel and thus exhibits bigger pores) before the proteins are being separated according to their size. This procedure enhances the sharpness of the bands within the gel.

Sample preparation (embryos)

Embryos were collected and dechorionized as described above (see 2.2.1.1). In case of mutant animals, homozygous embryos were manually separated for the GFP-expressing balancer chromosomes using UV binoculars. The embryos were homogenized with a micropestle in 2x sample buffer (about 2 embryos per 1µl of sample buffer) and heated for 5 min at 98°C. Lysates were centrifuged for 5 min at 14000rpm and room temperature, transferred into a fresh tube and directly used for gel electrophoresis or stored at -20°C.

Sample preparation (larvae)

Larvae were dissected in PBS, homogenized with a micropestle in 2x sample buffer (about 1 larval filet per 10µl of sample buffer) and heated for 5 min at 98°C. Lysates were centrifuged for 5 min at 14000rpm and room temperature, transferred into a fresh tube and directly used for gel electrophoresis or stored at -20°C.

Sample preparation (larval hemolymph)

About 50 larvae were collected and rinsed in a sieve. Larvae were then pinched with forceps at the mouth region and transferred into a 500 μ l tube, which was previously cut with a razor blade at the bottom. The small tube was inserted into a pre-chilled 1.5ml tube containing 10 μ l sample buffer and centrifuged for 10s on a benchtop microcentrifuge. Probes were immediately stored at -80°C until use and heated for 5 min at 98°C prior to gel electrophoresis.

Gel preparation

Gels were prepared using the Mini-PROTEAN Tetra handcast system (BioRad). Gels were compounded as described above (see 2.1.2). TEMED and APS initiate polymerization and were added just before casting the gel. The separating gel was layered with 70% ethanol in order to ensure a bubble-free meniscus. After polymerization of the separating gel, the ethanol was discarded, the stacking gel was cast on top and the comb was inserted.

Polymerized gels were inserted into the Mini-PROTEAN Tetra System chamber and running buffer was added. Combs were carefully removed and the resulting pockets were rinsed with running buffer in order to remove residual, unpolymerized parts of the gel.

Electrophoresis

Samples were denatured for 5 min at 98°C. Gels were loaded with 20 μ l of sample and 8 μ l of marker, respectively. Free pockets were filled with 20 μ l of 2x sample buffer to improve electrophoretic properties of the gel. Electrophoresis was started by applying 80V for 20 min (or until the running front reaches the separating gel). Voltage was then augmented to 120V until the running front reached the end of the gel.

2.2.4.7 Semi-dry western blot

Western blotting is used to detect specific proteins via immuno-labeling. The proteins, which have been separated according to their molecular weight, are now transferred onto a PVDF membrane. Specific binding of the HRP-conjugated antibody is visualized by the chemiluminescence reaction.

Protein transfer

The PVDF membrane needs to be activated by a short incubation in 100% methanol. Starting from the anode, one layer of API-soaked filter paper, one layer of APII-soaked filter paper and the activated PVDF membrane were piled up. The gel was removed from the gel chamber and the stacking part was discarded. The separating gel was placed on top of the membrane and three layers of KP-immersed filter paper were stacked upmost. Air bubbles in between the layers would prevent proper protein transfer and need to be removed using a blot roller after each layer. The lid (cathode) was mounted to the blotting sandwich and the voltage was applied. Protein transfer took place at 15V for 30 min (for 1 gel) or 45 min (2 gels).

Immunodetection

All incubation and washing steps took place on the rocker.

The membrane was transferred into a plastic bowl and briefly washed with TBST twice. Unspecific binding sites were blocked by incubation of the membrane with blocking solution (5% powdered milk in TBST) for 1h at room temperature. The membrane was then incubated with the primary antibody, diluted in blocking solution, at 4°C over night. The membrane was then washed with TBST three times for 10 min at room temperature. Secondary, HRP-conjugated antibody (diluted 1:7500 in blocking solution) was applied and the membrane was incubated for 2h at room temperature. The membrane was again washed with TBST three times for 10 min at room temperature and once with TBS. The membrane was incubated with a mix of 500µl peroxide solution and 500µl luminol/enhancer solution (Clarity Western ECL Substrate) for 3-5 min in darkness. Excess liquid was removed, the membrane was put between two layers of transparency film and imaged using the ChemiDoc MP System.

2.2.5 Microscopy

Confocal images were recorded using the laser scanning microscope 710 (Zeiss). Z-stacks were processed to maximum intensity projections, which were used for all figures. Embryonic and larval images are arranged with the dorsal part up and the anterior end to the left.

2.2.5.1 Whole mount imaging of intact *Drosophila* embryos

It is possible to track fluorescent constructs and their localization directly in the embryo. For this purpose, embryos were dechorionized as described above (see 2.2.1.1), transferred to an object slide with PBS and covered by an 18 x 18mm cover slip.

2.2.5.2 Whole mount imaging of intact *Drosophila* larvae

Through the translucent cuticle of *Drosophila* larvae, it is possible to directly image larvae, which express fluorescent markers without prior antibody staining procedures. For this purpose, larvae were immobilized in 65°C warm water for 1-2 seconds. The stretched, immobilized larvae were then transferred to an object slide with 70% glycerol in PBS and covered by 22 x 22mm cover slips.

2.2.6 Contributions

During this work I supervised several bachelor- and master students. Experiments were partly performed by the students listed in Table 2.27.

Table 2.27: Contributions

Result section	Partly performed by	Reference
3.1.1 <i>Beat</i> mutant alleles	Anna van de Venn	(Venn, 2012)
3.3 Side is constitutively expressed in larvae	Anne-Marie Bösenberg	(Bösenberg, 2016)
3.4 Beat expression during embryogenesis	Valentina del Olmo-Toledo	(del Olmo-Toledo, 2014)
3.7 Side and Beat deletion and fusion constructs	Vera Kühlmann Valentina del Olmo-Toledo	(Kühlmann, 2012; del Olmo-Toledo, 2014)
3.8 Larval innervation defects	Anne-Marie Bösenberg Vera Kühlmann Valentina del Olmo-Toledo Anna van de Venn	(Bösenberg, 2016; Kühlmann, 2012; del Olmo-Toledo, 2014; Venn, 2012)
3.9 Analysis of the Beat expression pattern	Valentina del Olmo-Toledo Anna van de Venn	(del Olmo-Toledo, 2014; Venn, 2012)
3.12 Interaction of Beat and Side <i>in vivo</i>	Anne-Marie Bösenberg Anna van de Venn	(Bösenberg, 2016; Venn, 2012)

3 Results

3.1 Side and beat mutant alleles

In two different forward mutagenesis screens using ethyl methanesulfonate (EMS) exposure, novel genes have been identified which are important for the correct formation of neuromuscular junctions (NMJs). Among these, four *beat* alleles (*beat*¹, *beat*², *beat*³ and *beat*^{*tric-1*}) and eight *side* alleles (*side*^{C137}, *side*^{D282}, *side*^{D609}, *side*^{H143}, *side*^{I1563}, *side*^{I306}, *side*^{K717} and *side*^{P45}) have been discovered (Aberle et al., 2002; Sink et al., 2001; Van Vactor et al., 1993). As EMS is known to induce point mutations, all available alleles have been sequenced in order to identify the underlying point mutations. Mutated alleles, which do not exhibit stop mutations, can give valuable hints at structurally or functionally important domains of Beat and Side.

3.1.1 Beat mutant alleles

As it was not possible to obtain all different mutant alleles, the *beat* mutations in the alleles *beat*² (sequenced in this work together with A. van de Venn (Venn, 2012)) and *beat*³ (sequenced by A. Bauke and reviewed in this work) have been sequenced. The deletion in *beat*^{C163} (Fambrough and Goodman, 1996) has been described before as gene inversion (Ashburner et al., 1999) and is also specified in Figure 3.1. *Beat*³ reveals a point mutation in the codon for lysine at position 235 causing a premature stop signal (AAG → TAG). *Beat*² exhibits a point mutation of the splice donor site directly downstream of exon 4 (GT → AT). The consequences have been evaluated on mRNA level. Sequencing of *beat*² cDNA obtained from homozygous L3 larvae showed that 108 base pairs of the coding sequence of exon 4 are lost on mRNA level. There is no frameshift emerging from this mutation. The modification on mRNA level results in an according loss of the 26 amino acids G111 up to I136 within the first immunoglobulin domain of Beat.

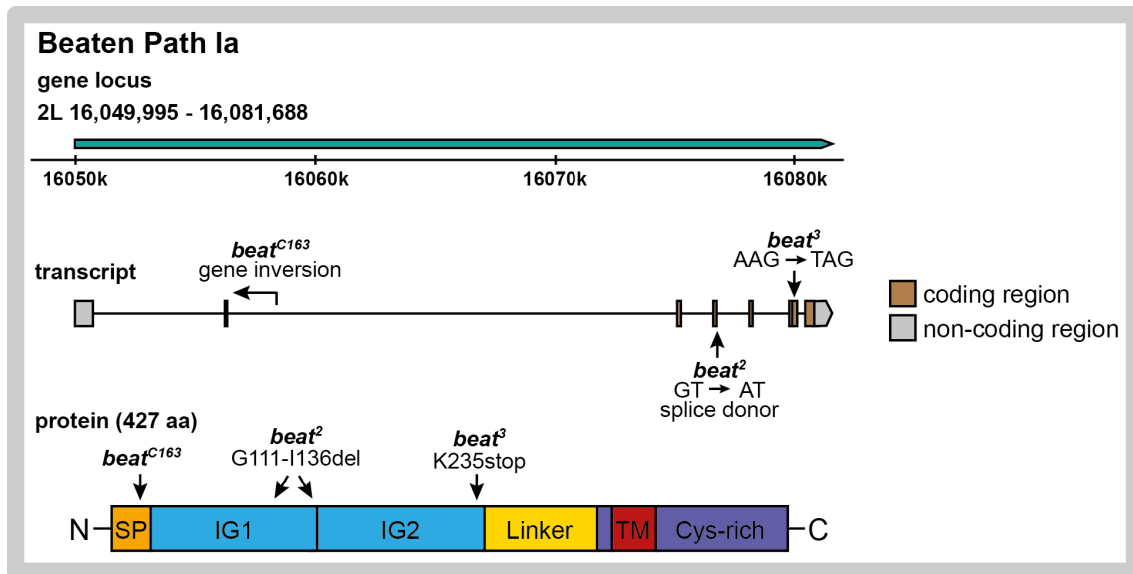


Figure 3.1: Survey of *beat* mutant alleles.

Beat^{C163} is characterized by a gene inversion in the second intron. This leads to a disruption of the Beat protein within the signal peptide. *Beat*² carries a point mutation of the splice donor site following exon 4 which results in alternative splicing within exon 4 and excision of amino acids 111 to 136 on protein level. *Beat*³ exhibits a point mutation, which causes a stop codon. The resulting *Beat*³ protein is thus reduced to 234 amino acids.

The nucleotide loss in *beat*² mRNA is probably due to the choice of a cryptic splice donor site (Roca et al., 2003) within exon 4, which is used in *beat*² as the original splice site consensus nucleotides MAGgttragt with M = A or C and R = A or G, according to the IUPAC nomenclature, capital letters = exon, small letters = intron, red = splice donor site (Mount et al., 1992). Here, the cryptic splice site would be CCGgttaaat and is thus close to the above mentioned consensus site.

3.1.2 Side mutant alleles

For *side*, the mutant alleles *side*^{C137}, *side*^{K717} (sequenced by H. Aberle and *side*^{C137} confirmed on mRNA level in this work), *side*^{I1563} and *side*^{I306} (sequenced by H. Aberle and confirmed in this work), as well as *side*^{D609} and *side*^{H143} (sequenced in this work) have been analyzed (Figure 3.2). Interestingly, it was possible to uncover two different amino acid exchange mutations in *side*^{I306} and *side*^{H143}. These mutations are located very close together within the C-terminal region of the first immunoglobulin domain and the linker domain separating the first and second immunoglobulin domain, respectively. *Side*^{I306} exhibits an exchange of the unpolar glycine to the polar aspartic acid within the first immunoglobulin domain. This glycine is highly conserved

in immunoglobulin domains of different molecules. *Side*^{H143} carries an exchange of the unpolar leucine to the polar, alkaline histidine in the linker between the first and second immunoglobulin domains. *Side*^{C137} harbors a mutation of the splice acceptor site upstream of exon 7 from AG → AA. Subsequent effects on transcription have been evaluated on mRNA level and reveal the deletion of the first nucleotide within exon 7, the G directly after the damaged splice site. The splicing machinery thus chooses as next available splice acceptor (indicated in red) the mutated A and the following G from exon 7. The splice site **cagGA** is accordingly degenerated into **caagA**. This leads to a frameshift of the reading frame of -1 in the transcript and a subsequent stop codon. The resulting amino acid sequence following the D376T mutation is GISQRVS* in the *Side*^{C137} protein. All other sequenced alleles contain a stop mutation within the extracellular domain of *Side* (see Figure 3.2), producing a truncated and secreted version of *Side*.

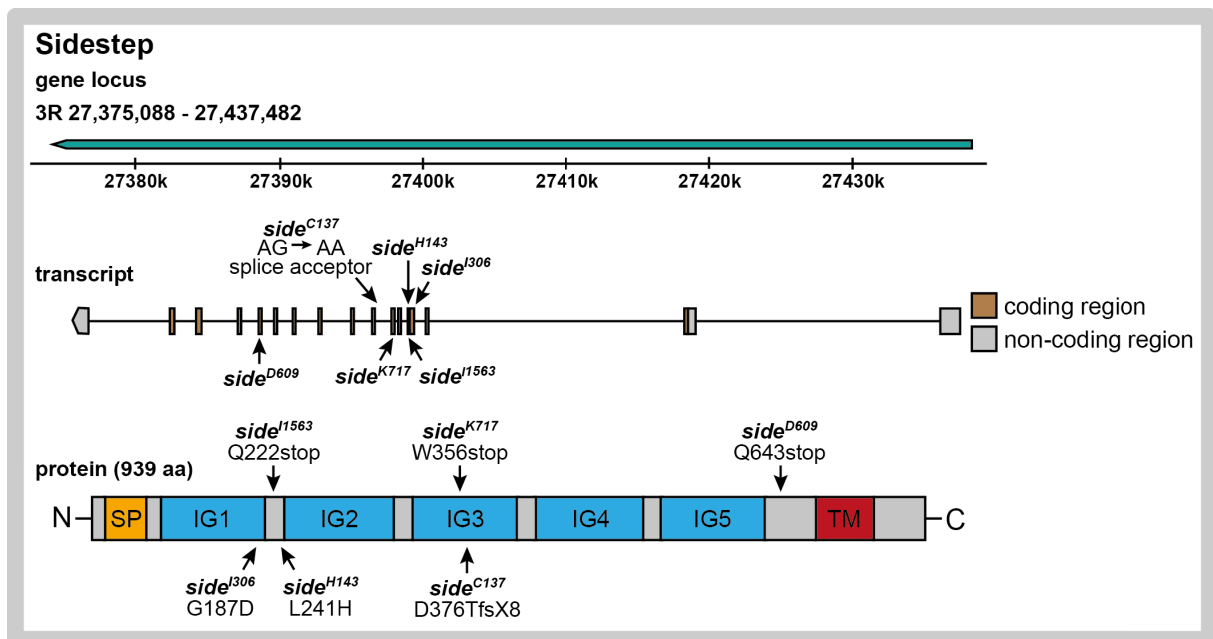


Figure 3.2: Characterization of *side* mutant alleles.

Side^{I306} and *side*^{H143} exhibit a single amino acid exchange mutation at position 187 and 241, respectively. *Side*^{C137} yields a splice acceptor mutation resulting in a frameshift and prompt protein truncation after seven amino acids. *Side*^{I1563}, *side*^{K717} and *side*^{D609} carry a stop mutation within the extracellular domain of *Side*.

Complementary analyses evaluating the extent of innervation defects caused by the combination of different *side* mutant alleles in third instar larvae were performed (data not shown). Complementation of *side*^{I306} and *side*^{H143} yielded weaker defects than in all other combinations of the *side* mutant alleles, indicating a small portion of

residual protein function and thus supporting the above findings of single amino acid exchanges.

In order to assess a potential influence of the mutations *side*^{I306} and *side*^{H143} on a binding pocket or the 3D structure of the protein, the protein structure was modeled using RaptorX structure prediction (Källberg et al., 2012). The highly conserved glycine at position 187 is predicted to be part of a β -sheet and is positioned right next to a turn disrupting the β -sheet (Figure 3.3, A'). According to the calculation, the structures of both the β -sheet and the turn region remain unaffected in *side*^{I306} (Figure 3.3, B'). Interestingly, the L241H mutation in *side*^{H143} is predicted to result in a conformational change into a helix at amino acids 183-185 (see purple structure in Figure 3.3, C'), very close to the G187.

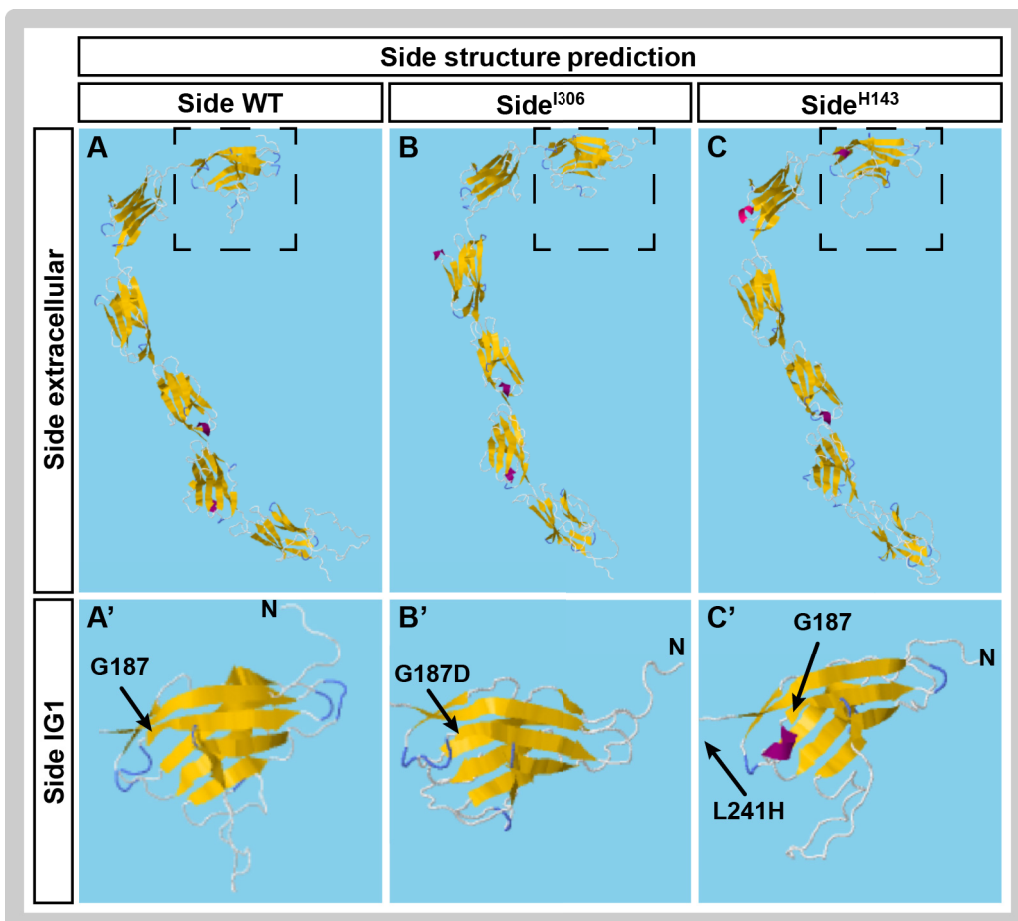


Figure 3.3: Structure prediction of Side.

The predicted effect of the amino acid exchange mutations on the protein structure of the first immunoglobulin domains in Side^{I306} and Side^{H143} are depicted (Källberg et al., 2012). Modeled protein structure of wild-type Side (A), Side^{I306} (B), Side^{H143} (C) and a magnification of the respective first immunoglobulin domain (A'-C').

3.2 Side expression during embryonic development

Due to its role as motor axonal guidance cue, Side is expressed in a spatially and temporally highly dynamic expression pattern during embryogenesis. Co-staining of motor axons and Side in FasII-GFP^{Mue397} exon trap embryos in previous studies showed that Side-signal is detectable just ahead of the navigating growth cones of motor axons during embryogenesis (Siebert et al., 2009).

Immunohistochemical stainings have been performed in order to assess a possible Side expression in *side* mutant embryos as well as in *beat* mutant embryos (Figure 3.4). According to the previously described Side expression pattern (Siebert et al., 2009; Sink et al., 2001), Side expression at embryonic stage 12 (Figure 3.4, A) is localized in glia cells flanking the ventral midline. In stage 13-14, Side is expressed on afferent sensory neurons (Figure 3.4, B). At stage 15, Side-signal becomes downregulated (Figure 3.4, C) and almost no Side-signal is detectable in stage 16-17 embryos (Figure 3.4, D), although Sink and colleagues reported Side expression in the muscles during this embryonic stage (Sink et al., 2001). *Beat* mutant embryos exhibit constitutive Side expression. In *beat*^{C163}, the Side expression pattern looks quite wild-type up to stage 14 and then fails to get downregulated (Figure 3.4, H). Similar, in *side*^{I306} and *side*^{H143}, both alleles harboring an amino acid exchange mutation, Side expression is very well detectable. *Side*^{H143} displays a more globular distribution of the Side-signal compared to the wild-type (arrows in Figure 3.4, I-L). Through stages 15-17, Side remains on neurons and is only slightly downregulated (Figure 3.4, L). *Side*^{I306} exhibits a signal very comparable to the wild-type up to stage 14 (Figure 3.4, M-N). In later stages, Side remains weakly, constitutively expressed (Figure 3.4, O-P). Still, the constitutive Side expression is stronger in *beat* mutant embryos than in *side*^{H143} or *side*^{I306} mutant embryos. Immunohistochemical stainings of *side*^{C137}, *side*^{I1563}, *side*^{D609} and *side*^{K717} mutant embryos show that no Side-signal is detectable in these homozygously mutant embryos and that the anti-Side antibody is thus not able to bind its epitope (Figure 3.4, Q-R). In contrast, heterozygous embryos carrying the fluorescent TM3, twist-GFP balancer, exhibit Side-signal (Figure 3.4, S-T).

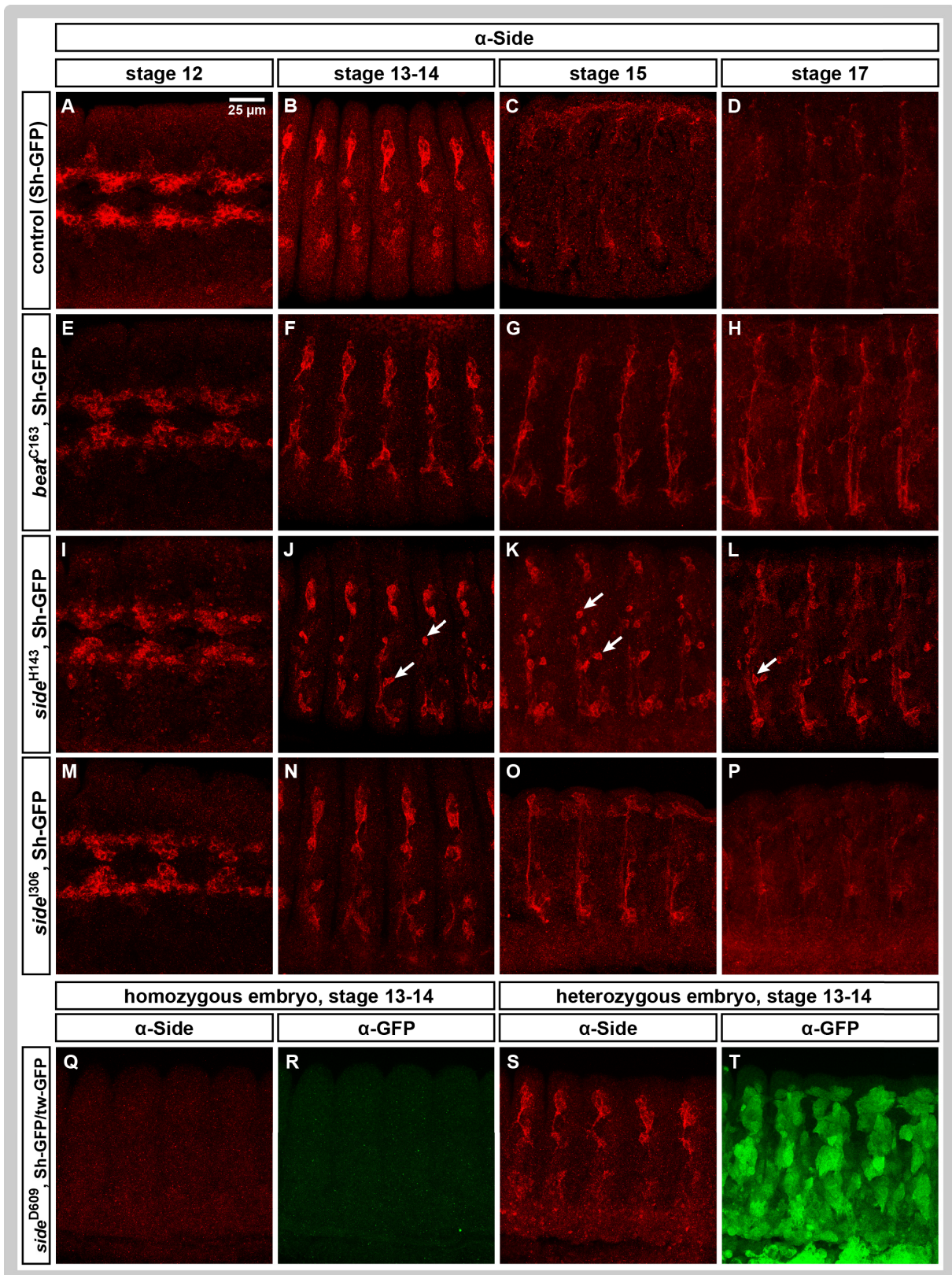


Figure 3.4: Side is constitutively expressed in *side* and *beat* mutant embryos.

Confocal images of embryonic, immunohistochemical stainings against Sidestep in wild-type and different, homozygously mutant alleles are shown. Side is expressed in a spatio-temporal highly dynamic pattern during embryogenesis. A-D: Wild-type Side expression starts at stage 12 in glia cells flanking the ventral midline (A). This expression becomes downregulated and instead sensory neurons commence to express Side at stage 13 (B). At stage 15, this expression starts to be downregulated (C) and late-stage embryos exhibit only very weak Side-signal (D). E-H: *Beat*^{C163} homozygous embryos display Side expression, which is very prominently visible on sensory neurons in late stages.

Results

I-L: *Side*^{H143} homozygous embryos display Side-signal, yet the expression pattern looks more cellular than in control embryos (arrows). In stage 17 embryos, the Side-signal is not downregulated. M-P: Young *side*^{I306} homozygous embryos up to stage 14 exhibit Side expression in the same manner as the control embryos. In late embryos, Side remains weakly expressed. Q-R: Homozygous *side*^{D609} mutant embryos, characterized by the lack of twist-GFP, do not exhibit Side-signal. S-T: Heterozygous embryos display both Side expression and twist-GFP expression. The confocal images in this and all following figures are maximum intensity projections and the orientation of the animals is dorsal up and anterior to the left.

Co-stainings with anti-Side and anti-Ank, a marker for motor- and sensory neurons, demonstrate that the ongoing Side expression in *side* and *beat* mutants co-localizes with the sensory neurons (see Figure 3.5). In *side*^{H143} mutant embryos, the Side protein seems to be localized in the membrane of the cell bodies and may not be properly transported into the sensory axons as it is the case in wild-type animals (see Figure 3.5, A-A').

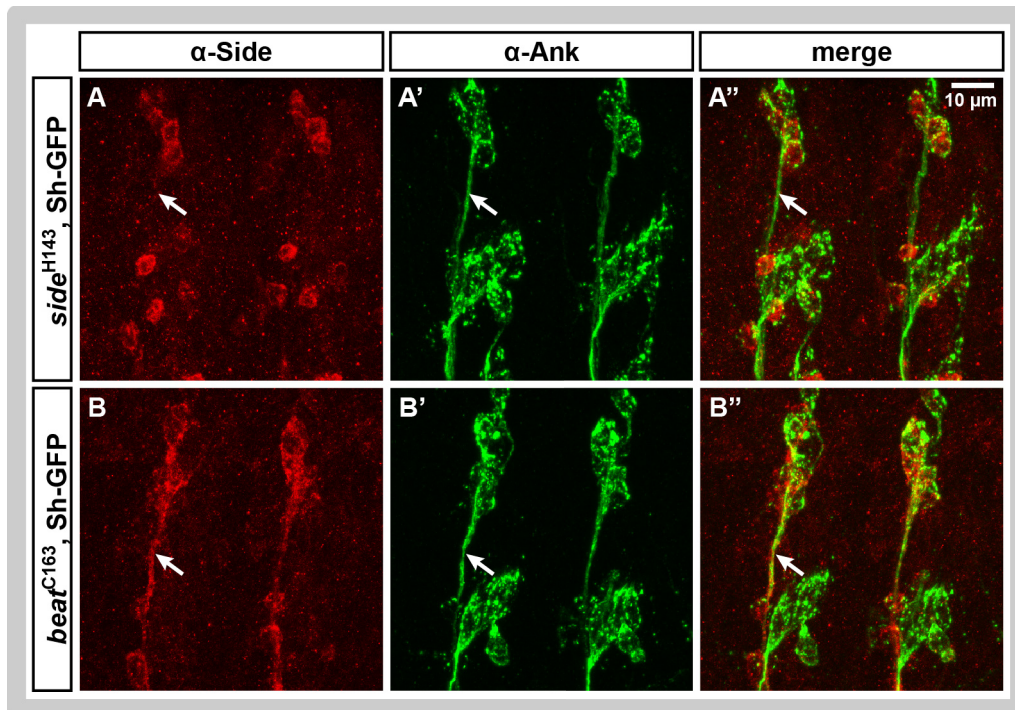


Figure 3.5: Side^{H143} protein is restricted to the cell bodies.

Co-stainings of stage 15 embryos with anti-Side and anti-Ank are depicted. A-A'': *Side*^{H143} homozygous embryos exhibit a cellular pattern of Side expression. B-B'': In *beat*^{C163} embryos, sensory neurons and their axons express Side.

Further demonstration of the lack of Side protein in some of the *side* mutant alleles has been performed by western blot analysis (Figure 3.6). The molecular weight of Side protein is predicted at 102 kDa. Embryos, which overexpress Side muscle-specifically as well as wild-type embryos provide a clear band at about 112 kDa and an additional signal at approximately 47 kDa. Homozygously mutant *side*^{I306} and

Results

side^{H143} embryos exhibit strong Side-signal at 112 kDa as well as the additional, lower band. Interestingly, embryos homozygous for the *side* mutant genotypes *side*^{C137}, *side*^{I1563}, *side*^{D609} and *side*^{K717} do not exhibit the Side-signal at 112 kDa but clearly show the lower band.

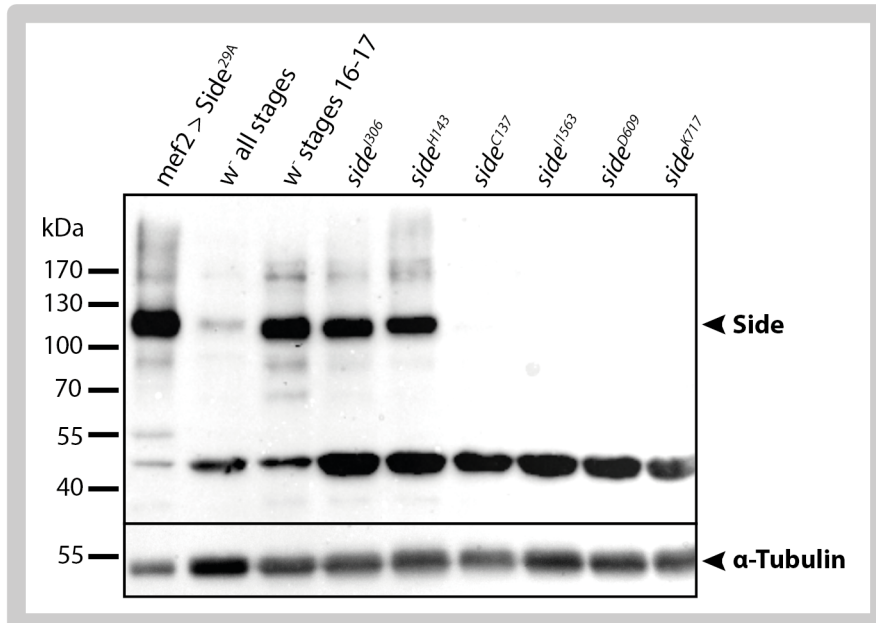


Figure 3.6: Side expression is not detectable in *side* mutant embryos, which contain a protein truncation.

A Western Blot analysis of homozygous embryos is depicted. Side-signal is detected at about 112 kDa. Older embryos exhibit stronger Side-signal compared to embryos of all stages. *Side*^{I306} and *side*^{H143} alleles exhibit Side-signal, whereas *side*^{C137}, *side*^{I1563}, *side*^{D609} and *side*^{K717} are negative for Side immunodetection. Besides, all different genotypes reveal a band at about 47 kDa.

Immunohistochemical stainings show that Side is downregulated in wild-type embryos in late developmental stages (Figure 3.4, D). Remarkably, western blot immunodetection reveals an increase of Side protein in stage 16-17 embryos (Figure 3.6, lane 2 and 3). The blot against α-Tubulin represents the amount of protein lysate loaded onto the gel and illustrates that the lysate from mixed embryonic stages (lane 2) was even employed in a higher concentration than the lysate from old embryonic stages and thus increases the difference of relative protein amount even more.

Taken together, the immunohistochemical stainings and western blot analysis support the sequencing results of milder mutations in the *side*^{I306} and *side*^{H143} alleles and the more drastic stop mutations found in *side*^{C137}, *side*^{D609}, *side*^{I1563} and *side*^{K717} mutant alleles. Furthermore, western blot analysis of old embryos revealed a high amount of Side protein. This finding might indicate that the epitope for the anti-Side antibody is being masked in late embryonic stages.

3.3 Side is constitutively expressed in larvae

Side occupies a crucial role in axon guidance during embryogenesis. The above western blot findings of increased Side protein level in late embryonic stages contradict the previously described downregulation of Side (Siebert et al. 2009). Larval Side expression has not been reported in the past, although our working group found evidence for a crucial function of Side during metamorphosis for the establishment of the correct motoneuronal wiring of the adult fly (Kinold, 2016). The endogenous Side protein level in different tissues of L3 larvae was therefore further analyzed by western blot (Figure 3.7).

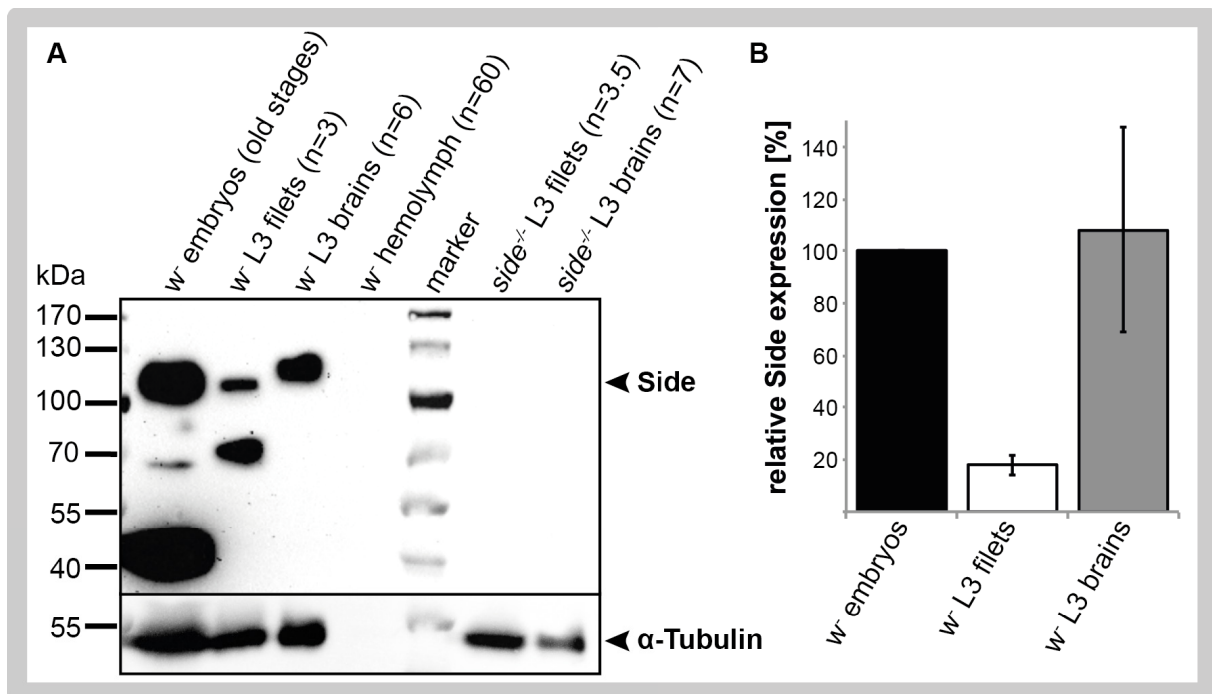


Figure 3.7: Western blot analysis reveals ongoing Side expression in L3 larvae.

Western blot analysis of embryos and larval tissues (L3) is shown. A: Side-signal can be strongly detected in stage 14-17 embryos. Larval filets and brains also exhibit Side-signal. In the larval hemolymph fraction containing secreted proteins, no Side expression can be detected. *Side*^{C137/11563} trans-heterozygous larvae do not exhibit protein expression. B: Quantification of the relative Side protein expression shows that Side expression in muscles is decreased, whereas Side expression in the brain remains elevated compared to the embryonic expression (n=2).

These experiments show that Side is persistently expressed in third instar larvae. Compared to late embryonic stages, Side expression is detectable, but reduced in larval filets consisting of muscle tissue and dermis (Figure 3.7 A, lane 2). The larval brain exhibits higher amounts of Side protein than the muscles (Figure 3.7 A, lane 3). Endogenous Side protein as well as α -Tubulin is not detectable in the hemolymph fraction, which contains secreted proteins (Figure 3.7 A, lane 4). *Side*^{C137/11563} trans-

heterozygous larvae serve as negative control and do not exhibit Side expression (Figure 3.7 A, lanes 4 and 5). Quantification of the relative Side expression (data from 2 individual western blots and normalized against α -Tubulin) confirms the tendency that larval brains exhibit similar amounts of Side as old embryos, whereas the expression level is decreased in larval muscles. Together with the results from A. Bösenberg, who detected endogenous Side protein also in first instar larvae in western blot (Bösenberg, 2016), these findings demonstrate that Side is constitutively expressed from embryonic development onwards up to third instar larvae. Here, Side is enriched in neuronal tissue.

To date, Side expression is not described in the literature. Still, Side is detectable as pattern of small dots at the synapse in third instar larvae in wild-type as well as Side mutant larvae (Figure 3.8, B-B''). However, the experiments described above have revealed a big discrepancy in late stage embryos between immunohistochemical Side protein detection and the detection of Side by western blot analysis. In order to further elucidate the larval expression pattern, a Side-GFP exon trap was utilized. The anti-Side antibody binds to an epitope in the extracellular domain of Side, whereas the GFP in the Side-GFP exon trap line is localized in the intracellular part of the protein. The GFP-signal of these embryos covers exactly the anti-Side-signal (Föhrenbach, 2016) and is specifically detectable in stage 17 embryos, where the anti-Side-signal is downregulated.

Intact, whole mount Side-GFP larvae exhibit only very little GFP-signal in the brain. Therefore, co-stainings with anti-GFP and anti-FasII (motor axons) were performed on larval filets and showed that GFP-signal of this exon trap line is detectable in the brain, marking the neuropil with the central synapses (Figure 3.8, A-A''). Further co-stainings of this genotype with anti-Side and anti-GFP showed complete overlap of the Side and GFP-signal in the brain (data not shown), thereby sustaining the western blot findings of high levels of Side protein in the larval brain. By contrast, the clustered Side-signal at the neuromuscular junction is not detected by the anti-GFP antibody.

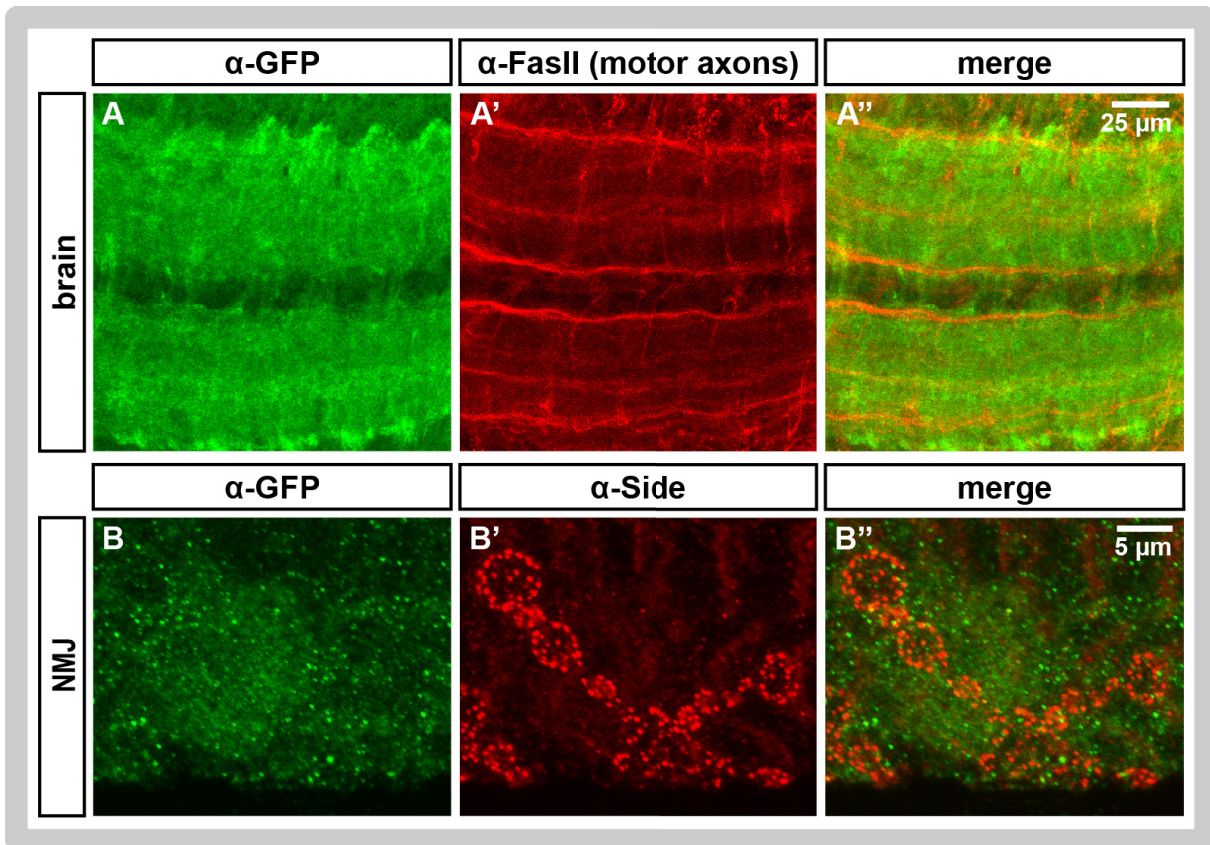


Figure 3.8: Side is constitutively expressed in the CNS of L3 larvae.

Confocal images of larval Side-GFP filets. A-A'': The neuropil in the brain exhibits specific GFP-signal. B-B'': The NMJs exhibit a clustered Side-signal. This signal is not reflected by the GFP-staining of the exon trap line.

3.4 Beat expression during embryogenesis

Beat is described to be expressed in cell bodies of the aCC and RP motoneurons, motor axons and growth cones (Fambrough and Goodman, 1996). Since there is no anti-Beat antibody commercially available, Beat antisera (directed against the linker region and the cys-rich domain of Beat, respectively) were produced in the context of this work (see Chapter 2.2.4.1) and examined for their specificity. Another Beat antiserum, which had been produced by A. Bauke during her master thesis, was also tested. The Beat antisera were examined in immunohistochemical stainings of embryos and in western blots.

Among the antisera directed against the Cys-rich domain of Beat, only the one generated in rabbit provides distinct signal motor axons, growth cones and sensory neurons. Although the tested preimmune serum does not exhibit specific signal in motor axons, overexpressed Beat is not specifically recognized and *beat* mutant embryos exhibit the same axonal staining. This antiserum thus lacks specificity.

Regarding the antisera directed against a peptide fragment of the Linker domain of Beat, the antibody produced in guinea pig, but not the one from rabbit, yields weak, distinct signal in motor axons with an enrichment of the signal in the growth cones (Figure 3.9, A-A''). Moreover, this antiserum recognizes muscle-specifically overexpressed Beat (Figure 3.9, B-B). However, *beat*^{C163} homozygously mutant embryos exhibit a similar weak staining of motor axons and growth cones as wild-type embryos (data not shown). Immunohistochemical stainings with the rabbit anti-Beat-Linker antiserum generated previously by A. Bauke do not provide any signal (data not shown).

The different antisera were further evaluated by western blot analysis. These studies were completed together with V. del Olmo-Toledo (del Olmo-Toledo, 2014). Only the guinea pig anti-Beat-Linker and the Beat antiserum generated by A. Bauke exhibit specific signal. Both antisera detect one distinct, intense band at about 38 kDa, which is exclusively detectable in the muscle-specific overexpression of Beat⁵. This band is not detectable in western blot against the guinea pig preimmune serum (data not shown). However, the expected molecular weight for the unprocessed Beat is about 48 kDa. Fambrough and Goodman reported a Beat signal for their anti-Beat antiserum at 43 kDa (Fambrough and Goodman, 1996).

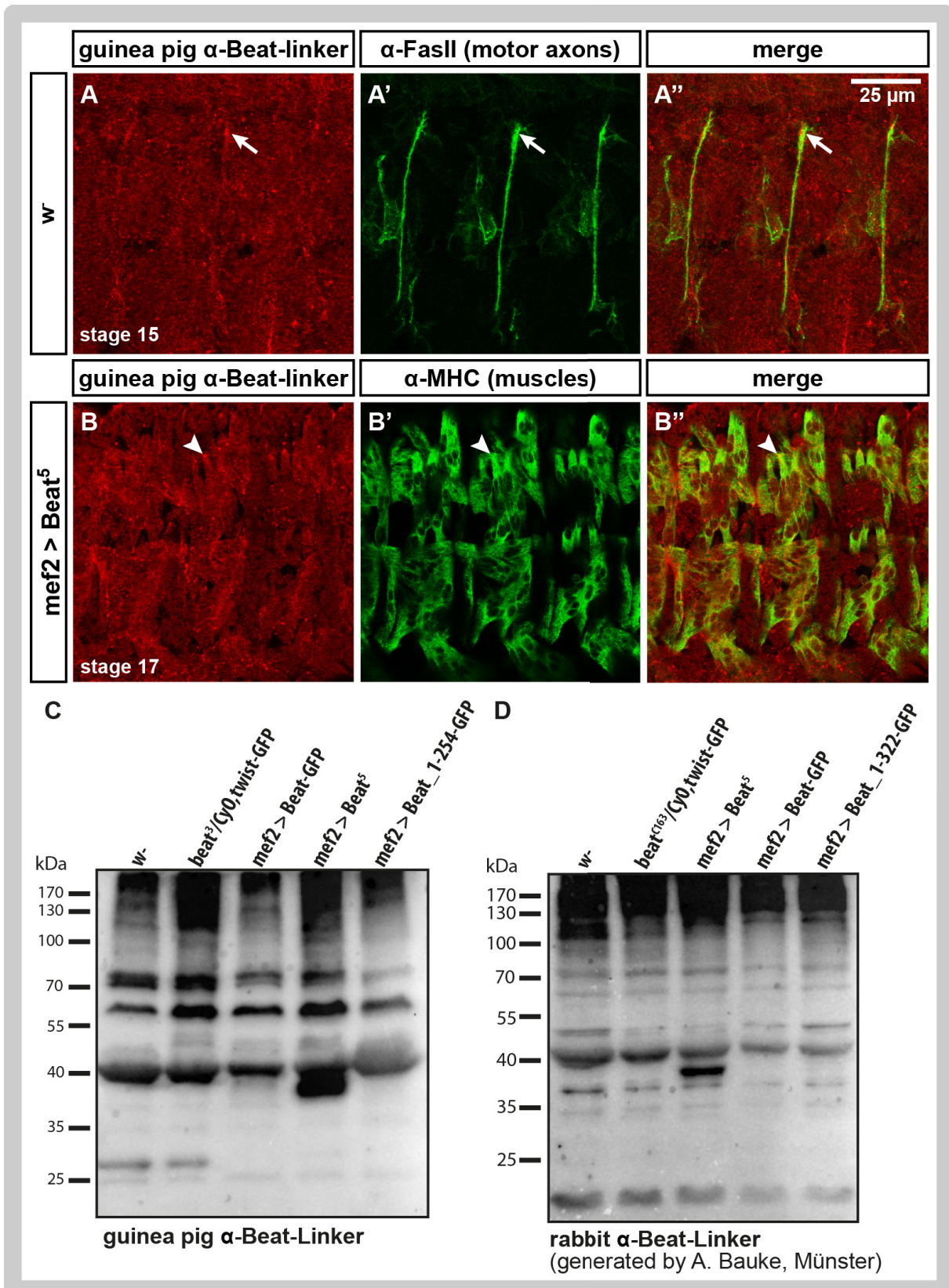


Figure 3.9: Guinea pig anti-Beat-Linker antiserum recognizes overexpressed Beat⁵.

Confocal images of embryos co-stained with anti-Beat-Linker antiserum as well as anti-FasII and anti-MHC, respectively, are depicted. A-A'': The Beat antiserum weakly labels embryonic motor axons. The signal is enriched in growth cones (arrows). B-B'': Muscle-specific overexpression of untagged Beat leads to staining of muscles (arrowheads). C-D: Both guinea pig anti-Beat-Linker and rabbit anti-Beat-Linker (Bauke, 2009) provide one specific band at about 38 kDa in the muscle-specific overexpression of the untagged full-length Beat.

3.5 *Side attracts motor axons*

The guidance molecules *Side* and *Beat* are essential for correct motoneuronal wiring. As Siebert and colleagues have shown, *Side* attracts motor axons towards their target cells (Siebert et al., 2009).

Here, the impact of *Side* loss of function versus *Side* gain of function on motor axons is illustrated in late embryos. In wild-type embryos, the motor axons grow out regularly and straight (Figure 3.10, A). At the end of embryogenesis, the motor axons have reached the dorsal muscle field. If *Side* is overexpressed muscle-specifically in early embryonic stages using the driver line *mef2-Gal4* (gain of function), the motor axons are prematurely drawn into the developing muscle fields. The dorsal muscle field remains uninervated (Figure 3.10, B). In *side* mutant embryos (loss of function), motor axons cannot grow out in a coordinated manner but display different guidance defects (Figure 3.10, C). Frequent pathfinding errors are defasciculation defects resulting in bypassing of the ventral muscle field, crossing of the hemisegmental boundary or stalling of motor axons.

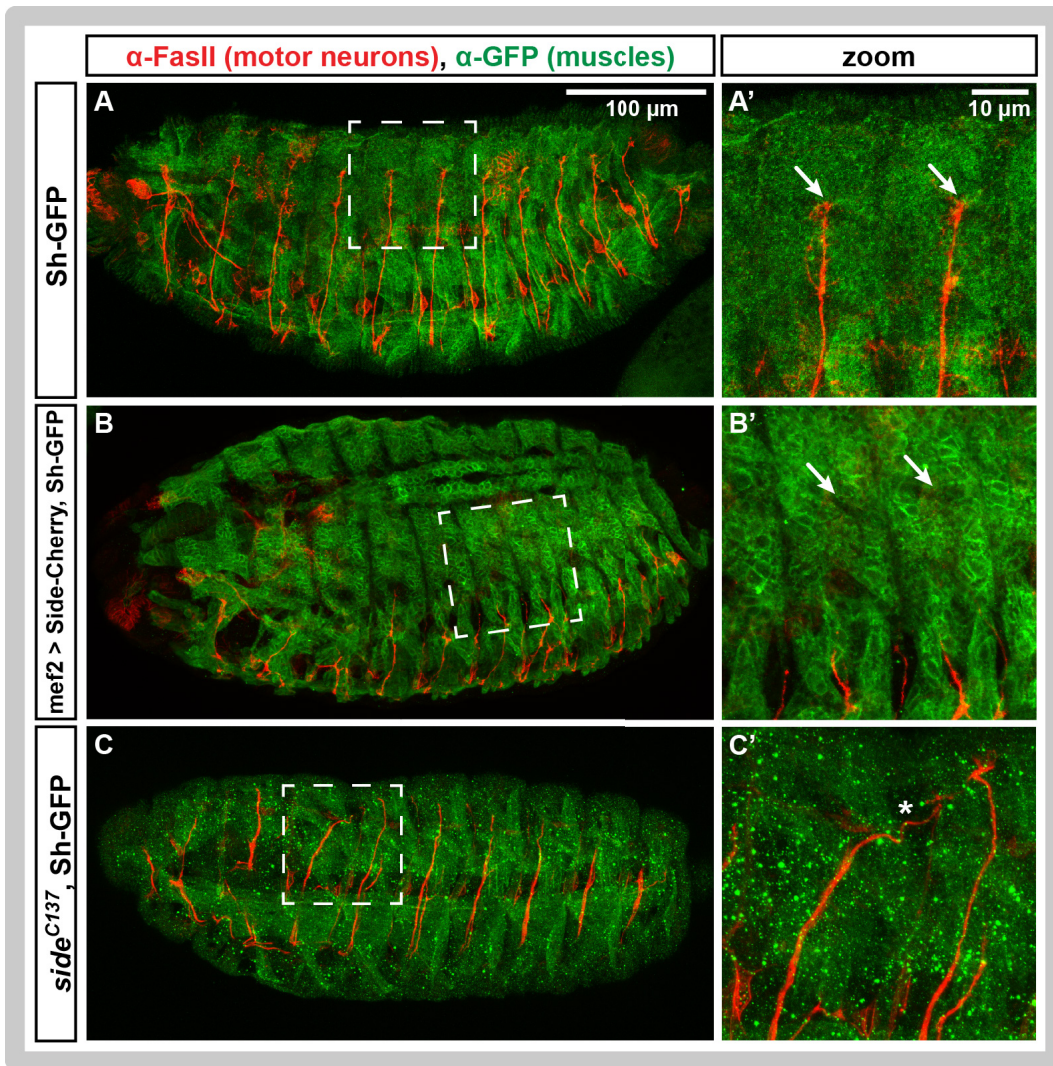


Figure 3.10: Overexpressed Side prematurely attracts motor axons.

Antibody staining of stage 17 embryos with anti-FasII and anti-GFP are shown. A-A': In wild-type embryos, motor axons grow out straight and reach the dorsal muscle field. B-B': Early, muscle-specific overexpression of Side prematurely attracts growth cones and motor axons thus constantly fail to innervate the dorsal muscles. C-C': In *side* mutant embryos, motor axons display various guidance defects. Arrows indicate dorsal muscles 9 and 1. The asterisk marks segmental border crossing of motor axons.

FasII is an axon guidance molecule, which mediates homophilic binding of motor axons. *FasII* loss of function mutant embryos exhibit defects in axon fasciculation (Grenningloh et al., 1991). FasII gain of function embryos with neuronal overexpression of FasII show axonal bypass, detour and stall phenotypes (Lin and Goodman, 1994).

The influence of the fasciculation molecule FasII was tested and evaluated in comparison to the premature attraction of motor axons mediated by Side overexpression. As immunohistochemical anti-FasII staining does not allow for visualization of motor axons in the background of muscle-specific FasII-overexpression, embryos of the FasII-GFP^{Mue397} exon trap were utilized to specifically

mark motor axons (Figure 3.11). Compared to control embryos, muscle-specific overexpression of FasII does not induce premature attraction of motor axons. These findings were also confirmed in larvae (data not shown).

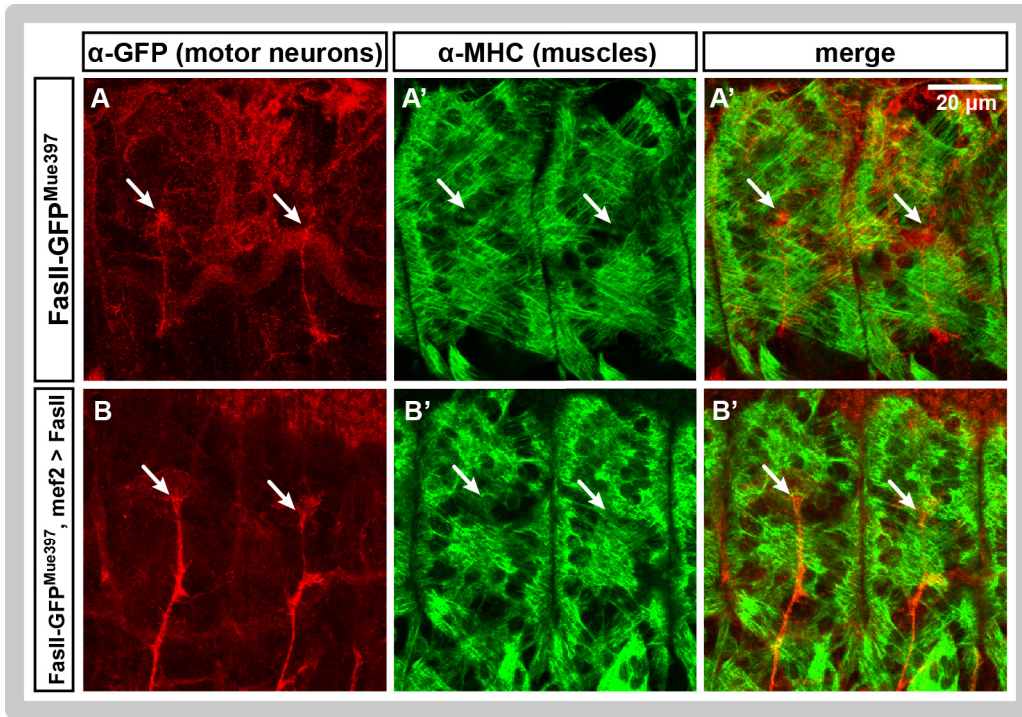


Figure 3.11: Overexpressed FasII does not attract motor axons.

Confocal images of dorsal muscles of stage 17 embryos are shown. A-A'': In control FasII-GFP exon trap embryos, motor axons reach the dorsal muscle field. B-B': Muscle-specific overexpression of FasII does not divert ISN motor axons from their pathway. The arrows indicate the growth cones of the ISN which have reached the dorsal-most muscles 1 and 9.

The muscle-specific overexpression of the adhesion molecule FasII, which is expressed on motor axons and mediates their fasciculation by homophilic binding, is thus not able to prevent motor axons from reaching the dorsal-most muscles. This reinforces the special role of Side to irreversibly attract motor axons and demonstrates the specific and very strong attraction of Side on motor axons.

3.6 Overexpression of Side induces synaptogenesis

The muscle-specific overexpression of Side does not only prematurely draw motor axons into the ventral muscle field, but also induces the formation of ectopic NMJs. Figure 3.12 illustrates how motor axons actively search for synaptic partners by growing along the muscles not straight forward as in the wild-type (see Figure 3.10), but take their route in a curved fashion.

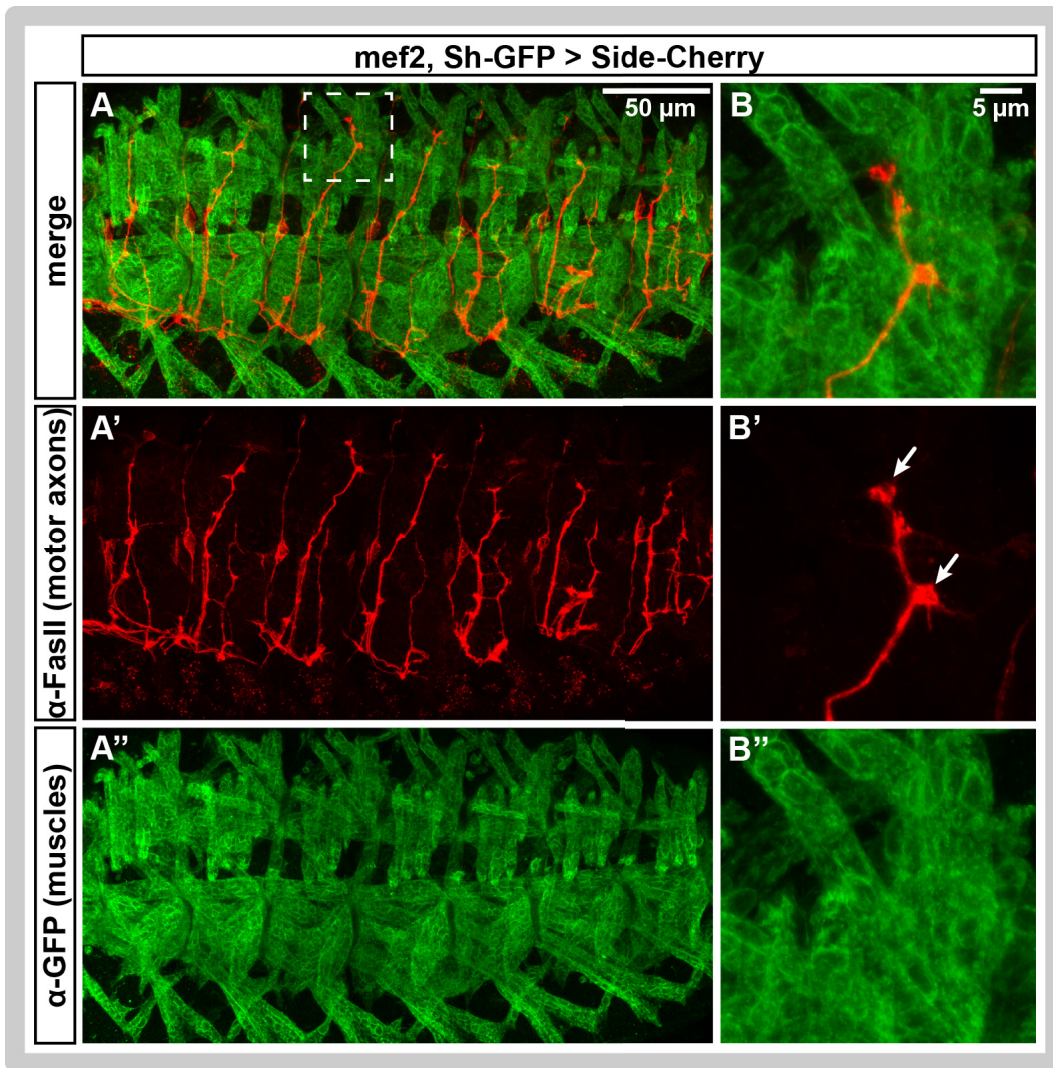


Figure 3.12: Overexpression of Side-Cherry draws axons into the ventro-lateral muscle field and induces the formation of ectopic synapses.

Confocal images of a stage 17 embryo, muscle-specifically overexpressing Side-Cherry. A-A'': Motor axons do not reach the dorsal muscle field but grow along the ventral and lateral muscles searching for synapse partners. B-B'': Motor axons form ectopic innervations on ventral and lateral muscles.

These ectopically formed synapses persist in third instar larvae. Figure 3.13 shows a ventral segment with normal innervation (A), the typical *side* mutant bypass phenotype due to embryonic defasciculation defects (B) and specific Side overexpression on muscle 12 in a *side* mutant background (C). The specific Side overexpression demonstrates that on muscle 12, ectopic NMJs are established and maintained. Remarkably, ectopic Side expression is able to overcome the habit that motor axons of a given bouton type can only once innervate each muscle. In the case of muscle 12 specific Side overexpression in an otherwise *side* mutant background, several type I NMJs, marked by Sh-GFP, are formed on muscle 12.

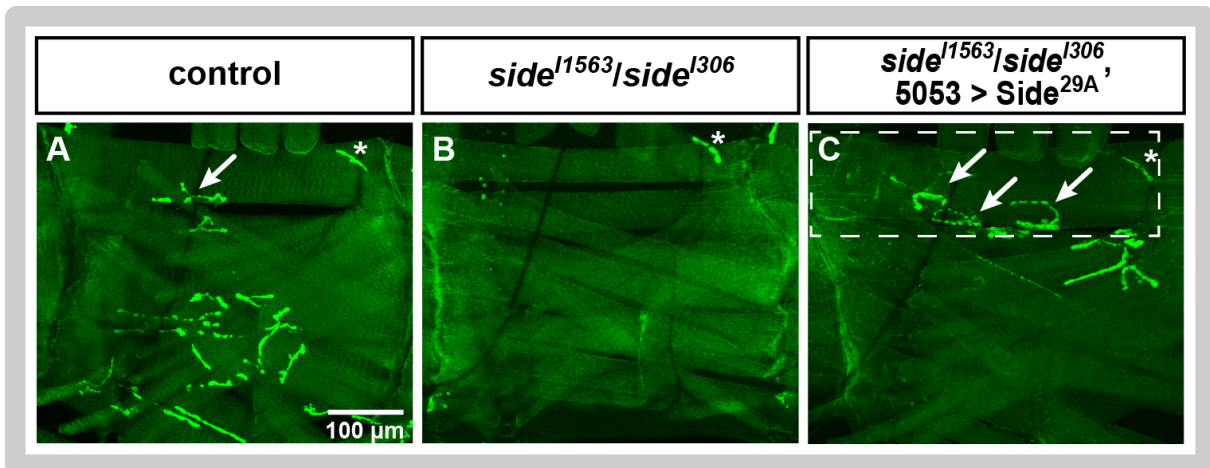


Figure 3.13: Side overexpression specifically induces synaptogenesis.

Wholemount preparations of Side loss- and gain of function L3 larvae are shown. Postsynapses are labeled with Sh-GFP. Arrows mark NMJs on muscle 12 and asterisks mark the NMJ of muscle 5, which is located diagonally to muscle 12 and is partly not visible due to microscope settings. A: Wild-type innervation pattern of the ventral muscle field. B: Drastic ventral bypass phenotype in a *side* mutant larva, leading to complete lack of innervation in this ventral hemisegment. C: Specific Side overexpression on muscle 12 in a *side* mutant background leads to the establishment of multiple NMJs on muscle 12 (marked by the dashed square), whereas the rest of the ventral muscle field exhibits typical *side* mutant innervation defects.

3.7 Side and Beat deletion and fusion constructs

In order to test the impact of modifications of different domains of Beat and Side proteins *in vivo*, different fluorescently labeled constructs were designed and transgenic fly stocks were generated. All constructs carry a UAS promoter and can thus be overexpressed in a tissue-specific manner *in vivo* using different Gal4 driver lines (see Chapter 2.2.1.4).

In order to assess the distribution of Beat in embryos and larvae, all Beat constructs (except for Beat⁵) were tagged with GFP (Figure 3.14). There are three full-length Beat constructs: The untagged Beat⁵, Beat-GFP and the doubly labeled GFP-Beat-Cherry. For the N-terminal deletion constructs as well as for GFP-Beat-Cherry, the endogenous signal peptide of Beat was employed in order to ensure the correct destination of the Beat protein. The gradually, C-terminally truncated constructs include deletions of different extents: a small part of the Cys-rich domain or the whole C-terminus up to the linker domain has been deleted in the different constructs. The respective construct designation bases on the amino acids of Beat present in this construct. The fusion construct BeatnewTM-GFP and the deletion construct Beat Δ TM-GFP are focused on the location of the putative transmembrane region at

position 324-343. The fusion constructs Beat₂₉₋₄₂₇-GFP and Beat₂₉₋₃₂₂-GFP contain an exogenous signal peptide to exclude the possibility of a second, yet undiscovered transmembrane anchoring in this region.

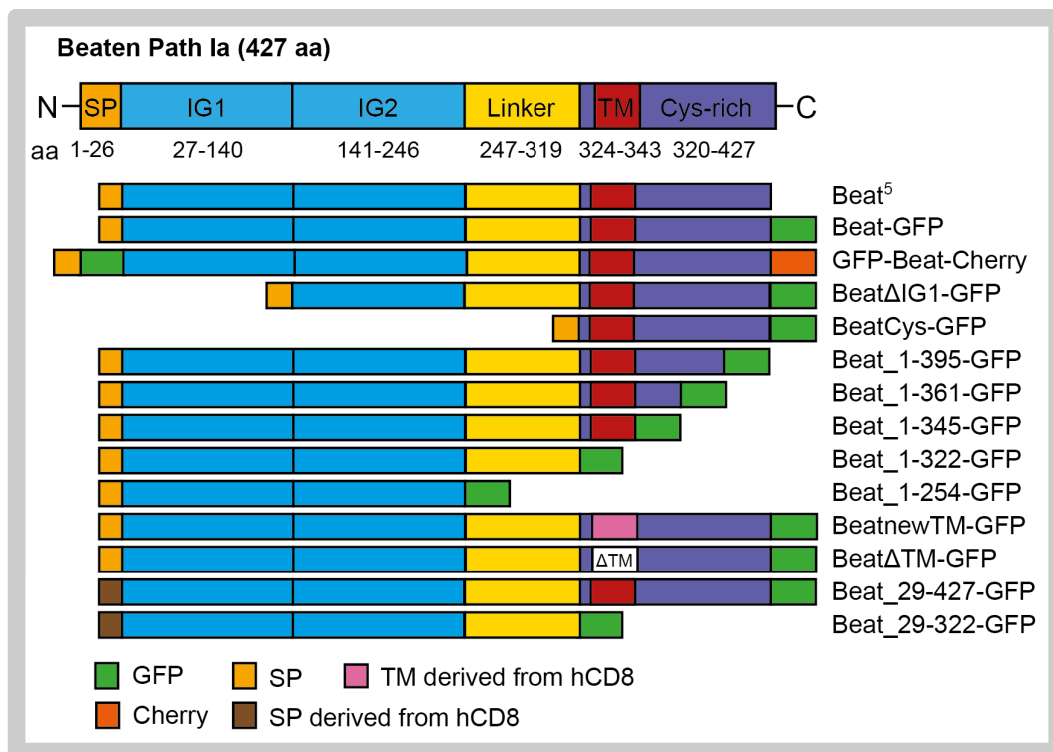


Figure 3.14: Schematic overview of the different Beat constructs.

The GFP-tagged Beat deletion and fusion constructs were integrated into the third chromosome. In the case of N-terminal modifications such as N-terminal deletion or the use of an N-terminal GFP-tag, the endogenous signal peptide (SP), marked in orange, was used to ensure correct direction of the construct. The endogenous transmembrane domain (TM) is labeled in dark red, whereas the transmembrane domain derived from hCD8 (used for BeatnewTM-GFP) is marked in pink. A signal peptide derived from hCD8, marked in brown, was used to assess whether the designated endogenous signal peptide holds any additional function.

Apart from the untagged full-length Side^{29A}, all other Side constructs were labeled with a C-terminal Cherry-tag (Figure 3.15). The doubly labeled GFP-Side-Cherry contains an additional N-terminal GFP-tag. Both GFP-Side-Cherry and SideΔIG1-Cherry contain the endogenous Side-signal peptide to ensure proper destination of the protein. In order to address the attractive effect of the first immunoglobulin domain (IG1) of Side on motor axons, the fusion constructs contain the Side IG1 fused to a spacer protein scaffold derived from the human CD8 (hCD8) and Fasciclin II (FasII), respectively. Both hCD8 and FasII are transmembrane proteins of the immunoglobulin superfamily. The human CD8 is a glycoprotein expressed on T-lymphocytes and mediates cell-cell contact. FasII is a *Drosophila* protein, which mediates fasciculation by homophilic binding of motor axons and thus also holds a

function in cell adhesion. Both proteins are good candidates to mediate the required stability in the cell membrane. As any possible attraction emanating from FasII should be ruled out, the FasII IG1 domain has been excised.

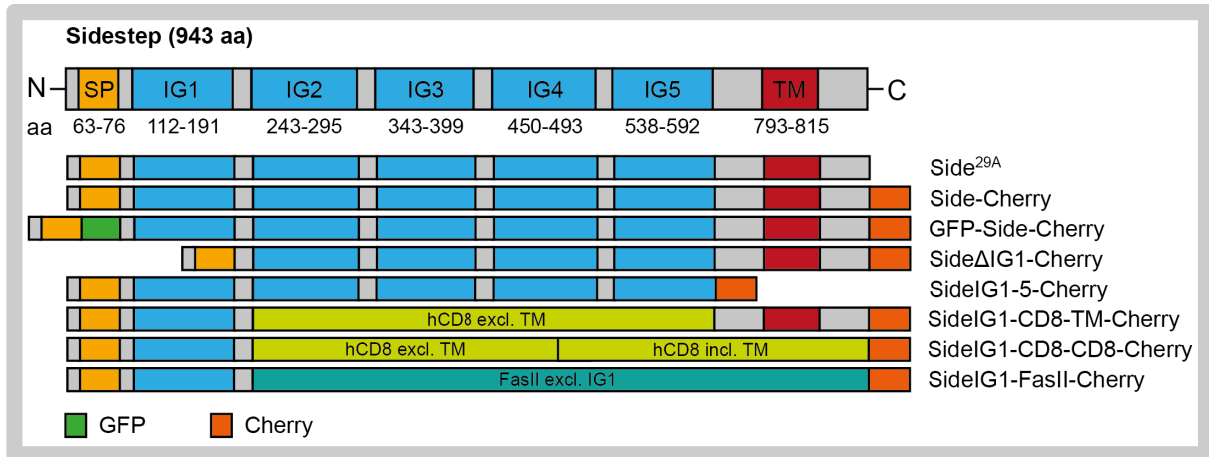


Figure 3.15: Side constructs.

Different, Cherry-tagged Side deletion and fusion constructs were integrated into the second chromosome.

3.8 Larval innervation defects

Embryonic pathfinding defects persist as larval innervation defects. *Side* and *beat* mutant animals as well as larvae overexpressing these guidance molecules exhibit severe innervation defects (Figure 3.18). In the case of *beat* mutant animals, the innervation phenotype can be rescued by presynaptic overexpression of full-length Beat cDNA (Figure 3.16). The innervation pattern was visualized using Sh-GFP, which marks muscles and postsynapses (see Chapter 1.3.1), by imaging intact L3 larvae. Estimation of the severity of innervation defects took place by fluorescent microscopy. During the bachelor thesis of A. Bösenberg (Bösenberg, 2016), the defects of some selected genotypes were counted and analyzed statistically.

3.8.1 Rescue of the *beat* mutant phenotype

The *beat* mutant phenotype can be rescued by presynaptic overexpression of full-length Beat cDNA. The functionality of different Beat constructs can thus be evaluated by their rescue ability regarding the innervation patterns of third instar larvae. Figure 3.16 shows a selection of different rescue genotypes. For facilitated comparison, representative images of the dorsal muscles 9/1 and 10/2 are depicted.

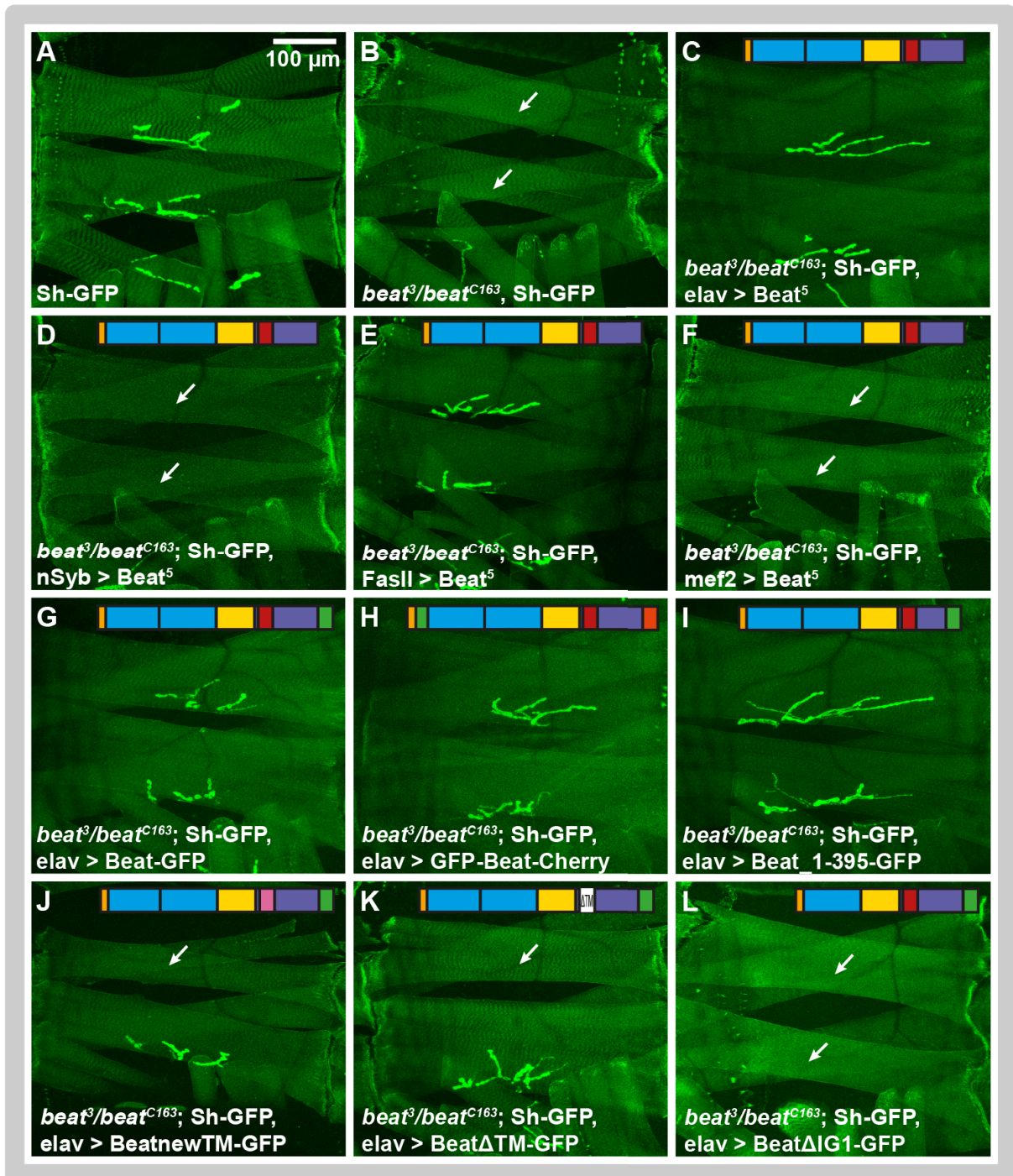


Figure 3.16: Presynaptic Beat overexpression rescues the *beat* mutant phenotype.

Muscles and postsynapses are marked by Sh-GFP in whole-mount larvae. A: Typical wild-type innervation pattern of dorsal muscles in a third instar larva. B: The *beat* mutant phenotype exhibits strong innervation defects. C: Early embryonic, presynaptic overexpression of Beat full-length cDNA rescues the mutant phenotype. D: Late embryonic, presynaptic overexpression of Beat cannot restore the innervation pattern. E: Restriction of Beat overexpression to motoneurons is sufficient for a rescue. F: Postsynaptic expression of Beat does not attenuate the *beat* mutant phenotype. G: Full-length Beat tagged to a C-terminal GFP is perfectly able to rescue. H: The N-terminal GFP-tag strongly impairs the rescue ability. I-J: Beat_1-395-GFP and BeatnewTM-GFP are able to partially restore the *beat* mutant innervation defects. K: BeatΔTM-GFP exhibits very little residual rescue capacity. L: Other Beat deletion and fusion constructs are hardly able to rescue. Arrows: innervation defects.

Compared to wild-type larvae, *beat* mutant larvae frequently display innervation defects (Figure 3.16, A-B). Early (*elav-Gal4*), but not late (*nSyb-Gal4*), embryonic pan-neuronal overexpression of full-length Beat cDNA rescues the *beat* mutant phenotype (Figure 3.16, C-D). Motoneuron-specific Beat overexpression restores the wild-type innervation pattern for the most part (Figure 3.16, E). Early, postsynaptic Beat overexpression does not reduce the *beat* mutant innervation defects (Figure 3.16, F), indicating a cell-autonomous function of Beat. The insertion of a C-terminal GFP-tag to the full-length Beat cDNA is able to fully rescue the mutant phenotype, whereas an N-terminal GFP-tag strongly reduces the rescue-ability (Figure 3.16, G-H). Among the Beat deletion- and fusion constructs, Beat_1-395-GFP and BeatnewTM-GFP can partially restore the wild-type innervation pattern (Figure 3.16, I-J). Beat Δ TM-GFP exhibits minimal rescue capacity (Figure 3.16, K). Other Beat constructs are not able to rescue (Figure 3.16, L).

Table 3.1 compiles the estimated rescue ability of all Beat constructs.

Table 3.1: Deletions or modifications of Beat domains highly impair the rescue ability.

The intensity of rescue capacity induced by presynaptic overexpression of the different Beat constructs in the *beat* mutant background (*beat³/beat^{C163}*; *elav*, Sh-GFP > construct) is illustrated. Column A: Construct designation. Column B: Schematic overview of Beat domains. Column C: Estimated rescue by presynaptic overexpression of the respective Beat construct. Estimated intensity of rescue capacity: - no rescue, + minor rescue, ++ moderate rescue, +++ about wild-type innervation.

A	B	C
Construct	Scheme	Rescue capacity
Beat ⁵		+++
Beat-GFP		+++
GFP-Beat-Cherry		+
Beat_1-395-GFP		+
Beat_1-361-GFP		(+)
Beat_1-345-GFP		(+)
Beat_1-322-GFP		-
Beat_1-254-GFP		-
Beat_29-427-GFP		(+)
Beat_29-322-GFP		-
Beat Δ IG1-GFP		-
BeatCys-GFP		-
BeatnewTM-GFP		+
Beat Δ TM-GFP		(+)

The exact rescue ability has been evaluated for some selected Beat constructs by counting the number of NMJs per hemisegment (Bösenberg, 2016).

The statistical analysis shows that Beat-GFP is able to fully restore the *beat* mutant innervation defects (Figure 3.17, A-D, $p < 0.001$) and compared to the control, there is no significant difference in the number of NMJs in any muscle field (data not shown). Interestingly, the partial rescue mediated by GFP-Beat-Cherry, Beat_1-395-GFP and BeatnewTM-GFP mostly applies to the ventral muscle field (Figure 3.17, B). The innervation pattern of the lateral compartment can be rescued only by Beat-GFP, but not by GFP-Beat-Cherry, Beat_1-395-GFP and BeatnewTM-GFP (Figure 3.17, C). By contrast, the dorsal muscle field is only rescued by full-length Beat-GFP but is even less innervated after rescue with the above-mentioned Beat constructs than in the *beat* mutant situation (Figure 3.17, D). These findings suggest that the ISN, which grows out prior to the other nerve fascicles and innervates the dorsal muscles, as well as the SNa, which innervates the lateral compartment, is not rescued if Beat is not returned in its full-length version. On the other hand, the guidance of the later outgrowing fascicles ISNb, ISNd and SNc is highly improved compared to the *beat* mutant larvae.

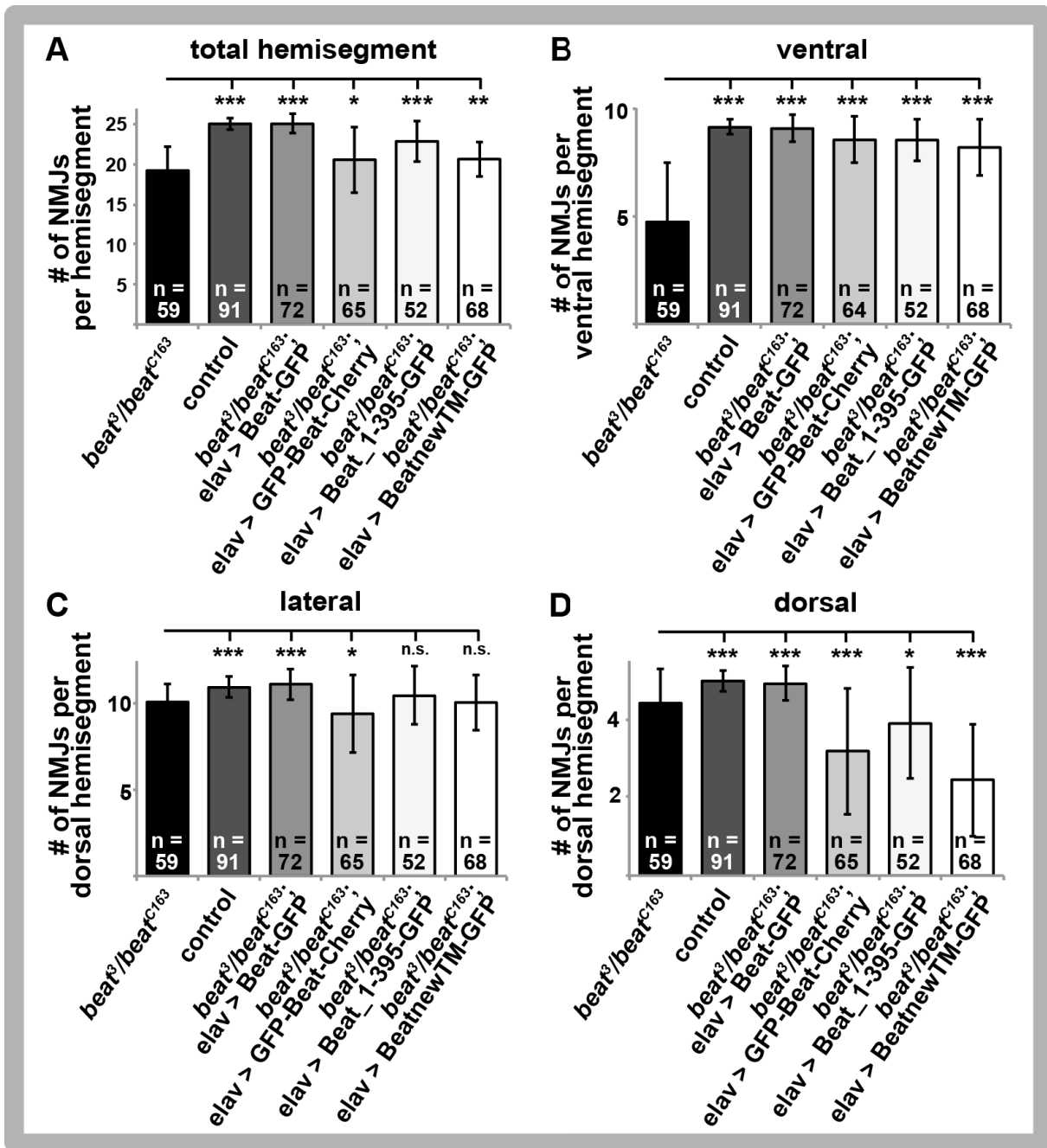


Figure 3.17: Rescue capacity of selected Beat constructs.

A: The total number of NMJs per hemisegment shows that presynaptic expression of Beat-GFP in the *beat* mutant background completely restores the wild-type innervation pattern. Other Beat constructs can partly rescue these innervation defects. B: The number of ventral NMJs is significantly increased by presynaptic expression of the analyzed Beat constructs compared to the *beat* mutant. C: In the lateral muscle field, only Beat-GFP is able to restore the innervation pattern. D: In the larvae rescued by expression of GFP-Beat-Cherry, Beat_1-395-GFP and BeatnewTM-GFP, the dorsal segments are even less innervated than the *beat* mutant. * $p \leq 0.05$, ** $p \leq 0.01$, *** $p \leq 0.001$.

3.8.2 Overexpression of Side and Beat induces innervation defects

Wild-type larvae exhibit a stereotypical innervation pattern of the abdominal segments (Figure 3.18, A). Due to the guiding role of Side and Beat during motor

axonal outgrowth and defasciculation, *side* and *beat* mutant larvae exhibit very strong defects especially in the ventral muscle field, but also in the lateral and dorsal compartment due to lack of defasciculation as well as stalling phenotypes of the motor axons (Figure 3.18, B-C). Pan-neuronal overexpression of Side-Cherry induces strong innervation defects in all compartments, especially in the dorsal muscle field, caused by excessive Side expression in neurons (Figure 3.18, D). Muscle-specific overexpression of Side-Cherry abolishes all dorsal innervation as well as part of the lateral innervation (Figure 3.18, E), as motor axons are drawn towards the developing muscle fields too early. This dorsal lack of innervation results in a curved body shape of the larvae with the ventral part being the convex side and the dorsal part being the concave side. Pan-neuronal overexpression of Beat-GFP does not influence the innervation pattern (data not shown). Muscle-specific overexpression of Beat-GFP induces defects in all body compartments (Figure 3.18, F).

The generated Beat and Side constructs, which carry modifications in the amino acid sequence of the original molecule, can thus be evaluated by their power to distract motor axons from their embryonic pathway induced by their overexpression. The findings of the disturbance of the correct larval innervation pattern then allow for conclusions regarding the functionality of the different domains of Beat and Side. In the following tables, the innervation defects induced by the overexpression of different constructs are summed up and estimated by their impact relative to the defects caused by the construct mediating the strongest effect.

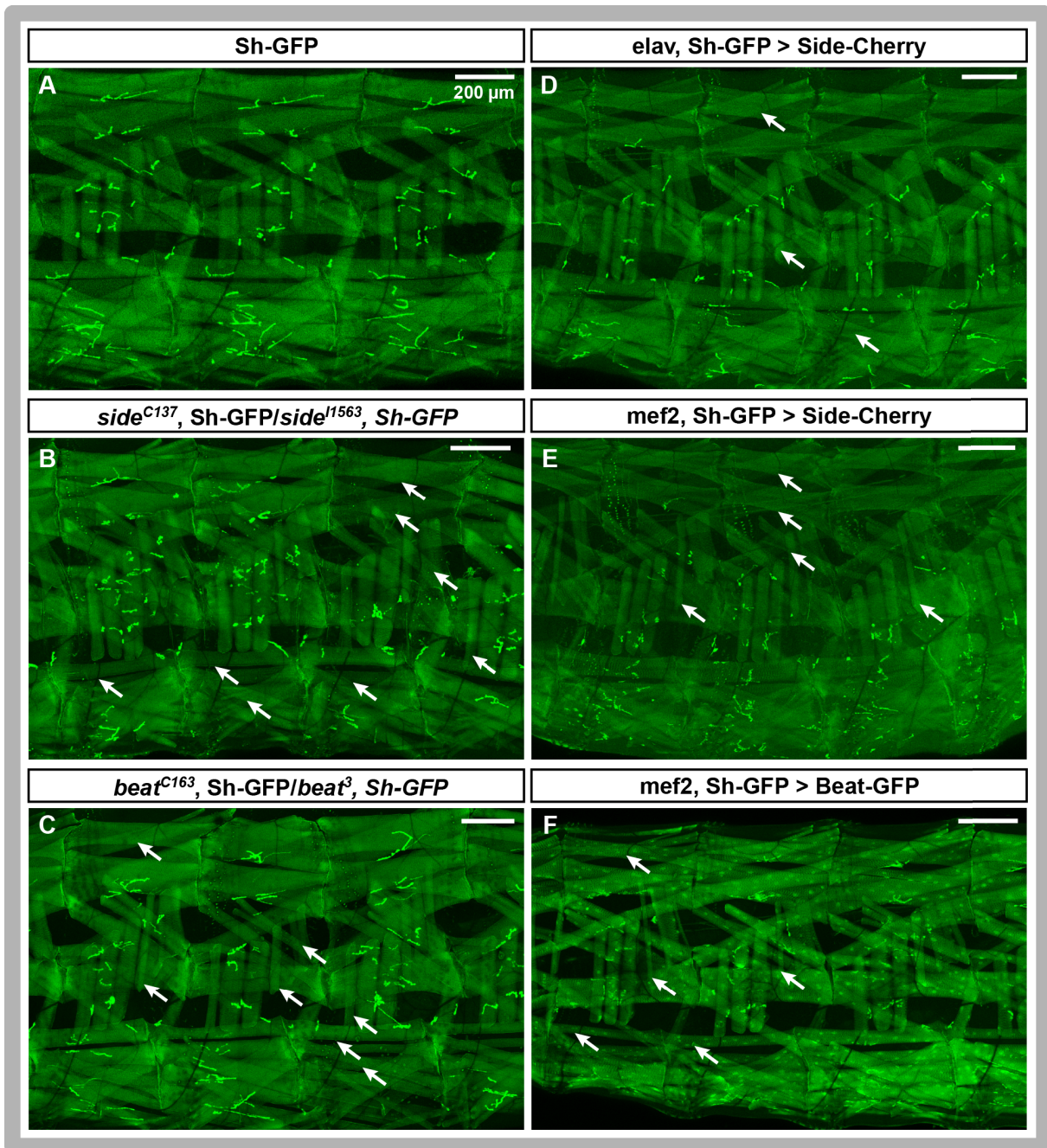


Figure 3.18: Larval innervation pattern of three adjacent hemisegments.

A: Wild-type innervation of control larvae. B-C: *Side* and *beat* mutant larvae exhibit similar, severe innervation errors especially in the ventral body part. D: Presynaptic overexpression of Side-Cherry induces innervation defects. E: Postsynaptic overexpression of Side-Cherry results in dorsally uninervated larvae. F: Postsynaptic overexpression of Beat-GFP induces strong innervation errors distributed among all body parts. Arrows indicate lack of innervation. Scale bars: 200 μm .

3.8.2.1 Innervation defects induced by overexpression of Side constructs

Table 3.2 illustrates the intensity of innervation defects induced by muscle- and neuron-specific overexpression of the different Side constructs. Pre- and postsynaptic overexpression of Side^{29A}, Side-Cherry and GFP-Side-Cherry lead to strong innervation defects with Side-Cherry and GFP-Side-Cherry mediating the

most severe phenotypes with the curved body shape, as described above. Muscle-specific overexpression of SideIG1+CD8-Linker-TM-Cherry and SideIG1-FasII-Cherry induces some minor innervation errors (with SideIG1-FasII-Cherry causing slightly more defects). Pan-neuronal expression of the SideIG1 fusion constructs does not lead to noticeable defects. Postsynaptic - but not presynaptic - expression of the secreted SideIG1-5-Cherry mediates some minor innervation defects. Pre- or postsynaptic expression of SideΔIG1-Cherry and SideIG1-CD8-CD8-Cherry does not lead to an increase of innervation defects compared to the wild-type.

Table 3.2: Pre- and postsynaptic overexpression of Side disturbs motor axonal wiring.

Column A: Construct designation. Column B: Schematic overview of Side domains. Column C: Innervation defects mediated by muscle-specific overexpression of different Side constructs. Column D: Innervation defects induced by neuronal overexpression of different Side constructs. Estimated intensity of innervation defects: - wild-type innervation pattern, + minor defects, ++ moderate defects, +++ strong defects.

Construct	Scheme	Intensity of innervation defects	
		mef2, Sh-GFP > construct	elav, Sh-GFP > construct
Side ^{29A}		++	++
Side-Cherry		+++	+++
GFP-Side-Cherry		+++	++
SideΔIG1-Cherry		-	-
SideIG1-5-Cherry		(+)	-
SideIG1+CD8-Linker-TM-Cherry		+	-
SideIG1-CD8-CD8-Cherry		-	-
SideIG1-FasII-Cherry		+	-

So interestingly, the Cherry-tagged full-length Side construct induces even more severe defects than the untagged Side^{29A}. The Side IG1 domain mediates attraction also when being fused to different linker proteins (SideIG1-FasII-Cherry and SideIG1+CD8-Linker-TM-Cherry), although not as strong as the original Side.

3.8.2.2 Innervation defects induced by overexpression of Beat constructs

Postsynaptic overexpression of Beat constructs leads to the presence of this guidance receptor in the muscles from about stage 14 onwards, additionally to the endogenous occurrence on motor axons and growth cones.

Table 3.3 compiles the wiring defects caused by postsynaptic overexpression of the different Beat constructs. The results indicate the importance of the different domains of Beat for its functionality.

Table 3.3: Postsynaptic overexpression of Beat impairs motor axonal connectivity.

The intensity of innervation defects induced by postsynaptic overexpression of the different Beat constructs (mef2, Sh-GFP > construct) is illustrated. Column A: Construct designation. Column B: Schematic overview of Beat domains. Column C: Innervation defects induced by overexpression of different Beat constructs. Estimated intensity of innervation defects: - wild-type innervation pattern, + minor defects, ++ moderate defects, +++ strong defects.

A	B	C
Construct	Scheme	Intensity of innervation defects
Beat ⁵		+++
Beat-GFP		+++
GFP-Beat-Cherry		+
Beat_1-395-GFP		+
Beat_1-361-GFP		-
Beat_1-345-GFP		-
Beat_1-322-GFP		-
Beat_1-254-GFP		-
Beat_29-427-GFP		-
Beat_29-322-GFP		-
BeatΔIG1-GFP		-
BeatCys-GFP		-
BeatnewTM-GFP		++
BeatΔTM-GFP		-

Muscle-specific overexpression of untagged Beat⁵ as well as Beat-GFP induce strong innervation defects throughout all body compartments. Overexpression of BeatnewTM-GFP leads to moderate innervation defects. Postsynaptic expression of GFP-Beat-Cherry and Beat_1-395-GFP induces several minor innervation errors. Overexpression of other Beat constructs, including Beat_29-427-GFP, does not disturb the innervation pattern noticeably. The guidance defects induced by the overexpression of GFP-Beat-Cherry are strongly diminished compared to those induced by ectopic expression of the untagged Beat or Beat-GFP. The C-terminal GFP-tag thus does not visibly disturb the functionality of Beat, whereas the N-terminal GFP-tag does. Furthermore, even the slightest deletion or modification in the amino acid sequence of Beat diminishes its functionality drastically.

3.8.2.3 Statistical analysis of innervation defects

The innervation defects caused by muscle-specific overexpression have been evaluated for some selected Side and Beat constructs by counting the NMJs per hemisegment (Bösenberg, 2016).

Side-Cherry induces severe defects, which are most prominent in the dorsal muscle field (with an average of 0.6 instead of 5 NMJs per dorsal hemisegment, see Figure 3.19, D) followed by defects in the lateral muscle field (7.8 instead of 11 NMJs, see Figure 3.19, C). By contrast, the number of ventral NMJs is slightly increased (Figure 3.19, B). These additional, ectopic NMJs are probably formed by some of the motor axons, which normally innervate the lateral and dorsal muscle fields. Postsynaptic overexpression of Side^{29A} also diminishes the dorsal innervation (with a mean of 2.7 instead of 5 NMJs, see Figure 3.19, D) but does not have strong effects on the lateral and ventral innervation. The functionality of the Side IG1 domain was evaluated by muscle-specific overexpression of the fusion constructs SideIG1-FasII-Cherry and SideIG1+CD8-Linker-TM-Cherry. These constructs induce some dorsal innervation defects (4.3 and 4.6, respectively instead of 5 NMJs, see Figure 3.19, D). Interestingly, in the lateral compartment, the innervation is slightly reduced by SideIG1-FasII-Cherry (10.3 instead of 11 NMJs, $p < 0.001$, see Figure 3.19, C) whereas SideIG1+CD8-Linker-TM-Cherry slightly diminishes the number of NMJs in the ventral muscle field (8.8 instead of 9.1, see Figure 3.19, B).

Postsynaptic overexpression of the secreted SideIG1-5-Cherry significantly decreases the innervation only in the ventral muscle field.

Muscle-specific overexpression of Beat-GFP induces significant innervation defects in all muscle fields (Figure 3.19, A-D). Beat₁₋₃₉₅-GFP, where the 32 C-terminal amino acids are deleted, slightly diminishes the number of NMJs, especially in the ventral muscle field.

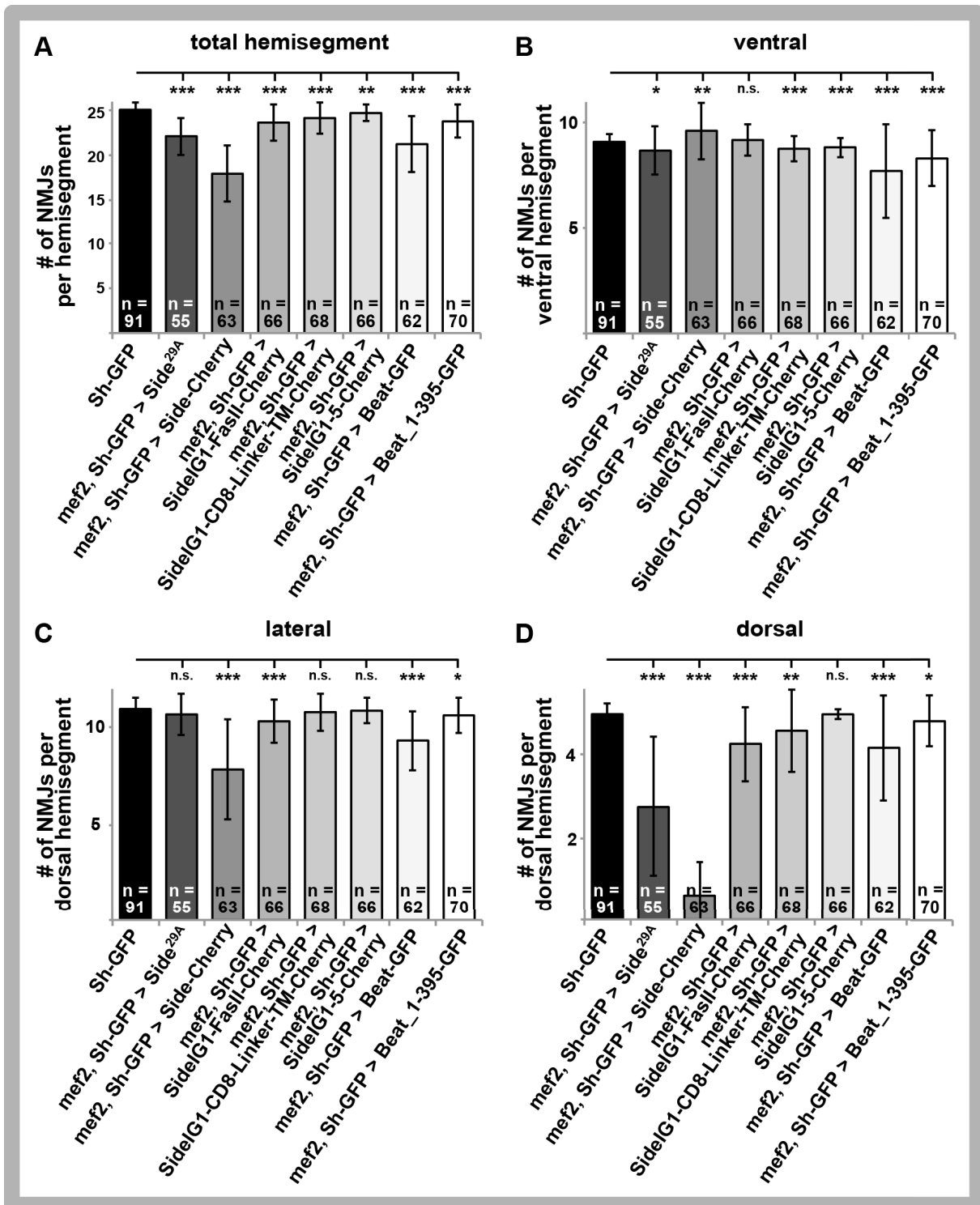


Figure 3.19: Postsynaptic overexpression of Side and Beat constructs induces innervation defects.

A: The number of NMJs per total hemisegment is reduced most severely by expression of Side-Cherry and Beat-GFP. B: Ventral defects are strongest induced by Beat-GFP. C: In the lateral compartment, most severe defects are induced by Side^{29A} and Side-Cherry, followed by Beat-GFP. D: Postsynaptic overexpression of Side^{29A} and Side-Cherry induces very strong dorsal innervation defects. * $p \leq 0.05$, ** $p \leq 0.01$, *** $p \leq 0.001$.

3.9 Analysis of the Beat expression pattern

Beat was previously characterized as secreted protein, as it does not contain a classical transmembrane domain. Furthermore, immunohistochemical stainings yielded an indistinct Beat-signal around axons and growth cones (Fambrough and Goodman, 1996). More recent studies contradict these findings. Firstly, bioinformatic algorithms predict a transmembrane region within the C-terminal, cysteine-rich region (Krogh et al., 2004). Secondly, Beat functions cell-autonomously in rescue experiments (Siebert et al. 2009 and Chapter 3.7.2). Thirdly, transiently transfected S2 cell did not secrete Beat-myc into the medium (Siebert et al., 2009).

In this work, the expression patterns of selected Beat constructs have been extensively tested for their embryonic and larval distribution *in vivo*. The embryonic, presynaptic expression pattern is especially interesting regarding the distribution of Beat. As Beat-GFP is able to fully rescue the *beat* mutant phenotype, the construct needs to be localized at neuronal compartments where it can mediate its necessary guidance receptor function. On the other hand, the muscle-specific expression pattern of the different Beat constructs can give valuable hints concerning the location of the transmembrane domain as it is easier to visualize.

3.9.1 Presynaptic Beat expression pattern

As Beat is naturally expressed on motor axons and expression with *elav-Gal4* rescues the mutant phenotype, the presynaptic expression pattern is of special interest. Unexpectedly, pan-neuronal overexpression of Beat-GFP with *elav-Gal4* (which has full rescue capacity) was not visible in embryonic or larval motor axons. Due to this fact, larval presynaptic overexpression was induced by *nSyb-Gal4*. The *nSyb* promoter drives expression pan-neuronally, similar to *elav-Gal4*, but starts expression in later embryonic stages and exhibits stronger larval expression. The presynaptic, larval expression pattern is listed in Table 3.4.

Results

Table 3.4: Larval, presynaptic expression pattern of Beat constructs.

Column A: Construct designation. Column B: Schematic overview of Beat domains. Column C-F: Presence of GFP-signal in the respective neuronal compartments. Estimated GFP-intensity: - no signal, (+) very weak signal, + weak signal, ++ moderate signal, +++ strong signal.

A nSyb > construct	B Scheme	Intensity of GFP-signal			
		C Brain cell bodies	D Brain neuropil	E Axons	F NMJs
Beat-GFP		+	(+)	-	-
GFP-Beat-Cherry		++	+++	++	+++
Beat_1-395-GFP		+	(+)	-	-
Beat_1-361-GFP		+	(+)	(+)	+
Beat_1-345-GFP		+	++	(+)	+
Beat_1-322-GFP		+	++	(+)	+
Beat_1-254-GFP		+	++	(+)	+
Beat_29-427-GFP		+	(+)	-	-
Beat_29-322-GFP		+	++	(+)	+
BeatΔIG1-GFP		(+)	-	-	-
BeatCys-GFP		(+)	-	-	-
BeatnewTM-GFP		+	+++	+	+
BeatΔTM-GFP		+	++	(+)	+

Interestingly, full-length Beat-GFP does not exhibit GFP-signal in motor axons, where it is embryonically expressed (Fambrough and Goodman, 1996). GFP-signal is only visible in the cell bodies of the brain and very weakly in the neuropil, which contains the central synapses. In contrast to these findings, GFP-Beat-Cherry exhibits strong N-terminal GFP-signal in motoneurons and very bright GFP-signal in the NMJs (but no C-terminal Cherry-signal in these compartments). The cell bodies and neuropil in the larval brain also show strong GFP-signal (and weak Cherry-signal). Surprisingly, the C-terminal truncation constructs also exhibit weak axonal as well as strong synaptic signal, if the construct does not exceed amino acids 1-361. They are all expressed in the cell bodies and neuropil in the brain. BeatnewTM-GFP exhibits rather vesicular, but intense GFP-signal in the axons and NMJs and localizes in the cell bodies of the brain as well as in the neuropil. BeatΔTM-GFP shows little expression in the axons but exhibits strong signal in the NMJs, cell bodies of the brain and the neuropil. BeatΔIG1-GFP and Beat-Cys-GFP, the N-terminal truncation constructs, only show weak signal in the cerebral cell bodies.

Due to the lack of a specific anti-Beat antibody, emphasis was placed on the embryonic, presynaptic expression pattern of Beat in order to visualize the subcellular distribution of this guidance receptor.

The larval findings of the strong axonal and synaptic expression of the N-terminally tagged GFP-Beat-Cherry construct made it feasible to visualize embryonic Beat expression in motor axons and growth cones using this construct (Figure 3.20). Co-staining with a marker for motoneurons shows Beat expression in motor axons, growth cones and cell bodies of the ventral nerve cord.

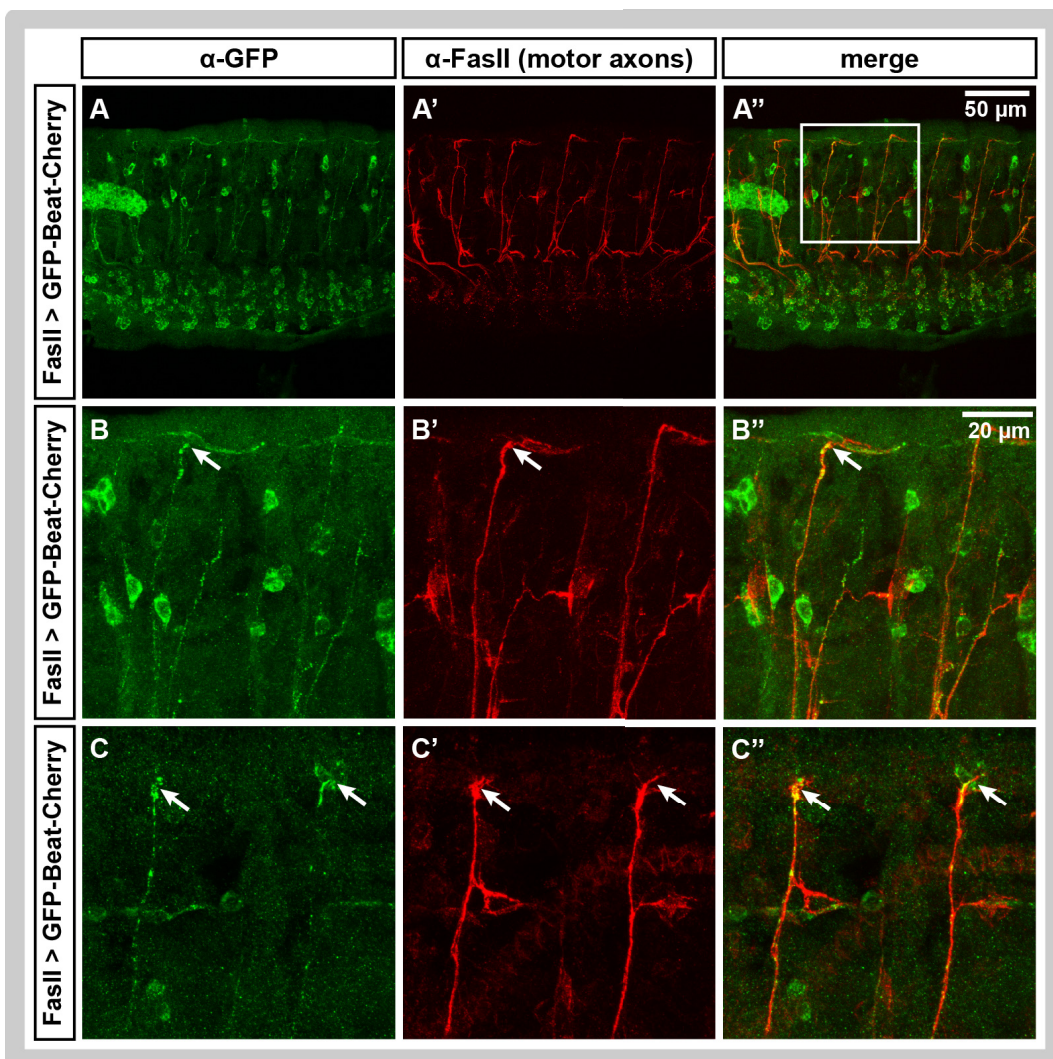


Figure 3.20: Motoneuron-specifically overexpressed GFP-Beat-Cherry is detectable at the growth cone.

Stage 17 embryos are shown. Detection of the Beat construct is effectuated via the N-terminal GFP-tag. A-A'': Beat can be detected in motor axons and cell bodies in the CNS. B-C'': The GFP-signal is visible in axons and is enriched in growth cones (arrows).

3.9.2 Postsynaptic Beat expression pattern

The larval, muscle-specific expression pattern of the different Beat constructs can provide clues about the existence and location of the transmembrane domain.

Muscle-specific overexpression of transmembrane and secreted, GFP-tagged control constructs mCD8-GFP and secret.Nrx-GFP exhibit membranous signal and a negative muscle pattern, respectively (Figure 3.21, A-B). Expression of mCD8-GFP shows staining of the NMJs whereas expression of secret.Nrx-GFP leads to enrichment at the lateral chordotonal organ. Postsynaptically expressed full-length Beat-GFP stains muscles and is enriched in the nuclei, but not at the NMJs (Figure 3.21, C). Out of the sequentially, C-terminally truncated Beat constructs, only Beat_1-395-GFP exhibits nuclear accumulation of GFP-signal (Figure 3.21, D). Beat_1-361-GFP shows staining of the membrane as well as slight accumulation around the nuclei (Figure 3.21, E). Beat_1-345-GFP, Beat_1-322-GFP and Beat_1-254-GFP exhibit very similar homogenous, membranous staining with slight enrichment at the attachment sites of the muscles (Figure 3.21, F-H). Introduction of an artificial signal peptide in Beat_29-322-GFP and Beat_29-427-GFP does not visibly change the expression pattern from that of the respective constructs with the endogenous signal peptide (Figure 3.21, I-J). Only in Beat_29-427-GFP, the membranous signal is a bit weaker than in Beat-GFP, whereas the accumulation in the nucleus persists. Interestingly, expression of Beat Δ IG1-GFP reveals a slight negative muscle pattern (Figure 3.21, K) and nuclear accumulation. Postsynaptic overexpression of Beat-Cys-GFP stains the muscle membranes only weakly but exhibits strong signal in the nucleus (Figure 3.21, L). Interestingly, excision of the putative transmembrane domain in Beat Δ TM-GFP leads to very bright and membranous staining of the muscles, which is enriched at the NMJs (Figure 3.21, M) with an expression pattern most similar to the control mCD8-GFP. Introduction of an artificial transmembrane domain in BeatnewTM-GFP leads to slight staining of the muscle membrane and shows distribution around the nuclei, probably in degradation particles (Figure 3.21, N). Replacement of the C-terminal GFP-tag with an N-terminal GFP-tag in GFP-Beat-Cherry leads to very bright expression with enrichment at the attachment sites (Figure 3.21, O). The C-terminal Cherry-tag stains muscles and is enriched in the nuclei in the same fashion as the C-terminal GFP-tag of Beat-GFP.

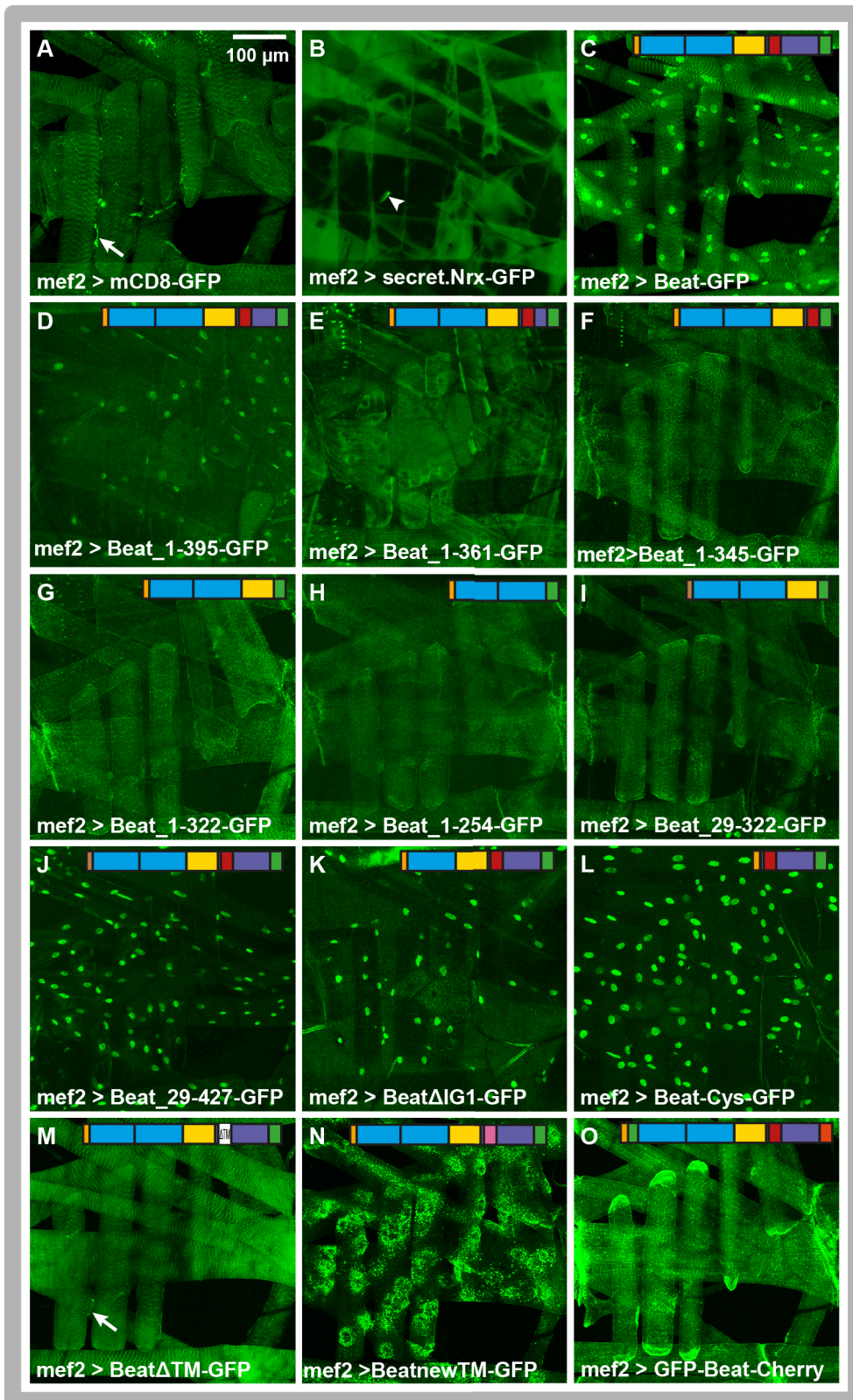


Figure 3.21: Full-length Beat-GFP does not display secretion in L3 larvae.

Larval, muscle-specific expression pattern of Beat deletion- and fusion constructs. A-B: Controls for membrane-anchored and secreted protein, respectively. Expression of mCD8-GFP stains muscle membranes and synapses (arrow). Expression of secret.Nrx-GFP stains the hemolymph and the lateral chordotonal organ (arrowhead). C: Full-length Beat-GFP exhibits fluorescence throughout muscle membranes as well as nuclei. D: Beat_1-395-GFP exhibits weak membranous staining and GFP-accumulation in the nucleus. E: Beat_1-361-GFP shows staining of the membrane. F-H: The C-terminal deletion constructs Beat_1-345-GFP, Beat_1-322-GFP and Beat_1-254-GFP all show the

Results

same homogenous, membranous staining. I: Beat₂₉₋₃₂₂-GFP, a C-terminal deletion construct with an exogenous signal peptide, exhibits the same homogenous, membranous staining as Beat₁₋₃₂₂-GFP. J: Beat₂₉₋₄₂₇-GFP displays membranous staining and GFP-accumulation in the nuclei. K: Beat Δ IG1-GFP exhibits a slightly secreted pattern with signal accumulation in the nuclei. L: Beat-Cys-GFP shows strong GFP accumulation in the nuclei and weak staining of the muscle membrane. M: Beat Δ TM-GFP stains the muscles very homogeneously and is slightly enriched at the NMJs (arrow). N: Overexpression of BeatnewTM-GFP leads to clustering of the construct around the nuclei and slight membranous staining. O: GFP-Beat-Cherry exhibits a very bright membranous staining with enrichment at the attachment sites.

Noteworthy, the nuclear accumulation of the GFP-signal is detectable only if the complete C-terminus is present in the construct or at least up to amino acid 395 (in Beat₁₋₃₉₅-GFP). Combined with the finding that neither expression of Beat Δ TM-GFP, nor of BeatnewTM-GFP exhibits nuclear enrichment, the amino acid sequence responsible for the C-terminal accumulation in the nucleus might be located between amino acids 322 and 395.

Unexpectedly, the muscle-specific expression pattern of whole larvae did not reveal a secreted expression pattern for any of the Beat constructs. In order to further address the question of a possible secretion, some selected Beat constructs were expressed muscle-specifically and whole embryos (stage 17) were imaged. The advantage of life imaging of embryos compared to the larval system is that a vitelline membrane surrounds the embryo and thus secreted proteins remain in the hemolymph and cannot be discarded.

Muscle-specific overexpression of mCD8-GFP exhibits a very bright signal in muscles (Figure 3.22, A). Expression of secret.Nrx-GFP by contrast shows a clear negative muscle pattern (Figure 3.22, B). Embryonic Beat-GFP exhibits cellular staining of the muscles with enrichment in small, vesicle-like structures (Figure 3.22, C). GFP-Beat-Cherry shows staining of the muscle surfaces with enrichment at the membranes and attachment sites (Figure 3.22, D). The C-terminal deletion constructs, which contain the putative transmembrane domain, exhibit weak muscular staining (Figure 3.22, E-G). The C-terminal deletion constructs Beat₁₋₃₂₂-GFP and Beat₁₋₂₅₄-GFP, which lack the predicted transmembrane domain, both exhibit a weak negative muscle-pattern (Figure 3.22, H-I). Beat Δ TM-GFP by contrast shows a clearly cellular expression pattern (Figure 3.22, J). Expression of BeatnewTM-GFP is also restricted to the muscles with a rather vesicular distribution (Figure 3.22, K). Overexpression of Beat Δ IG1-GFP is not detectable in life imaging (Figure 3.22, L).

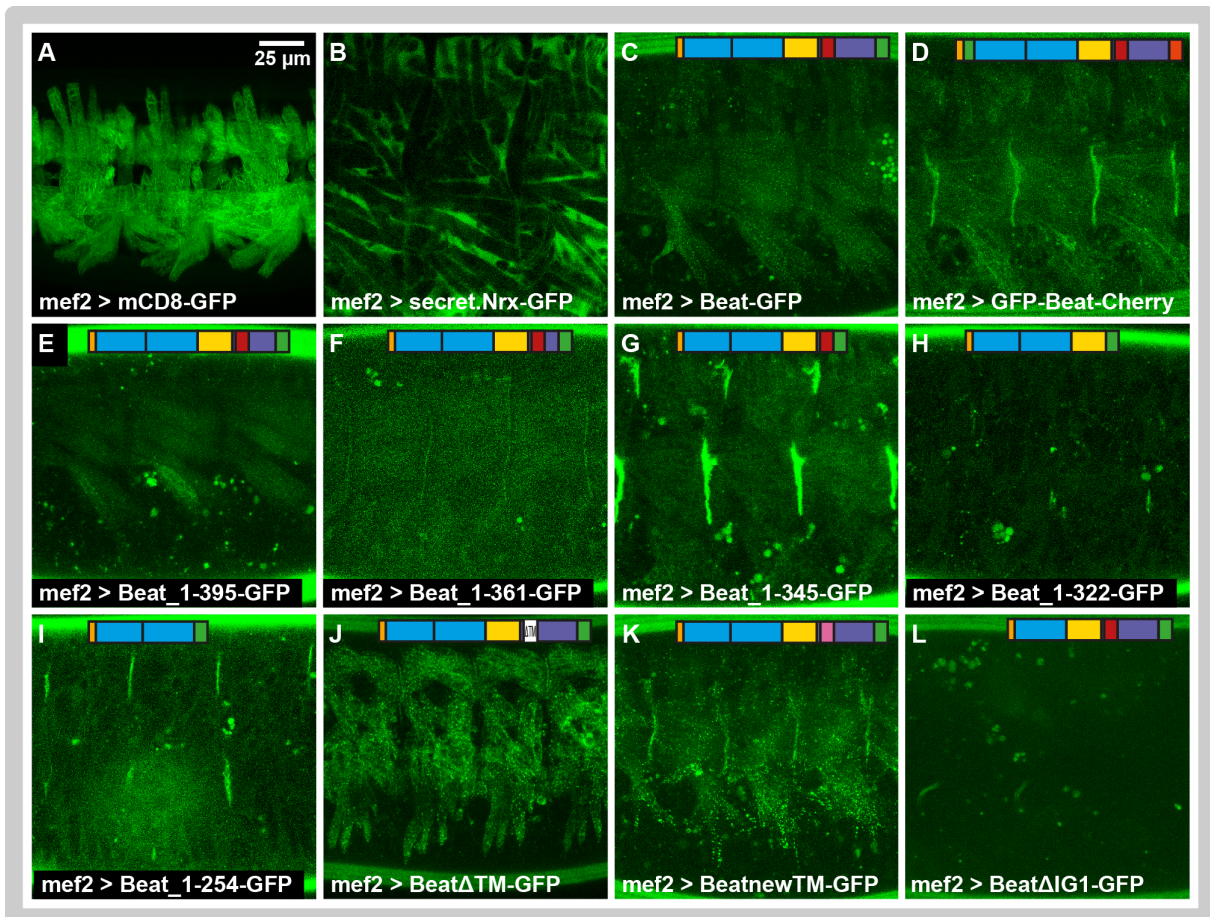


Figure 3.22: The C-terminal deletion constructs lacking the transmembrane domain exhibit a secreted fluorescence pattern in embryos.

Live-imaging of embryonic, muscle-specific overexpression of different Beat constructs. A-B: Controls for membrane-anchored versus secreted constructs. C-D: Expression of full-length Beat constructs exhibits cellular signal. E-G: C-terminal deletion constructs, which contain the predicted transmembrane region exhibit GFP-signal in the muscles. H-I: C-terminal deletion constructs lacking the putative transmembrane domain exhibit weak secreted GFP-signal. J: Exact excision of the predicted transmembrane region does not induce a secreted expression pattern. K: BeatnewTM-GFP exhibits vesicular expression, which is restricted to the muscles. L: Expression of BeatΔIG1-GFP is not detectable in the embryo.

These findings of life imaging whole embryos indicate a secretion of the constructs Beat_1-322-GFP and Beat_1-254-GFP into the hemolymph. By contrast, BeatΔTM-GFP is clearly associated with the muscle cells and does not provide a secreted expression pattern.

3.10 N- and C-terminal part of Beat segregate

Surprisingly, the GFP-signal diverges in the overexpression of C- and N-terminally tagged Beat constructs. Therefore, the pre- and postsynaptic expression pattern of the doubly tagged GFP-Beat-Cherry construct has been further characterized.

In the larval, presynaptic overexpression of GFP-Beat-Cherry, the C-terminal Cherry-tag is largely restricted to the soma of the motor neurons and is distributed intracellularly (Figure 3.23, A'-C'). The N-terminal GFP-tag by contrast localizes at the membrane of the cell bodies, in the neuropil, which contains the central synapses, as well as in the motor axons and NMJs in the periphery (Figure 3.23, A-C).

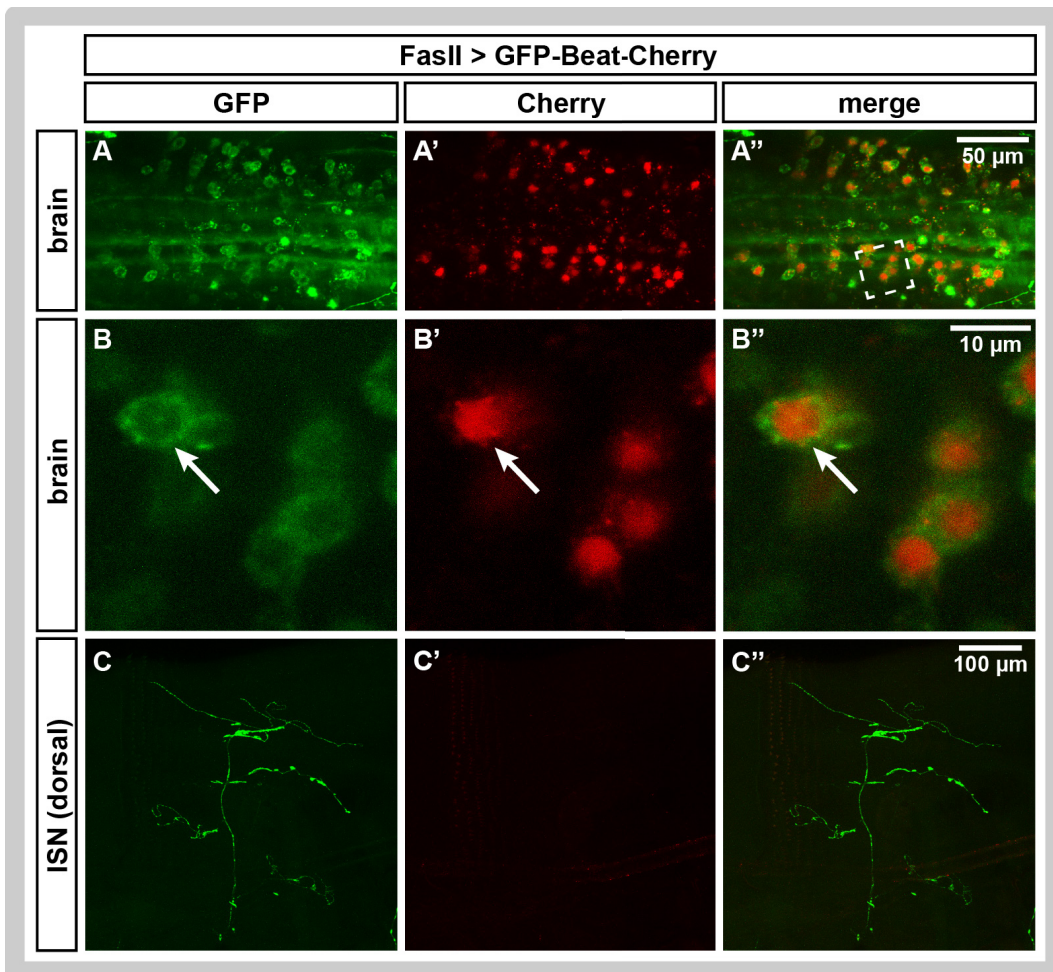


Figure 3.23: The N- and C-terminus of overexpressed GFP-Beat-Cherry segregate.

Confocal images display the presynaptic overexpression of doubly tagged GFP-Beat-Cherry in larvae. A-B'': In the larval brain, the GFP-tagged Beat N-terminus localizes in soma and central synapses of the motor neurons. The C-terminal Cherry-tag is largely restricted to the cell bodies. In these cell bodies, the N-terminal GFP-tag is located at the cell membrane, whereas the Cherry-tag distributes intracellularly. C-C'': The GFP-tagged Beat N-terminus, but not the Cherry-tagged C-terminus stains motor axons and NMJs in the periphery.

Similar findings can be observed in the postsynaptic overexpression of GFP-Beat-Cherry. Larval filets were prepared and nuclei were stained with DAPI. The native GFP- and Cherry-signal was imaged, as immunohistochemical procedures can produce slight artifacts in the expression pattern (e.g. accumulation around the

nuclei). The N-terminal GFP-signal distributes homogenously in the muscles, whereas the C-terminal Cherry-tag accumulates in the nuclei, as shown by the DAPI signal (Figure 3.24).

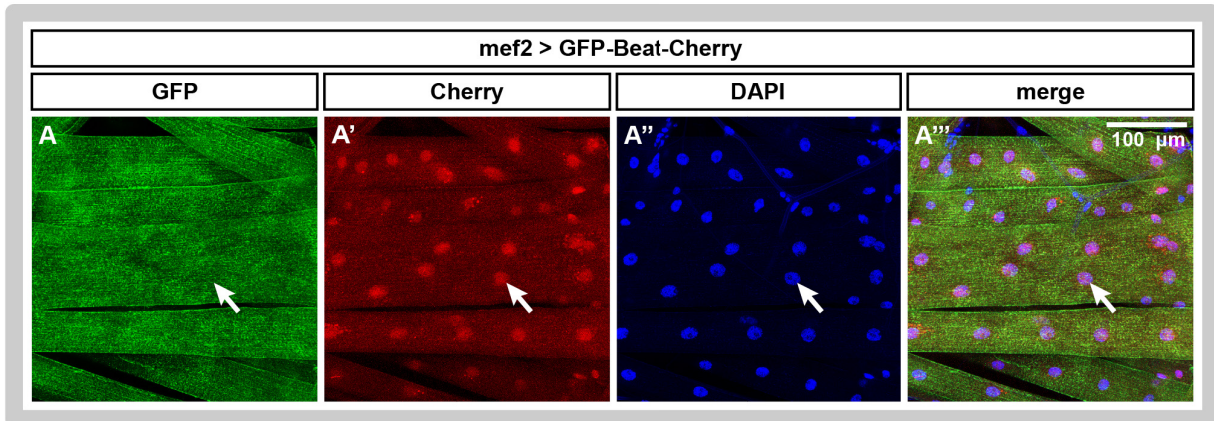


Figure 3.24: In postsynaptic overexpression, the N- and C-terminus of GFP-Beat-Cherry distribute differently.

Overexpression of Beat tagged at both its N- and C-terminus in larval muscles. A-A''': The Cherry-tagged Beat C-terminus, but not the GFP-tagged N-terminus co-localizes with nuclear DAPI staining.

Taken together, these results indicate a segregation of the N- and C-terminus of Beat in both pre- and postsynaptic overexpression.

3.11 Full-length Beat is not secreted in vivo

The extensive analysis of the Beat overexpression pattern in intact larvae and embryos did not yield explicit results concerning a possible secretion of specific Beat constructs. Further western blot analysis was performed using filets and hemolymph of third instar larvae overexpressing full-length and a C-terminally truncated Beat construct in muscles (Figure 3.25). The western blot reveals that both Beat-GFP and Beat_1-322-GFP are detectable in larval filets. Unexpectedly, Beat_1-322-GFP even exhibits a stronger signal than the full-length Beat-GFP. In the larval hemolymph fraction, Beat-GFP does not exhibit any signal, whereas Beat_1-322-GFP is clearly detectable. The blot against Tollold-related, a secreted protease, serves as positive control for the hemolymph fraction and reveals equal loading conditions.

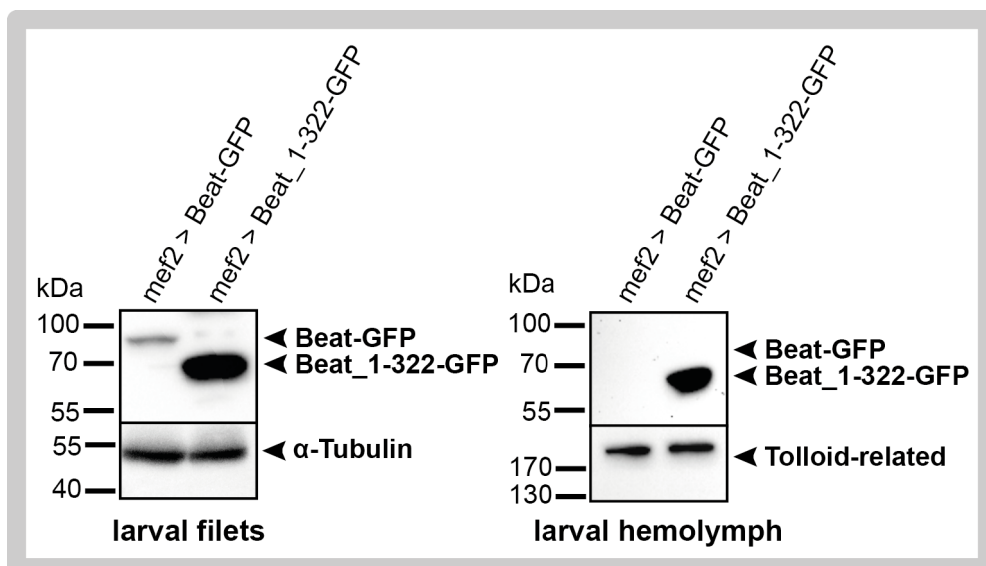


Figure 3.25: Beat-GFP is not secreted.

Western blot analysis of third instar larvae is shown. In larvae overexpressing Beat constructs, Beat-GFP and Beat_1-322-GFP are both detectable in muscles. By contrast, only Beat_1-322-GFP is secreted into the hemolymph, whereas Beat-GFP is not present in the hemolymph fraction.

3.11.1 Surface staining confirms the putative transmembrane domain

The location of the transmembrane domain was further approached by the method of surface staining. With this method, the probes are not permeabilized and the antibody can thus only bind to extracellular epitopes. Larval filets were prepared from animals overexpressing the different GFP-tagged Beat constructs muscle-specifically. Anti-GFP staining was performed using Alexa 647 as fluorophore coupled to the secondary antibody as to not interfere with the native GFP-signal. All overexpressed Beat constructs exhibit native GFP-signal, which is differently distributed (Figure 3.26, A-L). This confirms the findings of imaging intact larvae.

Full-length Beat with a C-terminal GFP-tag (Beat-GFP) does not exhibit extracellular anti-GFP staining (Figure 3.26, A'), indicating that the GFP-tag at the C-terminus is localized intracellularly. Swapping the GFP-tag to the N-terminus of Beat (GFP-Beat-Cherry) leads to intense extracellular GFP-signal (Figure 3.26, I').

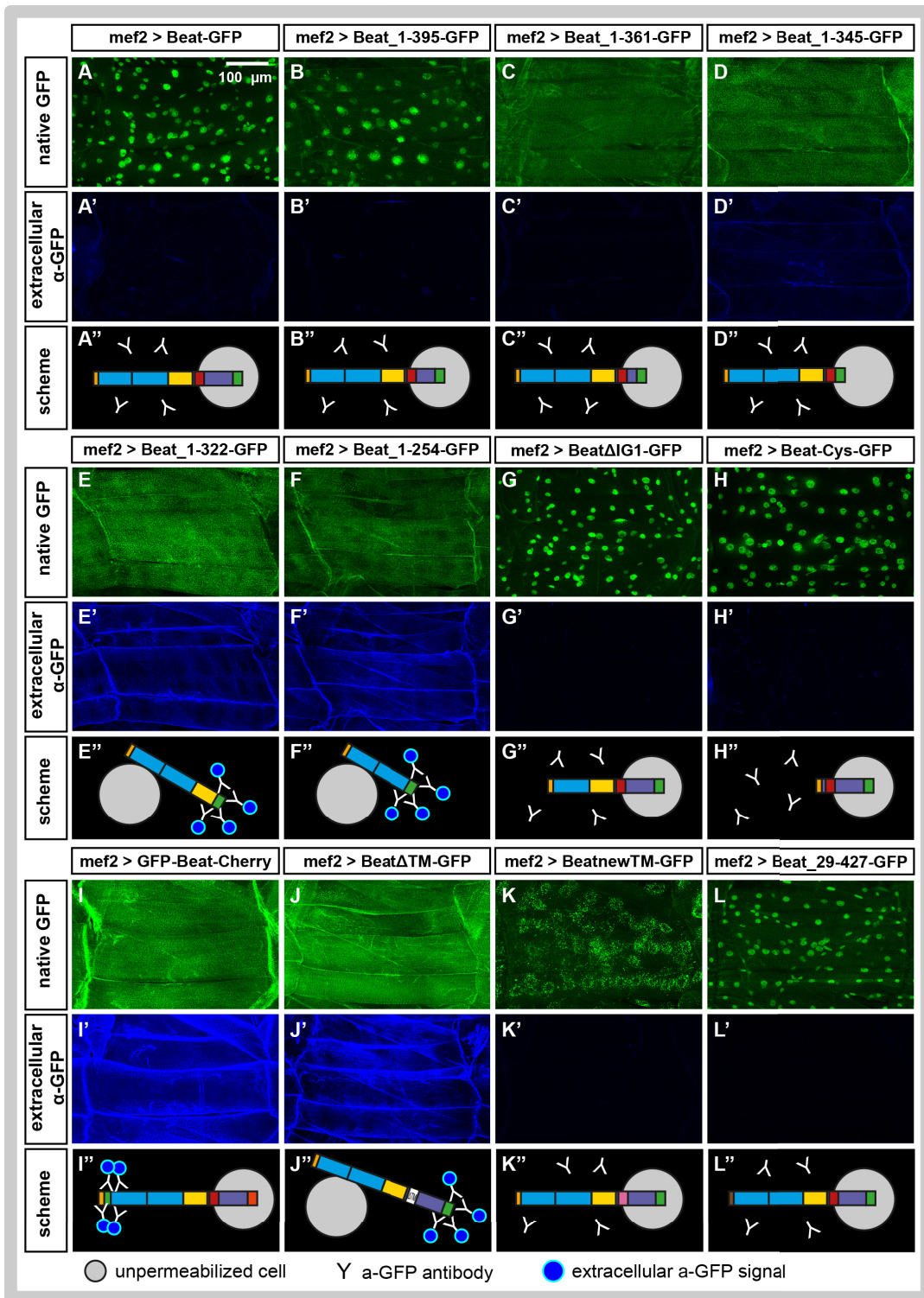


Figure 3.26: Surface stainings of larval filets postsynaptically overexpressing different Beat constructs indicate the existence and location of the putative transmembrane domain.

Confocal images of unpermeabilized larval filets. A-L: Native GFP-fluorescence of exogenously overexpressed, GFP-tagged Beat constructs. A'-L': Extracellular anti-GFP staining of unpermeabilized larval filets (labeled with Alexa 647). A''-L'': Schematic model of the orientation of the Beat construct in the cell. A-F'': Sequentially, C-terminally truncated constructs exhibit extracellular anti-GFP staining only if the construct does not exceed amino acids 1-322. G-H: N-terminal Beat deletion constructs do not show GFP-signal on the membrane surface. I-I'': N-terminal positioning of the GFP-tag of Beat leads to intense extracellular GFP-signal. J-J'': Excision of the potential second transmembrane domain leads to extracellular localization of the GFP-tag. K-K'': Introduction of an artificial transmembrane domain restores the intracellular localization of the GFP-tag. L-L'': Introduction of an exogenous signal peptide does not lead to extracellular GFP-signal.

C-terminal deletion constructs containing the putative transmembrane domain (Beat_1-395-GFP, Beat_1-361-GFP and Beat_1-345-GFP) do not provide GFP-signal of the surface staining (Figure 3.26, B'-D'). Only Beat_1-345-GFP shows slight anti-GFP-signal, probably because the anchoring of the transmembrane region is not stabilized by an intracellular cytoplasmic tail and thus some of these truncated Beat molecules might break from the membrane anchoring. By contrast, the C-terminal deletion constructs without the transmembrane region (Beat_1-322-GFP and Beat_1-254-GFP) exhibit clear extracellular anti-GFP-signal (Figure 3.26, E'-F'). N-terminal deletion constructs do not exhibit GFP-signal on the muscle surface (Figure 3.26, G'-H'). Excision of the putative transmembrane domain in Beat Δ TM-GFP leads to strong extracellular GFP-signal (Figure 3.26, J'). Introduction of an artificial transmembrane domain (BeatnewTM-GFP) abolishes the extracellular GFP-signal (Figure 3.26, K') by restoring the intracellular localization of the GFP-tag. Using an exogenous, well described signal peptide as sorting signal for full-length Beat (Beat_29-427-GFP) does not lead to extracellular GFP-signal (Figure 3.26, L').

Staining permeabilized probes as well as using a different driver line for the overexpression was used to control the specificity of the method of extracellular staining (Figure 3.27). The control immunohistochemistry of permeabilized larval filets overexpressing BeatnewTM-GFP muscle-specifically shows strong anti-GFP-signal, which displays a comparable distribution to the native GFP-signal (Figure 3.27, A-A'). The surface staining of unpermeabilized filets of the same genotype does not show anti-GFP-signal (Figure 3.27, B'). Strong overexposure of this negative surface staining reveals background signal (Figure 3.27, C'), verifying that antibodies have been administered in this staining, but did not bind specifically to the probe. Presynaptic overexpression of GFP-Beat-Cherry provides distinct, presynaptic signal in the surface staining (Figure 3.27, D'). Overexposure in the extracellular staining of presynaptic overexpression does not lead to postsynaptic background (Figure 3.27, E'), demonstrating that the antibodies bind specifically to the GFP-tag of the constructs.

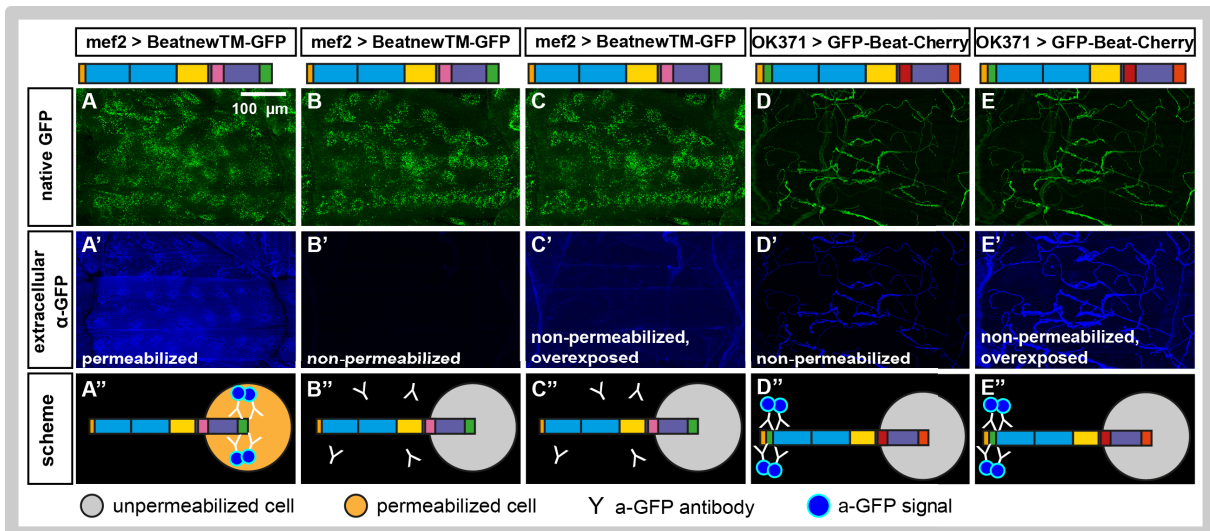


Figure 3.27: Control stainings with permeabilized and non-permeabilized larval filets verify the specificity of surface stainings.

A-E: Native GFP-fluorescence of exogenously overexpressed, GFP-tagged Beat constructs. A-A'': Control-immunohistochemistry with permeabilized probes leads to strong GFP-signal of BeatnewTM-GFP. B-B'': Non-permeabilized filets do not exhibit GFP-signal. C-C'': Overexposure of non-permeabilized filets reveals background, but no specific surface signal. D-D'': Surface staining of presynaptic overexpression of GFP-Beat-Cherry leads to distinct presynaptic GFP-signal. E-E'': Overexposure of presynaptic overexpression in non-permeabilized filets increases the specific GFP-signal but does not produce postsynaptic background.

Taken together, the results of the surface staining coincide with the expected protein structure and orientation, providing evidence that Beat indeed does span the membrane and that the transmembrane domain is localized at the predicted region.

3.11.2 Degradation of cytosolic GFP verifies the orientation of Beat

The method of degradation of cytosolic GFP was used to confirm the results concerning the transmembrane region and the orientation of Beat in the membrane. The fusion construct NSlmb-vhhGFP4 mediates the ubiquitination of GFP-tagged proteins, which then leads to degradation via the proteasome or the lysosome (Caussin et al., 2011). A single-domain antibody fragment, the vhhGFP4, is used to target GFP (Figure 3.28 C, orange part of NSlmb-vhhGFP4). The N-terminal component of the *Drosophila* Slmb (=NSlmb) is an F-box, which is part of the E3-ligase complex (Figure 3.28 C, bright blue part of NSlmb-vhhGFP4). The E3-ligase complex mediates the transfer of the ubiquitin from the E2 enzyme to the protein that is to be marked for degradation.

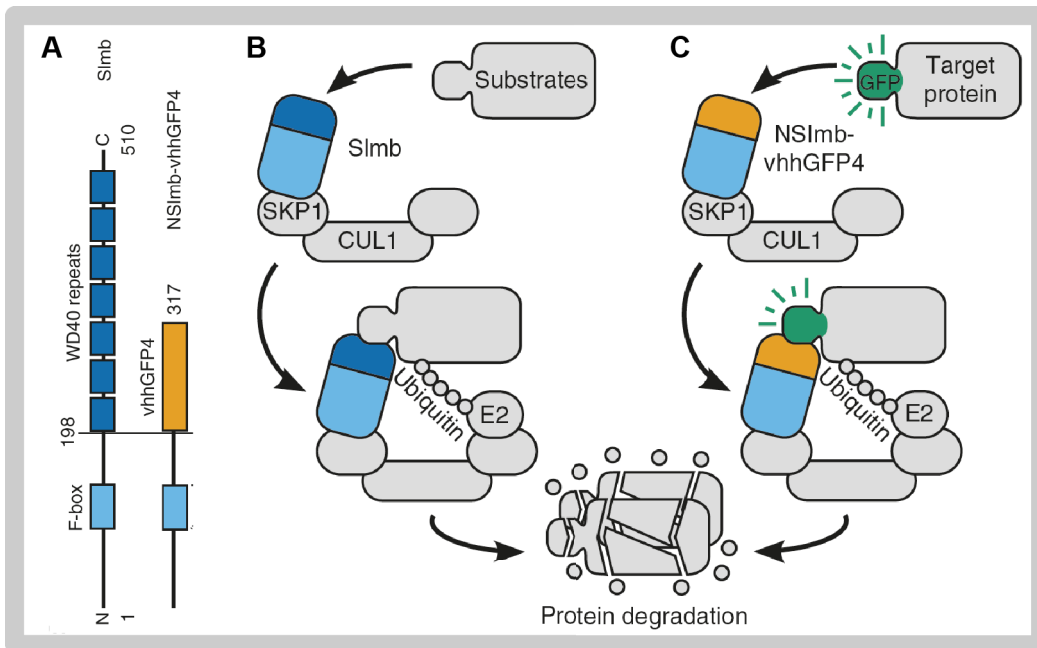


Figure 3.28: Protein ubiquitination mediated by NSlmb-vhhGFP4.

A: Slmb consists of the N-terminal F-box and the C-terminal WD40 repeats. NSlmb-vhhGFP4 is a fusion protein of the N-terminal F-box and the single-domain antibody fragment vhhGFP4. B: The WD40 part in Slmb (dark blue) is the protein interaction motif, which binds to its specific substrate. The F-box (bright blue) binds to SKP1 in the E3-ligase complex. C: The vhhGFP4-part (orange) of NSlmb-vhhGFP4 binds to GFP. The F-box (bright blue) binds to SKP1 in the E3-ligase complex. Target proteins are thus ubiquitinated and marked for degradation (modified from Caussinus et al., 2011).

Co-expressing UAS-NSlmb-vhhGFP4 together with GFP-tagged Beat constructs should thus lead to ubiquitination of the Beat constructs if the GFP-tag is located intracellularly in the cytosol and is thus accessible to the enzyme machinery for ubiquitination. Beat constructs were muscle-specifically overexpressed alone and in the presence of NSlmb-vhhGFP4, respectively (Figure 3.29). A total knockdown of GFP-signal could not be observed in any construct. Still, an alteration of the GFP-signal could be detected in those cases, where the GFP-tag is assumed to be localized intracellularly. All constructs were tested and selected constructs are illustrated in Figure 3.29.

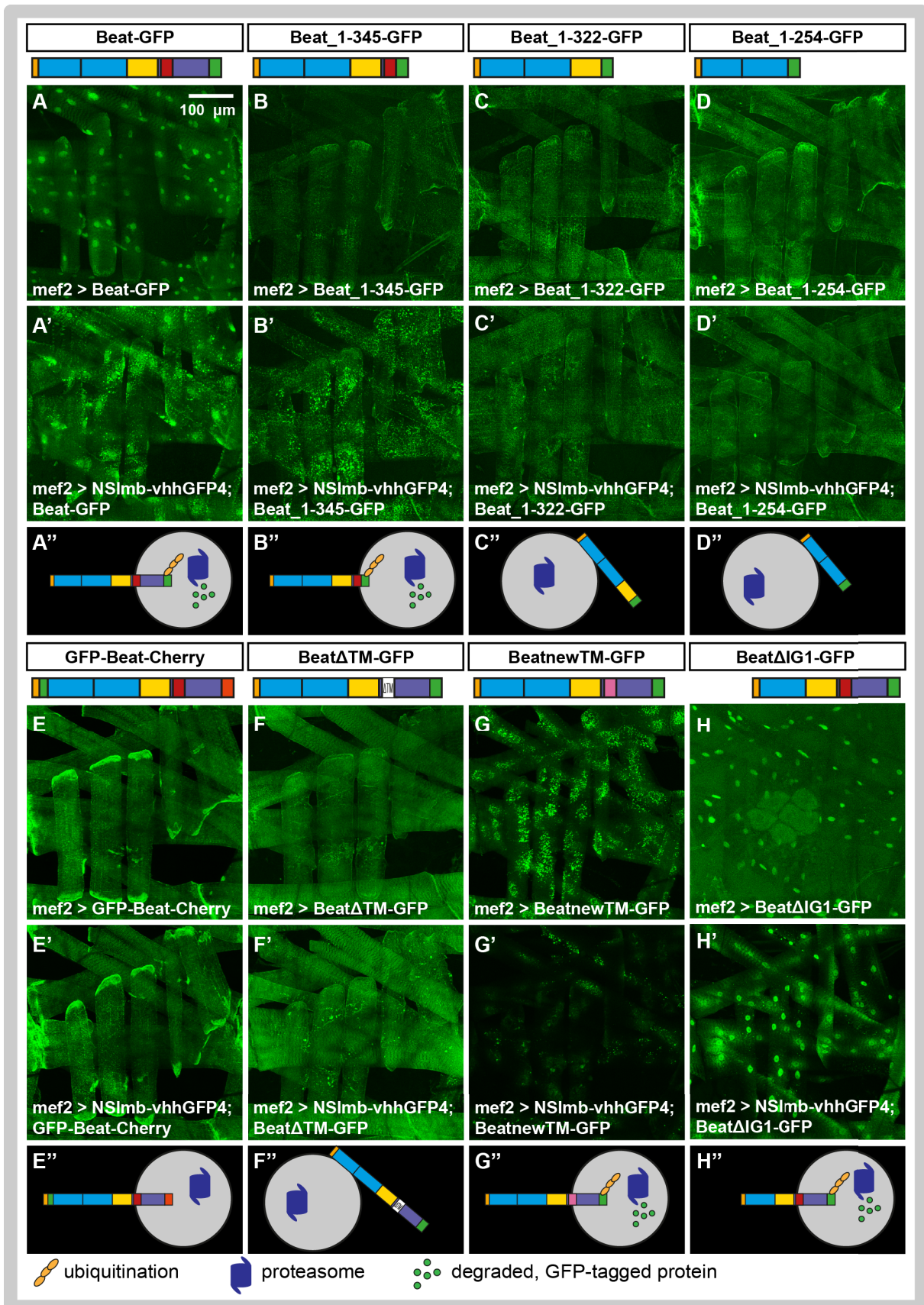


Figure 3.29: Degradation of cytosolic GFP in larvae verifies the orientation of Beat constructs. A-H: Postsynaptic overexpression of different Beat constructs. A'-H': Co-overexpression of NSImb-vhhGFP4 with different Beat constructs. A''-H'': Schematic model of the degradation of cytosolic, GFP-tagged proteins. Those constructs, where the GFP-tag is localized intracellularly, show an alteration of the GFP-signal in the co-expression with NSImb-vhhGFP4.

The GFP-signal of overexpressed Beat-GFP changes from a homogenous distribution in the muscles with nuclear accumulation to vesicular distribution with accumulation in and around the nuclei after co-expression with NSlmb-vhhGFP4 (Figure 3.29, A-A"). GFP-Beat-Cherry by contrast does not exhibit an alteration of the GFP-signal (Figure 3.29, E-E"). In the case of the C-terminal deletion constructs containing the predicted transmembrane region (Beat_1-395-GFP, Beat_1-361-GFP and Beat_1-345-GFP), the expression pattern got brighter with vesicular enrichment of fluorescence after co-expression with NSlmb-vhhGFP4 (Figure 3.29, B-B", not all constructs are shown). The C-terminal deletion constructs lacking the putative transmembrane domain (Beat_1-322-GFP and Beat_1-254-GFP) as well as Beat Δ TM-GFP do not show a modification of the expression pattern (Figure 3.29, C-C" and F-F"). In contrast, the N-terminal deletion constructs Beat Δ IG1-GFP and Beat-Cys-GFP as well as Beat_29-427-GFP exhibit a much brighter GFP-signal after co-expression with NSlmb-vhhGFP4, which does surprisingly not exhibit a vesicular distribution (Figure 3.29, H-H", not all constructs shown). The GFP-signal of BeatnewTM-GFP becomes strongly diminished by co-expression with NSlmb-vhhGFP4, but the distribution of the fluorescence remains the same (Figure 3.29, G-G").

Summed up, the ubiquitination of the GFP-tagged constructs by simultaneous expression of NSlmb-vhhGFP4 does not lead to complete degradation of the overexpressed Beat proteins. Still, a visible alteration in the expression pattern could be observed for all constructs with predicted intracellular GFP-tag, thereby confirming the findings of the surface staining and the predicted location of the transmembrane domain.

3.12 Interaction of Beat and Side in vivo

Former studies have shown that Side and Beat interact genetically in axonal pathway decisions (Siebert et al., 2009). Moreover, a direct interaction could be demonstrated *in vitro*. Cell aggregation experiments with transiently transfected S2 cells showed that adhesive aggregates formed only if both Beat-myc and Side-GFP were present in these cells (Siebert et al., 2009). This cell aggregation assay was confirmed with Kc167 cells (Pfarr, 2017). Large cell aggregates only formed if cells transfected with Side-GFP were mixed with cells transfected with Beat-Cherry.

During this work, further *in vivo* studies were carried out taking advantage of the Cherry-tagged Side constructs and GFP-labeled Beat constructs, which allow for concurrent imaging in intact larvae.

3.12.1 Beat and Side interact in simultaneous overexpression

Selected constructs were simultaneously overexpressed (Figure 3.30). In the muscle-specific overexpression, Side-Cherry exhibits a more or less evenly distributed expression pattern with clustered accumulations throughout the muscle (Figure 3.30, A, D and G). Beat-GFP is distributed very homogeneously throughout the muscle and exhibits nuclear accumulation (Figure 3.30, B). In the simultaneous overexpression, both Beat-GFP and Side-Cherry are redirected from their original expression pattern to form shared clusters around the nuclei (Figure 3.30, C-C"). Beat_1-322-GFP exhibits a weak muscle-specific expression with vesicular accumulation throughout the muscle (Figure 3.30, E). Co-overexpression with Side-Cherry leads to a highly increased GFP-signal and both constructs co-localize very strongly (Figure 3.30, F-F"). The better co-localization of Side-Cherry with Beat_1-322-GFP than with Beat-GFP might be due to the re-localization of the C-terminus of Beat-GFP, which carries the GFP-tag, into the nucleus. Muscle-specific overexpression of BeatnewTM-GFP shows vesicular enrichments around the nuclei and expression throughout the muscles (Figure 3.30, H). Concurrent expression of BeatnewTM-GFP and Side-Cherry results in strong clustering of both constructs around the nuclei and high co-localization (Figure 3.30, I-I").

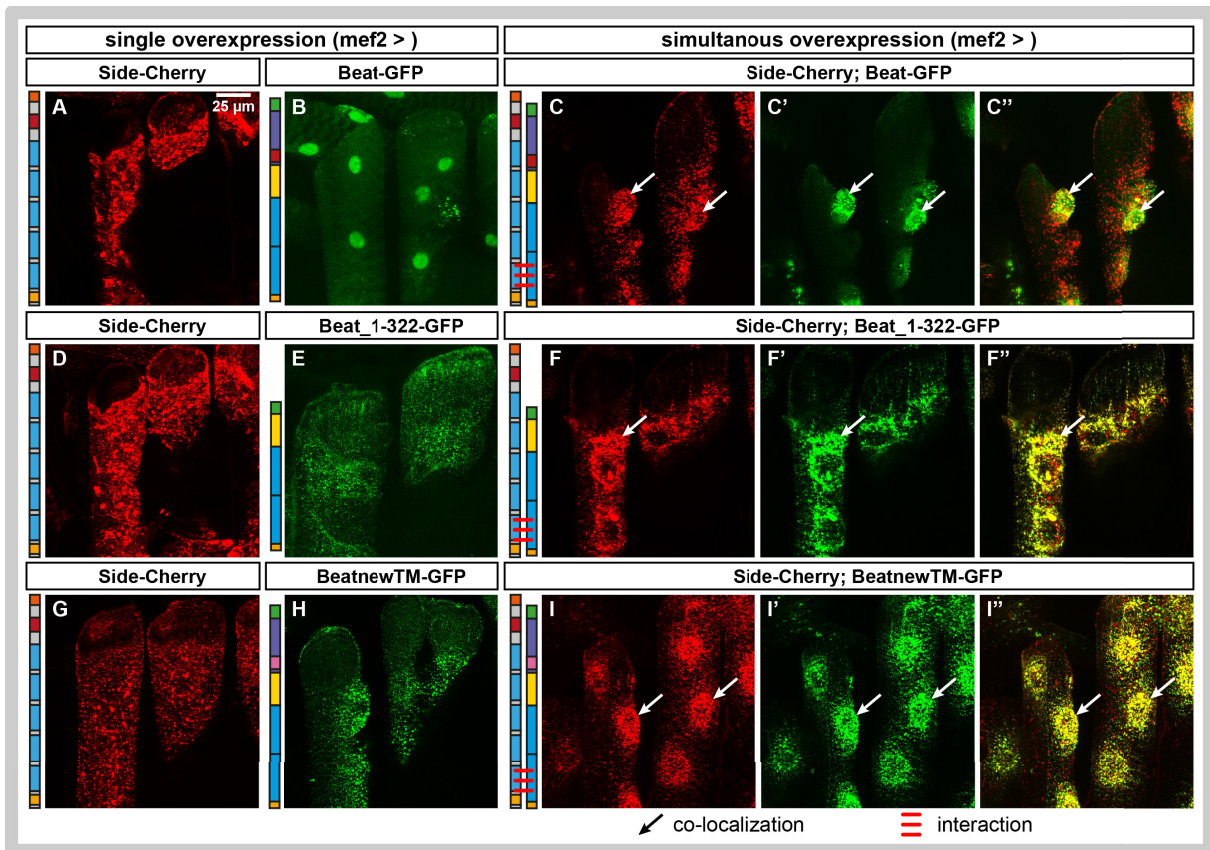


Figure 3.30: Side-Cherry and different GFP-tagged Beat constructs interact *in vivo*.

Confocal images of larval muscles 21 and 22 are shown in 63x magnification. A-B, D-E, G-H: Single expression pattern of Side-Cherry and GFP-tagged Beat constructs, respectively. C-C'': In simultaneous overexpression, Beat-GFP is redirected to form clusters with Side-Cherry. F-F'': Beat_1-322-GFP and Side-Cherry strongly co-localize when co-overexpressed. I-I'': Both Side-Cherry and BeatnewTM-GFP are strongly expressed around the muscle nuclei and co-localize.

Following the cell aggregation studies of Siebert and colleagues, A. Bauke performed further cell aggregation experiments. In her work, she was able to demonstrate that the respective first immunoglobulin domains of Beat and Side are necessary for their interaction *in vitro* (Bauke, 2009). The importance of these domains is now further investigated *in vivo*. Firstly, N-terminal deletion constructs (Beat Δ IG1-GFP and Side Δ IG1-Cherry) were overexpressed with the respective converse full-length construct (Figure 3.31, A-F''). Secondly, SideIG1+CD8-Linker-TM-Cherry (fusion construct of the Side IG1 domain fused to a CD8 linker) was co-overexpressed together with different Beat constructs (Figure 3.31, G-L''). Thirdly, the secreted SideIG1-5-Cherry was co-overexpressed with Beat-GFP (Figure 3.31, M-O''). Beat Δ IG1-GFP localizes mainly nuclear and exhibits a very weak muscle-specific expression (Figure 3.31, B). Co-overexpression with Side-Cherry does not alter any of their expression patterns (Figure 3.31, C-C''). The muscle-specific expression of Side Δ IG1-Cherry is distributed similar to Side-Cherry (Figure 3.31, D). *Vice versa*,

when co-expressing Side Δ IG1-Cherry together with Beat-GFP, neither of the single expression patterns is visibly altered (Figure 3.31, F-F''). Muscle-specific overexpression of SideIG1+CD8-Linker-TM-Cherry leads to a non-evenly distributed expression pattern with clusters around the nuclei (Figure 3.31, G + J). Simultaneous overexpression with Beat-GFP leads to slight co-localization of both constructs (Figure 3.31, I-I''). Co-overexpression with Beat_1-322-GFP causes strong redirection of the expression pattern of both constructs with strong co-localization (Figure 3.31, L-L''). Muscle-specific overexpression of the secreted SideIG1-5-Cherry does not stain the muscles at all (Figure 3.31, M). Instead, the construct enriches in some globular structures, which might be hemocytes taking up the secreted construct. Simultaneous expression of Beat-GFP retains SideIG1-5-Cherry from secretion (Figure 3.31, I-I''). Although some Cherry-signal is found in the described globular structures, a good portion of the construct is located in the muscles where it is enriched at the attachment sites and in clusters similar to the expression of Side-Cherry.

The experiments of simultaneous overexpression of Side and Beat constructs demonstrate that GFP-tagged Beat constructs containing the first IG domain are redirected to form clusters with Side-Cherry construct. Side Δ IG1-Cherry does not influence the Beat expression pattern. Both the Beat and Side IG1 domains are thus necessary for their interaction. Moreover, the Side IG1 domain is sufficient for the interaction, as co-overexpression of the fusion construct of the Side IG1 domain and a CD8 linker forms clusters with Beat constructs.

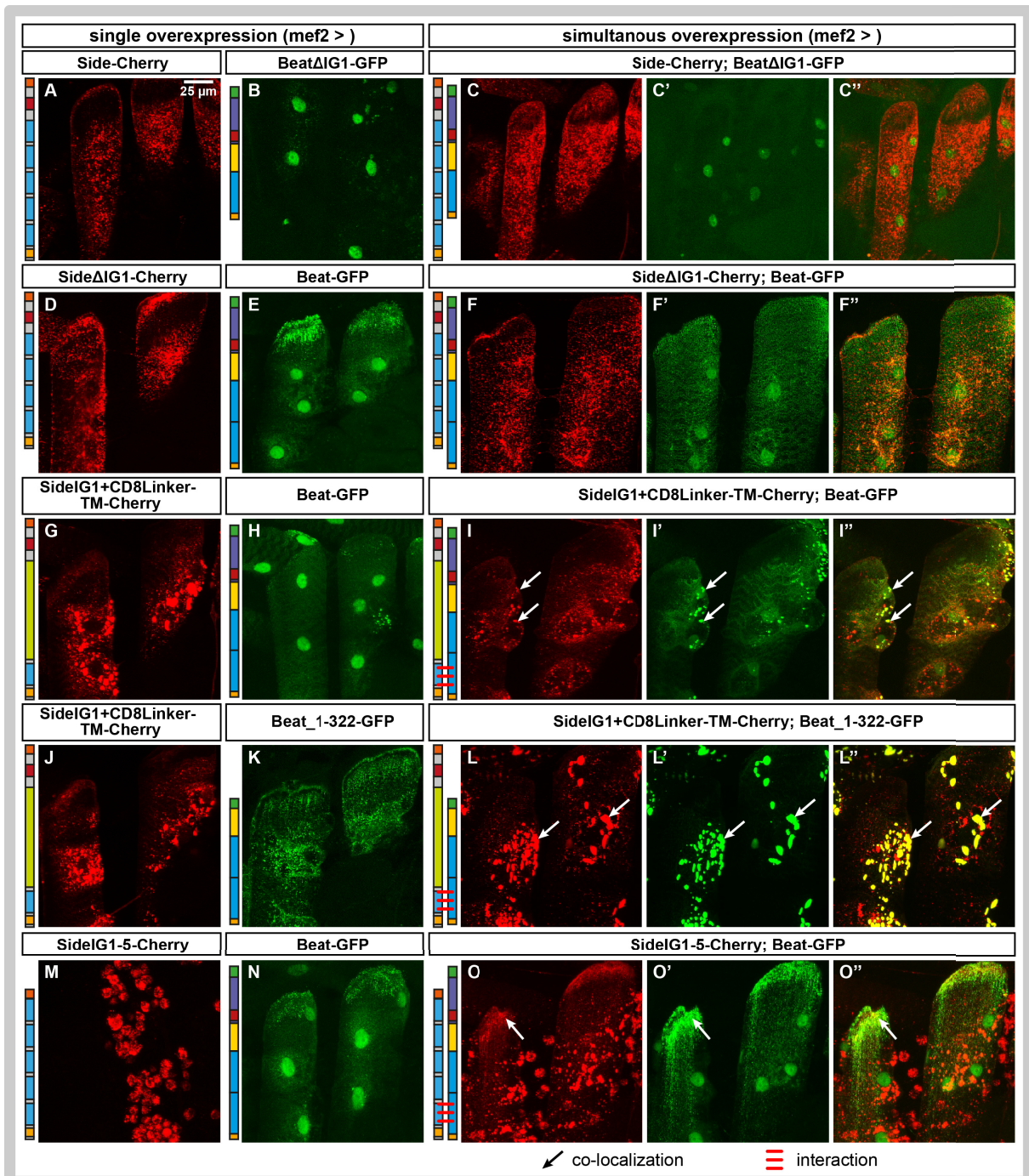


Figure 3.31: Simultaneous overexpression reveals that the respective first immunoglobulin domains of Beat and Side mediate their interaction *in vivo*.

Larval muscles 21 and 22 are shown in 63x magnification. A-B, D-E, G-H, J-K, M-N: Single expression pattern of Cherry-tagged Side constructs and GFP-tagged Beat constructs, respectively. C-C'': Deletion of the first IG domain in BeatΔIG1-GFP abolishes co-localization with Side-Cherry in co-overexpression. F-F'': Vice versa, deletion of the first IG domain in SideΔIG1-Cherry eliminates the redirection of Beat-GFP and accordingly the co-localization in simultaneous overexpression. I-I'' and L-L'': The first IG domain of Side fused to a linker protein without attractive function is sufficient for co-localization with Beat-GFP and Beat_1-322-GFP, respectively. O-O'': The secreted SideIG1-5-Cherry is retained in the muscles by simultaneous expression of Beat-GFP.

3.12.2 BeatnewTM-GFP biochemically interacts with Side-Cherry

The biochemical interaction between Side and Beat has been shown *in vitro* (Siebert et al., 2009), where Side and Beat were overexpressed in S2 cells. Side was able to co-precipitate Beat and *vice versa*. In order to show that Beat and Side also interact in *Drosophila*, co-immunoprecipitation (co-IP) was assessed *in vivo*, using larval lysates of animals individually overexpressing different Beat and Side constructs. The two different full-length Beat constructs (Beat-GFP and GFP-Beat-Cherry), as well as BeatnewTM-GFP, which strongly co-localizes with Side-Cherry in the simultaneous overexpression (see Figure 3.30), were tested for co-precipitation with Side^{29A} and Side-Cherry, respectively. As Side^{29A} and Side-Cherry are not integrated into the same genomic region of the second chromosome, larval filets overexpressing these constructs using the driver line *mef2-Gal4* had beforehand been tested in western blot for their intensity of protein expression (data not shown). This experiment revealed that Side^{29A} is expressed stronger than Side-Cherry.

The protein lysates of the different Beat constructs were precipitated with anti-GFP antibody and were then tested for their interaction with Side by western blotting (Figure 3.32, A).

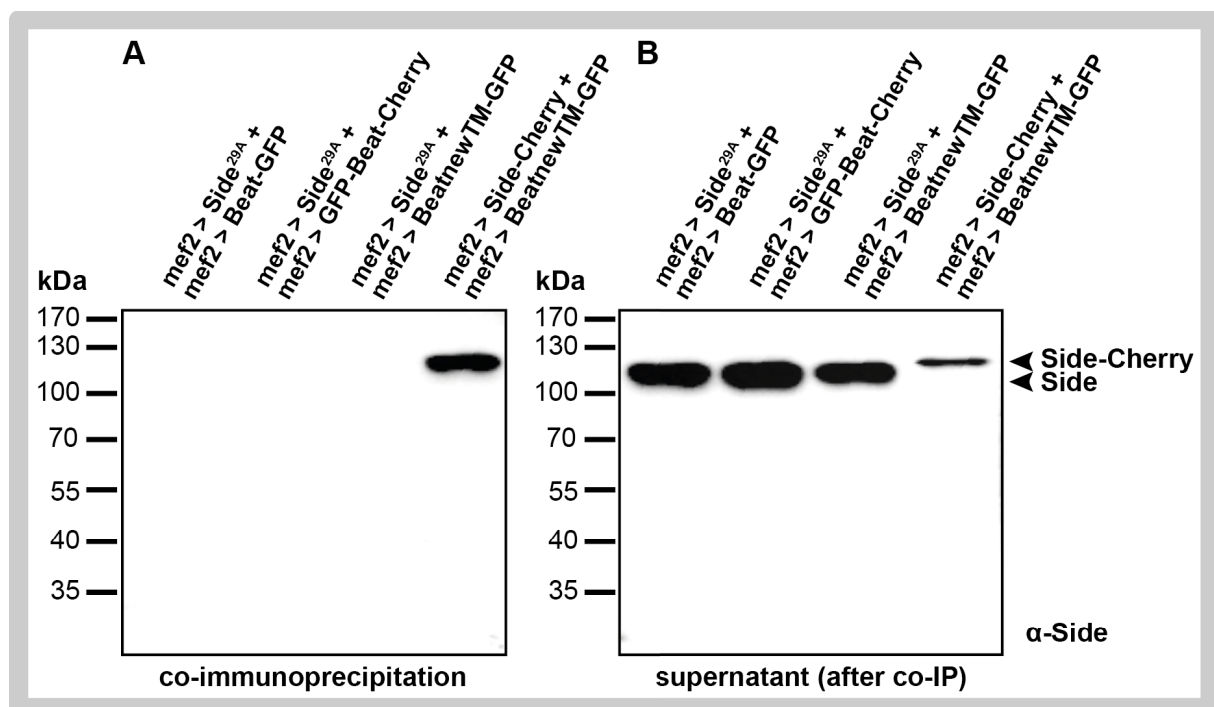


Figure 3.32: BeatnewTM-GFP is able co-precipitate Side-Cherry.

Different combinations of protein lysates from larval protein overexpression were mixed, precipitated with anti-GFP antibody and subsequently tested for Side-signal in western blot analysis. A: Beat-GFP and GFP-Beat-Cherry were not able to co-precipitate Side^{29A}. BeatnewTM-GFP was able to co-precipitate Side-Cherry, but not Side^{29A}. B: In the lysate fraction after co-IP, all Side constructs can be clearly detected.

Unexpectedly, only Side-Cherry could be co-precipitated by BeatnewTM-GFP. None of the three tested Beat constructs were able to precipitate Side^{29A}. The supernatant of the mixed protein lysates after co-immunoprecipitation were also tested for Side-signal (Figure 3.32, B). Side protein is detectable in all probes and the protein amount is lowest in the combination of BeatnewTM and Side-Cherry, supporting the results of the co-precipitation of Side-Cherry and thus depletion of the constructs from the supernatant (Figure 3.32, A, lane 4).

3.12.3 Overexpression of Beat-GFP traps endogenous Side

If Beat and Side indeed interact *in vivo*, it should be possible to manipulate the endogenous Side by overexpression of a Beat construct. As it is possible to stain for endogenous Side, it was further assessed whether overexpression of Beat-GFP relocates the endogenous Side-signal. In young embryos, no alteration of the Side expression pattern was observed for pre- or postsynaptic overexpression of Beat-GFP (data not shown). These findings show that Side is still expressed and regulated in the correct manner. In old embryos by contrast, Side fails to get downregulated but is trapped in different tissues, according to the tissues of Beat overexpression (Figure 3.33 and Figure 3.34).

Wild-type embryos exhibit a downregulated Side expression in late stage embryos (Figure 3.33, A-A''). Muscle-specific overexpression of Beat-GFP traps endogenous Side on the muscle surface and on attachment sites in late embryonic stages (arrows and arrowheads in Figure 3.33, B-B''). In earlier embryonic stages, Side is expressed in the normal, wild-type fashion (data not shown). In contrast, overexpression of Beat Δ IG1-GFP in muscles is not able to trap endogenous Side to the muscle surface (Figure 3.33, C-C''). In the muscle-specific overexpression of Side-Cherry, the exogenously expressed Side is strongly detectable. In embryonic stage 17, when the muscles are completely established, Side-Cherry is intensely expressed on the muscle surface (Figure 3.33, D-D''). No accumulation at the attachment sites is visible. In the ventral muscle field, there are enrichments of Side-signal (Figure 3.33, D-D'', asterisk), which were identified as NMJs by co-staining with anti-DvGlut, a marker for motoneurons and NMJs (data not shown).

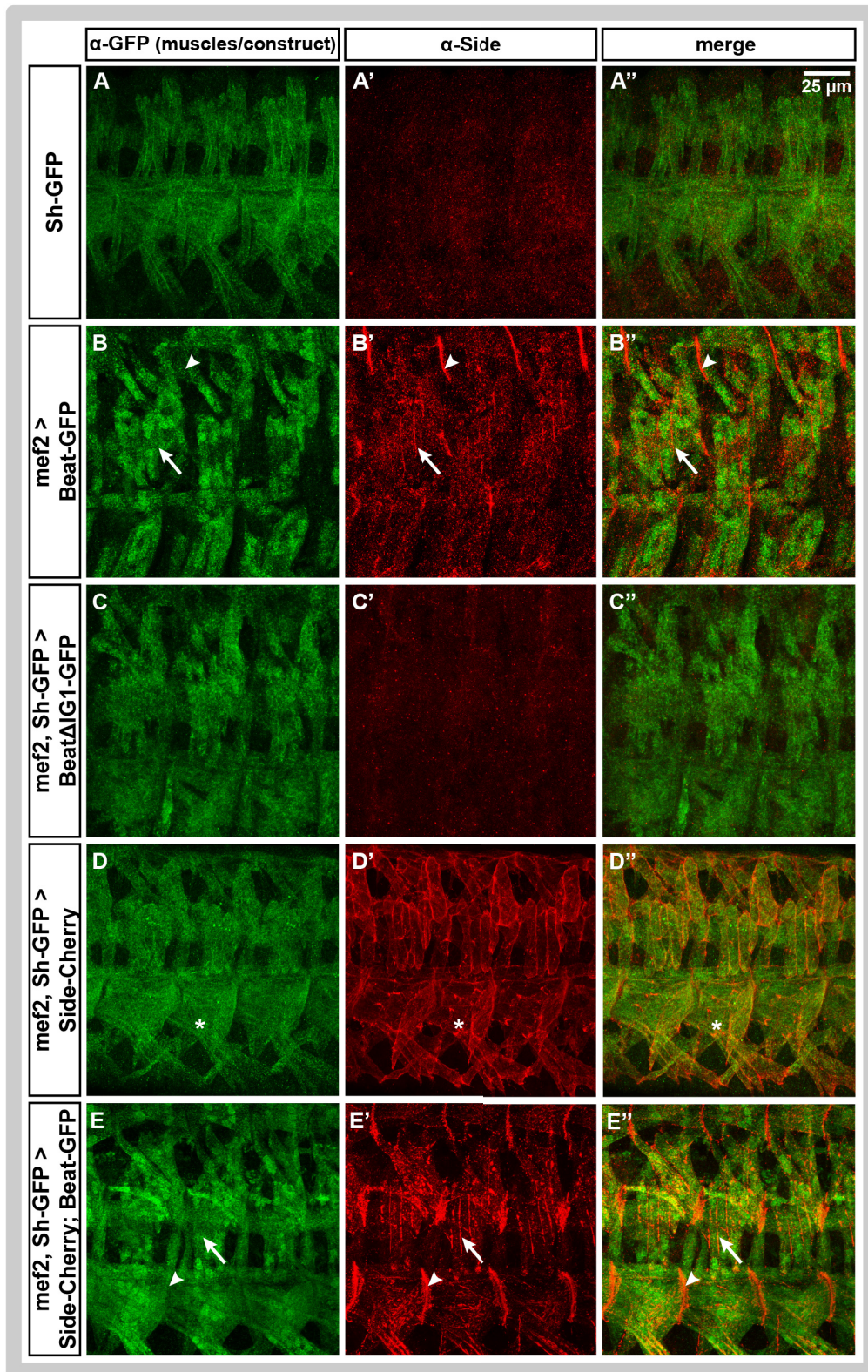


Figure 3.33: Postsynaptic Beat-GFP traps endogenous Side on the muscle surface.

Confocal images of stage 17 embryos. A-A'': In late stage control embryos, Side expression is mostly downregulated. B-B'': Muscle-specific overexpression of Beat-GFP leads to endogenous Side-signal on the muscle surface (arrows) and on attachment sites (arrowheads) in late stage embryos. C-C'': Beat Δ IG1-GFP is not able to trap endogenous Side. D-D'': Muscle-specifically overexpressed Side-Cherry is enriched in the muscle membranes and exhibits clusters of accumulation (asterisks). E-E'': If both Side-Cherry and Beat-GFP are simultaneously overexpressed, the expression pattern of Side-Cherry changes compared to the single overexpression (compared to D'). Side-Cherry is enriched on the muscle surface (arrows) and on attachment sites (arrowheads).

In the simultaneous postsynaptic overexpression of Beat-GFP and Side-Cherry, Side-signal is enriched on the muscle surface and attachment sites (Figure 3.33, E-E’), similar to the situation of Beat-GFP overexpression but to a stronger degree.

As the innervation defects caused by muscle-specific overexpression of Side-Cherry are strongly diminished by simultaneous overexpression of Beat-GFP (Figure 3.36, C), the question arises whether the Side expression is downregulated in this double expression genotype. Although the distribution of the Side-signal has changed compared to the single overexpression of Side-Cherry, Side is still strongly expressed.

These experiments demonstrate that expression of Beat-GFP in muscles thus captures endogenous Side on the muscle surface in late embryos without interrupting the early Side expression pattern.

Interestingly, presynaptic overexpression of Beat-GFP traps endogenous Side in motor axons and synapses as well as in sensory neurons (Figure 3.34). Pan-neuronal, motoneuronal and sensory overexpression of Beat-GFP leads to constitutive Side expression. The strongest Side-signal in motor axons and NMJs is induced by motoneuron-specific expression of Beat-GFP (Figure 3.34, B-B’). Sensory neuron specific overexpression of Beat-GFP captures Side strongly on sensory neurons of stage 17 embryos (Figure 3.34, D-D’). The early Side expression pattern remains unchanged (data not shown).

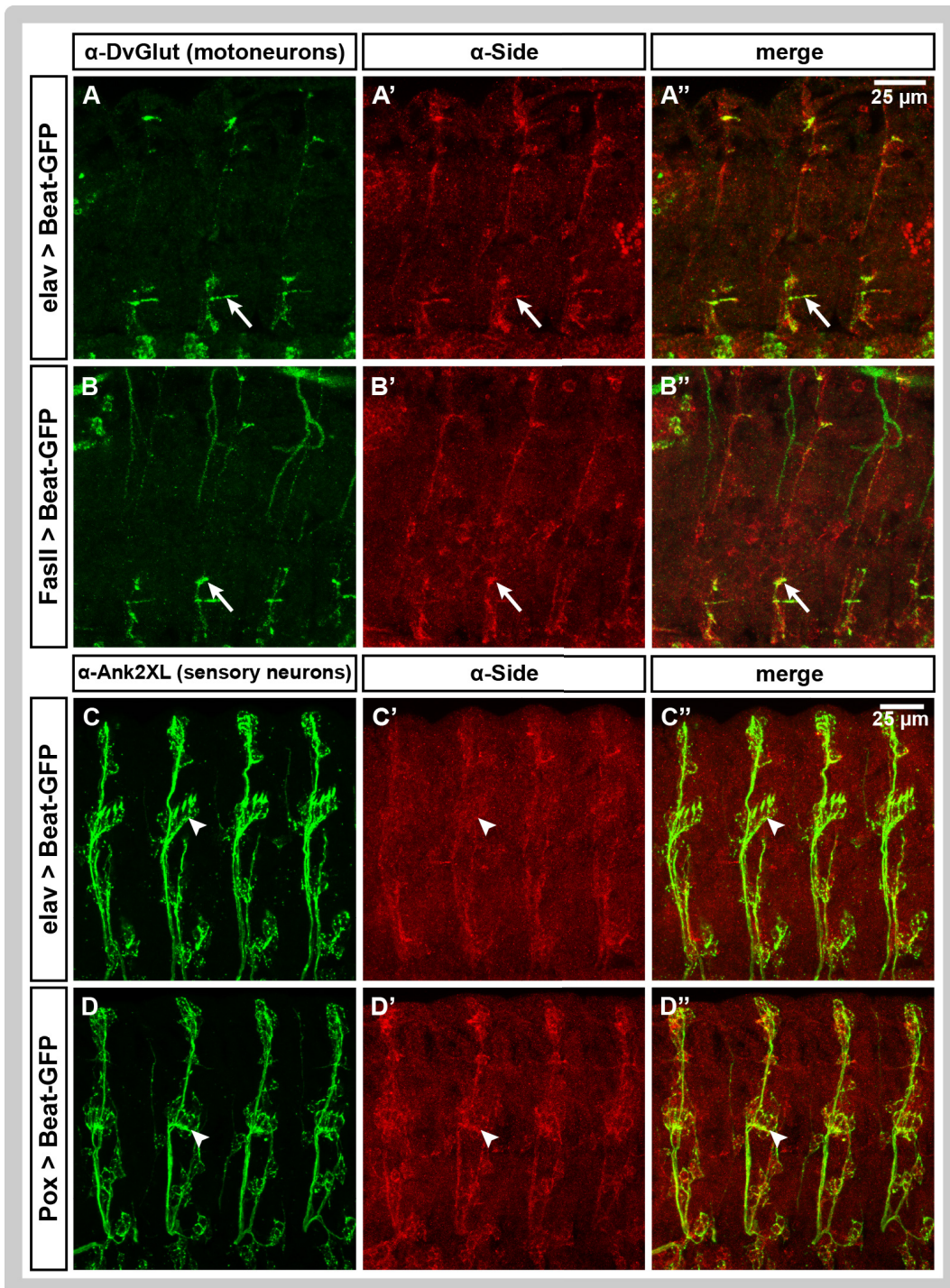


Figure 3.34: Presynaptic Beat-GFP traps endogenous Side on motor- and sensory neurons.

Stage 17 embryos are shown. A-A'' and B-B'': Co-staining with anti-DvGlut shows that pan-neuronal and motoneuron-specific overexpression of Beat-GFP traps Side in motoneurons and NMJs. C-C'' and D-D'': Pan-neuronal and sensory neuron-specific Beat-GFP expression catches Side on sensory neurons. Arrows: NMJs, arrowheads: sensory neurons of lateral chordotonal organs.

It was further tested, whether Beat-expressing motor axons and growth cones are able to attract the secreted SideIG1-5-Cherry construct. Therefore, intact embryos of the FasII-GFP^{Mue397} exon trap line were imaged. FasII is expressed motoneuron-specifically and thus motor axons are marked by GFP in the FasII-GFP^{Mue397} exon

trap animals. The images of this experiment reveal that the Cherry-signal is not accumulated around motor axons and growth cones and that the secreted construct is thus not attracted by motor axons (arrows in Figure 3.35, A-B'').

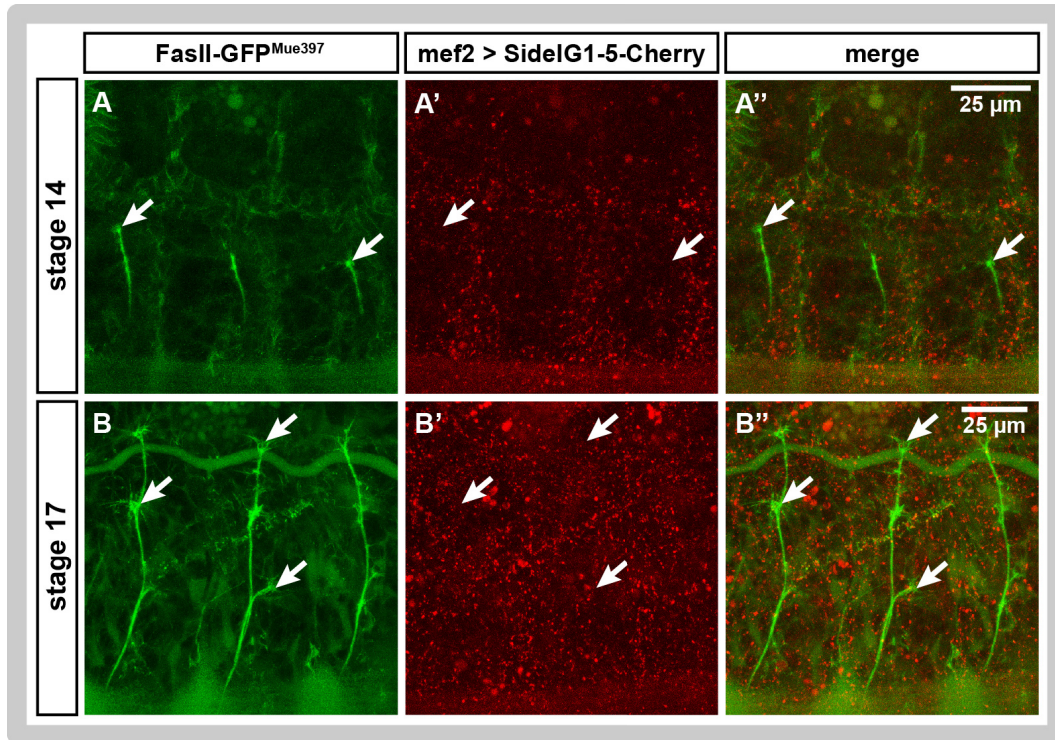


Figure 3.35: Endogenous Beat is not able to trap secreted SidelG1-5-Cherry at growth cones. Live imaging of FasII-GFP^{Mue397}; mef2 > SidelG1-5-Cherry embryos. Motoneurons are labeled in green, muscle-specific overexpression of secreted SidelG1-5-Cherry is shown in red. A-A'': Outgrowing motoneurons at stage 14 do not co-localize with SidelG1-5-Cherry. B-B'': Late stage embryos do not show enrichment of SidelG1-5-Cherry at growth cones or choice points. Arrows depict growth cones.

3.12.4 Interaction of Side and Beat neutralize the attractive effect of Side

Muscle-specific overexpression of Side-Cherry induces severe dorso-lateral innervation defects (see Chapter 3.8.2). In the simultaneous, postsynaptic overexpression of Side-Cherry and Beat-GFP, these dorsal innervation defects are largely decreased. As the innervation defects of this genotype cannot be counted in intact larvae due to excess Beat-GFP fluorescence outshining the Sh-GFP-signal, immunohistochemical stainings on larval filets were performed (Figure 3.36, A-C). The typical array of innervations mediated by the respective genotype is depicted (Figure 3.36, A'-C'). Simultaneous, muscle-specific expression of Side-Cherry and Beat-GFP mostly restores the wild-type innervation pattern compared to the overexpression of Side-Cherry alone.

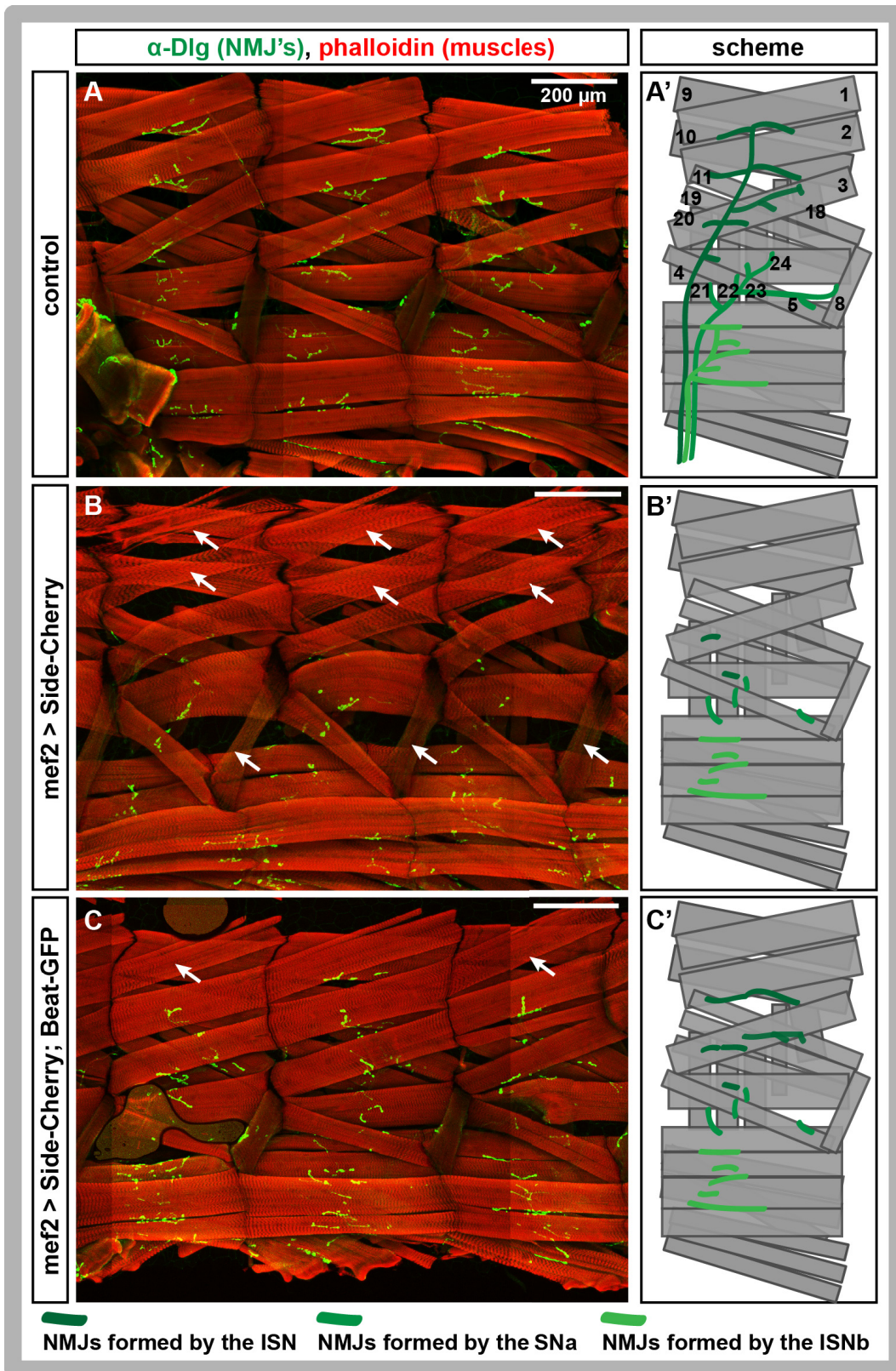


Figure 3.36: Simultaneous expression of Beat-GFP strongly diminishes innervation defects caused by postsynaptic overexpression of Side-Cherry.

Confocal images (tilesacans) of larval filets. Postsynapses are marked by anti-Dlg and muscles are stained with phalloidin. **A:** In wild-type larvae, all dorsal muscles are innervated. **B:** Postsynaptic overexpression of Side-Cherry induces severe dorso-lateral innervation defects. **C:** Additional overexpression of Beat-GFP largely rescues the severity of the innervation defects caused by Side-Cherry. **A'-C':** Schematic overview of typical innervations per genotype, assigned to NMJs formed by the ISN, SNa and ISNb. **A'** additionally illustrates the nomenclature of the dorso-lateral muscles.

Results

Remarkably, uninnervated muscles exhibit much less Cherry and GFP fluorescence (data not shown), indicating a correlation between functional wiring of a muscle and the strength of transgene expression.

The innervations of muscles normally innervated by the ISN and SNa were counted and are listed in Table 3.5. The percentage of innervated muscles was calculated and the significance of differences in the innervation frequency was analyzed using the χ^2 test.

Table 3.5: Counting of NMJs reveals significant innervation defects throughout the dorso-lateral compartment of Side-Cherry overexpressing larvae.

Column A: Muscle nomenclature. Column B: Percentage of innervated muscles of control larvae and respective number of counted muscles. Column C: Postsynaptic overexpression of Side-Cherry leads to most drastic reduction of innervated muscles. The p-value (χ^2 , calculated against the control) reveals highly significant differences for most muscles. Column D: Percentage of innervated muscles of larvae co-overexpressing Side-Cherry and Beat-GFP, the respective number of counted muscles and p-values calculated against the control and against the single overexpression of Side-Cherry, respectively. N.s.: not significant, *p ≤ 0.05, **p ≤ 0.01, ***p ≤ 0.001.

Muscle	B		C			D			
	Control Innervation	n	mef2 > Side-Cherry Innervation	n	p (vs B)	mef2 > Side-Cherry; Beat-GFP Innervation	n	p (vs B)	p (vs C)
ISN									
1	100 %	53	2.2 %	91	***	34.9 %	83	***	***
9	100 %	56	1.0 %	96	***	19.0 %	79	***	***
2	100 %	52	11.1 %	99	***	88.9 %	90	*	***
10	100 %	56	3.1 %	98	***	75.0 %	88	***	***
3	100 %	56	65.0 %	100	***	98.9 %	93	n.s.	***
4	98.3 %	58	94.1 %	102	n.s.	94.9 %	78	n.s.	n.s.
11	98.0 %	51	29.3 %	99	***	96.5 %	86	n.s.	***
19	100 %	56	66.7 %	96	***	97.8 %	89	n.s.	***
20	98.0 %	51	47.9 %	96	***	90.7 %	75	n.s.	***
18	100 %	44	9.9 %	91	***	94.7 %	76	n.s.	***
SNa									
21	100 %	50	81.7 %	82	**	98.7 %	76	n.s.	**
22	100 %	50	78.8 %	85	**	93.2 %	73	n.s.	*
23	100 %	51	70.0 %	82	***	91.9 %	74	n.s.	***
24	98.1 %	53	9.0 %	89	***	62.3 %	69	***	***
5	98.3 %	58	89.8 %	98	n.s.	97.9 %	94	n.s.	*
8	100 %	56	40.0 %	100	***	84.6 %	91	**	***

All muscles of the regarded dorso-ventral region except for muscles 4 and 5 are significantly affected by the Side-Cherry overexpression. Remarkably, additional overexpression of Beat-GFP is able to significantly improve the innervation in all cases (except for muscle 4, which is not much affected by Side-Cherry expression anyway). The varying number of counted muscles (n) is due to imaging conditions of the larval filets, where some muscles of deeper layers could not always be evaluated. Figure 3.37 visualizes the innervation defects of the different genotypes. Black muscles indicate up to 100% innervation, light grey muscles indicate 0-10% innervation.

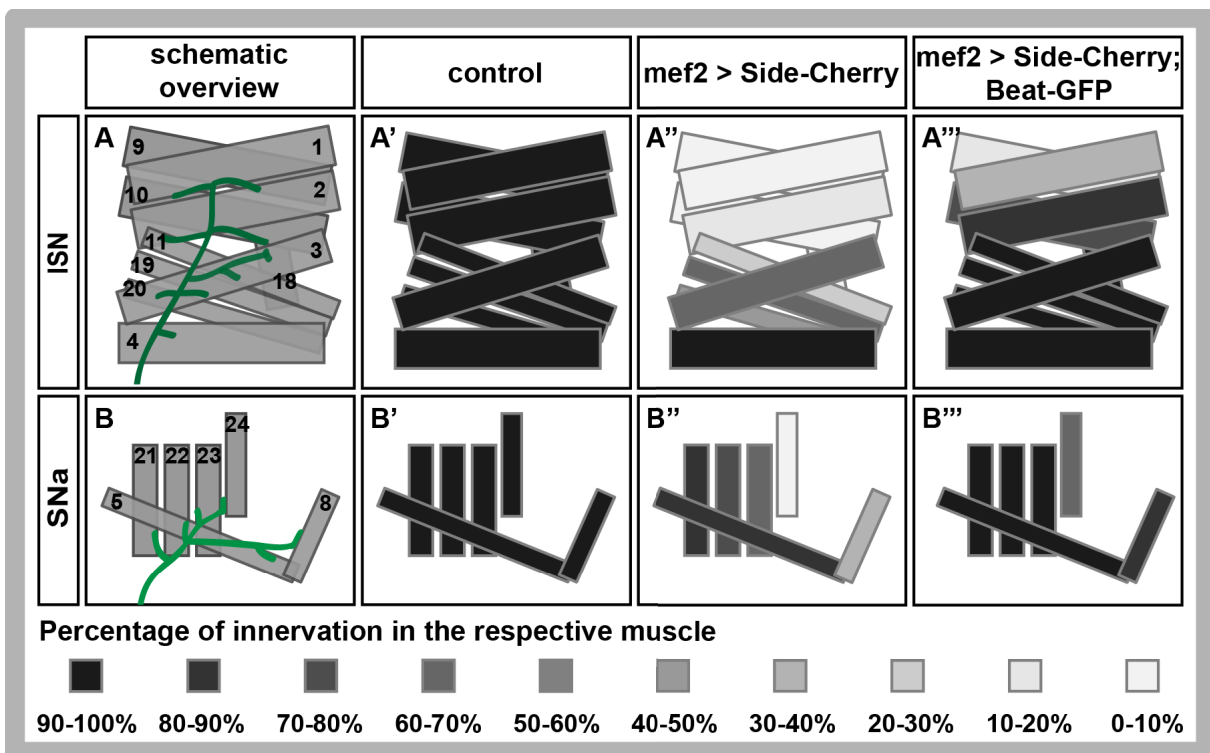


Figure 3.37: Muscles at the outmost end of the ISN and SNa are most severely affected by muscle-specific overexpression of Side-Cherry.

Schematic illustration of quantitative analysis of larval innervation defects. A-B: Muscle nomenclature and ideal innervation path off the ISN and SNa, respectively. A'-B': In control larvae, roughly 100% of all dorsal and lateral muscles are innervated, as indicated by the black color. A''-B'': Postsynaptic overexpression of Side-Cherry leads to drastic lack of innervation, especially at the most distant part of the ISN and SNa (light grey color of the muscles). A'''-B''': Additional, simultaneous overexpression of Beat-GFP restores a good portion of the missing innervations.

As only postsynapses and not complete motor axons were labeled with anti-Dlg, the disturbed pathway in the overexpression genotype cannot be reconstructed with these data. Still, the way the NMJs are positioned on the muscles, in many cases it becomes clear that the ISN and SNa do not follow the ideal, wild-type pathway. For example the NMJ on muscle 5 of the Side-Cherry overexpression genotype is in

most cases situated at a wrong position (dislocated NMJ), indicating that this muscle might be innervated by some other fascicle than the SNa or that the SNa pathway is severely diverted from its original track.

Taken together, these experiments demonstrate that simultaneous overexpression of Beat-GFP restores the most part of the innervation defects induced by postsynaptic overexpression of Side-Cherry.

4 Discussion

The prerequisite to percept and adequately react to internal as well as external stimuli is a precise neuronal wiring. Beat and Side strongly contribute to the process of motor axonal guidance during embryogenesis. In this work, the mechanisms of the Beat and Side interaction were characterized *in vivo* including the identification and verification of structurally important domains for interaction, membrane anchoring and signal transduction.

4.1 Missense mutations in Side and Beat impede their functionality

Single point mutations in Beat and Side, which lead to the typical *beat*- and *side*-specific guidance defects, can provide valuable clues about functionally or structurally important domains of these guidance molecules. All truncated forms of Side proteins in the analyzed *side* alleles are null alleles and lead to loss-of-function phenotypes. Evidently, the C-terminal domain of the Side protein, which provides the membrane anchoring, is essential for its function. Moreover, two different single amino acid exchange mutations, G187D in *side*^{I306} and L241H in *side*^{H143}, were found among the analyzed *side* alleles. The mutations are located within the first immunoglobulin domain and the linker domain separating the first and second immunoglobulin domain, respectively. Both these alleles *side*^{I306} and *side*^{H143} harbor an exchange mutation of an unpolar amino acid, which is predicted to be part of a β -sheet in both cases, in favor of a polar amino acid. The glycine at position 187, which is affected in *side*^{I306}, is part of the F-strand β -sheet and is highly conserved among different immunoglobulin domains (Bieber et al., 1989; Williams and Barclay, 1988). It could thus critically contribute to proper spatial conformation of the first immunoglobulin domain, as such domains are characterized by multiple β -sheets, with each two β -sheets forming antiparallel β -strands. These antiparallel β -sheets form a hydrophobic interior by inwards-pointing hydrophobic amino acids, which alternate with outwards-pointing hydrophilic residues (Williams and Barclay, 1988). On the one hand, the exchange of an unpolar amino acid into a polar one most likely disturbs the correct folding of the β -sheet and therefore might interrupt proper formation of the secondary protein structure within this region. In the literature, different cases are reported, where the substitution of a single amino acid disturbs

some part of the protein structure. Firstly, an R628P mutation in the $\alpha 3$ subunit of the Integrin $\alpha 3\beta 1$ was reported to partially disrupt two β -sheets (Yamada and Sekiguchi, 2013). Secondly, a missense mutation in Keratin 25 (KRT25), a type I keratin, which is associated with wooly hair in humans and mice, was recently identified. This L317P variant is described to result in the disruption of an α -helical domain, which possibly interferes with the heterodimerization with type II keratins (Ansar et al., 2015). On the other hand, the unstructured “turn” region in between the two β -sheets could serve as binding pocket for the guidance receptor Beat and might be directly affected. This option could be further tested by the generation of a Side construct with a modified protein sequence in this region and subsequent overexpression experiments *in vivo*, thereby analyzing the impact of this construct on axon guidance. However, the single amino acid exchanges in *side*^{I306} and *side*^{H143} result in strong guidance defects according to the *side* mutant phenotype. This shows that these mutations highly impair the Side protein function, probably by impeding the binding of the interaction partner Beat.

*Beat*³ exhibits a stop mutation leading to a truncation of the linker- and the Cys-rich region including the potential transmembrane domain. The severe guidance defects might confirm the function of Beat as membrane-bound guidance receptor and furthermore indicate a signaling role of the Beat C-terminus. The mutation in *beat*² is characterized as point mutation in the splice donor site resulting in the deletion of 26 amino acids (G111 up to I136) within the first immunoglobulin domain. This mutation shows that also for Beat, the external-most first immunoglobulin domain is crucial to convey the protein function.

4.2 Side is constitutively expressed

Side is expressed in a highly dynamic, spatio-temporally restricted pattern during embryogenesis (Siebert et al., 2009; Sink et al., 2001), marking a substrate pathway for the outgrowing motor axons. Among the available *side* mutant alleles, only *side*^{I306} and *side*^{H143} exhibit Side protein expression. In all other alleles, no Side protein is detectable, neither in immunohistochemical stainings nor in western blot analysis. This confirms the sequencing results of stop mutations versus single amino acid exchange mutations. Remarkably, Side^{H143} protein expression is restricted to the cell bodies (Figure 3.5, A-A”) and not localized on the axons of the sensory neurons. The

axon initial segment, which separates the somatodendritic and the axonal compartments, plays an important role in the trafficking regulation of neuronal proteins. It holds both a function as surface diffusion barrier and intracellular traffic filter (Leterrier and Dargent, 2014). Lipids and membrane proteins can thus not freely diffuse through the axon initial segment, but their transmission is restricted. Similarly, the vesicular transport and diffusion of intracellular molecules into the axon is regulated. Axonal enrichment of proteins can take place via different mechanisms (Winckler and Mellman, 2010). Firstly by direct polarized delivery of proteins targeted to the axon from the secretory pathway. Secondly the indirect polarized delivery by transcytosis redirects membrane proteins into the appropriate domain by selective endocytosis. Thirdly the nonpolarized delivery and selective retention keeps randomly diffusing membrane proteins at the desired location by attachment via appropriately placed cytoskeletal scaffolds or adjacent cells. Side protein structure modeling using RaptorX suggests that the secondary structure is affected by an additional helix in the first and second immunoglobulin domains of Side^{H143} (see Figure 3.3 C, purple structures). RaptorX is used for bioinformatic modeling of protein structures by several working groups, as for example (Goswami, 2015; Panda and Mahapatra, 2017). According to the predicted additional helices within the immunoglobulin domains, the mutation in *side*^{H143} might result in incorrect protein folding and thus could disturb any of the above-mentioned mechanisms for transportation of the Side^{H143} protein into the axons of the sensory neurons. Most likely, the interaction of Beat with Side^{H143} protein is strongly impaired. In case of residual interaction, the restriction of the Side expression to the cell bodies would still strongly perturb the correct pathfinding by preventing the fasciculation of motor axons with the ingrowing sensory axons. Instead, motor axon growth cones would continue searching for alternative guidance information.

Western blot analysis confirms the findings that in homozygous *side*^{I306} and *side*^{H143} mutant embryos, Side protein is detectable. Moreover, Side^{I306} and Side^{H143} proteins exhibit exactly the same molecular weight as the native Side, which is predicted to have a molecular weight of 102 kDa and is detectable at about 112 kDa, probably due to posttranscriptional modifications. Homozygous *side* mutant embryos of all other tested alleles do not exhibit the band at 112 kDa. Interestingly, the anti-Side antibody recognizes a second prominent band at about 47 kDa in wild-type embryos as well as in all different *side* mutant alleles. This might be due to unspecific binding

of the antibody, as it is also the case in third instar larvae, where wild-type as well as *side* mutants exhibit a distinct, dotted pattern recognized by the anti-Side antibody at the NMJs (see Figure 3.8, B-B’). Another option would be that there is an unknown, alternative splice-isoform of Side, which can still be transcribed in *side* mutants. The possibility of a different splice-isoform could be checked by western blot analysis of embryos containing a *side* deficiency, which widely spans the whole *side* gene locus. In wild-type embryos, Side expression is largely downregulated in immunohistochemical stainings of stage 17 embryos, but persistently stains the CNS (Siebert et al., 2009; Sink et al., 2001). Larval Side expression has not been described before. Unexpectedly, western blot analysis revealed an increase of Side protein from mid-stage to late stage wild-type embryos and showed considerable amounts of Side protein in the larval brain and slight amounts in larval muscle tissue. The detected larval Side-signal seems to be specific, as in trans-heterozygous *side*^{C137}/*side*^{I1563} larvae, the anti-Side antibody does not recognize any protein. These findings emphasize that, in contrast to previous findings, Side is constitutively expressed or not degraded in larval neuronal and muscular tissue. Interestingly, the Side-signal runs at a slightly higher band in brains than in embryos and larval filets. This might implicate different posttranscriptional modifications of the Side protein or the presence of a different splice-isoform in the brain. There are four known splice-isoforms of the *side* gene, which encode proteins between 929 and 986 amino acids. The previously characterized version of Side is *side*-RA and encodes for a 939 amino acid protein (Sink et al., 2001). The longest isoform is *side*-RC, which encodes for a protein consisting of 986 amino acids. Furthermore, embryos exhibit an additional, unspecific signal at about 47 kDa (which is also present in *side* mutant embryos) and a specific Side-signal at about 67 kDa (which is not detectable in *side* mutant embryos), whereas an additional, specific band in larvae is only present in filets at roughly 70 kDa, which might be an unknown splice variant or a processed form of Side. This latter option would argue for a potential cleavage of some part of the protein, for example after interaction with its receptor. In this context, the matrix-metalloprotease Tolloid-related (Tlr) might be a potential candidate to downregulate Side expression on intermediate targets by cleavage after contact between Side and Beat (Bauke, 2009; Kinold, 2016).

Stainings of Side-GFP exon trap third instar larvae revealed specific signal exclusively in the neuropil of the brain, where the central synapses are located. This

GFP-signal overlaps with the signal from the anti-Side antibody. Interestingly, a mass-spectrometry screen using membrane fraction proteins from adult *Drosophila* heads detected the presence of Side-RB protein (Aradska et al., 2015). These findings firstly support the results of Side expression beyond embryogenesis and secondly encourage the findings of brain-associated Side expression.

The convergence of Beat-expressing growth cones and Side-expressing intermediate and final targets during axon guidance makes these molecules a pair of leading proteins for contact adhesion prior to synapse formation. Side might therefore play an additional role for example in processes of synaptic stabilization and growth, as supported by the Side-signal found in boutons of neuromuscular junctions. Unexpected, this distinct-looking Side-signal is also present in all *side* mutant larvae. The hypothesis, whether this synaptic staining might represent the lower band of embryonic western blot Side-signal, was discouraged though by the finding that *side* mutant larvae did not exhibit any Side-signal in western blot analysis. However, former works have already proposed a role of Side to promote synaptogenesis (de Jong et al., 2004), which will be discussed in Chapter 4.5. Furthermore, the late larval Side expression could be a further hint for a repeated role in axon guidance during metamorphosis, as adult *side* mutants exhibit strong locomotion defects and innervation defects (Kinold, 2016).

In *side*^{I306}, *side*^{H143} and *beat*^{C163} mutant embryos, Side is constitutively detectable in sensory neurons of late embryos. Immunohistochemistry suggests a downregulation of wild-type Side protein in late embryonic stages, whereas western blot analysis indicates a constitutive and even increased protein level. The epitope for the anti-Side antibody must be located somewhere in between the second immunoglobulin domain and the transmembrane domain, as it does recognize the construct SideΔIG1-Cherry, but not SideIG1+Linker-TM-Cherry. The discrepancy between immunohistochemical detection and western blot might be due to a masking of the antigen epitope in late embryonic stages in the native Side protein, for example by an ongoing interaction between Side and Beat or by the formation of higher complexes. The antibody could thus no longer bind to the Side epitope in immunohistochemical stainings. In SDS gel electrophoresis, proteins are denatured and the epitope might consequently become unmasked. The hypothesis of the masked Side antigen epitope is supported by the findings that immunohistochemical stainings of Side-GFP exon trap embryos yield constitutive signal using the anti-GFP antibody, which binds

to the intracellular GFP-insert, whereas the signal from the anti-Side antibody, which recognizes an extracellular epitope, becomes downregulated in late stage embryos (Föhrenbach, 2016). In the case of *side* and *beat* mutants, the interaction between these proteins would be drastically reduced (in case some residual protein function exists in *side*^{I306} and *side*^{H143}) or totally abolished. The Side antigen epitope would consequently remain unaffected, permitting constitutive, embryonic Side detection in immunohistochemistry. The observation that the constitutive Side expression is stronger in *beat*^{C163} than in *side*^{I306} and *side*^{H143} embryos supports the possibility of minor, residual protein function in *side*^{I306} and *side*^{H143} mutant animals, as indicated by complementary analyses. This option could be tested by overexpression of Beat-GFP in these mutant backgrounds and evaluation of a potential relocation of the endogenous Side^{I306} or Side^{H143} protein. Another possibility to examine if residual protein function is left would be the generation of Side constructs carrying the *side*^{I306} and *side*^{H143} mutation and subsequent overexpression experiments evaluating the content of larval innervation defects.

In summary, the examination of Side expression during embryonic and larval developmental stages indicates a constitutive role for Side, which might involve synaptic processes.

4.3 Endogenous Beat expression

Fambrough and Goodman reported embryonic Beat expression in motor neurons and growth cones (Fambrough and Goodman, 1996), using an anti-Beat antiserum directed against an epitope within the amino acid region 245-318. As this antiserum is no longer available, emphasis was laid on the generation of a new antibody for the detection of the endogenous Beat protein, because to date it is only possible to visualize overexpressed Beat *in vivo*. Former efforts to reproduce the anti-Beat antiserum employed the same amino acid sequence as epitope for immunization as previously used by Fambrough. However, this antiserum has not been sufficient successful, as it only recognizes overexpressed, but no endogenous Beat (Bauke, 2009).

In the context of this work, a new approach using two different peptide-fragments derived from the linker region (aa 286-299) and the intracellular Cys-rich region (aa 376-389), respectively, has been made. Both fragments have been used for

immunization of a rabbit and a guinea pig each, as the immune response can be highly variable in different species. Out of the resulting antisera, only the rabbit anti-Beat-Cys and the guinea pig anti-Beat-Linker provide signal of specific structures in immunohistochemical stainings. The rabbit anti-Beat-Cys antiserum marks motor axons and growth cones as well as sensory neurons. Muscle-specifically overexpressed Beat is slightly detectable, but overrun by the neuronal staining. The guinea pig anti-Beat-Linker antiserum exhibits strong background, and motor axons and growth cones are weakly, but distinctly, labeled. Overexpressed Beat is clearly detectable. However, in both cases these neuronal structures are also weakly visible in *beat*^{C163} mutant embryos. As *beat*^{C163} is a loss of function mutation due to a gene inversion (Ashburner et al., 1999; Fambrough and Goodman, 1996) within the signal peptide of Beat, no protein should be detectable in these mutant embryos. These findings indicate that the protein fragments chosen for immunization are not exclusively specific for the Beat protein. Interestingly, both the antisera derived from immunization with the different parts of Beat yield motor axonal labeling, and thus represent the formerly described and expected Beat expression pattern.

Further evaluation of the generated Beat antisera in western blot analysis did not yield specific bands for the endogenous Beat, compared to the blots incubated with preimmune-sera. Solely the guinea pig anti-Beat-Linker recognizes a specific band at about 37 kDa in the overexpression of untagged Beat, substantiating the specific detection of Beat overexpression with this antibody in immunohistochemical stainings. The predicted molecular weight of full-length Beat is 48 kDa and Fambrough and colleagues detected Beat at 43 kDa in western blot (Fambrough and Goodman, 1996). Still, the band at 37 kDa is also detectable using the rabbit anti-Beat-Linker antiserum generated by A. Bauke and also exclusively in the overexpression. These findings indicate that the endogenous Beat expression might be too weak for western blot detection among the unspecific bands. The detected overexpressed protein at 37 kDa could either undergo posttranscriptional modifications or it might experience processing like for example cleavage of some part of the protein, like it is discussed in Chapter 4.4.2.

4.4 *Beat is a type I transmembrane protein*

Beat is expressed on motor axons and was in former studies described as secreted molecule, which regulates the defasciculation of motor axons from the main nerve branch into the periphery (Fambrough and Goodman, 1996). Further studies of our working group found evidence that Beat acts cell-autonomously, as the *beat* mutant phenotype is only rescued by presynaptic, but not postsynaptic expression of full-length Beat cDNA (Siebert et al., 2009 and this work, Chapter 3.7.1). Moreover, *in vitro* experiments indicated that S2 cells transfected with different Beat constructs secrete C-terminal Beat deletion constructs lacking the putative transmembrane domain into the medium (Bauke, 2009). These data suggest a role for Beat as a transmembrane receptor for Side. In this work, the transmembrane domain and the orientation of Beat was further verified in different *in vivo* approaches by analyzing overexpressed constructs in *Drosophila*.

4.4.1 Localization of Beat constructs

Although Beat is naturally expressed on motor axons, pan-neuronal expression of Beat-GFP is hardly visible in embryos or larvae. GFP-signal is only detectable in the cell bodies in the brain and slightly in the neuropil containing the central synapses, but not on motor axons. By contrast, swapping the GFP-tag to the Beat N-terminus produces very intense signal in motor axons and NMJs. Immunohistochemical stainings of motoneuron-specific overexpression of this N-terminally tagged construct in embryos yields good signal and shows the localization of Beat on motor axons and growth cones, thereby providing evidence for the location and functionality of endogenous Beat on motor axons. Other Beat constructs exhibit GFP-signal in motor axons, if the C-terminal part of Beat is truncated or if the transmembrane domain is manipulated (constructs lacking at least 66 C-terminal amino acids, such as Beat_1-361-GFP or shorter constructs, as well as BeatnewTM-GFP and BeatΔTM-GFP exhibit staining of the axons and NMJs).

In muscle-specific, larval overexpression of Beat constructs, the expression pattern is also highly affected by modifications in the Beat sequence. Nuclear GFP accumulation is visible if the C-terminus and the endogenous, predicted transmembrane domain are present or a maximum of 32 C-terminal amino acids have been deleted (among the C-terminal deletion constructs, only Beat_1-395-GFP

exhibits this nuclear accumulation). Surprisingly, a secreted expression pattern like for secret.Nrx-GFP is not visible in larvae, only Beat Δ IG1-GFP exhibits a slight negative muscle pattern. Together with the observation that the severely C-terminally truncated Beat constructs Beat_1-254-GFP and Beat_1-322-GFP exhibit clear membranous signal in both pre- and postsynaptic, larval expression, this raises the question if there might actually be a second transmembrane domain within the very N-terminal part of Beat. As a second transmembrane domain is indeed predicted at amino acid position 11-28 (Rost and Liu, 2004, <https://www.predictprotein.org>), the constructs Beat_29-427-GFP and Beat_29-322-GFP, where amino acids 1-28 are exchanged for a signal peptide sequence from human CD8, were therefore designed to address the possibility of a second transmembrane domain in this region. However, the expression studies do not indicate a different localization of these constructs compared to Beat-GFP and Beat_1-322-GFP, respectively. The possibility of a second transmembrane domain was therefore not confirmed.

All other constructs, including those with deleted transmembrane regions, exhibit GFP-signal, which is associated with the muscles. Surprisingly, Beat Δ TM-GFP does not exhibit a secreted pattern, but even yields very bright and homogenous staining of the muscles. This might indicate that certain regulatory sequences have been excised in this construct. In the embryonic overexpression, a slight secreted expression pattern could be identified for Beat_1-322-GFP and Beat_1-254-GFP. Expression in intact embryos is useful to image weak, secreted expression, as the vitelline membrane prevents that any secreted proteins get discarded. The expression of Beat_1-322-GFP and Beat_1-254-GFP is not very strong in larvae, which might explain that the secreted expression pattern is difficult to detect in embryos. Still, these findings support the *in vitro* results that Beat contains a transmembrane domain. However, the secreted Beat constructs seem to be somehow retained at the cell membrane or in the extracellular matrix. Subsequent western blot analysis using larvae that muscle-specifically overexpress Beat-GFP and Beat_1-322-GFP show a clear secretion of the truncated construct. Beat_1-322-GFP, but not Beat-GFP, gets secreted and is thus detectable in the larval hemolymph fraction. Consistent with the imaging of intact larvae, both constructs are detectable in western blots from larval filets, arguing for a partial retention of Beat_1-322-GFP at the muscle membrane.

4.4.2 C- and N-terminus of Beat segregate

Further investigation of the doubly tagged GFP-Beat-Cherry indicate that the C- and N-terminal signal diverge from each other both in pre- and postsynaptic overexpression. In motoneuron-specific expression, the C-terminal Cherry-signal is restricted to the soma of the motoneurons, whereas the N-terminal GFP-tag exhibits a membranous signal throughout all compartments of the motoneurons with bright fluorescence in axons and NMJs. In muscle-specific expression, the membranous signal of the N-terminal GFP is by far brighter than the C-terminal Cherry. By contrast, Cherry intensely accumulates in the nuclei of the muscles. It is possible that the C-terminal tag gets cleaved off. On the other hand, these findings might imply that Beat could be cleaved and the C-terminus gets translocated into the nucleus, where it might fulfill downstream signaling functions like for example the regulation of downstream target gene expression. The generation of antibodies for immunodetection of endogenous Beat has not been completely successful, yet western blot detection of overexpressed Beat⁵ with anti-Beat-Linker antiserum yielded a specific signal at about 37 kDa. The expected molecular weight is 48 kDa and was formerly reported at 43 kDa (Fambrough and Goodman, 1996). The anti-Beat-Linker antiserum is directed against a peptide sequence within the linker region and might thus detect the N-terminal part of a cleaved version of Beat. Indeed, the N-terminal part of Beat up to and including the linker region is calculated at 36 kDa. These findings might indicate a cleavage of Beat in between the linker region and the transmembrane region with a subsequent translocation of the C-terminal part of Beat. Still, western blot analysis using anti-GFP antibody for detection did not confirm these findings and further western blot analyses detecting different cellular fractions of overexpressed GFP-tagged Beat constructs with anti-GFP antibodies have so far not been successful (data not shown). However, the question remains, whether the endogenous Beat receptor behaves in the same way as the overexpressed Beat.

The possibility of an interaction between Side and Beat leading to this putative cleavage and translocation of the Beat C-terminus into the nucleus was disproved. Firstly, Beat-Cys-GFP, which lacks the complete extracellular part and thus the interaction domain for Side (see Chapter 4.6), exhibits nuclear accumulation. Secondly, in a *side* mutant background, overexpressed Beat-GFP still exhibits the nuclear GFP accumulation (data not shown). It was further tested whether the nuclear accumulation of Beat-GFP might be dependent on some interacting

pathfinding molecule such as Tlr. Muscle-specific expression of Beat-GFP in a *tlr* mutant background displays the same nuclear GFP accumulation as the wild-type (data not shown). Cleavage or other modifications are thus not mediated by Side or Tlr. There is the possibility that another molecule associated with axon guidance like for example *Drosophila* Leucocyte antigen related (Dlar), which controls the defasciculation of certain motor axons (Krueger et al., 1996), might be involved in the translocation behavior. On the other hand, this segregation behavior of Beat observed in the overexpression might simply be an artifact without biological relevance.

However, the analysis of the postsynaptic expression pattern of the different Beat constructs allows for narrowing down the region, which is responsible for the translocation. The nuclear accumulation is observed in full-length Beat-GFP, in the C-terminal deletion construct Beat_1-395-GFP as well as in both N-terminal deletion constructs Beat Δ IG1-GFP and Beat-Cys-GFP. This indicates that the C-terminal amino acid sequence somewhere in between amino acids 361 and 395 might play a role, as Beat_1-361-GFP does not exhibit this nuclear accumulation. Indeed, a low probability for a nuclear localization signal is predicted around the amino acids 360-400 (Nguyen Ba et al., 2009, <http://www.moseslab.csb.utoronto.ca/NLStradamus/>). Another idea would be that the sequence KQKQKQRQ at amino acids 380-387 is positioned in a β -sheet in a way that the positive KKKR residues would all stick to one side of the β -sheet and might thus form a nuclear localization sequence. Both possibilities would meet the above-mentioned criteria of lying approximately in between amino acids 361-395. Moreover, modeling for DNA binding predicts a potential DNA binding site within the Cys-rich domain of Beat in the full-length Beat at amino acids 401-425 and in the truncated Beat_1-395 at amino acids 389-395 (Hwang et al., 2007; Kuznetsov et al., 2006 <http://lcg.rit.albany.edu/dp-bind/>). For Beat_1-361, there is no binding site predicted within the Cys-rich region. A role in DNA binding would explain the translocation into the nucleus and indicate that the Beat C-terminus might be involved in the transcription of target genes. Still, the region around the transmembrane domain also seems to play a role, as the C-terminus is completely present in BeatnewTM-GFP and there is no nuclear accumulation visible. If the hypothesis is correct that Beat gets cleaved in between the linker and the transmembrane region prior to the translocation, then the findings

make sense that both the C-terminus and the transmembrane domain need to be present in the construct to achieve the nuclear accumulation of the C-terminus.

Future experiments could further concentrate on the retrieval of the nuclear fraction of overexpressed Beat-GFP. These experiments might provide evidence for the cleavage and nuclear translocation of the Beat C-terminus.

4.4.3 Orientation of Beat and localization of the transmembrane domain

In order to further confirm the existence and the exact position of the transmembrane domain, two different approaches of firstly marking extracellular GFP-tags by surface stainings and secondly degrading cytosolic GFP-tags have been used.

Staining unpermeabilized larval filets marks only extracellular GFP-tags and reflects exactly the expected staining behavior of all Beat constructs. C-terminal deletions of at least 105 amino acids (in Beat_1-322-GFP and Beat_1-254-GFP) as well as the exact excision of the predicted transmembrane domain lead to very strong extracellular GFP-signal, whereas the introduction of an artificial transmembrane region restores the intracellular position of the C-terminal GFP-tag.

The method to degrade cytosolic GFP did not completely downregulate the GFP-signal. Still, cytosolic GFP-signal was visibly altered. In cases of rather weak muscular GFP-signal like for example in BeatCys-GFP and Beat Δ IG1-GFP, it was even enhanced. This indicates that these constructs might be tightly regulatory controlled and GFP in degradation particles is thus brighter visible than the construct in its original overexpression pattern. For constructs with an expected extracellular localization of the GFP-tag, the GFP-signal is not altered. In order to quantify the degradation extent of the different constructs, western blot analysis could be further carried out, since Urban and colleagues reported a marked downregulation of Rad21-EGFP protein level by overexpression of NSImb-vhhGFP4 (Urban et al., 2014).

Taken together, both experiments exactly confirm the expectations of the localization of the GFP-tag in all different constructs. This further verifies the existence and also the location of the predicted transmembrane domain *in vivo*.

4.5 Side attracts motor axons and induces synaptogenesis

Neuromuscular connectivity is established by a symphony of guidance molecules, which direct the outgrowing motor axons towards their targets. Side and Beat are major key players in this embryonic process (Aberle, 2009a, 2009b; Siebert et al., 2009). Beat-expressing motor axons follow a Side labeled substrate pathway, presumably by contact adhesion (Figure 4.1, A-A').

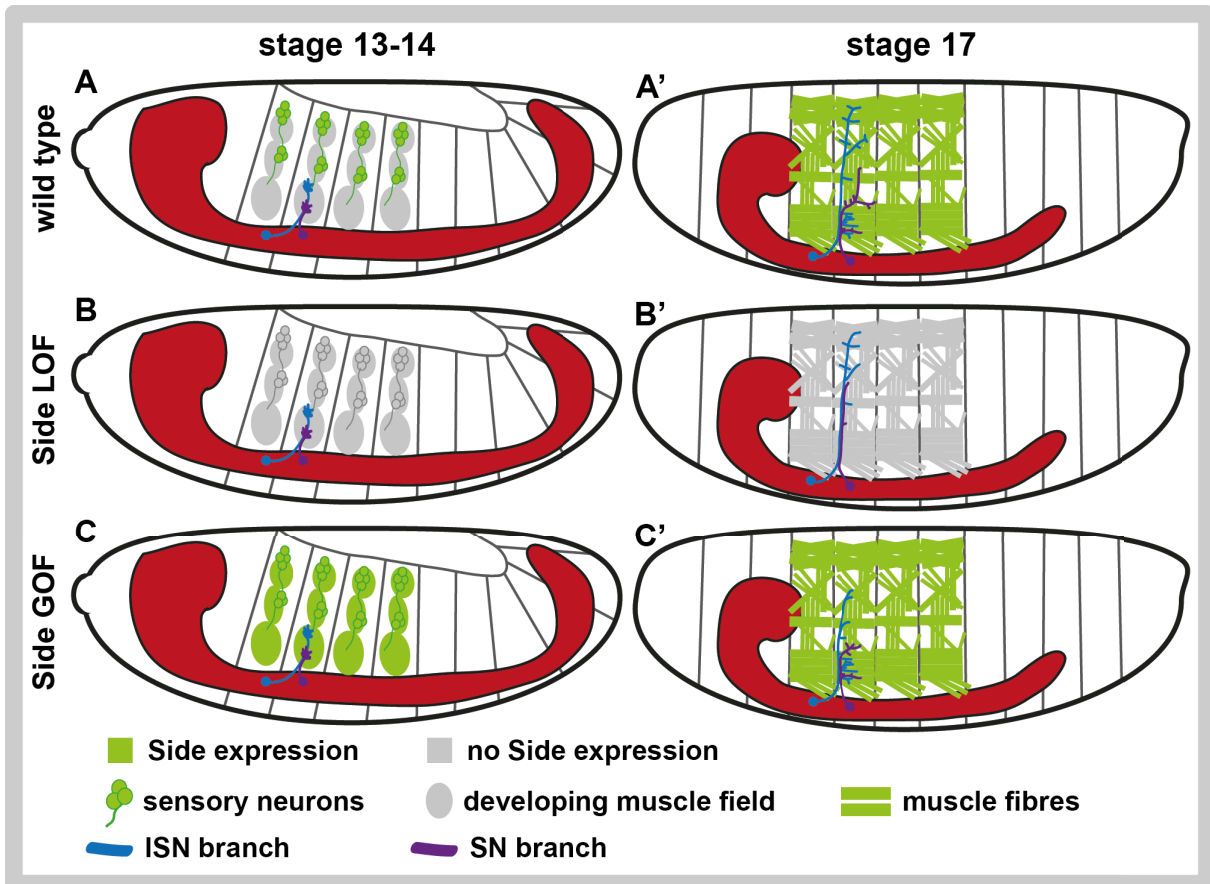


Figure 4.1: Schematic overview of guidance defects induced by Side loss of function (LOF) versus Side gain of function (GOF).

A-A': Motoneurons follow a Side-positive substrate pathway towards their target muscles. In stage 13-14 wild-type embryos, the ingrowing sensory neurons express Side and guide motor axons into the periphery. The developing muscles do not yet express Side. In stage 17 embryos, muscles express Side and thus draw the respective motor axons towards the positions where NMJs will be established. B-B': *Side* mutant embryos do not express Side. Motor axons grow out into the periphery but fail to defasciculate from the main nerve bundle into the appropriate muscle fields. C-C': In embryos, which overexpress Side muscle-specifically, the motor axons are prematurely attracted by the Side-expressing muscle precursors and fail to grow further towards the dorsal region.

Motoneuronal guidance is highly perturbed in *side* as well as *beat* mutant animals. These loss of function larvae exhibit severe innervation defects, mostly in the ventral muscle region due to bypassing of motor axons (Siebert et al., 2009). The typical bypass defects are based on the lack of the attractive guidance cue Side in the

intermediate and final targets (in *side* mutants, see Figure 4.1, B-B') or on the lack of the motor axon guidance receptor Beat (in *beat* mutants). In larvae overexpressing Side in a muscle-specific manner (gain of function), Side is prematurely expressed in the developing muscles from stage 13 onwards (Figure 4.1, C). This ectopic Side expression overlies the endogenous expression pattern and strongly attracts growth cones. Motor axons are thus prematurely drawn towards the developing ventral muscle fields and cannot further follow the endogenous Side trail (Figure 4.1, C').

Side overexpression does not only attract and guide motor axons, but also leads to the establishment of ectopic synapses. It was reported that the misexpression of synaptogenic molecules in inappropriate partners promote the formation of ectopic synapses (Jin, 2002). These findings suggest that Side does not only play a role in the formation of ectopic synapses, but also takes part in the regular establishment of NMJs. Former studies have shown that ectopic Side expression on muscles encourages motor axon targeting and subsequent synaptogenesis and indicated that FasII is required to stabilize the synaptic contacts (de Jong et al., 2004). As direct interaction partner of Beat, Side might contribute to early synaptic stabilization via contact adhesion with Beat on the growth cones. Furthermore, Side might recruit vesicles containing postsynaptic molecules such as glutamate receptors, Neuroligin or scaffold proteins and thus promote synaptogenesis.

4.6 Beat and Side interact via their first IG domains in vivo

Former cell aggregation experiments provided evidence that the cooperation of Beat and Side during axon guidance occurs by direct interaction. These studies with transiently transfected S2 cells have shown that adhesive aggregates only formed if both Beat-myc and Side-GFP were present in these cells (Siebert et al., 2009). A further study using a different cell line confirmed these results by demonstrating that transiently transfected Kc167 cells formed adhesive aggregates if both Beat-Cherry and Side-GFP were present (Pfarr, 2017 and J. Kinold, personal communication).

Among the identified *side* mutant alleles, there are two different alleles, *side*^{I306} and *side*^{H143}, carrying a missense point mutation within the first immunoglobulin domain and the linker region separating the first and second immunoglobulin domain, respectively (see Chapter 3.1.2). Similarly, there is a deletion of 26 amino acids within the first immunoglobulin domain of Beat in *beat*² (see Chapter 3.1.1). All three

mutations lead to severe motor axon guidance defects with the characteristic *side* and *beat* mutant phenotype. This knowledge indicates a crucial function of the first immunoglobulin domains of both Side and Beat. In addition, A. Bauke was able to demonstrate in further cell aggregation experiments that cells transfected with Beat-constructs lacking the first immunoglobulin domain did not form aggregates with Side-Cherry transfected cells. Vice versa, cells transfected with SP-myc-Side Δ IG1 did not cluster with Beat-GFP transfected cells (Bauke, 2009). These *in vitro* findings were now further expanded and the function of the different structural domains of Beat and Side were assessed *in vivo* using a variety of fluorescently labeled deletion and fusion constructs in several different experiments.

4.6.1 Beat and Side interact in simultaneous overexpression

The tagging of Beat constructs with GFP and Side constructs with Cherry allows for a concurrent overexpression of Beat and Side in the same animal and easy evaluation of both their expression patterns by imaging intact larvae. Beat and Side constructs containing their respective first immunoglobulin domains interact in living animals, thereby relocating their expression patterns and exhibiting co-localization of the GFP and Cherry-signals to different extents. Some of the simultaneously overexpressed constructs are probably retained in the export machinery and are thus visible as fluorescent clusters in the endoplasmic reticulum and the golgi vesicles. Secretory and membrane proteins are folded in the endoplasmic reticulum and retained in this cellular compartment, until correctly folded. If the proper conformation of a protein is not achieved after several folding cycles, the protein is targeted for degradation (Vincenz-Donnelly and Hipp, 2017). If Side and Beat molecules already bind to each other during protein biosynthesis and before proper protein folding has been completed, then the agglutination could probably prevent the formation of the native tertiary structure and proteins might not be exported but marked for protein decay. Postsynaptically overexpressed Beat₁₋₃₂₂-GFP seems to be retained on the cell membrane, but does not induce innervation defects. This might be explained by a spatial conformation of this truncated Beat construct, which would not allow for interaction with the endogenous Side (see Figure 4.2, C). The possibility of a precocious interaction between Beat₁₋₃₂₂-GFP and Side-Cherry in the endoplasmic reticulum in the simultaneous overexpression would then explain the

discrepancy between the potential lack of interaction with the endogenous Side and the observed strong co-localization in the concurrent overexpression of these constructs.

The respective first immunoglobulin domains of Beat and Side are necessary for their interaction. Beat and Side constructs lacking the first immunoglobulin domain do not co-localize or redirect the protein expression, if co-expressed with the converse full-length construct, indicating that no binding between these proteins can take place. The first immunoglobulin domain of Side is sufficient for its interaction with Beat, as SideIG1+CD8-Linker-TM-Cherry exhibits slight co-localization with Beat-GFP and strong co-localization with Beat_1-322-GFP. Both Side-Cherry and SideIG1+CD8-Linker-TM-Cherry show more signal overlap with Beat_1-322-GFP than with Beat-GFP. It was observed that the C-terminus of the overexpressed Beat-GFP, which contains the GFP-tag, segregates from the N-terminus, which contains the interaction domain for Side, and translocates into the nuclei of the muscles (see Chapter 4.4.2). The interaction domain might consequently not be associated with the GFP-tagged C-terminus in the processed Beat molecules, which would inhibit spatial contact with the Side constructs and therefore explain the observation of less co-localization.

4.6.2 BeatnewTM-GFP biochemically interacts with Side-Cherry

To date, it was not possible to detect biochemical interaction between Side^{29A} and different Beat constructs. Still, BeatnewTM-GFP is able to biochemically interact with Side-Cherry and precipitate this construct. These results together with the observation of the strong increase of innervation defects induced by ectopic expression of Side-Cherry compared to Side^{29A}, indicate that the biochemical affinity of Side-Cherry towards endogenous Beat as well as Beat constructs might be higher. In future experiments, Side-Cherry will be tested as biochemical interaction partner for different Beat constructs. These experiments will provide further information about the interaction behavior with differently modified Beat constructs.

4.6.3 Overexpression of Beat-GFP traps endogenous Side

Overexpressed Beat is not only able to interact with ectopic Side, but is also able to bind and redirect endogenous Side. Embryos overexpressing Beat-GFP in different

pre- and postsynaptic tissues were stained for endogenous Side. These experiments show that in stage 17 embryos, Side is always trapped in the tissues where Beat-GFP is overexpressed instead of getting downregulated. Muscle-specific overexpression of Beat Δ IG1-GFP does not have an effect on Side expression, providing further evidence that the first immunoglobulin domain of Beat is necessary for interaction with Side.

Vice versa, the hypothesis that the secreted SideIG1-5-GFP, which is redirected towards the Beat-GFP expression in simultaneous, muscle-specific overexpression (see Figure 3.31, M-O''), might cluster around endogenous Beat on motor axons and growth cones could not be verified. This could be due to the situation that the secreted SideIG1-5-GFP, which is visible in punctual clusters in the embryo, might be taken up by macrophages or hemocytes. These cells would thus incorporate the constructs and the first immunoglobulin domain would consequently not be accessible for the Beat proteins on motor axons.

4.6.4 Binding of Side to co-overexpressed Beat restores axon guidance

Additional to their physical interaction in the simultaneous overexpression, the interaction of muscle-specifically overexpressed Beat and Side functionally inhibits the attractive guidance effect of ectopic Side on growth cones. Early, postsynaptic overexpression of Side-Cherry induces dramatic dorsal and lateral innervation defects. The concurrent overexpression of Beat-GFP highly significantly reduces these defects in all muscles, which are affected highly significantly by Side-Cherry, as calculated with the χ^2 -test (see Table 3.5). These results further confirm the findings of the interaction of ectopically expressed Beat and Side. The interaction of Beat-GFP and Side-Cherry in the simultaneous overexpression redirect their expression patterns. The strong reduction of attraction might thus be caused by the situation that Side-Cherry does not completely reach the cell-surface. Yet, these findings possibly also indicate that the interaction of simultaneously overexpressed Beat and Side is able functionally block the Side domain, which is responsible for guiding motor axons.

4.6.5 Larval innervation defects

Motor axonal guidance errors during embryogenesis manifest as larval innervation defects in many cases. The *side* and *beat* loss of function and gain of function phenotypes are highly persistent and can easily be assessed by imaging intact larvae. The possibility to rescue the *beat* mutant phenotype on the one hand and to deliberately induce innervation defects by the overexpression of Side or Beat constructs on the other hand allows for the estimation of the extent of functionality of the different generated constructs.

4.6.5.1 TM and first IG domains are crucial for the functionality of Beat

The functionality of Beat constructs can be evaluated firstly by their rescue capacity of presynaptic expression in the *beat* mutant background and secondly by their ability to provoke innervation defects by muscle-specific overexpression. Presynaptic overexpression of full-length Beat cDNA completely rescues the *beat* mutant phenotype and restores the wild-type innervation pattern in third instar larvae. The rescue capacity of different Beat constructs is thus an important tool to evaluate their functionality, as it does not only rate the interaction with Side, but also considers possible further mechanisms necessary for steering decisions. By contrast, the muscle-specific overexpression of Beat induces innervation defects. These defects probably result from a cis-interaction of the ectopically overexpressed Beat with the endogenous Side on the muscle surface (Figure 4.2). The Side guidance molecules would then largely be blocked for trans-interaction with the endogenous Beat receptors on motor axons. Due to the masking of the attractive effect of this guidance molecule, the growth cones would consequently fail to innervate their correct target muscles.

The untagged Beat and the C-terminally tagged Beat-GFP exhibit very comparable functionality. Firstly, both constructs fully rescue the *beat* mutant phenotype, and secondly both constructs induce severe innervation defects throughout all body compartments by muscle-specific overexpression. The insertion of the N-terminal GFP-tag by contrast largely reduces the rescue ability as well as the induced innervation defects, arguing for a spatial impairment of the first immunoglobulin domain by the GFP-tag. Interestingly, BeatnewTM-GFP is able to induce moderate innervation defects, whereas it is only slightly able to rescue. The noteworthy

induction of innervation defects argues for the ability to interact with Side and mask its guidance effect. By contrast, the reduction of the rescue capacity compared to Beat-GFP implies a crucial role of the replaced amino acids of the transmembrane domain, like for example for a cleavage and subsequent nuclear translocation of the C-terminus, which might mediate important signaling information. Beat_1-395-GFP, the C-terminal deletion construct where only a small portion of the intracellular part of Beat has been removed (32 amino acids), is also highly impaired in its functionality, as evaluated by both the rather mild resulting innervation defects and the rescue capacity of only approximately 70%. The considerable reduction of rescue capacity implies a crucial role of the C-terminal part of the receptor. Still, if the first immunoglobulin domain is responsible for binding to Side, one will expect similar guidance defects induced by muscle-specific expression as for Beat-GFP. Postsynaptic overexpression of other deletion constructs do not lead to visibly impaired innervation, whereas Beat_1-361-GFP, Beat_1-345-GFP, Beat_29-427-GFP and Beat Δ TM-GFP are able to slightly improve the *beat* mutant phenotype in rescue experiments. Surprisingly, Beat_29-427-GFP is not able to induce innervation defects in ectopic expression. In this construct, the endogenous signal peptide has been replaced by a signal peptide derived from the human CD8 molecule and the Beat sequence is else unaffected. This result indicates that the real signal peptide might be a bit shorter than the predicted one, thus withdrawing a small portion of the Beat N-terminus in Beat_29-427-GFP. Interestingly, the statistical analyses revealed that rescue with BeatnewTM-GFP, Beat_1-395-GFP and GFP-Beat-Cherry restores a big part of the ventral innervation, but renders the dorsal muscle field more defective than it the case in the *beat* mutant background. This indicates that the ISN, which grows out prior to the other fascicles and innervates the dorsal muscle field, is guided a lot worse than the later outgrowing and ventrally innervating ISNb, ISNd and SNc. Elav-Gal4 drives expression in all postmitotic neurons. Expression of the constructs thus begins with the onset of motor axonal outgrowth. One explanation might be that the deletion- and fusion constructs need more time to fold correctly and to be transported into the axons and growth cones than Beat-GFP. Another possibility is that these constructs recognize the Side guidance molecules, but the signaling of these modified Beat receptors is impaired, thus slowing down the pioneering growth cone of the ISN.

These studies with the different Beat deletion- and fusion constructs reveal that even slight modifications in the Beat sequence highly disturb the ability to rescue the mutant phenotype or induce innervation defects. Figure 4.2 illustrates the estimated cis-interaction between the respective Beat constructs and Side and the possibly accompanied masking of the attractive effect of Side. After all, it remains unclear, why the transmembrane C-terminal deletion constructs Beat_1-361-GFP and Beat_1-345-GFP do not induce innervation defects. As all constructs have been sequenced prior to injection into the fly and positive transformants have been verified in PCR and western blot analysis, any cloning- and insertion mistakes can be ruled out.

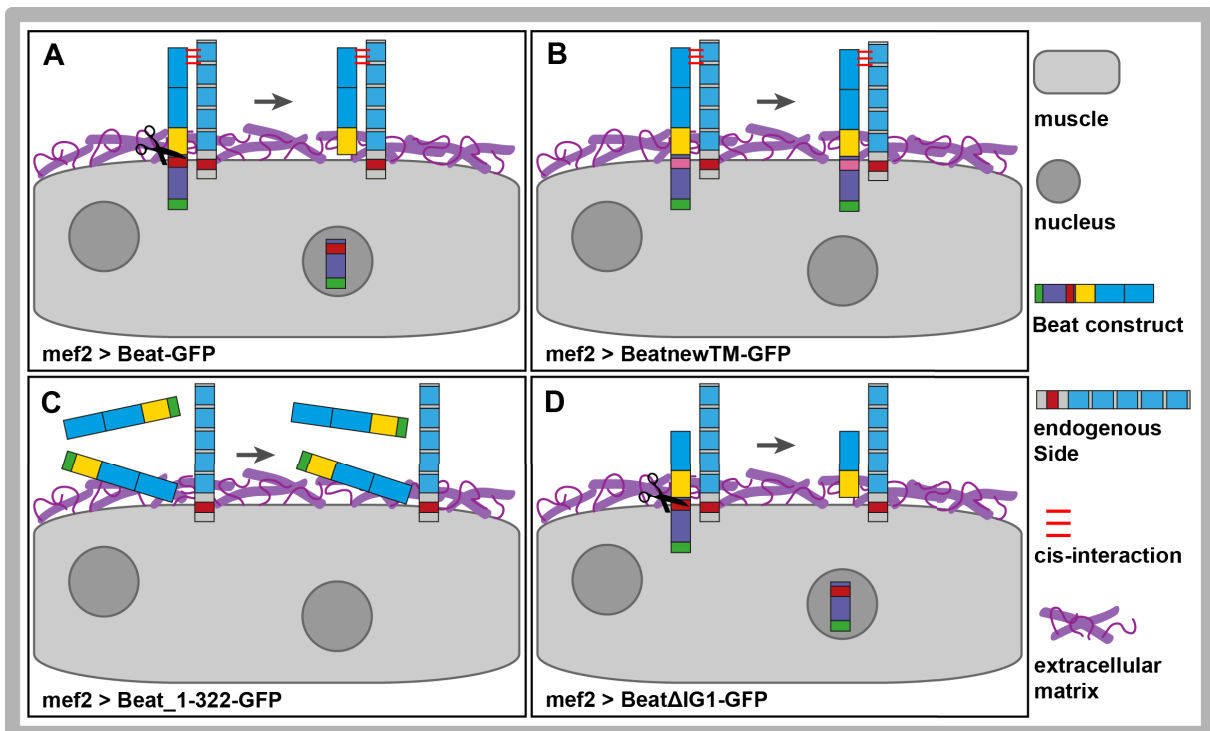


Figure 4.2: Schematic model of muscle-specific overexpression of Beat constructs and their estimated interaction with endogenous Side.

A: Overexpressed Beat-GFP binds to Side. The C-terminal part of Beat probably gets cleaved and is translocated into the nucleus. B: BeatnewTM-GFP probably binds to endogenous Side and thus masks the guidance molecule for endogenous Beat. The analysis of the expression pattern indicates that the C-terminus does not get translocated into the nucleus, as no nuclear GFP accumulation is detectable. C: Beat_1-322-GFP gets secreted and is in part possibly somehow attached to the muscle, for example via the extracellular matrix. Interaction with endogenous Side is probably not possible, thereby not impairing its function. D: Beat Δ IG1-GFP lacks the interaction domain and can therefore not bind to Side. Cleavage and translocation of the C-terminus still take place.

Figure 4.3 explains the hypothesized functionality of different Beat constructs in rescue experiments via trans-interaction with Side and nuclear translocation of the C-terminus. Regarding a possible function of the Beat C-terminus in signal

transduction, it makes sense that even slight modifications in the C-terminal part impair its rescue capacity.

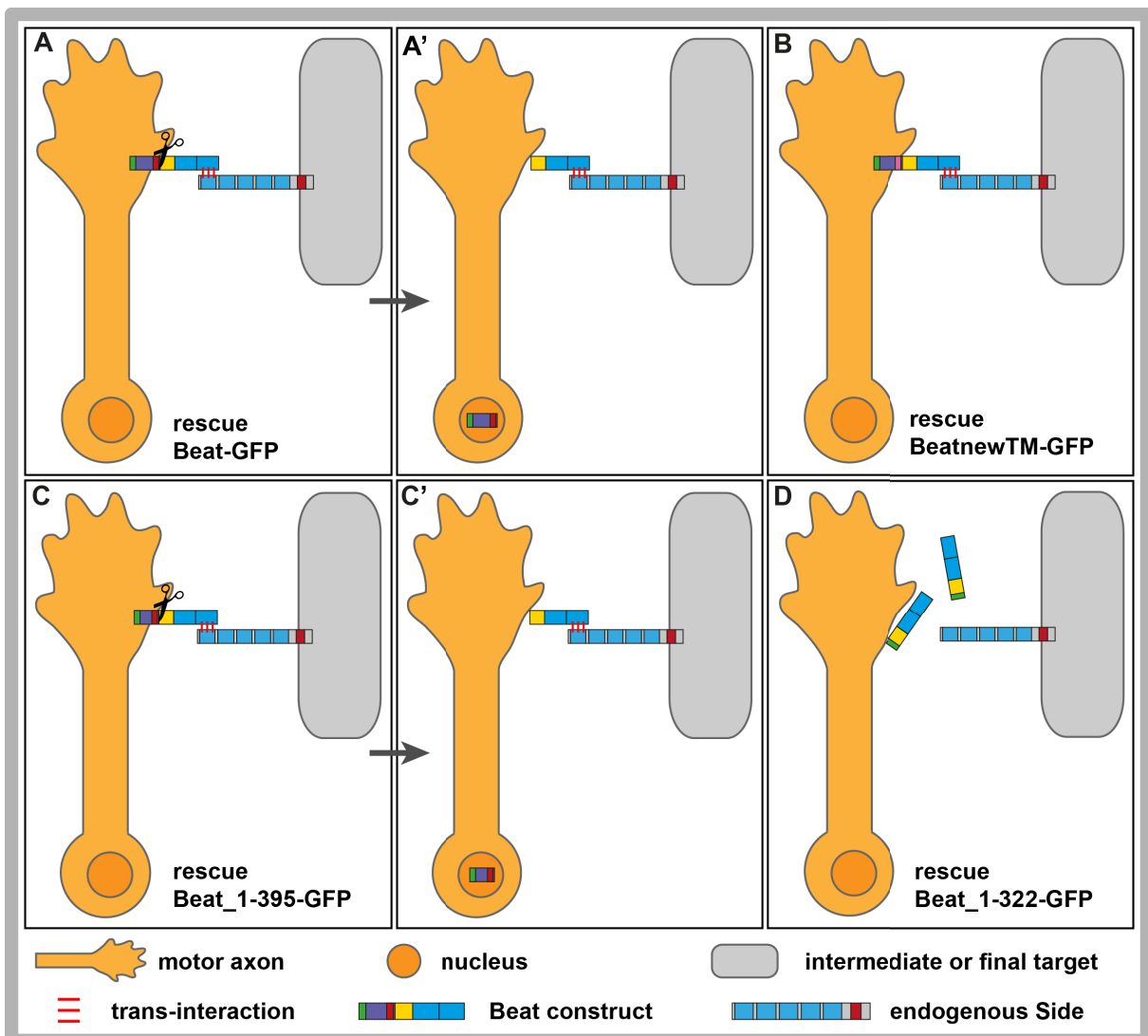


Figure 4.3: Illustration of presynaptic Beat constructs and how they possibly interact with endogenous Side in rescue experiments.

A-A': Beat-GFP fully rescues the *beat* mutant phenotype. The Beat C-terminus possibly gets translocated into the cell body. B: BeatnewTM-GFP probably fully interacts with Side, but is only partly able to rescue. The translocation of the C-terminus might therefore be crucial for proper signal transduction. C-C': The C-terminal deletion construct Beat_1-395-GFP interacts with Side and its C-terminus is translocated. It conveys reduced rescue capacity, indicating that the complete C-terminus is important for signal transduction. D: Beat_1-322-GFP is probably secreted and some molecules might be anchored to the axon extracellularly.

4.6.5.2 The first IG domain conveys the attractive impact of Side

Ectopic Side expression draws motor axons towards the tissues of Side overexpression (de Jong et al., 2005; Siebert et al., 2009; Sink et al., 2001, this work). The scenario of muscle-specific Side expression has been explained in detail above (see Chapter 4.5 and Figure 4.1). In the pan-neuronal overexpression, Side

remains persistently present on motoneurons and sensory neurons. On the one hand, the ectopic Side on motoneurons might interact with the endogenous Beat receptors on motor axons in cis-conformation and thus block them from detecting the correct Side labeled pathway. On the other hand, the persistent Side-expression on sensory neurons could inhibit the defasciculation of motor axons from the sensory axons, which normally occurs at the choice point of the dorsal bidendritic neuron. This hypothesis is encouraged by former work of Sink and colleagues, who found that expression of Side on all neurons leads to an embryonic defasciculation phenotype similar to the *side* mutant phenotype (Sink et al., 2001). The overall larval innervation defects mediated by the presynaptic overexpression of Side are less drastic than the defects provoked by the postsynaptic overexpression of Side. So generally, the muscle-specific, ectopic Side-expression might provide higher sensitivity in the evaluation of mild innervation defects, whereas the presynaptic overexpression can provide higher sensitivity in the evaluation of strong innervation defects.

Unexpectedly, the untagged Side^{29A} induces fewer defects than Side-Cherry or GFP-Side-Cherry. Compared to Side^{29A}, Side-Cherry mediates most dramatic effects in the muscle-specific overexpression: in the dorsal compartment, Side-Cherry completely abolishes innervation, and also the lateral muscle field exhibits highly reduced innervation, especially in the muscles, which are normally innervated by the more distal part of the SNa. In the ventral compartment by contrast, this construct leads to the establishment of more synapses than in the wild-type, probably based on many ectopic NMJs caused by the axons of the ISN and SNa, which failed to grow out into the dorsal and lateral muscle field. Western blot quantification ruled out the possibility of a stronger transcription of Side-Cherry, which is integrated in the Φ 51C landing site, compared to Side^{29A}, which is randomly integrated (J. Kinold, personal communication). Another reason could be that the C-terminal Cherry-tag might prevent some sort of regulatory process, thus rendering the tagged constructs more stable. However, the functionality of Side does not seem to be impaired by the C-terminal Cherry-tag. The N-terminal GFP-tag mildly weakens functionality compared to Side-Cherry, as the innervation defects induced by presynaptic overexpression are slightly reduced. The secreted SideIG1-5-Cherry induces very mild defects in the muscle-specific overexpression, mainly in the ventral muscle region. This indicates that the secreted Side molecules contain the binding site for Beat and slightly inhibit

the receptor, thus provoking a mild version of the *beat* mutant bypass phenotype. If the first immunoglobulin domain of Side, which is considered as potential interaction domain, is removed in Side Δ IG1-Cherry, the construct is not able to induce innervation defects, as expected. On the other hand, fusing the first immunoglobulin domain of Side to a linker scaffold is sufficient to induce innervation defects. In SideIG1-FasII-Cherry, only the signal peptide and the first immunoglobulin domain of Side domain are present and fused to FasII (without the first immunoglobulin domain of FasII). As former studies have shown that muscle-specifically overexpressed FasII is not able to induce larval innervation errors (del Olmo-Toledo, 2014) or prevent motor axons from reaching the dorsal-most muscles (Figure 3.11), the observed innervation defects in the dorsal and lateral muscle fields must be exclusively owed to the attractive effect of the first immunoglobulin domain of Side. Moreover, the Side-endogenous membrane anchoring is obviously not crucial for the functionality, because SideIG1+CD8-Linker-TM-Cherry (which includes the Side transmembrane domain) and SideIG1-FasII-Cherry (which is anchored via the FasII transmembrane domain) both provoke slight innervation defects in the postsynaptic overexpression. However, the distance between the cell-surface and the first immunoglobulin domain of Side is probably critical for its functionality, as SideIG1-CD8-CD8-Cherry does not induce innervation defects.

4.7 Conclusion and outlook

Side is one of the most effective identified guidance molecules in *Drosophila*, strongly and irreversibly attracting motor axons towards their target muscles via interaction with its guidance receptor Beat. During this work, important domains of both molecules, including their interaction domain and the transmembrane domain of Beat, have been characterized *in vivo*. These findings further substantiate that axon guidance via Side and Beat is a key mechanism. As Side expression is persistently found in the embryonic and larval brain (Siebert et al., 2009; this work), and Beat expression was also reported in a small number of cells with unknown function in the embryonic brain (Fambrough and Goodman, 1996), this contact-adhesion mediated guidance principle could also apply in the guidance of central axons. Moreover, since Beat and Side both belong to protein families, which are highly conserved in related species (Aberle, 2009b), similar guidance mechanisms might be preserved in other insects.

This work further provides evidence for an important functional role of the Beat C-terminus, possibly during signal transduction. In future experiments, it would be interesting to study the motor axonal cytoskeleton in different rescue genotypes using full-length and C-terminal truncated Beat constructs to find hints about how Beat signal transduction influences the cytoskeleton and mediates growth cone steering.

Index of Tables

Table 2.1: Equipment.....	18
Table 2.2: Chemicals and solvents.....	18
Table 2.3: Kits and reagents.....	20
Table 2.4: Buffers.....	21
Table 2.5: Media and solutions.....	23
Table 2.6: Fly stocks.....	24
Table 2.7: Oligonucleotides.....	26
Table 2.8: Oligonucleotides used for OE-PCR and subsequent Topo-cloning of Beat constructs.....	28
Table 2.9: Oligonucleotides used for OE-PCR and subsequent Topo-cloning of Side constructs.....	30
Table 2.10: General plasmids.....	32
Table 2.11: Gateway pENTR/D-Topo vectors.....	32
Table 2.12: Gateway destination vectors.....	33
Table 2.13: Primary antibodies.....	35
Table 2.14: Secondary antibodies.....	35
Table 2.15: Software.....	36
Table 2.16: Mix for injection.....	37
Table 2.17: Reverse transcription.....	42
Table 2.18: Standard PCR.....	43
Table 2.19: Extension PCR.....	45
Table 2.20: Overlap PCR.....	45
Table 2.21: Purification PCR.....	46
Table 2.22: Mix for Topo cloning.....	47
Table 2.23: Sample preparation for sequencing.....	47
Table 2.24: List of employed <i>E. coli</i> strains.....	48
Table 2.25: Components of a restriction digest.....	50
Table 2.26: Components of the LR reaction.....	51
Table 2.27: Contributions.....	58
Table 3.1: Deletions or modifications of Beat domains highly impair the rescue ability.....	80
Table 3.2: Pre- and postsynaptic overexpression of Side disturbs motor axonal wiring.....	85
Table 3.3: Postsynaptic overexpression of Beat impairs motor axonal connectivity..	86
Table 3.4: Larval, presynaptic expression pattern of Beat constructs.....	90
Table 3.5: Counting of NMJs reveals significant innervation defects throughout the dorso-lateral compartment of Side-Cherry overexpressing larvae.....	116

Index of Figures

Figure 1.1: Embryonic origin of motor axons.	3
Figure 1.2: Larval neuromuscular system.	4
Figure 1.3: Stereotypic innervation pattern of <i>Drosophila</i> larval body wall muscles.	5
Figure 1.4: Protein structure of Beaten path Ia.	9
Figure 1.5: Protein structure of Sidestep.	11
Figure 1.6: Schematic illustration of the dynamic Side expression in spatial relation to the outgrowing motoneurons.	12
Figure 1.7: Schematic model of Side-expressing tissues guiding Beat-positive motor axons towards their final targets.	13
Figure 1.8: Schematic overview of the motor axon cytoskeleton and surrounding guidance cues.	14
Figure 2.1: Schematic model of directed gene expression via the Gal4/UAS-system.	39
Figure 2.2: Peptide-antibodies generated at Biogenes.	52
Figure 3.1: Survey of <i>beat</i> mutant alleles.	60
Figure 3.2: Characterization of <i>side</i> mutant alleles.	61
Figure 3.3: Structure prediction of Side.	62
Figure 3.4: Side is constitutively expressed in <i>side</i> and <i>beat</i> mutant embryos.	64
Figure 3.5: Side ^{H143} protein is restricted to the cell bodies.	65
Figure 3.6: Side expression is not detectable in <i>side</i> mutant embryos, which contain a protein truncation.	66
Figure 3.7: Western blot analysis reveals ongoing Side expression in L3 larvae.	67
Figure 3.8: Side is constitutively expressed in the CNS of L3 larvae.	69
Figure 3.9: Guinea pig anti-Beat-Linker antiserum recognizes overexpressed Beat ⁵	71
Figure 3.10: Overexpressed Side prematurely attracts motor axons.	73
Figure 3.11: Overexpressed FasII does not attract motor axons.	74
Figure 3.12: Overexpression of Side-Cherry draws axons into the ventro-lateral muscle field and induces the formation of ectopic synapses.	75
Figure 3.13: Side overexpression specifically induces synaptogenesis.	76
Figure 3.14: Schematic overview of the different Beat constructs.	77
Figure 3.15: Side constructs.	78
Figure 3.16: Presynaptic Beat overexpression rescues the <i>beat</i> mutant phenotype.	79
Figure 3.17: Rescue capacity of selected Beat constructs.	82
Figure 3.18: Larval innervation pattern of three adjacent hemisegments.	84
Figure 3.19: Postsynaptic overexpression of Side and Beat constructs induces innervation defects.	88
Figure 3.20: Motoneuron-specifically overexpressed GFP-Beat-Cherry is detectable at the growth cone.	91
Figure 3.21: Full-length Beat-GFP does not display secretion in L3 larvae.	93
Figure 3.22: The C-terminal deletion constructs lacking the transmembrane domain exhibit a secreted fluorescence pattern in embryos.	95
Figure 3.23: The N- and C-terminus of overexpressed GFP-Beat-Cherry segregate.	96
Figure 3.24: In postsynaptic overexpression, the N- and C-terminus of GFP-Beat-Cherry distribute differently.	97
Figure 3.25: Beat-GFP is not secreted.	98

Index of Figures

Figure 3.26: Surface stainings of larval filets postsynaptically overexpressing different Beat constructs indicate the existence and location of the putative transmembrane domain.....	99
Figure 3.27: Control stainings with permeabilized and non-permeabilized larval filets verify the specificity of surface stainings.....	101
Figure 3.28: Protein ubiquitination mediated by NSlmb-vhhGFP4.	102
Figure 3.29: Degradation of cytosolic GFP in larvae verifies the orientation of Beat constructs.	103
Figure 3.30: Side-Cherry and different GFP-tagged Beat constructs interact <i>in vivo</i>	106
Figure 3.31: Simultaneous overexpression reveals that the respective first immunoglobulin domains of Beat and Side mediate their interaction <i>in vivo</i>	108
Figure 3.32: Beatnew TM -GFP is able co-precipitate Side-Cherry.....	109
Figure 3.33: Postsynaptic Beat-GFP traps endogenous Side on the muscle surface.	111
Figure 3.34: Presynaptic Beat-GFP traps endogenous Side on motor- and sensory neurons.....	113
Figure 3.35: Endogenous Beat is not able to trap secreted Side ^Δ G1-5-Cherry at growth cones.	114
Figure 3.36: Simultaneous expression of Beat-GFP strongly diminishes innervation defects caused by postsynaptic overexpression of Side-Cherry.	115
Figure 3.37: Muscles at the outmost end of the ISN and SNa are most severely affected by muscle-specific overexpression of Side-Cherry.	117
Figure 4.1: Schematic overview of guidance defects induced by Side loss of function (LOF) versus Side gain of function (GOF).	131
Figure 4.2: Schematic model of muscle-specific overexpression of Beat constructs and their estimated interaction with endogenous Side.	138
Figure 4.3: Illustration of presynaptic Beat constructs and how they possibly interact with endogenous Side in rescue experiments.	139

References

- Aberle, H. (2009a). Searching for guidance cues: follow the Sidestep trail. *Fly 3*, 270–273.
- Aberle, H. (2009b). No sidesteps on a beaten track: motor axons follow a labeled substrate pathway. *Cell Adh. Migr.* 3, 358–360.
- Aberle, H., Haghghi, a. P., Fetter, R.D., McCabe, B.D., Magalhães, T.R., and Goodman, C.S. (2002). Wishful thinking encodes a BMP type II receptor that regulates synaptic growth in *Drosophila*. *Neuron* 33, 545–558.
- Ansar, M., Raza, S.I., Lee, K., Irfanullah, Shahi, S., Acharya, A., Dai, h., Smith, J.D., Shendure, J., Bamshad, M.J., et al. (2015). A homozygous missense variant in type I keratin KRT25 causes autosomal recessive woolly hair. *J. Med. Genet.* 52, 676–680.
- Aradska, J., Bulat, T., Sialana, F.J., Birner-Gruenberger, R., Erich, B., and Lubec, G. (2015). Gel-free mass spectrometry analysis of *Drosophila melanogaster* heads. *Proteomics* 15, 3356–3360.
- Araújo, S.J., and Tear, G. (2003). Axon guidance mechanisms and molecules: lessons from invertebrates. *Nat. Rev. Neurosci.* 4, 910–922.
- Ashburner, M., Misra, S., Roote, J., Lewis, S.E., Blazej, R., Davis, T., Doyle, C., Galle, R., George, R., Harris, N., et al. (1999). An Exploration of the Sequence of a 2.9-Mb Region of the Genome of *Drosophila melanogaster*: The Adh Region. *Genetics* 153, 179–219.
- Atwood, H.L., Govind, C.K., and Wu, C.F. (1993). Differential ultrastructure of synaptic terminals on ventral longitudinal abdominal muscles in *Drosophila* larvae. *J. Neurobiol.* 24, 1008–1024.
- Bate, M., and Broadie, K. (1995). Wiring by fly: The Neuromuscular System of the *Drosophila* Embryo. *Neuron* 15, 513–525.
- Bate, M., Landgraf, M., and Ruiz-Gomez, M. (1999). Development of larval body wall muscles. *Int. Rev. Neurobiol.* 43, 25–44.
- Battye, R., Stevens, A., and Jacobs, J.R. (1999). Axon repulsion from the midline of the *Drosophila* CNS requires slit function. *Development* 126, 2475–2481.
- Bauke, A.-C. (2009). Structure-function analysis of the axon guidance molecules Beaten path and Sidestep. Master Thesis. University of Münster.
- Bazan, J.F., and Goodman, C.S. (1997). Modular structure of the *Drosophila* Beat protein. *Cell Press* 7, 338–339.
- Beuchle, D., Schwarz, H., Langegger, M., Koch, I., and Aberle, H. (2007). *Drosophila* MICAL regulates myofilament organization and synaptic structure. *Mech. Dev.* 124, 390–406.
- Bieber, A.J., Snow, P.M., Hortsch, M., Patel, N.H., Jacobs, J.R., Traquina, Z.R., Schilling, J., and Goodman, C.S. (1989). *Drosophila* neuroglian: A member of the immunoglobulin superfamily with extensive homology to the vertebrate neural adhesion molecule L1. *Cell* 59, 447–460.
- Bischof, J., Maeda, R.K., Hediger, M., Karch, F., and Basler, K. (2007). An optimized transgenesis system for *Drosophila* using germ-line-specific phiC31 integrases. *Proc.*

Natl. Acad. Sci. U. S. A. *104*, 3312–3317.

Bösenberg, A.-M. (2016). Funktionelle Analyse von Sidestep und Beaten path la Fusions- und Deletionskonstrukten durch Quantifizierung larvaler Innervierungsdefekte in *Drosophila melanogaster*. Bachelor Thesis. Heinrich Heine University.

Bossing, T., Udolf, G., Doe, C.Q., and Technau, G.M. (1996). The embryonic central nervous system lineages of *Drosophila melanogaster*. *Dev. Biol.* *189*, 41–64.

Brand, A.H., and Perrimon, N. (1993). Targeted gene expression as a means of altering cell fates and generating dominant phenotypes. *Development* *118*, 401–415.

Broadie, K., and Bate, M. (1993a). Muscle development is independent of innervation during *Drosophila* embryogenesis. *Development* *543*, 533–543.

Broadie, K., and Bate, M. (1993b). Activity-Dependent Development of the Neuromuscular Synapse during *Drosophila* Embryogenesis. *Neuron* *11*, 607–619.

Campos-Ortega, J.A., and Hartenstein, V. (1997a). The Embryonic Development of *Drosophila melanogaster*. Chapter 11: Central nervous system. *Springer 2*, 233–269.

Campos-Ortega, J.A., and Hartenstein, V. (1997b). The Embryonic Development of *Drosophila melanogaster*. Chapter 4: Musculature. *Springer 2*, 109–123.

Caussin, E., Kanca, O., and Affolter, M. (2011). Fluorescent fusion protein knockout mediated by anti-GFP nanobody. *Nat. Publ. Gr.* *19*, 117–121.

Chiba, A. (1999). Early development of the *Drosophila* neuromuscular junction: a model for studying neuronal networks in development. *Int. Rev. Neurobiol.* *43*, 1–24.

Chiba, a, and Keshishian, H. (1996). Neuronal pathfinding and recognition: roles of cell adhesion molecules. *Dev. Biol.* *180*, 424–432.

Chiba, A., Hing, H., Cash, S., and Keshishian, H. (1993). Growth Cone Choices of *Drosophila* Motoneurons in Response to Muscle Fiber Mismatch. *J. Neurosci.* *13*, 714–732.

Colamarino, S.A., and Tessier-Lavigne, M. (1995). The Axonal Chemoattractant Netrin-I Is Also a Chemorepellent for Trochlear Motor Axons. *Cell* *81*, 621–629.

Culotti, J.G., and Merz, D.C. (1998). DCC and netrins. *Development* *10*, 609–613.

Dent, E.W., Gupton, S.L., and Gertler, F.B. (2011). The Growth Cone Cytoskeleton in Axon outgrowth and guidance. *Cold Spring Harb. Perspect. Biol.* *1*, 1–40.

Desai, C.J., Gindhart, J.G., Goldstein, L.S.B., and Zinn, K. (1996). Receptor Tyrosine Phosphatases Are Required for Motor Axon Guidance in the *Drosophila* Embryo. *Cell* *84*, 599–609.

Dickson, B.J. (2002). Molecular Mechanisms of Axon Guidance. *Science* *298*, 1959–1964.

Fambrough, D., and Goodman, C.S. (1996). The *Drosophila* beaten path Gene Encodes a Novel Secreted Protein That Regulates Defasciculation at Motor Axon Choice Points. *Cell* *87*, 1049–1058.

Featherstone, D.E., and Broadie, K. (2000). Surprises from *Drosophila*: genetic mechanisms of synaptic development and plasticity. *Brain Res. Bull.* *53*, 501–511.

Fernandes, J., and Keshishian, H. (1995). Neuromuscular development in *Drosophila*: insights from embryos and pupae. *Curr. Opin. Neurobiol.* *5*, 10–18.

- Föhrenbach, M. (2016). Analyse verschiedener GFP-Exontrap-Linien in *Drosophila melanogaster* und die weiterführende Charakterisierung einer Insertion im Gen des axonalen Wegfindungsmoleküls Sidestep. Bachelor Thesis. Heinrich Heine University.
- Goodman, C.S. (1996). Mechanisms and Molecules that control Growth Cone Guidance. *Annu. Rev. Neurosci.* *19*, 341–377.
- Goodman, C.S., Bastiani, M.J., Doe, C.Q., du Lac, S., Helfand, S.L., Kuwada, J.Y., and Thomas, J.B. (1984). Cell recognition during neuronal development. *Science* *225*, 1271–1279.
- Gorczyca, M., Augart, C., and Budnik, V. (1993). Insulin-like receptor and insulin-like peptide are localized at neuromuscular junctions in *Drosophila*. *J. Neurosci.* *13*, 3692–3704.
- Goswami, A.M. (2015). Structural modeling and in silico analysis of non-synonymous single nucleotide polymorphisms of human 3beta-hydroxysteroid dehydrogenase type 2. *Meta Gene* *5*, 162–172.
- Grenningloh, G., Rehm, E.J., and Goodman, C.S. (1991). Genetic analysis of growth cone guidance in *Drosophila*: fasciclin II functions as a neuronal recognition molecule. *Cell* *67*, 45–57.
- Halpern, M.E., Chiba, A., Johansen, J., and Keshishian, H. (1991). Growth Cone Behavior Underlying the Development of Synaptic Connections in *Drosophila* Embryos. *J. Neurosci.* *11*, 3227–3238.
- Harrelson, A.L., and Goodman, C.S. (1988). Growth cone guidance in insects: fasciclin II is a member of the immunoglobulin superfamily. *Science* *242*, 700–708.
- Ho, S.N., Hunt, H.D., Horton, R.M., Pullen, J.K., and Pease, L.R. (1989). Site-directed mutagenesis by overlap extension using the polymerase chain reaction. *Gene* *77*, 51–59.
- Hoang, B., and Chiba, A. (2001). Single-cell analysis of *Drosophila* larval neuromuscular synapses. *Dev. Biol.* *229*, 55–70.
- Hwang, S., Gou, Z., and Kuznetsov, I.B. (2007). Sequence analysis DP-Bind: a web server for sequence-based prediction of DNA-binding residues in DNA-binding proteins. *Bioinformatics* *23*, 634–636.
- Jia, X.-X., Gorczyca, M., and Budnik, V. (1993). Ultrastructure of Neuromuscular Junctions in *Drosophila*: Comparison of Wild Type and Mutants with Increased Excitability. *J Neurobiol.* *24*, 1025–1044.
- Jin, Y. (2002). Synaptogenesis: Insights from worm and fly. *Curr. Opin. Neurobiol.* *12*, 71–79.
- Johansen, J., Halpern, E., Johansen, M., and Keshishian, H. (1989). Stereotypic Morphology of Glutamatergic Synapses on Identified Muscle Cells of *Drosophila* Larvae. *J. Neurosci.* *9*, 710–725.
- de Jong, S., Cavallo, J. a, Rios, C.D., Dworak, H. a, and Sink, H. (2004). Target recognition and synaptogenesis by motor axons: responses to the sidestep protein. *Int. J. Dev. Neurosci.* *23*, 397–410.
- de Jousineau, C., Bataillé, L., Jagla, T., and Jagla, K. (2012). Diversification of Muscle Types in *Drosophila*. Upstream and Downstream of Identity Genes. *Curr.*

Top. Dev. Biol. 98, 277–301.

Källberg, M., Margaryan, G., Wang, S., Ma, J., and Xu, J. (2012). RaptorX server: A Resource for Template-Based Protein Structure Modeling. *Methods Mol. Biol.* 1137, 17–27.

Kevenaar, J.T., and Hoogenraad, C.C. (2015). The axonal cytoskeleton: from organization to function. *Front. Mol. Neurosci.* 8, 44.

Kidd, T., Bland, K.S., and Goodman, C.S. (1999). Slit is the midline repellent for the robo receptor in *Drosophila*. *Cell* 96, 785–794.

Kinold, J.C. (2016). Function and regulation of the axon guidance molecules Sidestep and Beaten path 1a in *Drosophila melanogaster*. Dissertation. Heinrich Heine University.

Koch, I., Schwarz, H., Beuchle, D., Goellner, B., Langeegger, M., and Aberle, H. (2008). *Drosophila* Ankyrin 2 Is Required for Synaptic Stability. *Neuron* 58, 210–222.

Kolodkin, A.L., and Tessier-Lavigne, M. (2011). Mechanisms and molecules of neuronal wiring: A primer. *Cold Spring Harb. Perspect. Biol.* 3, 1–14.

Krogh, A., Sonnhammer, E.L.L., and Ka, L. (2004). A Combined Transmembrane Topology and Signal Peptide Prediction Method. *J. Mol. Biol.* 338, 1027–1036.

Krueger, N.X., Vactor, D. Van, Wan, H.I., Gelbart, W.M., Goodman, C.S., and Saito, H. (1996). The Transmembrane Tyrosine Phosphatase DLAR Controls Motor Axon Guidance in *Drosophila*. *Cell* 84, 611–622.

Kühlmann, V. (2012). Genetische Analyse funktionaler Domänen der motoaxonalen Wegfindungsmoleküle Sidestep und Beaten path 1a in *Drosophila*. Bachelor Thesis. Heinrich Heine University.

Kuznetsov, I.B., Gou, Z., Li, R., and Hwang, S. (2006). Using Evolutionary and Structural Information to Predict DNA-Binding Sites on DNA-Binding Proteins. *Proteins Struct. Funct. Bioinforma.* 64, 19–27.

Lahey, T., Corczyca, M., Jia, X., and Budnik, V. (1994). The *Drosophila* Tumor Suppressor Gene *d / g* Is Required for Normal Synaptic Bouton Structure. *Cell* 13, 823–835.

Landgraf, M., and Thor, S. (2006). Development of *Drosophila* motoneurons: Specification and morphology. *Semin. Cell Dev. Biol.* 17, 3–11.

Landgraf, M., Bossing, T., Technau, G.M., and Bate, M. (1997). The origin, location, and projections of the embryonic abdominal motoneurons of *Drosophila*. *J. Neurosci.* 17, 9642–9655.

Landgraf, M., Baylies, M., and Bate, M. (1999). Muscle founder cells regulate defasciculation and targeting of motor axons in the *Drosophila* embryo. *Curr. Biol.* 9, 589–592.

Lee, T., and Luo, L. (1999). Mosaic Analysis with a Repressible Neurotechnique Cell Marker for Studies of Gene Function in Neuronal Morphogenesis. *Neuron* 22, 451–461.

Leterrier, C., and Dargent, B. (2014). No Pasaran! Role of the axon initial segment in the regulation of protein transport and the maintenance of axonal identity. *Semin. Cell Dev. Biol.* 27, 44–51.

- Lewis, A.K., and Bridgman, P.C. (1992). Nerve growth cone lamellipodia contain two populations of actin filaments that differ in organization and polarity. *J. Cell Biol.* *119*, 1219–1244.
- Lin, D.M., and Goodman, C.S. (1994). Ectopic and increased expression of Fasciclin II alters motoneuron growth cone guidance. *Neuron* *13*, 507–523.
- Lin, D.M., Fetter, R.D., Kopczynski, C., Grenningloh, G., and Goodman, C.S. (1994). Genetic Analysis of Fasciclin II in *Drosophila*: Defasciculation, Refasciculation and Altered Fasciculation. *Neuron* *13*, 1055–1069.
- Lin, D.M., Auld, V.J., and Goodman, C.S. (1995). Targeted Neuronal Cell Ablation in the *Drosophila* Embryo: Pathfinding by Follower Growth Cones in the Absence of Pioneers. *Neuron* *14*, 707–715.
- Long, J.B., and Van Vactor, D. (2013). Embryonic and larval neural connectivity: progressive changes in synapse form and function at the neuromuscular junction mediated by cytoskeletal regulation. *Wiley Interdiscip. Rev. Dev. Biol.* *2*, 747–765.
- Lopez, J. (1998). Embryonic Expression Patterns of GAL4 Enhancer Trap Lines. *Pers. Commun. to FlyBase*.
- Lowery, L.A., and Van Vactor, D. (2009). The trip of the tip: understanding the growth cone machinery. *Nat. Rev. Mol. Cell Biol.* *10*, 332–343.
- Mahr, A., and Aberle, H. (2006). The expression pattern of the *Drosophila* vesicular glutamate transporter: A marker protein for motoneurons and glutamatergic centers in the brain. *Gene Expr. Patterns* *6*, 299–309.
- Marqués, G. (2005). Morphogens and synaptogenesis in *Drosophila*. *J. Neurobiol.* *64*, 417–434.
- Meyer, F., and Aberle, H. (2006). At the next stop sign turn right: the metalloprotease Tolloid-related 1 controls defasciculation of motor axons in *Drosophila*. *Development* *133*, 4035–4044.
- Mount, S.M., Burks, C., Herts, G., Stormo, G.D., White, O., and Fields, C. (1992). Splicing signals in *Drosophila*: Intron size, information content, and consensus sequences. *Nucleic Acids Res.* *20*, 4255–4262.
- Nagarkar-Jaiswal, S., Lee, P.-T., Campbell, M.E., Chen, K., Anguiano-Zarate, S., Cantu Gutierrez, M., Busby, T., Lin, W.-W., He, Y., Schulze, K.L., et al. (2015). A library of MiMICs allows tagging of genes and reversible, spatial and temporal knockdown of proteins in *Drosophila*. *Elife* *4*, 1–28.
- Nguyen, T., Jamal, J., Shimell, M.J., Arora, K., and O'Connor, M.B. (1994). Characterization of tolloid-related-1: A BMP-1-like Product That Is Required during Larval and Pupal Stages of *Drosophila* Development. *Dev. Biol.* *166*, 569–586.
- Nguyen Ba, A.N., Pogoutse, A., Provart, N., and Moses, A.M. (2009). NLStradamus: a simple Hidden Markov Model for nuclear localization signal prediction. *BMC Bioinformatics* *10*, 202.
- Nose, A., Mahajan, V.B., and Goodman, C.S. (1992). Connectin: A Homophilic Cell Adhesion Molecule Expressed on a Subset of Muscles and the Motoneurons That Innervate Them in *Drosophila*. *Cell Press* *70*, 553–567.
- del Olmo-Toledo, V. (2014). Beaten path la and Sidestep: cloning and analysis of fusion constructs and study of homologous genes for axon guidance phenotypes

- induced by RNA interference. Master Thesis. Heinrich Heine University.
- Panda, S.K., and Mahapatra, R.K. (2017). In-silico screening, identification and validation of a novel vaccine candidate in the fight against *Plasmodium falciparum*. *Parasitol. Res.* *116*, 1293–1305.
- Pfarr, C. (2017). Untersuchung der Rolle von Beaten path la und Tolloid-related in der Sidestep-vermittelten axonalen Wegfindung und die Auswirkung fehlerhafter Muskelinnervierung auf das lokomotorische Verhalten von *Drosophila melanogaster*. Bachelor Thesis. Heinrich Heine University.
- Pipes, G.C.T., Lin, Q., Riley, S.E., and Goodman, C.S. (2001). The Beat generation: a multigene family encoding IgSF proteins related to the Beat axon guidance molecule in *Drosophila*. *Development* *128*, 4545–4552.
- Raper, J.A. (2000). Semaphorins and their receptors in vertebrates and invertebrates. *Curr. Opin. Neurobiol.* *10*, 88–94.
- Raper, J., and Mason, C. (2010). Cellular Strategies of Axonal Pathfinding. *Cold Spring Harb. Perspect. Biol.* 1–22.
- Raper, A., Bastiani, M., and Goodman, C.S. (1983). Pathfinding by neuronal growth cones in grasshopper embryos. I. Divergent choices made by the growth cones of sibling neurons. *J. Neurosci.* *3*, 20–30.
- Rasse, T.M., Fouquet, W., Schmid, A., Kittel, R.J., Mertel, S., Sigrist, C.B., Schmidt, M., Guzman, A., Merino, C., Qin, G., et al. (2005). Glutamate receptor dynamics organizing synapse formation in vivo. *Nat. Neurosci.* *8*, 898–905.
- Ritzenthaler, S., Suzuki, E., and Chiba, A. (2000). Postsynaptic filopodia in muscle cells interact with innervating motoneuron axons. *Nat. Neurosci.* *3*, 1012–1017.
- Roca, X., Sachidanandam, R., and Krainer, A.R. (2003). Intrinsic differences between authentic and cryptic 5' splice sites. *Nucleic Acids Res.* *31*, 6321–6333.
- Rost, B., and Liu, J. (2004). The PredictProtein server. *Nucleic Acids Res.* *31*, 3300–3304.
- Rothberg, J.M., Hartley, D.A., Walther, Z., and Artavanis-Tsakonas, S. (1988). Slit: An EGF-homologous locus of *D. melanogaster* involved in the development of the embryonic central nervous system. *Cell* *55*, 1047–1059.
- Rothberg, J.M., Roger Jacobs, J., Goodman, C.S., and Artavanis-Tsakonas, S. (1990). Slit: An extracellular protein necessary for development of midline glia and commissural axon pathways contains both EGF and LRR domains. *Genes Dev.* *4*, 2169–2187.
- Schuster, C.M., Davis, G.W., Fetter, R.D., and Goodman, C.S. (1996). Genetic Dissection of Structural and Functional Components of Synaptic Plasticity. I. Fasciclin II Controls Synaptic Stabilization and Growth. *Neuron* *17*, 641–654.
- Serpe, M., Ralston, A., Blair, S.S., and O'Connor, M.B. (2005). Matching catalytic activity to developmental function: tollid-related processes Sog in order to help specify the posterior crossvein in the *Drosophila* wing. *Development* *132*, 2645–2656.
- Siebert, M., Banovic, D., Goellner, B., and Aberle, H. (2009). *Drosophila* motor axons recognize and follow a Sidestep-labeled substrate pathway to reach their target fields. *Genes Dev.* *23*, 1052–1062.

- Sink, H., and Whitington, P.M. (1991). Location and connectivity of abdominal motoneurons in the embryo and larva of *Drosophila melanogaster*. *J. Neurobiol.* 22, 298–311.
- Sink, H., Rehm, E.J., Richstone, L., Bulls, Y.M., and Goodman, C.S. (2001). Sidestep Encodes a Target-Derived Attractant Essential for Motor Axon Guidance in *Drosophila*. *Cell* 105, 57–67.
- Tessier-Lavigne, M., and Goodman, C.S. (1996). The Molecular Biology of Axon Guidance. *Science* 274, 1123–1133.
- Urban, E., Nagarkar-Jaiswal, S., Lehner, C.F., and Heidmann, S.K. (2014). The Cohesin Subunit Rad21 Is Required for Synaptonemal Complex Maintenance, but Not Sister Chromatid Cohesion, during *Drosophila* Female Meiosis. *PLoS Genet.* 10, e1004540.
- Van Vactor, D., Sink, H., Fambrough, D., Tsoo, R., and Goodman, C.S. (1993). Genes that control neuromuscular specificity in *Drosophila*. *Cell* 73, 1137–1153.
- Venn, A. van de (2012). Expressionsanalyse von Beaten path la Deletionskonstrukten in *Drosophila melanogaster*. Bachelor Thesis. Heinrich Heine University.
- Vincenz-Donnelly, L., and Hipp, M.S. (2017). The Endoplasmic Reticulum: A Hub of Protein Quality Control in Health and Disease. *Free Radic. Biol. Med.* 108, 383–393.
- Weitkunat, M., and Schnorrer, F. (2014). A guide to study *Drosophila* muscle biology. *Methods* 68, 2–14.
- Wilkinson DG (2001). Multiple roles of EPH receptors and ephrins in neural development. *Nat. Rev. Neurosci.* 2, 155–164.
- Williams, A.F., and Barclay, A.N. (1988). The immunoglobulin superfamily-domains for cell surface recognition. *Annu. Rev. Immunol.* 6, 381–405.
- Winckler, B., and Mellman, I. (2010). Trafficking guidance receptors. *Cold Spring Harb. Perspect. Biol.* 2, 1–18.
- Yamada, M., and Sekiguchi, K. (2013). Disease-associated single amino acid mutation in the calf-1 domain of integrin alpha-3 leads to defects in its processing and cell surface expression. *Biochem. Biophys. Res. Commun.* 441, 988–993.
- Zinn, K. (2009). Choosing the road less traveled by: A ligand-receptor system that controls target recognition by *drosophila* motor axons. *Genes Dev.* 23, 1042–1045.
- Zito, K., Fetter, R.D., Goodman, C.S., and Isacoff, E.Y. (1997). Synaptic clustering of Fasciclin II and Shaker: essential targeting sequences and role of Dlg. *Neuron* 19, 1007–1016.
- Zito, K., Parnas, D., Fetter, R.D., Isacoff, E.Y., and Goodman, C.S. (1999). Watching a synapse grow: Noninvasive confocal imaging of synaptic growth in *Drosophila*. *Neuron* 22, 719–729.

Index of Abbreviations

aa	amino acid
aCC	anterior corner cell
Ank	Ankyrin-2XL
APS	ammonium persulfate
bp	base pair
Beat	Beaten path Ia
cDNA	copy DNA
CNS	central nervous system
Cy	cyanine dyes
Cys	cysteine
DAPI	4',6-diamidino-2-phenylindole
DNA	deoxyribonucleic acid
dNTP	deoxyribonucleotide triphosphate
DTT	dithiothreitol
DvGlut	<i>Drosophila</i> vesicular glutamate transporter
EDTA	ethylenediaminetetraacetic acid
EGTA	ethylene glycol tetraacetic acid
elav	Embryonic lethal, abnormal vision
EMS	ethyl methanesulfonate
et al.	<i>et alii</i> , and other
FasII	Fasciclin II
GFP	Green fluorescent protein
GOF	gain of function
h	hour
hCD8	human cluster of differentiation 8
HRP	horse raddish peroxidase
IG	immunoglobulin domain
IP	immunoprecipitation
ISN	intersegmental nerve
IUPAC	International Union of Pure and Applied Chemistry
kDa	kilo Dalton
l	liter
L3	third instar larva
LBD	lateral bidendritic neuron
LOF	loss of function
LSN	lateral segmental neurons
M	molar
mef2	Myocyte enhancer factor 2
MHC	Myosin heavy chain
min	minute
ml	milliliter
mRNA	messenger RNA
n	number
NDS	normal donkey serum
NGS	normal goat serum
nm	nanometer
NMJ	neuromuscular junction
Nrx	Neurexin

Index of Abbreviations

n.s.	not significant
NSlmb	N-terminal component of the <i>Drosophila</i> Slmb
nSyb	neuronal Synaptobrevin
OE-PCR	overlap-extension PCR
PAGE	polyacrylamide gel electrophoresis
PBS	phosphate buffered saline
pCC	posterior corner cell
PCR	polymerase chain reaction
PTX	phosphate buffered saline with 0.1% triton X-100
PVDF	polyvinylidene difluoride
RNA	ribonucleic acid
RNase	ribonuclease
rpm	rounds per minute
RT	room temperature
S2 cells	Schneider 2 cells
SDS	sodium dodecyl sulfate
sec	second
Sh	Shaker
Side	Sidestep
Slmb	Supernumerary limbs
SN	segmental nerve
SOC	super optimal broth
SP	signal peptide
TAE	Tris acetate EDTA buffer
TBS	Tris buffered saline
TBST	Tris buffered saline with 0.1% triton X-100
TE	Tris EDTA buffer
TEMED	tetramethylethylenediamine
Tlr	Tolloid-related
TM	transmembrane domain
TN	transverse nerve
Tris	tris-(hydroxymethyl)ammoniummethan
tw-GFP	twist-GFP
UAS	upstream activating sequence
UTR	untranslated region
vhh	variable domain of <i>Camelidae</i> heavy chain antibodies
VIN	ventral intersegmental neurons
VUM	ventral unpaired neuron
WT	wild-type

Eidesstattliche Erklärung

Ich versichere an Eides statt, dass die Dissertation von mir selbstständig und ohne unzulässige fremde Hilfe unter Beachtung der „Grundsätze zur Sicherung guter wissenschaftlicher Praxis an der Heinrich-Heine-Universität Düsseldorf“ erstellt worden ist.

Des Weiteren erkläre ich hiermit, dass die Dissertation bisher noch nicht an einer anderen Fakultät eingereicht worden ist und es somit noch keinen bisherigen Promotionsversuch gegeben hat.

Düsseldorf, den 09. Juni 2017

.....

(Caroline Heymann)

Danksagung

An dieser Stelle möchte ich meinen Dank all denjenigen aussprechen, die diese Arbeit ermöglicht und mich dabei tatkräftig unterstützt haben. Diese Arbeit wurde am Institut für funktionelle Zellmorphologie unter der Leitung von Professor Hermann Aberle angefertigt. Ich möchte mich ganz herzlich bei Hermann bedanken für die Möglichkeit, die Arbeit in seiner Gruppe durchzuführen, sowie für seine Betreuung und kreativen Ideen. Zudem bedanke mich bei Professor Eckhard Lammert für die freundliche Übernahme des Zweitgutachtens sowie für die Gedankenanstöße im Institutsmeeting.

Ein ganz großer Dank gilt den aktuellen und ehemaligen Mitgliedern unserer Arbeitsgruppe. Besonders Jaqueline und Christine möchte ich für ihre Unterstützung und ihre wissenschaftlichen Anregungen danken. Darüber hinaus macht Eure tolle Art einen großen Anteil an der harmonischen und familiären Atmosphäre dieser Gruppe aus und ich hoffe, dass unsere Freundschaft noch lange bestehen bleibt! Jaqueline, danke für Deinen Beistand in Rat und Tat während des praktischen und des theoretischen Teils dieser Arbeit. Marcel, als Herz unserer Abteilung bist Du immer zur Stelle wenn etwas gebraucht wird. Danke dafür, ohne Dich wären wir oft aufgeschmissen! Nicht zuletzt möchte ich mich bei meinen Studenten bedanken für ihr Mitwirken an diversen Projekten, Klonierungen, Injektionen und Auszählungen.

Ich möchte mich von ganzem Herzen bei meiner Familie, insbesondere bei meinem Mann, meinem Sohn und meiner Mutter, bedanken. Ohne Deine tolle Unterstützung und Rückhalt, Alex, hätte ich nicht so viel Zeit und Durchhaltevermögen in diese Arbeit investieren können. Ulrike, Du kümmerst Dich so hingebungsvoll um Niklas, und bist immer zur Stelle wenn Not am Mann ist. Und natürlich Niklas, Du zeigst mir immer wieder die wirklich wichtigen Dinge im Leben. Danke dafür!

Zudem möchte ich mich ganz herzlich bei meinen Freunden bedanken, für Euer Verständnis und die Ermutigungen während dieser Zeit.